# Photo-induced Oxygen Atom Transfer with molybdenum and tungsten dioxo complexes

Thorsten Dreher

Doctor of Philosophy

University of York

Chemistry

April 2022

# Abstract

To date, only a few examples of photo-catalysed oxygen atom transfer (OAT) with molybdenum and tungsten containing complexes have been reported, and these suffer from poor performance or require extensive synthesis. This work investigates new simple molybdenum and tungsten complexes that overcome these shortcomings.

Sixteen molybdenum (VI) dioxo and two tungsten (VI) dioxo complexes with substituted Schiff base SAP ligands (SAP = salicylidene amino phenol) were synthesised and characterised by NMR-, ATR-IR- and UV-Vis spectroscopies, mass spectrometry and elemental analysis. Substituent position and stereo-electronic properties were varied to study their influence on the metal complex properties and catalytic activity. UV-Vis and emission spectroscopic measurements revealed little difference between complexes except when additional chromophores were present. Excited state lifetimes of selected complexes were in the range of 2 to 6 ns.

The ability of the complexes to catalyse OAT between DMSO and $PPh_3$ under irradiation was screened. Conversions up to 78 % after 3 h were observed, with some complexes being inactive.

The most active complex (**Mo-2**) was used to study the substrate scope. Several different phosphines and sulfoxides were tested. While conversion changed with the substrate a clear trend was not observed.

Further information on the mechanism was obtained from the stoichiometric reaction between **Mo-2** and $PPh_3$**.** Analysis of the reaction mixture after irradiation suggested the formation of molybdenum (IV), likely in the triplet state.

Reaction kinetics were found to depend strongly on the solvent used and, particularly, on the concentration of **Mo-2.** Below 1 mM the reaction rate increased linearly with catalyst concentration while above 1mM it decreased exponentially.

Three mechanisms for photoactivated OAT have been discussed expanding on the mechanism found in thermal OAT, one involving the formation of radical molybdenum and triphenyl phosphine species. None of the mechanisms can fully explain the results obtained and further work is needed.

# Table of Contents

# Table of Figures

# Table of Schemes

# Table of Tables

# Acknowledgments

This thesis would not have been possible without the help of many people.

First of all, I thank my supervisors Anne and Richard for their support, guidance and valuable critique during this project.

Thank you to the technicians and the analytical services. In particular Heather and Alex for keeping the NMR running, training and troubleshooting; Lawrence for help with the fluorescence and lifetime measurements.

A big thank you to past and present members of the AKDK and RED groups and E002 for help in general but more importantly for making my time here more enjoyable, in particular Ben, James, Connor, Lisa, Ros, Sophie, Lukas, Nat, Abbey, Ben, Alex, Nia, Will, Joy, Mina, Peter, Jon and Rajat.

Und zu guter Letzt, meinen Eltern und meinem Bruder für die Unterstützung auf dem langen Weg der mich zu diesem Punkt geführt hat: Vielen Dank!

# Declaration

I declare that the work presented in this thesis is original and my own. The research was carried out between October 2017 and April 2022 under the supervision of Prof. Anne-K. Duhme-Klair and Dr. Richard E. Douthwaite at the University of York. No part of this thesis has been submitted for other qualifications at this or any other university. Sources are acknowledged as references. The following work was done by other researchers:

-Mass spectrometry was performed by Dr. K. Heaton, Dr. R. Cercola, and Mr. A Lopez.

- Elemental analysis was performed by Dr. G. McAllister

- Single crystal X-ray crystallography was performed by Mr. T. Tanner and Dr. A. Whitwood

-Synthesis and characterisation of **L-11**, **L-12**, **L-13**, **L-14**, **L-15**, **L-16**, **Mo-11**, **Mo-12**, **Mo-13**, **Mo-14**, **Mo-15** and **Mo-16** and catalytic testing of **Mo-11**, **Mo-12**, **Mo-13**, **Mo-14**, **Mo-15** and **Mo-16** was in part performed by Mrs. K. Morgan

Thorsten Dreher

# Chapter 1 Introduction

## 1.1 The environmental impact of chemistry

There is a clear need to reduce the human impact on the environment in terms of energy consumption leading to emission of climate affecting $CO_2$ as well as production of harmful waste and by-products.

Many industrial processes producing important chemicals are operated under high temperature or pressure which requires large amounts of energy thus leading to $CO_2$ release.[1] Among these are oxidations, with the oxidation of alcohols playing an important part in production of pharmaceuticals and fine chemicals.[2] Another important reaction is the epoxidation of olefins both for production of fine chemicals as well as large scale compounds like polymers.[3]

The sun provides free, renewable energy sufficient to meet future energy needs.[4] There are many potential ways of using this energy including the production of electricity by photovoltaic solar cells, solar thermal heating, photocatalytic and photoelectrochemical production of chemical fuels as a means of storage (so called solar fuels like hydrogen or methanol) and the production of useful chemicals. However, there remain many challenges to realising economically viable processes based on many of these technologies.

While clean electricity or solar fuels could be used to heat up reaction mixtures and activate thermal reactions, a potentially more efficient way is to directly use sun light to activate reactions *via* a photocatalyst. The use of sunlight could suffer from too low and fluctuating irradiance compared to light sources usually used in laboratories during the development of photocatalysts. The combination of a photocatalyst and an artificial light source could still be less energy intense than a high temperature thermal process and avoid the use of fossil fuels.

Oxidation reactions on the industrial or laboratory scale, still rely mostly on oxidants such as organic peroxides, DMSO, permanganate, chromate or iodosyl benzene that themselves are toxic and produce waste.[5] They also need to be made in the first place and transported, again requiring energy.

$H_2O_2$ might seem like a good alternative given it is an effective oxidant, as its use only produces water as by-product and it is efficient from the perspective of active oxygen species to overall weight ratio. On the down side water is always present in the reaction and more importantly $H_2O_2$ production requires an energy intensive process.[6]

A better solution would be to produce $H_2O_2$ via a less energy consuming route or to use a process that does not rely on such oxidants but instead uses oxygen gas/air or water, ideally under ambient conditions.

Another alternative would be to use a species as an oxygen source where reduction of this species is beneficial, either because the reduced species can be used in subsequent reactions or because it is less harmful.

## 1.2 Oxygen Atom Transfer

The type of reaction this work is focussed on is oxygen atom transfer (OAT). OAT is a redox process with very specific characteristics in which a species A is oxidised while formally gaining an oxygen atom, while species D is reduced and loses an oxygen atom.

$$A + D^{2+}O^{2-} \rightleftharpoons A^{2+}O^{2-} + D$$

*Scheme 1-1: OAT between two species A and DO.*

In this process the oxygen being transferred retains the formal oxidation state -2 in both reactant and product. The formal oxidation state of species A and D changes by +2 and -2, respectively.

Oxygen atom transfer is a common type of reaction but usually not recognised as such. An example of an industrially relevant OAT process is the production of syngas shown in Scheme 1-2.[7]

$$CH_4 + CO_2 \rightleftharpoons 2\,CO + 2\,H_2$$

*Scheme 1-2: Production of syngas, an example of OAT.[7]*

In most applications of OAT, the aim is to oxidise / reduce a substrate hence the oxygen donor / acceptor is considered a by-product. Examples of oxygen donors include PhIO, peroxides (*m*-chloro-perbenzoic acid, *t*-BuOOH, $H_2O_2$), N-oxides (pyridine-N-oxide), S-oxides (DMSO, biotin-S-oxide) while phosphines ($PPh_3$), sulfides and protons can accept oxygen. As the donor or acceptor, respectively, is required in stoichiometric quantities, significant amounts of waste can result unless the by-product is water.

Examples of OAT in biology will be presented in sections 1.3.1 and 1.3.2.

**Reactivity in OAT**

In order to predict whether reaction occurs between an oxygen donor and an acceptor, a thermodynamic scale has been devised.[8] Similar to standard redox-potentials, the enthalpy of reaction for a number of pairs X/XO have been obtained. OAT from XO to Y occurs if $\Delta H_{X/XO} > \Delta H_{Y/YO}$, assuming $|T\Delta S| << |\Delta H|$.

A few selected examples are shown in Table 1-1.

*Table 1-1: Thermodynamic reactivity scale for OAT. Data taken from Holm and Donahue.* [8]

| $X + \frac{1}{2} O_2 = XO$ | | | |
|---|---|---|---|
| X | XO | $\Delta H_{X/XO}$ / kcal mol$^{-1}$ | |
| $H_2O$ | $H_2O_2$ | +34.1 | Gas phase |
| tBuOH | tBuOOH | +15.9 | |
| $Me_2S$ | $Me_2SO$ | -27.1 | |
| O | $O_2$ | -59.6 | |
| $Ph_3P$ | $Ph_3PO$ | -73.8 | |
| | | | |
| $PhCO_2H$ | $PhCO_3H$ | +4.3 | Solid phase |
| $NaClO_3$ | $NaClO_4$ | -4.9 | |
| $Ph_3P$ | $Ph_3PO$ | -69.9 | |
| Mg | MgO | -144 | |

From Table 1-1 it would, for example, be predicted that $PPh_3$ is oxidised by $O_2$ which does in fact happen. The reaction is, however, slow,[9] especially between solid $PPh_3$ and air emphasising the importance of reaction kinetics.

## 1.2.1 Metal centred Oxygen Atom Transfer

OAT is mostly encountered involving metals and metal-based OAT is the focus of this work. One of the first examples of such a reaction is the reaction between $OsO_2$ and chlorate yielding $OsO_4$ reported by Hofmann in 1912.[10] It was not until the work of Halperin and Taube in 1950 employing $^{18}O$-labelling that OAT became popular as the labelling now allowed identification of the oxygen acceptor / donor in a reaction system.[11,12]

In general, OAT involving metals can be divided into primary and secondary OAT, Scheme 1-3. [12]

primary OAT

$$M^{z+2}O_{a+1}L_n + X \rightleftharpoons M^{z}O_aL_n + XO \tag{1}$$

secondary OAT

$$M^{z+2}O_aL^{l}_{n} + L' \rightleftharpoons M^{z}O_{a-1}L^{l}_{n-1}L' + L^{l+2}O \tag{2}$$

$$M^{z+1}(L^{l}O_a)_n + X \rightleftharpoons M^{z}(L^{l}O_a)_{n-1}(L^{l-1}O_{a-1}) + XO \tag{3}$$

*Scheme 1-3: Primary and secondary oxygen atom transfer.*

Primary OAT corresponds to the general case in Scheme 1-1 where one species is the metal oxo complex $[MO_aL_n]$ which transfers one of its oxo ligands to a species X. The reactants X/XO are oxygen atom acceptor/donor, the oxidation state of M changes by ±2 as a consequence of atom transfer only and the oxygen transferred is directly bound to M as a terminal or bridging group.

An example of primary OAT is the reaction of an iron porphyrin complex with $PPh_3$:

$$\mathrm{FeO(TMP)} + \mathrm{PPh_3} \longrightarrow \mathrm{Fe(TMP)} + \mathrm{OPPh_3}$$

*Scheme 1-4: Reaction of an iron porphyrin oxo complex with $PPh_3$. TMP = meso-tetramesitylporphyrinate.*[13]

In secondary OAT, there are two different cases. In reaction 2, binding of a ligand L' leads to an internal redox reaction and formation of ligand oxide OL which may dissociate as depicted or stay bound. In contrast to reaction 1, the incoming species L' is not the oxo acceptor. In reaction 3, both the metal and a ligand L are reduced when oxygen is transferred.

The following reaction between two titanium porphyrin complexes is an example of secondary OAT as the reaction proceeds *via* ligand reduction of the peroxide:

$$[\mathrm{(OEP)Ti(O_2)}] + [\mathrm{(TTP)Ti)PhC{\equiv}CPh)}] \longrightarrow [\mathrm{(OEP)Ti{=}O}] + \mathrm{PhC{\equiv}CPh}$$

*Scheme 1-5: OAT between two titanium porphyrin complexes. OEP = octaethylporphyrinato, TTP = meso-tertaphenylporphyrinato.*[14]

The remainder of this work will focus on primary OAT.

## 1.3 Properties and occurrence of Molybdenum and Tungsten

Molybdenum and tungsten have found use due to their high melting points and hardness. Tungsten and tungsten alloys are used in high temperature applications, *e.g.* electrodes for welding and as tungsten carbide in tools like drills.[15] Molybdenum is an additive in steel and increases strength and hardness and corrosion- and wear resistance.[16] Molybdenum sulfide is used to remove sulfur from petrol and molybdenum oxide in the oxidation of alcohols.[17]

The abundances of molybdenum and tungsten in different environments are listed in Table 1-2, together with those of iron for comparison. Despite its low abundance, molybdenum is essential to most organisms, from single cell species to humans. Currently, more than 50 molybdenum enzymes are known, most of which are found in prokaryotes (single celled organisms). Tungsten is used much less and mostly found in archaea, which are mostly thermophilic anaerobes.[18]

*Table 1-2: Abundance of molybdenum, tungsten and iron.*[19]

| | Abundance / ppb by atoms | | |
|---|---|---|---|
| | Mo | W | Fe |
| Universe | 0.1 | 0.003 | 20 000 |
| Crustal rock | 230 | 120 | 23 000 000 |
| Ocean | 0.64 | 0.004 | 0.33 |
| Human body | 7 | / | 6 700 |

Molybdenum and tungsten are primarily involved in catalysing redox reactions, mostly oxygen atom transfer to and from carbon, nitrogen and sulfur. Their chemical properties make molybdenum and tungsten suitable for their role in organisms. Oxidation states from 6+, 5+ and 4+ (molybdenum can even have 3+ in the nitrogenases) are accessible under physiological conditions thereby allowing catalysis of both one-electron and two-electrons redox reactions.[20] Although molybdenum has a strong affinity for oxygen it can relatively easily lose a single oxygen which makes molybdenum complexes excellent catalysts for oxygen atom transfer (Scheme 1-1). In organisms, water / protons are typically involved as the donor / acceptor in oxygen atom transfer with molybdenum and tungsten enzymes.

## 1.3.1 The active centre of molybdo- and tungsto-enzymes

After first purification of xanthine oxidase by Dixon and Thurlow[21] in 1924 the first crystal structure of an Mo enzyme, the aldehyde oxido-reductase isolated from *Desulfovibrio gigas* was recorded by Romão and co-workers in 1995.[22]
Formate dehydrogenase from *Clostridium thermoaceticum*, the first tungsten enzyme, was only purified in 1983 by Yamamoto and co-workers[23] and the first crystal structure reported in 1995 even before that of molybdenum by Chan and co-workers of the aldehyde ferredoxin oxidoreductase from *Pyrococcus furiosus*.[24] From these as well as structures of other enzymes (*e.g.* dimethylsulfoxide reductase from *Rhodobacter sphaeroides* and sulfite oxdase from chicken liver)[25,26] the active centres of the molybdo- and tungsto-enzymes were identified.

Apart from a few exceptions, molybdenum and tungsten are contained within the enzymes as mononuclear centres coordinated *via* sulfur to one or two pyranopterin cofactors (Figure 1-1), the remaining coordination sites are filled by oxygen, sulfur, nitrogen or selenium.

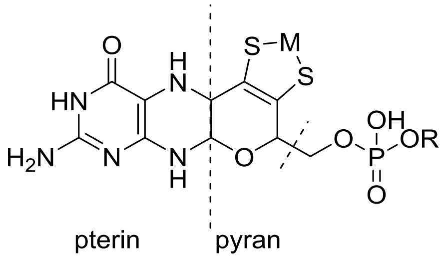

M = Mo, W
R = H, cytidine, guanosine, adenosine

*Figure 1-1: Structure of the pyranopterin cofactor of molybdenum and tungsten enzymes.*

The cofactor consists of a pterin molecule fused to a substituted pyran. The pyran bears the thiolate ligands which coordinate to the metal as well as a phospho ester. In eukaryotes this ester is a simple mono ester (R=H) whereas in prokaryotes it is usually a diester bound to nucleosides (cytidine, guanosine or adenosine).[20]

Figure 1-1 depicts the cofactor in the closed pyran form which has been found in the crystal structures of most molybdenum enzymes.[27] The existence of the open form has, however, brought about the hypothesis that closing and opening could be involved in the catalytic process.[28]

The exact role of the cofactor is still unclear but could include serving as an anchor point for and modulating the redox potential of the metal and allowing for efficient electron transfer between the metal and other redox active centres of the enzyme.[20,27]

In nitrogenases which are of great importance for the fixation of atmospheric nitrogen, molybdenum is part of a $[MoFe_7S_9C]$ cluster, whereas in the recently isolated “orange protein” it is found in the linear $[S_2MoS_2CuS_2MoS_2]$ cluster whose function is not yet completely understood.[20]

In the following sections the enzymes capable of OAT will be presented. The separation of the molybdo- and tungsto-enzymes into (sub)classes is based on their active centre and the type of reactions they catalyse, and different classifications based on these criteria have been made too.[20]

### 1.3.1.1 The subclasses and active centres of pyranopterin-containing molybdo-enzymes

Based on the structure of their active centre and the reactions catalysed, molybdo enzymes have been categorised into three main classes: Xanthine oxidase (XO), Sulfite oxidase (SO) and DMSO reductase (DMSOR), with several subclasses.[29]

**Xanthine oxidase**

The active centre of the xanthine oxidase (XO) class is shown in Figure 1-2 consisting of the pyranopterin bound molybdenum with an oxo and a hydroxo ligand. The fifth coordination site is filled depending on the enzyme subclass with sulfur being the most common. Oxygen is found in the inactive form of carbon monoxide dehydrogenase, XO and the active form of aldehyde oxidase, selenium in nicotinate dehydrogenase.[30] In CO dehydrogenases, the active centre is binuclear, containing an additional sulfide bridged copper, Mo-S-Cu-S(Cys).[31] XO class enzymes generally possess additional redox-active sites such as iron sulfur clusters and FAD (flavin adenine dinucleotide), where electrons from the molybdenum centre are transferred to $O_2$ or $NAD^+$ (nicotinamide adenine dinucleotide).[32]

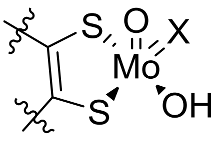

X= S, Se, O, S-Cu-S(Cys)

*Figure 1-2: Coordination sphere of Mo in the active centre of Xanthine oxidase class enzymes.[33] The dithiolene represents the pyranopterin unit (Figure 1-1).*

Members of this class catalyse the oxidative hydroxylation of various substrates. The oxidation of xanthine, and its precursor, after which this class of enzymes is named, is shown in Scheme 1-6.

XO is part of the purine metabolism in humans and animals and is one of the most studied enzymes, particular the XO obtained from cows milk and discovered in 1902.[31,34]

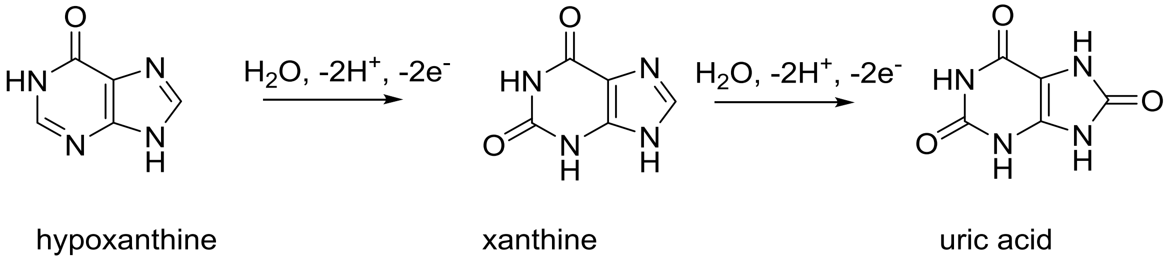

*Scheme 1-6: Stepwise oxidation of hypoxanthine to uric acid.*[35]

Other examples of this class include aldehyde oxidase and oxidoreductase, converting aldehydes to acids or CO dehydrogenase converting CO to $CO_2$.[29]

**Sulfite oxidase**

The active centre of sulfite oxidases is similar to that of xanthine oxidase but contains two oxo ligands. The fifth coordination site is occupied by a cysteine sulfur giving a square pyramidal geometry (Figure 1-3).

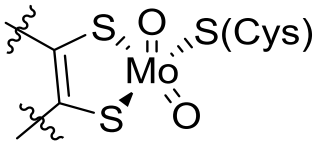

*Figure 1-3: Coordination sphere of Mo in the active centre of sulfite oxidase class enzymes.*[33] *The dithiolene represents the pyranopterin unit (Figure 1-1).*

The reaction that gave its name to this class is the oxidation of sulfite to sulfate, $SO_3^{2-} + H_2O \text{-->} SO_4^{2-} + 2e^- + 2H^+$

Another similar reaction catalysed by members of this family is the oxidation of nitrite to nitrate. In general, all members of the SO class catalyse reactions on substates containing sulfur or nitrogen.[36]

Sulfite oxidase is part of the catabolism of sulfur containing proteins. Disruption in the function of this enzyme leads to accumulation of toxic sulfite.[36]

**DMSO reductase**

DMSO reductase differs from the two previous classes in that molybdenum is bound to two pyranopterin units in a trigonal prismatic geometry (Figure 1-4). One oxo ligand and one hydroxide alkoxide, thiolate or selenolate complete the coordination sphere.[33]

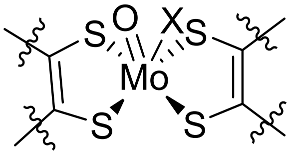

X =OH, O(Ser), O(Asp), S(Cys), Se(Cys)

*Figure 1-4: Coordination sphere of Mo in the active centre of DMSO reductase class enzymes.* [33] *The dithiolenes represent the pyranopterin units (Figure 1-1).*

The reaction that gave its name to this class is the reduction of DMSO to DMS, $DMSO + 2e^{-} + 2H^{+}$ -> $DMS + H_2O$, as DMSO reductase was the first in this class to be characterised by x-ray crystallography.[37]

The DMSO reductase class is the most diverse of the three, catalysing various reactions including reactions other than OAT, for example sulfur atom transfer or the addition of water to ethyne to give acetaldehyde.[20] A few selected examples are given in Table 1-3.

*Table 1-3: Examples of subclasses of the DMSO reductase family and reactions catalysed. Adapted from.* [29]

| Subclass | Reaction |
|---|---|
| Biotin sulfoxide reductase | Biotin-S-oxide $+2H^{+} + 2e^{-}$ -> Biotin + $H_2O$ |
| Trimethylamine-N-oxide reductase | $ONEt_3 + H^{+}$ + NADH-> $NEt_3 + H_2O$+ $NAD^{+}$ |
| Nitrate reductase (dissimilatory) | $NO_3^{-} + 2e^{-} + 2H^{+}$ -> $NO_2^{-} + H_2O$ |
| Formyl-methanofuran dehydrogenase | Formyl-methanofuran + $H_2O$ -> methanofuran + $CO_2 + 2e^{-} + H^{+}$ |
| Arsenite oxidase / Arsenate reductase | $AsO_3^{3-} + H_2O$ <-> $AsO_4^{3-} + 2e^{-} + 2H^{+}$ |

Members of this class are exclusively found in prokaryotes.

### 1.3.1.2 The active centre of pyranopterin-containing tungsto-enzymes

The active sites of tungsto-enzymes are similar to those of the DMSO reductases. Tungsten is bound to two pyranopterin units in a trigonal prismatic or a distorted octahedral geometry. The remaining coordination sites are filled by oxygen, sulfur or selenium (Figure 1-5).[20]

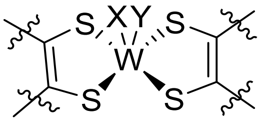

X,Y = S, Se, O, O(Asp), S(Cys),
Se(Cys)

*Figure 1-5: Coordination sphere of W in the active centre of tungsto-enzymes.[20] The dithiolenes represent the pyranopterin units (Figure 1-1).*

The members of this class catalyse diverse reactions. Selected examples are shown in Table 1-4.

*Table 1-4: Reactions catalysed by tungsto-enzymes.[38]*

| Enzyme | Reaction |
|---|---|
| Aldehyde oxidoreductase | $RCHO + H_2O <-> RCOOH + 2H^+ + 2e^-$ |
| N-Formylmethanofuran dehydrogenase | $RNHCHO + H_2O <-> RNH_3^+ + CO_2 + H^+ + 2e^-$ |
| Formate dehydrogenase | $HCO_2^- <-> CO_2 + H^+ + 2e^-$ |
| Acetylene hydratase | $HC{\equiv}CH + H_2O <-> CH_3CHO$ |

Molybdenum analogues are known for many of these enzymes. As for the structurally similar DMSO reductases, tungsto-enzymes are only found in prokaryotes.

## 1.4 Selected models for active centres of OAT-performing enzymes

In order to understand the molybdenum and tungsten enzymes and potentially apply the principles that govern their catalytic activity to perform OAT on substrates relevant to chemical synthesis, models of the active centres of these enzymes have been designed. Even before the first crystal structures of molybdo- and tungsto-enzymes were obtained models have been synthesised based on the spectroscopic and chemical studies of the enzymes .[39]

The degree to which the active centre was accurately modelled varied, but common to these complexes is their ability to catalyse thermal OAT. Models of these enzymes have usually focussed on a particular aspect be it the thiolene ligand, the metal core or the reactivity.

A complete model not only needs the appropriate atoms in the first coordination sphere, directly coordinated to the metal, but also in the second coordination sphere including the pyranopterin.

Synthesis of the pyranopterin has been attempted but due to its instability outside the enzyme without coordinated metal, it could only be synthesised in a highly protected form, shown in Figure 1-6.[40]

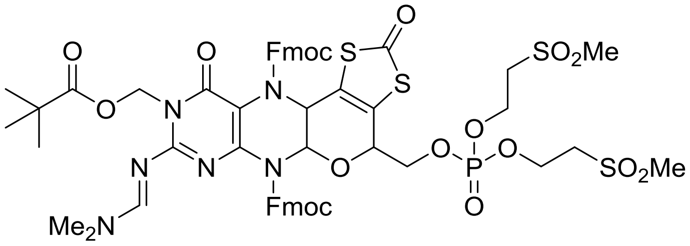

Figure 1-6: Structure of protected pyranopterin as synthesised by Bradshaw et al.[40]

In regard to the metal core, several issues were encountered.[38] Features found in the active centre had not been for known molybdenum complexes until their discovery in the crystal structure. The uncommon MoOS core of the XO class contains the highly reactive sulfido ligand but has been obtained in the complex $[MoOS(OSiPh_3)_2)phen)]$.[41] Stabilising the five coordinate $MoO_2$ centre of the SO class in the presence of three reducing thiolate ligands proved challenging. Lastly, the pair $Mo(VI)O_2$ / Mo(IV)O had been the natural choice for the metal core due to its frequent occurrence in conventional molybdenum chemistry. Crystal structures of the active centres of the xanthine oxidase and the DMSO reductase classes, however, revealed that using Mo(VI)O / Mo(IV) would be more accurate, but complexes containing this pair were barely known or studied.[38] Similar arguments apply to the tungsten enzymes.

The number of models is vast since any complex containing the $[MoO_2]^{2+}$ group models the active site. Many examples of complexes with this group have been reported, although often these complexes take inspiration from molybdo-enzymes rather than claiming to model their active centres. [33,42–44]

A selection of models will be presented in the following sections. Further examples are discussed with regard to the mechanism of OAT in chapter 3.1.

### 1.4.1 Enzyme models containing sulfido ligands

A close model of the active site of XO enzymes requires the $[MoO_2S(dithiolene)]$ or $[MoO(OH/H_2O)S(dithiolene)]$ unit, however, no such complex has been reported yet.[45] A complex with the $[MoO_2S]$ core, but no dithiolene ligand has been reported by Zhang *et al.*[46] The 1,4,7-trimethyl-1,4,7-triazacyclononane ($Me_3tacn$) ligand was used to obtain **1-1** (shown in Figure 1-7) from the trioxo analogue. The authors were not investigating models for enzymes, however, and no OAT or other reactions with **1-1** were performed.

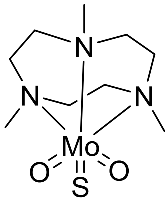

**1-1**

*Figure 1-7: A Model for the active site of XO enzymes.* [46]

Another model of the XO class of enzymes, containing the [Mo*O₃S*] core, was synthesised by Thapper and co-workers.[41] **1-2** (Figure 1-8) was obtained from [$MoO_3S$] with $ClSiPh_3$ and $Me_4$phen and the presence of the [MoOS]$^{2-}$ core was confirmed by elemental analysis, $^1$H NMR, mass spectrometry, x-ray crystallography structure and EXFAS measurements. Bond lengths of 1.71 and 2.18 Å of Mo=O and Mo=S, respectively, agreed well with values for xanthine oxidase. Reactivity, however, did not replicate the enzyme. Reaction with the oxygen acceptor $PPh_3$ yielded $SPPh_3$ quantitatively, due to the lower bond energy of Mo=S. In addition, sulfide transfer resulted in the reduced [Mo(IV)] which quickly abstracted chloride from the solvent $CH_2Cl_2$ to give the Mo(V) complex **1-3.**

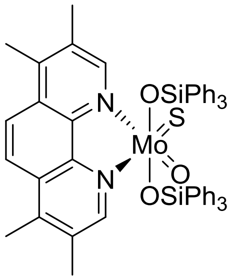

**1-2**

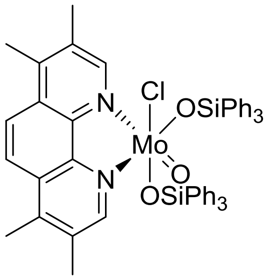

**1-3**

*Figure 1-8: Structure of a model of the active centre of XO enzymes (left)***,** *and the product of the reaction of* ***1-2*** *with* *$PPh_3$, (right).*

The active centres of enzymes of the DMSO reductase and tungsto-enzyme classes are very similar, both contain two pyranopterins. This close similarity is reflected in isoenzymes, two enzymes that catalyse the same reaction within a species, but differ in their properties, one uses molybdenum, the other tungsten. An example is the *Methanobacterium wolfei* which possesses both a tungsten and a molybdenum formylmethanofuran dehydrogenase.[47,48]

The first model of tungsten formate dehydrogenase (**1-4**, Figure 1-9) was synthesised by Groysman and Holm but neither its crystal structure nor its reaction with formate has been reported.[49] The related complexes **1-5** and **1-6** were the first structurally characterised models that showed the relevant substrate binding.[45,50]

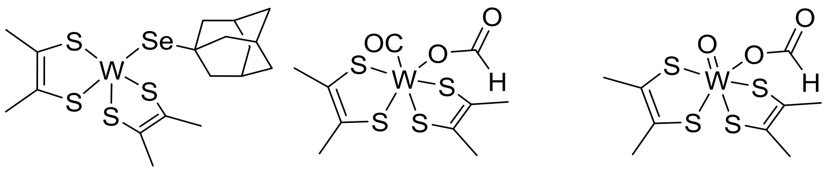

**1-4** **1-5** **1-6**

*Figure 1-9: A Model of the active site of tungsten formate dehydrogenase containing a selenothiolate ligand (left)[49] and two models showing substrate binding (right).[45,50]*

The complexes in Figure 1-10 form another interesting system of models, synthesised by Das *et al.* to model the active site of aldehyde oxidoreductase.[51] In contrast to earlier models, **1-7** showed reactivity relevant to the enzyme as it reacted with crotonaldehyde (3-butene aldehyde) to yield crotonic acid in low yields. Catalytic aldehyde oxidation was, however, not achieved. In addition, reaction of **1-7** with aldehyde yielded **1-8** with the dissociated $S_2^{2-}$ presumed to have reacted with remaining aldehyde to yield thio aldehyde. **1-8** could also be obtained from **1-7** via double sulfur atom transfer to $PPh_3$ whereas the back reaction can be achieved with elemental sulfur. **1-7** could be prepared from **1-9** with $H_2S$ which could also be reduced to **1-8** via OAT to $PPh_3$. The three complexes displayed an interesting oxygen / sulfur atom transfer dynamic.

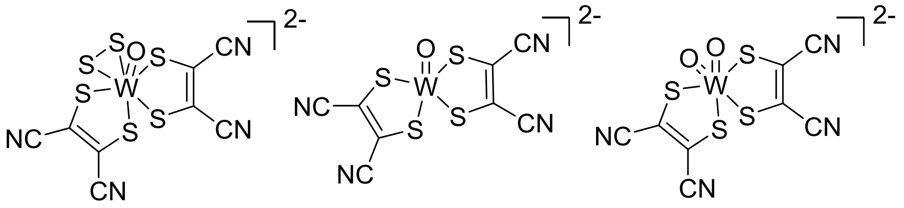

**1-7** **1-8** **1-9**

*Figure 1-10: Structures of complexes related to active site of aldehyde oxidoreductase.[51]*

### 1.4.2 Enzyme models containing the $MO_2$-core

Models containing the $MO_2$-core (M= Mo, W) have usually easier synthesis and higher stability than models containing sulfido ligands.

The active centre of the sulfite oxidase class contains the $MoO_2$-core. An example for a model of this class are **1-10** and **1-11**, shown in Figure 1-11, which are related to the tungsten complexes of the previous section (Figure 1-9 and Figure 1-10). **1-10** and **1-11** were synthesised before crystallographic information on the active centre was available and contained two dithiolene ligands. **1-10** was found to be a functional enzyme model of sulfite oxidase, catalysing the oxidation of sulfite to sulfate whereas **1-11** was found to model the structure of the low pH form of the enzyme, with an EPR signal similar to that of sulfite oxidase.[52]

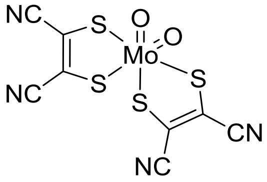

**1-10**

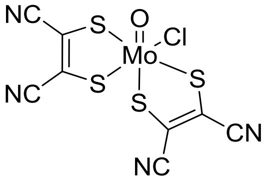

**1-11**

*Figure 1-11: Structure of a model for the active site of the sulfite oxidase class.*

Molybdenum and tungsten dioxo complexes are numerous and contain various types of ligands. Still, at their ($MO_2$-)core they can be regarded as enzyme models. Often in the study of these complexes substitution at the ligand is done to change the spectroscopic or steric properties of the complexes and in particular their OAT reactivity.

A few more examples of molybdenum and tungsten dioxo complexes are shown in Figure 1-12.

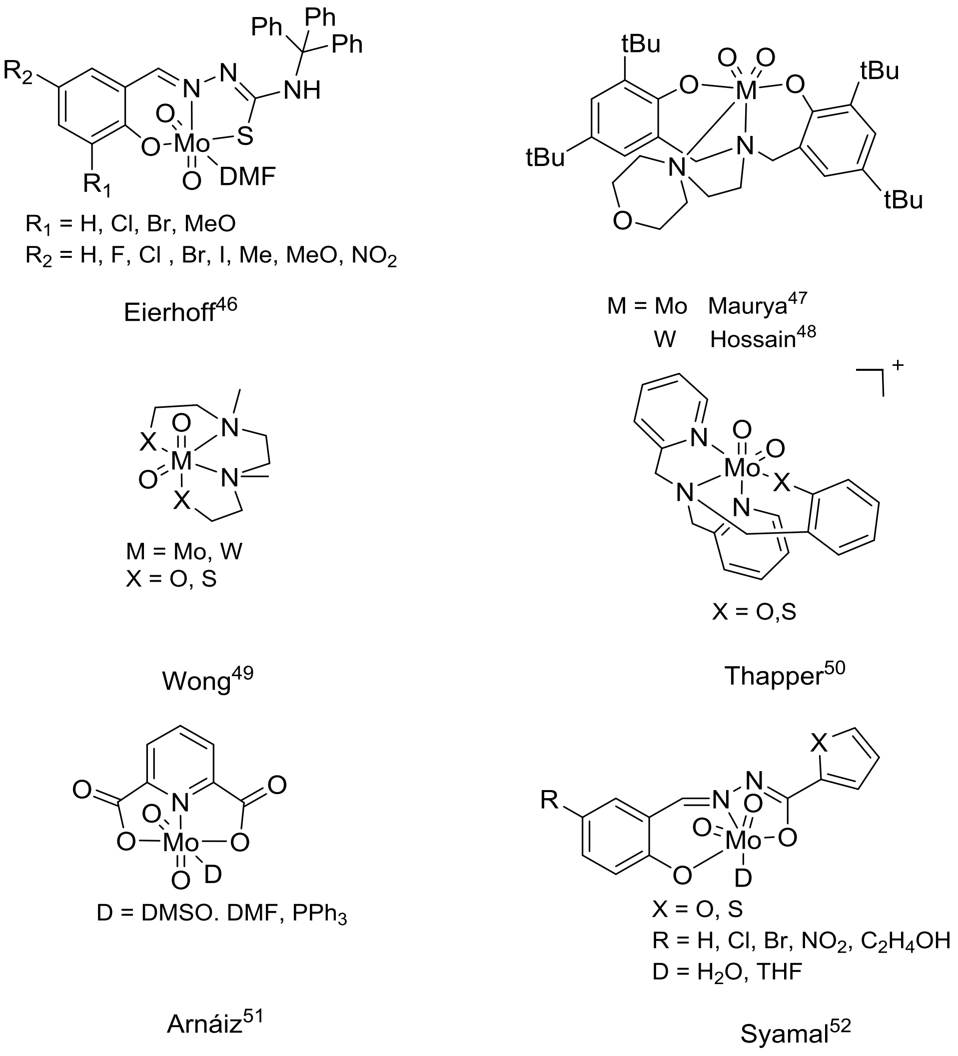

$R_1$ = H, Cl, Br, MeO

$R_2$ = H, F, Cl , Br, I, Me, MeO, $NO_2$

Eierhoff[46]

M = Mo Maurya[47]

W Hossain[48]

M = Mo, W

X = O, S

Wong[49]

X = O,S

Thapper[50]

D = DMSO. DMF, $PPh_3$

Arnáiz[51]

X = O, S

R = H, Cl, Br, $NO_2$, $C_2H_4OH$

D = $H_2O$, THF

Syamal[52]

*Figure 1-12: Structures of various molybdenum and tungsten dioxo complexes.*

Figure 1-13 shows two unusual molybdenum complexes, a mono oxo complex employing a tris pyrazolyl borate ligand that is connected to an iron porphyrin via a catechol, and a dioxo complex bearing two ferrocenium substituted imino pyridine ligands. The connected redox active iron centres model the iron centres found in sulfite oxidases and were found to stabilise Mo(V) over Mo(IV) after OAT.[60,61]

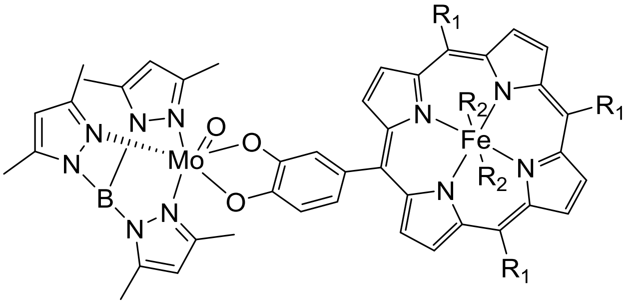

$R_1$ = 4-Me-Ph
$R_2$ = N-Me-imidazole

Basu[53]

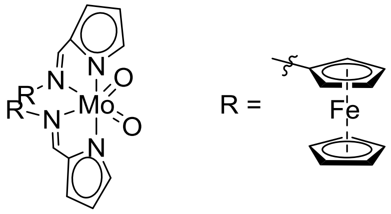

Hanauer[54]

*Figure 1-13: Two molybdenum complexes bearing redox active iron centres.*

As oxygen atom transfer is common for many metals, artificial enzymes and cofactor with metals other than molybdenum and tungsten in the active centre have been envisaged as potential drugs against molybdenum cofactor disease.[62] Figure 1-14 shows two oxo bis-dithiolene complexes with molybdenum and rhenium.[62] Both complexes showed extremely low reaction rates during OAT from DMSO to $PPh_3$ (40 mol% catalyst), [Mo] reached completion after 67 days whereas [Re] only reached 45 % after 73 days. The reaction rates suggested the existence of very different mechanisms, contrary to initial assumption, but these were not further investigated. Despite the poor catalytic performance [Re] is the first rhenium complex closely similar first coordination sphere to that of the molybdenum cofactor to show OAT reactivity at all.

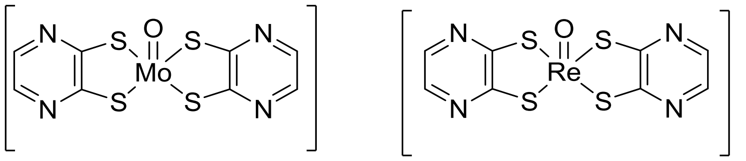

*Figure 1-14: Structures of two oxo bis-dithiolene complexes with molybdenum and rhenium.[62]*

## 1.4.3 Examples of photoactivated OAT

The model complexes presented thus far only performed thermal OAT – if they were tested and showed activity to begin with. Examples of photoactivated OAT are rare, particularly where a molybdenum or tungsten complex performs OAT as described in the dual role as OAT- and photo catalyst. Four related examples are shown below.

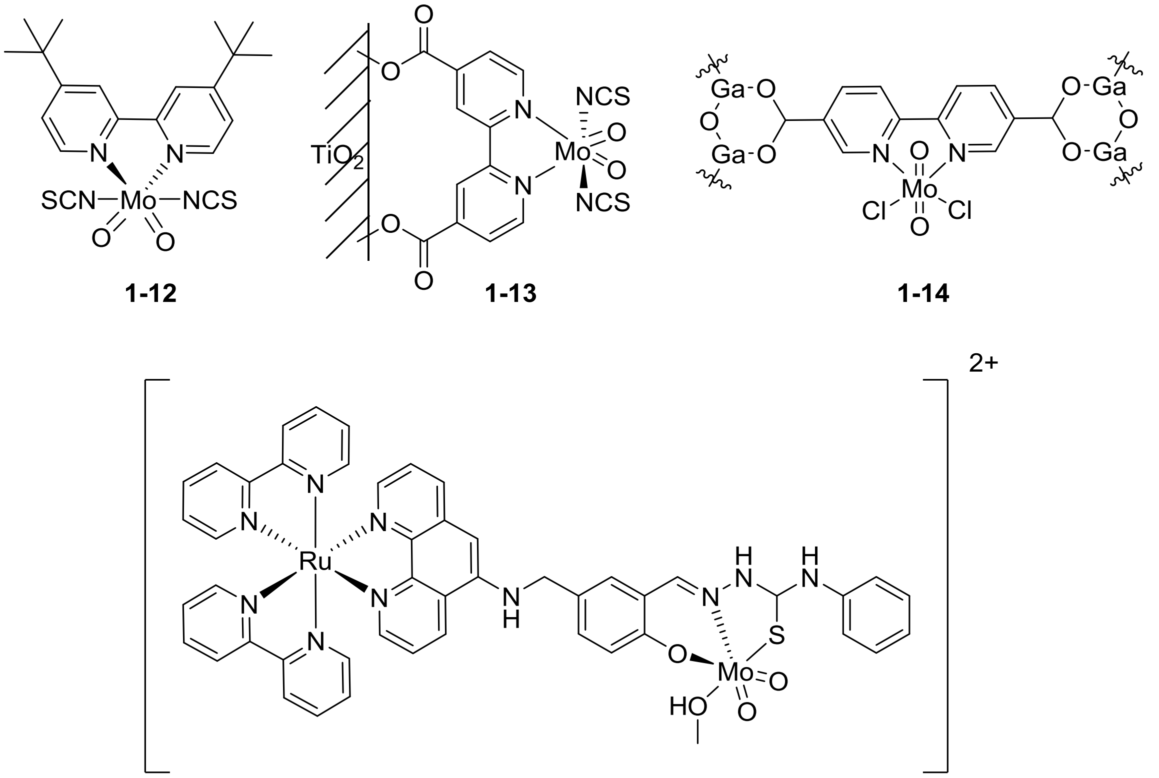

**1-12** **1-13** **1-14**

**1-15**

*Figure 1-15: Structures of four Mo complexes used in photoactivated OAT: a simple molybdenum complex[63], anchored to a semiconductor[64], anchored in a metal organic framework[65], as part of a dyad.[66]*

Complex **1-12** was used to oxidise arylalkanes (tetraline, ethyl benzene) to the corresponding ketones catalytically with DMSO under irradiation, but the underlying mechanism is not clear, possibly involving alkane radicals. In addition, yields and turnover numbers were very low which could suggest decomposition / deactivation of the catalyst.[63]

The Mo complex anchored to $TiO_2$ **1-13** has been used in photo-activated OAT from molecular oxygen to terpenes.[64] Here, absorbance of a photon by the titania leads to formation of an electron-hole-pair and electron flow away from the Mo centre. The use of titania made it necessary to perform the reaction in a cyclic manner do avoid formation of superoxide anion and hydroxyl radical species from photoactivated titania and oxygen. Oxidation of the substrates was done under nitrogen during irradiation, while regeneration of the catalyst was done under oxygen and in the absence of light.

Complex **1-14** consists of a gallium metal organic framework (MOF) where molybdenum is coordinated to a bipyridine linker.[65] This system performed OAT from oxygen to terpenes. Although the presence of molybdenum gave rise to an additional absorbance band in the UV-Vis spectrum and the light source used matched this region, contribution from the semiconducting MOF cannot be excluded as no mechanistic studies were performed. Plateauing of the reaction at 60 % conversion after 10 hours in a 18 h long experiment as well as a drop in activity to 40 % when the catalyst is recycled suggest deactivation.

The dyad **1-15** is conceptually similar to the $TiO_2$ system, the ruthenium moiety functions as the photoactive part with a molybdenum centre that performs OAT covalently linked to allow for electron flow.[66] With the help of the redox mediator methyl viologen, **1-15** transferred oxygen from DMSO to $PPh_3$. The disadvantage of this system is the multistep synthesis, partially under inert atmosphere, and the use of the precious metal ruthenium. The system also requires a redox mediator.

An example of a tungsten dioxo complex that performs photo-activated OAT is shown inFigure 1-6.

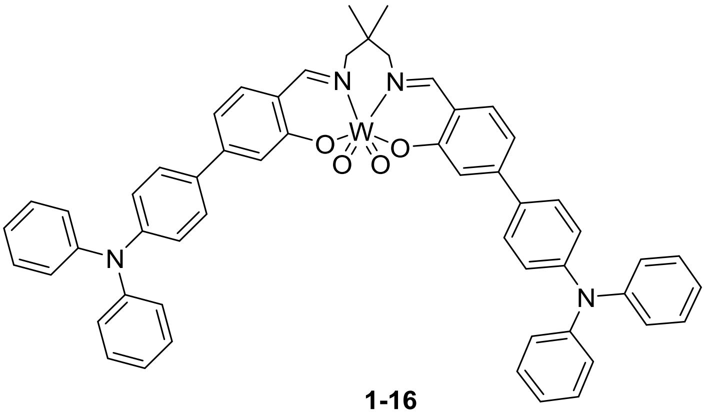

**1-16**

*Figure 1-16: Structure of a photo active tungsten dioxo complex.*[67]

Complex **1-16** has been used to catalyse the photo activated dehydrogenation of secondary alcohols and dienes in air (Scheme 1-7). The oxidation of alcohols only yielded 52 % and 16 % conversion after 12 hours whereas conversion of the dienes was quantitatively, benefitting from the additional driving force of generating an aromatic compound. The OAT in these reactions is more of a by-product as no oxygen is transferred to or from compounds under investigation. The reactions in Scheme 1-7 are thought to proceed via hydrogen atom abstraction by the tungsten complex resulting in formation of water and the reduced mono oxo complex which is regenerated by $O_2$. A mechanism where the complex acts as a photosensitizer generating reactive oxygen species is also possible. Similar to the dyad **1-15,** synthesis of **1-16,** particularly of the ligand, is more elaborate.[67]

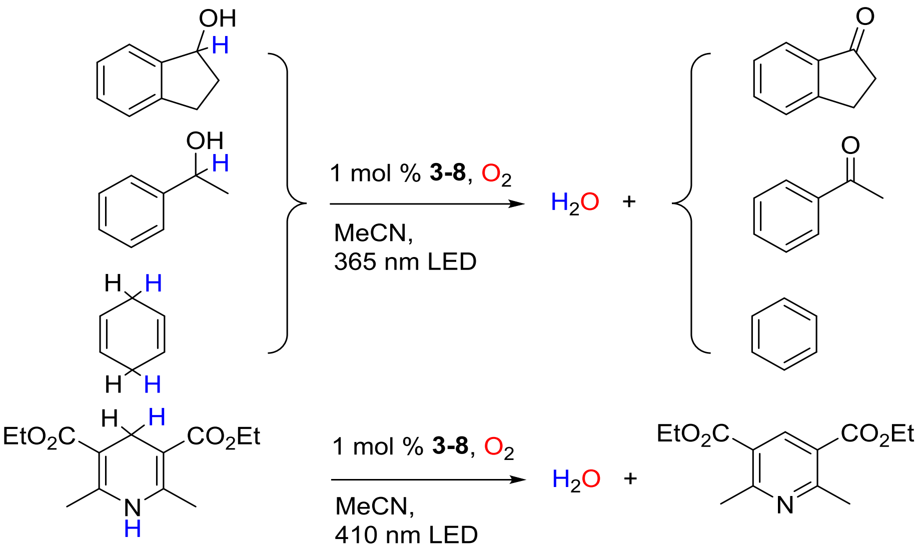

*Scheme 1-7: Dehydrogenations catalysed by **1-16**.*

## 1.5 Project aims

Taking inspiration from the molybdo- and tungsto-enzymes, this project aims to develop molybdenum and tungsten dioxo complexes that can perform oxygen atom transfer. The vast majority of the model systems reported in the literature thus far perform OAT under thermal conditions, in some cases requiring temperatures > 100 °C. It is therefore desirable to employ a different mechanism to activate OAT, the use of light. While photo-activated OAT systems are known, these are limited to a few examples and require more elaborate syntheses and expensive metals, their practical use is more complex, or they have poor performance.

Molybdenum and tungsten on the other hand are abundant metals, and the SAP (**s**alicylidene **a**mino **p**henol, 2-[(E)-(2-Hydroxybenzylidene)amino]phenol) system allows for easy synthesis making the complexes developed in this work more attractive.

Individual objectives of the project were:

- To investigate the potential of newly made complexes to act as photocatalysts in OAT using the model reaction between $PPh_3$ and DMSO
- To modify the SAP-based ligand to improve activity
- To study the substrate scope
- To investigate the underlying mechanism and differences between thermal and photoactivated OAT

# Chapter 2 Synthesis and Characterisation

## 2.1 Introduction

### 2.1.1 Schiff bases

A class of compounds often used as ligands are Schiff bases. They are obtained through the reaction of an aldehyde and an amine (see Scheme 2-1) and have been named after one of the first to study this type of reaction, Hugo Schiff.[68] Based on the choice of constituents, ligands of varying size and coordination number can be obtained. Bi- tri- and tetradentate ligands are commonly found where in addition to the imine nitrogen, further *N*-, *O*- or *S*-containing groups act as donors to the metal; some examples are shown below (Figure 2-1). Ligand denticity up to seven is rare but has been employed with various metals.[69]

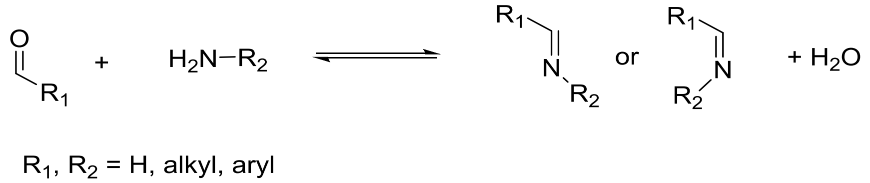

*Scheme 2-1: General scheme of the synthesis of a Schiff base through condensation between an amine and an aldehyde.*

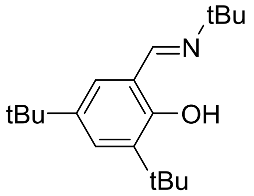

**2-1**

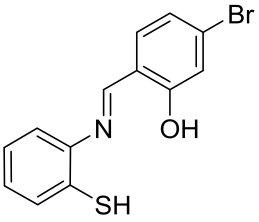

**2-2**

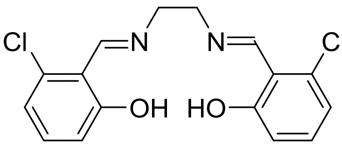

**2-3**

*Figure 2-1: Examples of Schiff bases with different denticity and coordinating groups.*[70–72]

Schiff bases have been studied extensively, as isolated or as ligands in metal complexes.
In biological systems, Schiff bases are found as intermediates in transamination[73] or light perception in humans[74] and have shown antibacterial, antifungal and antimalaria activity.[75] They are also used as chemical sensors to detect anions and metal cations.[76–78]

Complexation of various metals with Schiff bases has increased the interest in these ligands and the field of potential applications. Among the long list of reactions catalysed by Schiff base complexes are polymerisations, oxidations and coupling reactions.[79] Their biological properties include antibacterial, anti-tumour and anti-inflammatory activity.[80–82] The use of Schiff base complexes in light emitting diodes[83] or photovoltaic materials[84] has also been investigated.

Of importance for this thesis is the use of Schiff bases as easily made and modified ligands particularly as models for the active centre of enzymes. (see Chapter 1)

## 2.1.2 Choice of ligand backbone used in this work

In this work a Schiff base made from hydroxy benzaldehyde and hydroxy aniline was chosen as the core structure for a tridentate O,N,O-ligand (shown in Figure 2-2 alongside the molybdenum complex employing this ligand). The reasoning behind this choice of ligand is outlined below. Substituents were introduced to this structure, which is commonly referred to as **SAP**, from its trivial name **s**alicylidene **a**mino**p**henol, to modify the properties of the ligands and subsequently the complexes made thereof.

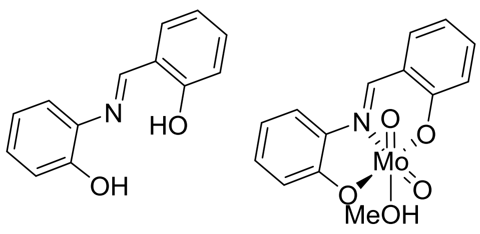

**L-1** **Mo-1**

*Figure 2-2: Structure of the SAP ligand **L-1** (left) and the molybdenum dioxo complex **Mo-1** based on this ligand (right).*

Initial studies had used disubstituted bipyridines as bidentate ligands and attempted to synthesise complexes of the form [$MoO_2(SCN)_2L$] (L = 2,2'-bipyridine, substituted in the 4 and 4' positions with COOH or COOMe). These complexes were however found to be unstable in solution yielding the free bipyridine ligand after a few hours.

The use of a ligand that provides a third binding site was expected to provide a stable complex. A tetradentate ligand clearly would have provided even more stability but would have meant that all six coordination sites were filled (four by the ligand and two for both oxo groups). With a tridentate ligand, the sixth coordination site is usually filled by a labile solvent molecule that could provide a binding site for the substrate during the OAT. Alternatively, introduction of a specific molecule in this site could provide a means to study the complex with a specific technique (spectroscopic handle) or allow to tune the properties of the complex further

The central part of the ligand was chosen to be an imine group which would serve as one of the coordinating groups. In addition, having this imine group allows to assemble the ligand from two separately synthesised parts (the amine and the aldehyde). This separation simplifies modification of the ligand as reactions on one part can be carried out without affecting the other. Separation also introduces a modularity to the ligand meaning that , for example, one amine can be combined easily with different aldehydes to produce various ligands when screening for optimal properties.

The two remaining coordinating groups were chosen to be oxygen donors. Nitrogen, oxygen and sulfur are all common donor atoms used to bind to molybdenum and all combinations of the three are employed.[85,86] Sulfur is predominant in enzymes[87] but studies would start with oxygen to facilitate synthesis, with the option to exchange one or two of them for sulfur on an optimised system later on.

The last point to be considered in the design of the ligand was the way the two oxygen donors would be connected to the imine group. The length of the linker between the three donors was chosen so that 5- or 6-membered rings would form in the complex for their greater stability.[88] These requirements can be fulfilled by having the amine and aldehyde (that form the imine) in the *ortho* position to two phenols groups. Two aromatic benzene rings connected by the imine group form a conjugated system where modification of electronic properties may be transferred across the ligand and onto the molybdenum centre.[89]

Additionally, aryl groups greatly improve stability of the Schiff base as purely aliphatic ones decompose or polymerise easily.[72]

### 2.1.3 Design of substituted ligands

With the backbone of the ligand established, further modifications were made. Substituents were introduced to modify certain properties of the ligand and their effect on OAT was then studied. Figure 2-3 shows the positions where substituents were introduced.

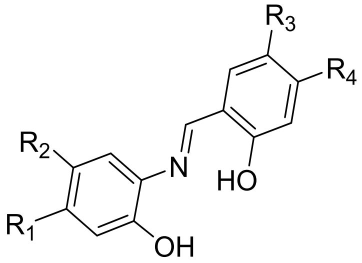

*Figure 2-3: Structure of the SAP ligand backbone with sites $R_1$-$R_4$ where substituents will be introduced.*

The main property to be modified is the electron density of the ligand which would influence the electron density of the metal centre. Electron donating or withdrawing groups were therefore introduced.

The imine group introduces a small asymmetry into the SAP ligand which makes the $R_1$/$R_4$ and $R_2$/$R_3$ positions inequivalent. A second distinction is made on each aromatic ring. Substituents $R_1$/$R_2$ are in the *para* position to the imine group and the *meta* position to the oxygen or *vice versa*. These positional aspects are interesting with regards to how the electronic effects are transferred onto the metal centre and the oxo ligands. Substituents $R_1$ to $R_4$ could have different effects depending on whether the electron flow is primarily conveyed through one of the phenol oxygens or the imine nitrogen.

An acidic proton was introduced to the ligand in the form of a carboxylic acid group to study its effect on OAT. Schiff bases containing acid groups are known but presence of an acidic proton could lead to increased hydrolysis of the imine bond under OAT conditions or interfere with OAT by binding to the (transferred) oxo ligand.

The optical properties of the ligand were modified in two ways. A substituent was introduced to shift absorption more into the visible region and increase the potential to use sunlight. The emissivity of the ligand was tuned through an amine substituent or the simultaneous substitution of an electron withdrawing and an electron donating group.

## 2.2 Synthesis and characterisation of SAP-based ligands

The ligands were obtained through condensation reactions between suitable hydroxy benzaldehydes and amino phenols. Most of these precursors were commercially available, with the exception of the hydroxy-formyl benzoic acid methyl ester (**2**)[90,91] and the hydroxy-amine benzoic acid methyl esters (**3, 4)** which were synthesised following reported procedures.[92]

Schiff base formation from amine and aldehyde precursors was carried out as shown for **L-1** in Scheme 2-2, adapting a reported procedure.[93] The Schiff base ligands were obtained in good yields (70 to 90 %). The structures of all ligands made in this work are shown in Table 2-1.

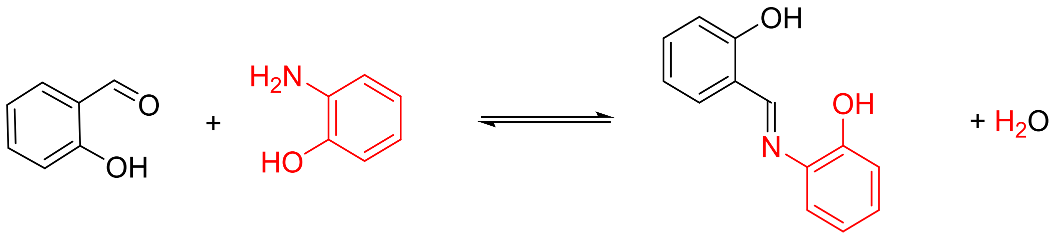

**2-4** **2-5** **L-1**

*Scheme 2-2: Synthesis of **L-1** from the aldehyde (black) and amine (red) components. Conditions: EtOH , reflux, 6 h. The origin of the two phenol rings in the ligand - from the aldehyde or amine component - is evident and will be used to reference substituent position: aldehyde ring (black) and amine ring (red).*

*Table 2-1: Structure of the SAP-based ligands studied in this work.*

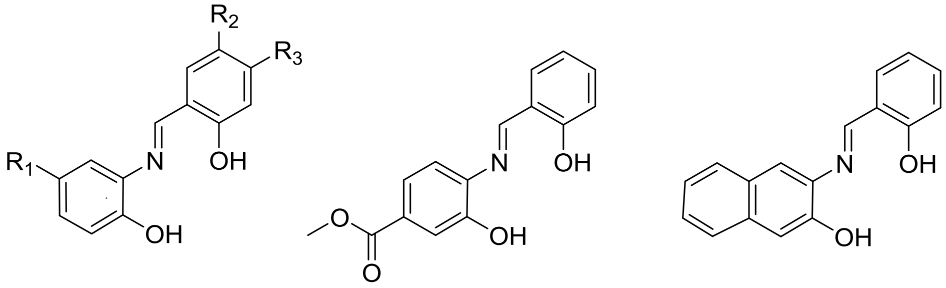

**L-11$^{COOMe,H}$**

**L-16$^{naph}$**

| R$_1$ | R$_2$ | R$_3$ | # |
|---|---|---|---|
| H | H | H | L-1$^{H,H}$ |
| COOMe | COOMe | H | L-2$^{COOMe,COOMe}$ |
| COOH | COOH | H | L-3$^{COOH,COOH}$ |
| COOMe | H | NEt$_2$ | L-4$^{COOMe,H}$ |
| COOMe | COOH | H | L-5$^{COOMe,COOH}$ |
| COOH | COOMe | H | L-6$^{COOH,COOMe}$ |
| COOH | H | H | L-7$^{COOH,H}$ |

| R$_1$ | R$_2$ | R$_3$ | # |
|---|---|---|---|
| H | COOH | H | L-8$^{H,COOH}$ |
| COOMe | H | H | L-9$^{COOMe,H}$ |
| H | COOMe | H | L-10$^{H,COOMe}$ |
| NO$_2$ | H | H | L-12$^{NO2,H}$ |
| CF$_3$ | H | H | L-13$^{CF3,H}$ |
| SO$_2$NH$_2$ | H | H | L-14$^{SO2NH2,H}$ |
| H | H | NEt$_2$ | L-15$^{H,Et2N}$ |

The identity and purity of the ligands were confirmed by $^1$H and $^{13}$C NMR spectroscopy, FTIR spectroscopy, elemental analysis and mass spectrometry. Characteristic bands in the IR spectra of the ligands are the imine group stretching bands around 1590 to 1620 cm$^{-1}$ in all ligands and carbonyl group stretching bands around 1670 to 1720 cm$^{-1}$ in ligands **L-2** to **L-11**.

A typical $^1$H NMR spectrum, of **L-1**, recorded in DMSO-d$_6$, is shown below (Figure 2-5). The main characteristic resonance in the NMR spectrum is the resonance of the imine proton (-C*H*=N-) appearing as a singlet at 8.96 ppm (between 8.63 and 9.24 ppm for the different ligands). The spectrum also shows two resonances at 13.76 and 9.71 ppm attributed to the OH groups. Due to hydrogen bonding as depicted in Figure 2-4 the phenol proton of the aldehyde ring is shifted further downfield; involvement of the second OH group in hydrogen bonding is not observed.[94]

The characterisation data of **L-1** is consistent with reported data.[95,96] Characterisation data of all ligands can be found in the experimentals section.

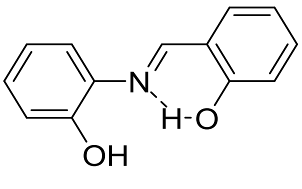

*Figure 2-4: Structure of **L-1** with H-bonding.*

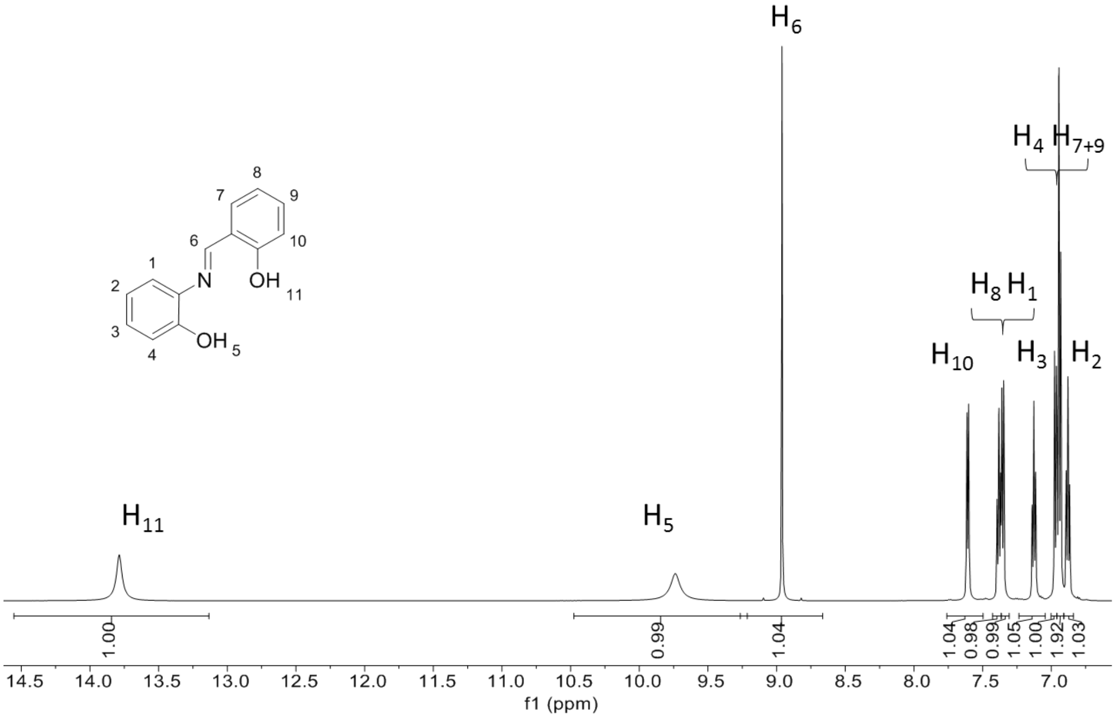

*Figure 2-5: $^1$H NMR spectrum of **L-1** in DMSO-$d_6$.*

## 2.3 Synthesis of dioxo complexes and characterisation

### 2.3.1 Synthesis of molybdenum and tungsten complexes

The SAP-based molybdenum complexes were synthesised through ligand exchange on the complex [$MoO_2(acac)_2$], **5**, (acac = acetylacetonate) which was obtained from the sodium molybdate salt ($Na_2MoO_4$) and acetylacetone adapting a reported procedure.[97] Formation of the precursor and **SAP**-based complexes is depicted in Scheme 2-3.

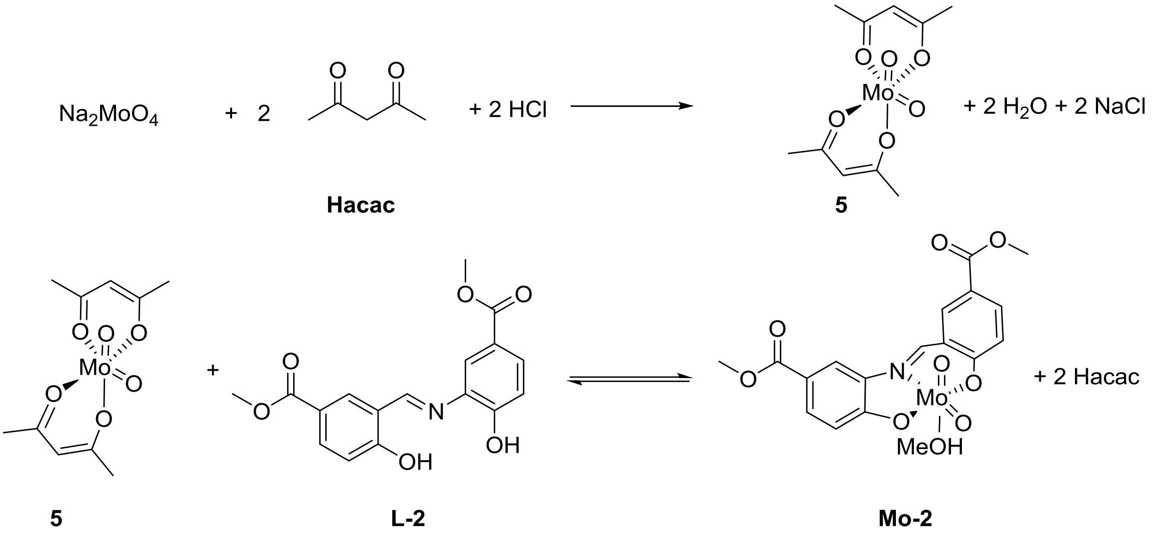

*Scheme 2-3: Synthesis of **5** and **Mo-2** as a model for the general procedure. Reaction conditions: a) 1 h in the dark, b) MeOH, 4 h RT.*

Synthesis of tungsten complexes was attempted following the protocol established for molybdenum by using sodium tungstate instead of sodium molybdate. [$WO_2(acac)_2$], however, could not be isolated and an alternative route was chosen instead, in which the ligand was directly reacted with the sodium tungstate (Scheme 2-4).

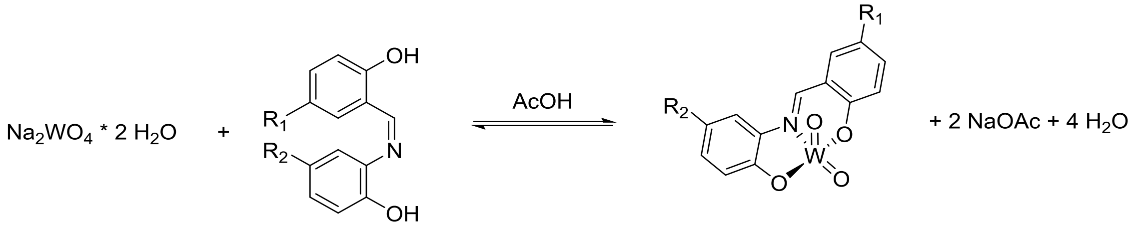

*Scheme 2-4: Synthesis of the tungsten complexes. Conditions: in boiling MeOH, 20 h.*

Formation of the molybdenum and tungsten complexes was confirmed by $^1H$ and $^{13}C$ NMR spectroscopy, mass spectrometry, elemental analysis and FTIR spectroscopy. Characterisation data can be found in the experimentals section. A more detailed discussion of $^1H$ NMR and FTIR spectroscopic data and crystal structures can be found in sections 2.3.2, 2.3.2 and 2.3.4 respectively.

All molybdenum complexes are shown in Figure 2-6 with their structures depicted as suggested by analytical data and discussed in section 2.3.5, and the two tungsten complexes are shown in

Figure 2-7. (Note: An overview of the structures of all synthesised complexes and the substrates used later in this project can be found in the appendix).

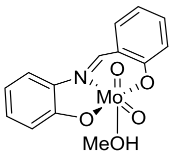

**Mo-1$^{H,H}$**

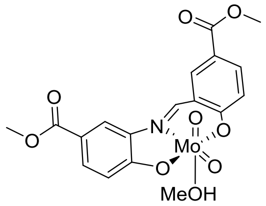

**Mo-2$^{COOMe,COOMe}$**

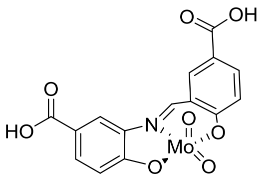

**Mo-3$^{COOH,COOH}$**

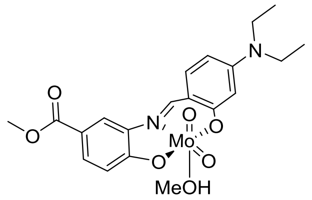

**Mo-4$^{COOMe,NEt2}$**

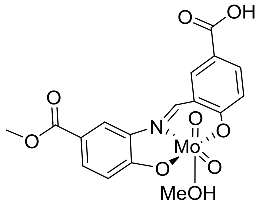

**Mo-5$^{COOMe,COOH}$**

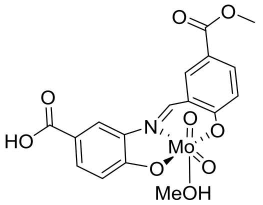

**Mo-6$^{COOH,COOMe}$**

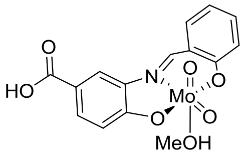

**Mo-7$^{COOH}$**

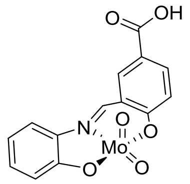

**Mo-8$^{H,COOH}$**

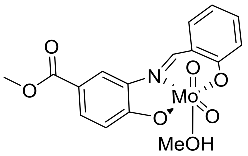

**Mo-9$^{COOMe}$**

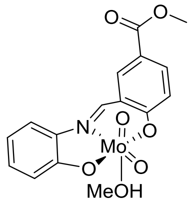

**Mo-10$^{H,COOMe}$**

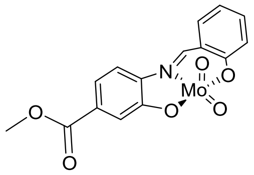

**Mo-11$^{COOMe}$**

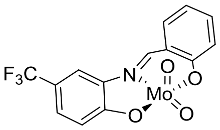

**Mo-12$^{CF3}$**

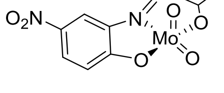

**Mo-13$^{NO2}$**

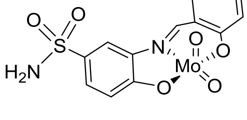

**Mo-14$^{SO2NH2}$**

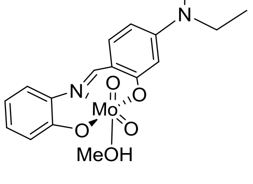

**Mo-15$^{H,NEt2}$**

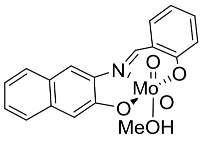

**Mo-16$^{Naph}$**

*Figure 2-6: Structure of the complexes synthesised in this project. Structures for **Mo-3, Mo-8, Mo-12, Mo-13, Mo-14** have been simplified for clarity.*

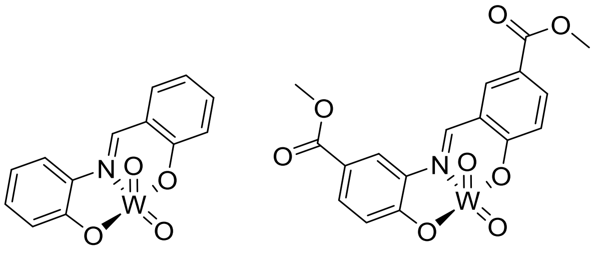

**W-1** **W-2**

*Figure 2-7: Structure of the tungsten complexes **W-1** and **W-2**.*

Complexes are mostly yellow/orange in colour except for **Mo-3, Mo-8, Mo-12, Mo-13, Mo-14, W-1** and **W-2** which are brown. Solubility of molybdenum complexes is high in DMSO and DMF, moderate in MeOH and acetone (up to 8 mM) and low in MeCN (up to 0.8 mM). Solubility of **W-1** and **W-2** is low, only in strongly coordinating solvents like DMSO and DMF are they appreciably soluble. Dissolution is also slower compared to **Mo-1** and **Mo-2**.

The molybdenum complexes are stable in air in their solid form although loss of bound solvent over time has been observed.[98] They can be dried *in vacuo,* but equally lose the bound solvent above 140 °C and decompose above 300 °C. **W-1** and **W-2** are stable in air, and no change was observed upon heating up to 350 °C.

Figure 2-6 depicts the structures that include MeOH for most of the molybdenum complexes. In these cases, the structures shown are evidenced by characterisation data. In contrast to their Mo counterparts, the **W-1** and **W-2** do not contain MeOH as evidenced by its absence in $^1$H NMR spectra and in the crystal structure of **W-1**. For complexes that do not contain MeOH, the solid state structure is more complex (consisting of Mo-dimers or oligomers, as discussed later (section 2.3.5).

Mass spectra (LIFDI) of all complexes showed the presence of molybdenum or tungsten, respectively, by their isotope patterns as shown in Figure 2-8 for **Mo-1** and **W-1**. The most intense peaks m/z in all complexes matched the formula $^{98}MoO_2L$ and $^{184}WO_2L$, respectively. Any solvent incorporated into the complex would have been lost under analysis conditions. Higher masses were not detected.

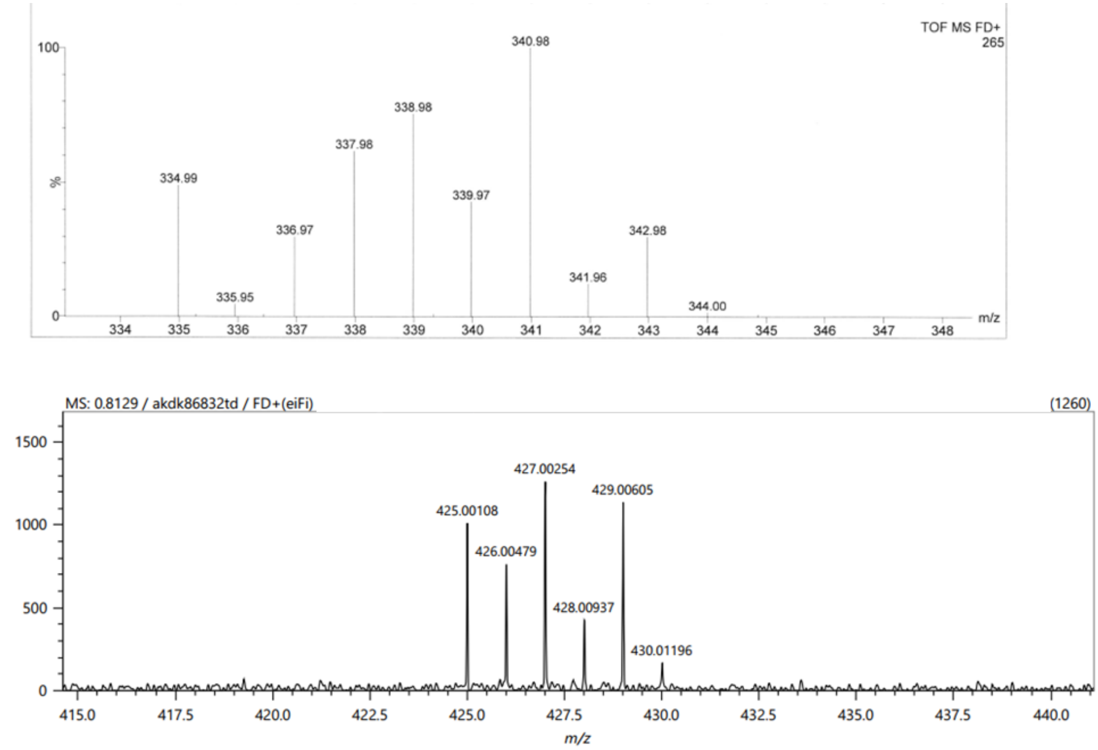

*Figure 2-8: LIFDI-MS spectrum of* ***Mo-1,*** *(top) and* ***W-1****(bottom) showing Mo and W isotope patterns.*

## 2.3.2 Crystal structure of Mo-2$^{COOMe,COOMe}$, Mo-7$^{COOH,H}$ and W-1$^{H,H}$ and comparison to literature data

Single crystals of **Mo-2** (yellow needles) suitable for structural analysis were obtained from recrystallisation from a hot, concentrated solution of the compound in MeOH. The compound crystallised in the monoclinic system, space group P2$_{1/c}$. Single crystals of **Mo-7** (yellow needles) suitable for structural analysis were obtained through slow evaporation of a concentrated solution of the compound in THF. **Mo-7** crystallised in the triclinic system, space group P-1. Single crystals of **W-1** were obtained from recrystallisation from a hot, concentrated solution of the compound in DMSO. The compound crystallised in the monoclinic system, space group P2$_{1/c}$ Crystal data are listed in Table 2-2, selected bond lengths and angles in Table 2-3; ORTEP plots of **Mo-2**, **Mo-7** and **W-1** together with literature examples are shown in Figure 2-9, Figure 2-10, Figure 2-11, Figure 2-13 and Figure 2-14.

The ligand in **Mo-2** was disordered and therefore modelled with refined occupancies in two positions (0.857 : 0.143). Bond lengths and angles are listed for the major species. In addition, constraints and restraints on pairs of atoms were employed (see appendix).

In **Mo-7**, highly disordered THF was modelled using a solvent mask and the carboxylic acid proton located by difference map (see appendix).

**W-1** was disordered, and tungsten, the imine bridge, the phenoxy oxygens and DMSO were modelled with refined occupancies in two positions (0.541 : 0.459; see appendix).

*Table 2-2: Crystal data for* ***Mo-2*** *,* ***Mo-7*** *and* ***W-1*** *.*

| | **Mo-2**$^{COOMe,COOMe}$ | **Mo-7**$^{COOH,H}$ | **W-1**$^{\mathbf{H},H}$ |
|---|---|---|---|
| Empirical formula | $C_{18}H_{17}MoNO_9$ | $C_{20}H_{21}MoNO_7$ | $C_{17}H_{21}NO_6S_2W$ |
| Formula weight | 487.27 | 491.32 | 583.32 |
| Temperature / K | 110.00(10) | 110.00 (14) | 109.9 (4) |
| Crystal system | Monoclinic | Triclinic | Monoclinic |
| Space group | $P2_1/c$ | P-1 | $P2_1/c$ |
| a/Å | 6.8609(2) | 6.7460 (4) | 12.48131 (15) |
| b/Å | 31.9207(9) | 12.9235 (11) | 6.72402 (8) |
| c/Å | 8.6525(3) | 13.1613 (11) | 23.5573(3) |
| α/° | 90 | 61.601 (9) | 90 |
| β/° | 97.813(3) | 87.263 (6) | 94.1359(11) |
| γ/° | 90 | 80.349 (6) | 90 |
| Volume/Å$^3$ | 1877.36(11) | 994.39 (15) | 1971.89 (4) |
| Z | 4 | 2 | 4 |
| $\rho_{calc}$ / g/cm$^3$ | 1.724 | 1.641 | 1.965 |
| μ/mm$^{-1}$ | 6.208 | 5.806 | 13.141 |
| F(000) | 984.0 | 500 | 1136.0 |
| Crystal size/mm$^3$ | 0.31 × 0.088 × 0.047 | 0.173 x 0.03 x 0.01 | 0.24 x 0.16 x 0.13 |
| Radiation | Cu Kα (λ = 1.54184) | CuKα (λ = 1.54184) | CuKα (λ = 1.54184) |
| 2Θ range for data collection/° | 10.686 to 134.16 | 7.642 to 134.156 | 7.1 to 134.156 |
| Index ranges | -8 ≤ h ≤ 8, -34 ≤ k ≤ 38, -10 ≤ l ≤ 10 | -8 ≤ h ≤ 7, -15 ≤ k ≤ 14, -14 ≤ l ≤ 15 | -14 ≤ h ≤ 14, -8 ≤ k ≤ 7, -28 ≤ l ≤20 |
| Reflections collected | 12024 | 6214 | 12136 |
| Independent reflections | 3349 [$R_{int}$ = 0.0489, $R_{sigma}$ = 0.0429] | 3537 [$R_{int}$ = 0.0423, $R_{sigma}$ = 0.0597] | 3503 [$R_{int}$ = 0.0233, $R_{sigma}$ = 0.0219] |
| Data/restraints/parameters | 3349/5/298 | 3537/0/245 | 2502/24/285 |
| Goodness-of-fit on F$^2$ | 1.092 | 1.019 | 1.105 |
| Final R indexes [I>=2σ (I)] | $R_1$ = 0.0339, w$R_2$ = 0.0850 | $R_1$ = 0.0345, w$R_2$ = 0.0834 | $R_1$ = 0.0246, w$R_2$ = 0.0529 |
| Final R indexes [all data] | $R_1$ = 0.0398, w$R_2$ = 0.0888 | $R_1$ = 0.0394, w$R_2$ = 0.0870 | $R_1$ = 0.0265, w$R_2$ = 0.0538 |
| Largest diff. peak/hole / e Å$^{-3}$ | 0.52/-0.82 | 0.61/-0.81 | 0.89/-0.87 |

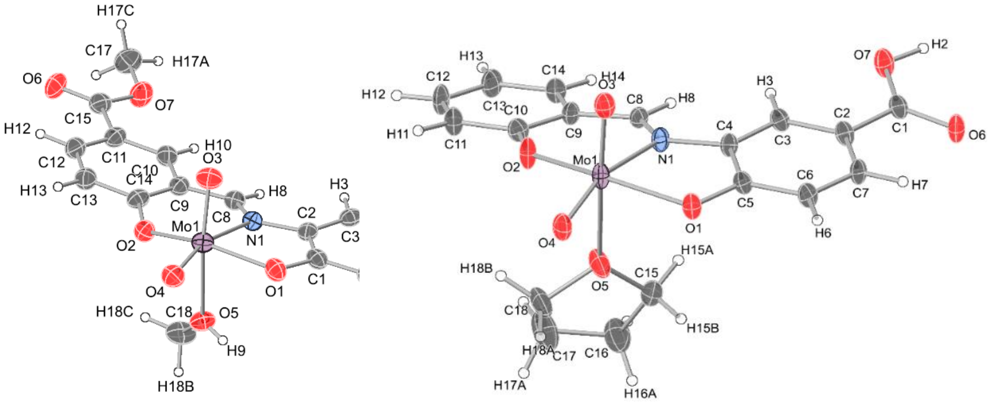

*Figure 2-9: ORTEP plots (50 % probability) of the crystal structures of **Mo-2** (OC-6-24-C, left) and **Mo-7-THF** (OC-6-24-C, right).*

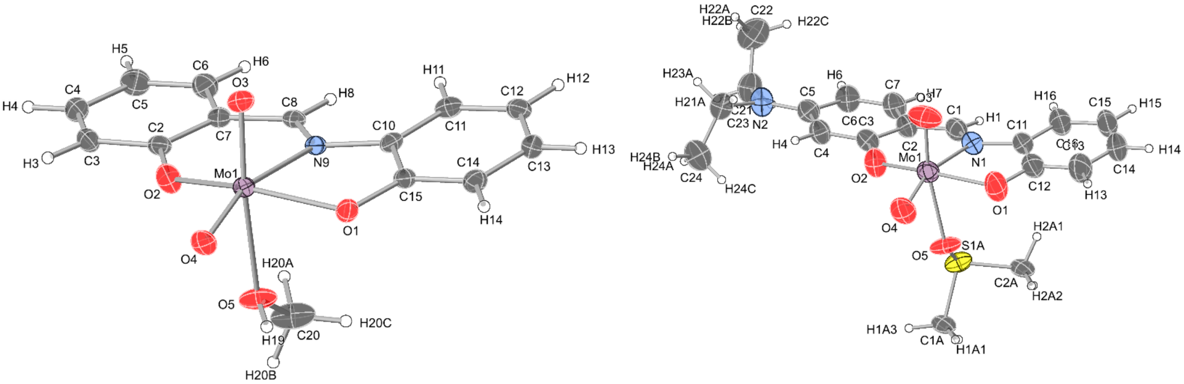

*Figure 2-10: ORTEP plots (50 % probability) of the literature crystal structures of **Mo-1** (OC-6-24-C, top) [99] and **Mo-15-DMSO** (OC-6-43-A, bottom). [100]*

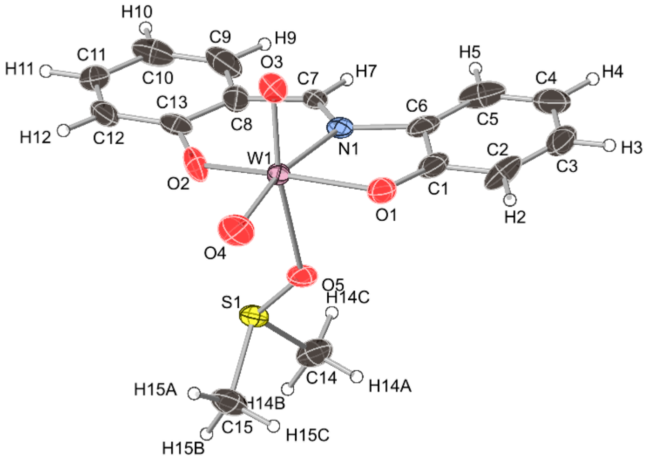

*Figure 2-11: ORTEP plot (50 % probability) of the crystal structure of **W-1-DMSO** (OC-6-43-A).*

Table 2-3: Selected bond angles and distance in **Mo-2**, **Mo-7** and **W-1** (this work) and **Mo-1** and **Mo-15** (taken from literature).[99,100]

| | **Mo-2**$^{COOMe,COOMe}$ | **Mo-7**$^{COOH}$ | **Mo-1**$^{H,H}$ (99) | **Mo-1**$^{H,H}$ (100) | **Mo-15**$^{H,NEt2}$ (100) | **W- 1**$^{H,H}$ |
|---|---|---|---|---|---|---|
| Formula | **[MoO$_2$(L-2)(MeOH)]** | **[MoO$_2$(L-7)(THF)]** | **[MoO$_2$(L-1)(MeOH)]** | **[MoO$_2$(L-1)(DMSO)]** | **[MoO$_2$(L-15)(DMSO)]** | **[WO$_2$(L-1)(DMSO)]** |
| **Bond distance / Å** | | | | | | |
| M-O1 | 1.966(2) | 1.982 (2) | 1.995 (2) | 1.943 (4) | 1.973 (3) | 1.938(8) |
| M-O2 | 1.938(3) | 1.942 (2) | 1.924 (3) | 1.929 (4) | 1.927 (3) | 1.987 (14) |
| M=O3 (axial) | 1.695(2) | 1.691 (2) | 1.699 (2) | 1.686 (3) | 1.688 (4) | 1.69 (4) |
| M=O4 (eq) | 1.705(2) | 1.702 (2) | 1.712 (2) | 1.697 (4) | 1.698 (3) | 1.711 (4) |
| M-O5 (solvent) | 2.309(2) | 2.344 (3) | 2.322 (3) | 2.267 (7) | 2.234 (3) | 2.228 (6) |
| M-N | 2.322(4) | 2.266 (3) | 2.280 (2) | 2.2813 (8) | 2.265 (3) | 2.288 (7) |
| **Bond angle / °** | | | | | | |
| O3=M=O4 | 105.67 (12) | 104.65 (12) | 105.24 (8) | 104.84 (18) | 105.20 (17) | 105.9 (3) |
| O1-M-N | 73.07 (10) | 74.77 (9) | 74.06 (7) | 70.4 (2) | 74.7 (4) | 75.2 (3) |
| O2-M-N | 81.06 (12) | 81.88 (10) | 81.95 (7) | 86.7 (2) | 82.22 (11) | 79.9 (4) |
| O1-M-O2 | 147.54 (12) | 152.61 (10) | 150.34 (8) | 152.0 (2) | 152.78 (16) | 151.2 (4) |
| N-M-O5 | 78.4 (5) | 77.30 (10) | 82.95 (6) | 78.5 (3) | 74.51 (12) | 78.1 (2) |
| O3=M-O2 | 97.66 (12) | 97.11 (10) | 99.99 (8) | 98.08 (18) | 101.86 (13) | 96.9 (4) |
| O1-M-O5 | 77.68 (10) | 82.24 (9) | 80.23 (7) | 71.1 (2) | 71.8 (4) | 78.1 (2) |
| O3=M-O5 | 165.59 (11) | 170.75 (10) | 173,19 (7) | 165.8 (2) | 169.1 (5) | 167.3 (2) |
| O3=M-N | 89.07 (12) | 94.01 (11) | 90.27 (7) | 89.7 (3) | 92.86 (15) | 89.3 (2) |
| O4=M-N | 163.66 (11) | 160.67 (11) | 162.55 (8) | 163.8 (3) | 160.63 (15) | 164.8 (2) |

Standard deviation in parentheses. Data given for the enantiomer shown in figures above.

The crystal structures of **Mo-2** and **Mo-7** shows the ligand coordinating meridionally as a dianion. The two dioxo groups and a solvent molecule complete the remaining coordination sites resulting in a distorted octahedral geometry with the metal outside the plane formed by the ONO-ligand and the equatorial oxo group. Bond angles around the metal deviate from the octahedral angle of 90 ° for atoms mutually *cis, e.g.* the angle between the two oxo ligands is around 105 °, or 180 ° for atoms mutually *trans, e.g.* the angle between phenolic oxygens is between 147 and 153 °. The Schiff base ligand itself is not planar, the aromatic rings form an angle of 6.2 ° (**Mo-2** ) and 14.4 °

(**Mo-7**) which is common in these complexes (*e.g.* 6.7 ° in **Mo-1**) .[101–105] The ligand alone e.g. **L-1** when not restricted through binding to a metal centre is also not planar, the aromatic rings form an angle of 10.8 °.[106] The **SAP** ligand system was initially chosen with the idea that a conjugated system (the two aromatic rings together with the imine group) would be beneficial for stability and mediating redox chemistry. The difference in nonplanarity of the ligand between **Mo-2** and **Mo-7** is likely a result of the different packing in the solid state. In solution the arrangement of the aromatic rings is less restrained and there may be no difference between **Mo-2** and **Mo-7** and the aromatic rings could be planar.

In **Mo-2** and **Mo-7** the two oxo ligands are mutually cis , forming an angle of around 105 ° which is in line with reports in the literature for **Mo-1** and **Mo-15** as well as similar complexes with the **SAP** backbone. The lengths of the metal-oxo bonds are also similar between all.[99–105]

The crystal unit cell contains a racemic mixture of the complex, one molecule per asymmetric unit which generates the second enantiomer through an inversion centre (**Mo-2**, **Mo-7**) or glide plane (**Mo-2**).

Intermolecular hydrogen bonds are observed between the ester group on the former aldehyde ring and MeOH in **Mo-2**, and between acid groups in **Mo-7** (Figure 2-12). Formation of these pseudo dimers may contribute to the observed behaviour upon heating: complexes lose the bound solvent above 140 °C and start to decompose above 300 °C, but do not melt. In the absence of suitable substituents, hydrogen bonds can still form between bound solvent and a phenol oxygen as in **Mo-1**.[99]

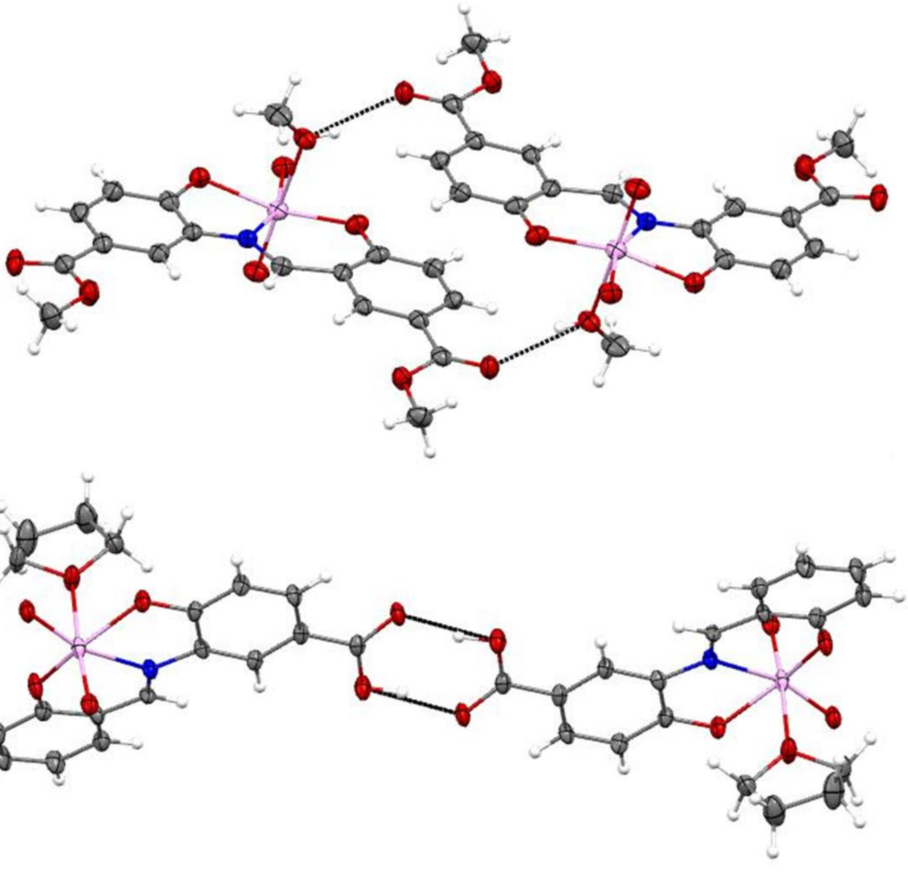

*Figure 2-12: ORTEP plots (50 % probability) of the crystal structures of **Mo-2** (top) and **Mo-7-THF** (bottom) showing intermolecular hydrogen bonding.*

In addition to hydrogen bonding, π-interactions are also observed. The crystal structure of **Mo-7** shows π- π interactions with the aromatic rings offset and a C-C distance of 3.343 Å whereas in **Mo-2** the aromatic rings involved are offset and also angled at a 30 ° with a C-C distance of 3.248 Å.

The crystal structure of **W-1** is practically identical to the molybdenum complexes, a distorted octahedral geometry with a meridionally coordinated SAP ligand, two cis-dioxo groups and one solvent molecule around the metal centre. Bond lengths and angles are within the range seen for SAP based molybdenum complexes, the only difference being the phenoxy-tungsten distances with tungsten closer to the oxygen on the aldehyde ring (O2) than molybdenum. Hydrogen bonding or π-interactions are not observed.

Only three more crystal structures of tungsten complexes based on the SAP ligand are known[107], shown in

Figure 2-13 and Figure 2-14. In **[WO($O_2$)L-1-HMPA]** the equatorial dioxo ligand is replaced by $O_2^{2-}$ leading to the two phenoxy and other oxo ligands moving away from the metal (distances of 1.972(79), 1.9825(8) and 1.6897(84) Å, respectively, in **[WO($O_2$)L-1-HMPA]** compared to 1.929(65), 1.9308(73) and 1.7033(67) Å in **W-1-HMPA**) while the nitrogen and solvent oxygen move closer (distances of 2.2114(115) and 2.1386(67) Å in **[WO($O_2$)L-1-HMPA]** compared to 2.2627(88) and 2.1748(108) Å in **W-1-HMPA**). The bond lengths and bond angles of **W-1** (Table 2-3) fit within the range observed in these literature examples while being closest to those of **W-1-HMPA** which only differs in the bond solvent.

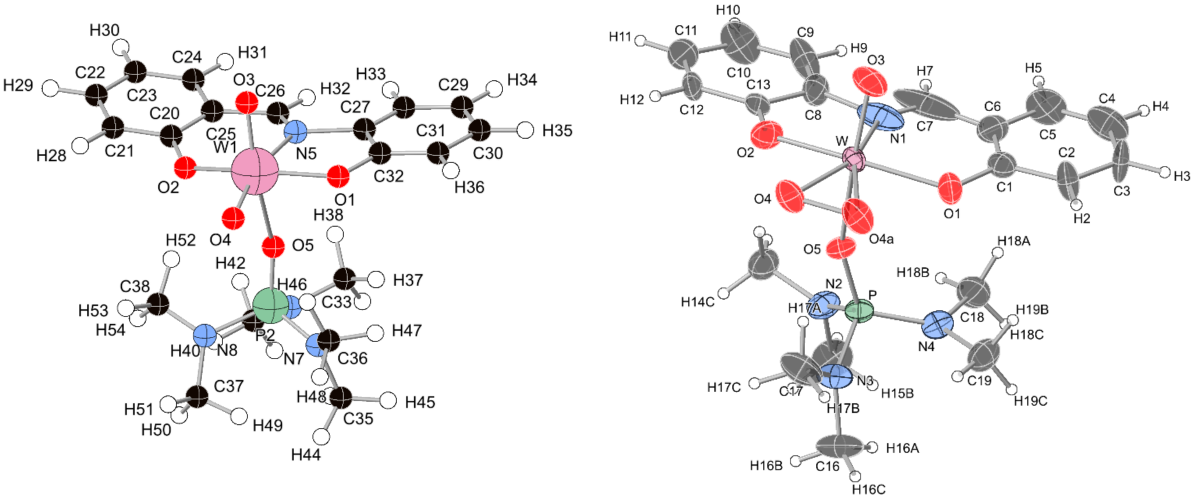

*Figure 2-13: Ball and stick representation of the crystal structure of **[W-1-HMPA]** (left, a thermal ellipsoid model was not available)* [108]*, ORTEP plot (50 % probability) of the crystal structure of **[WO($O_2$)L-1-HMPA]** (right).*[109] *Data taken from the literature.*

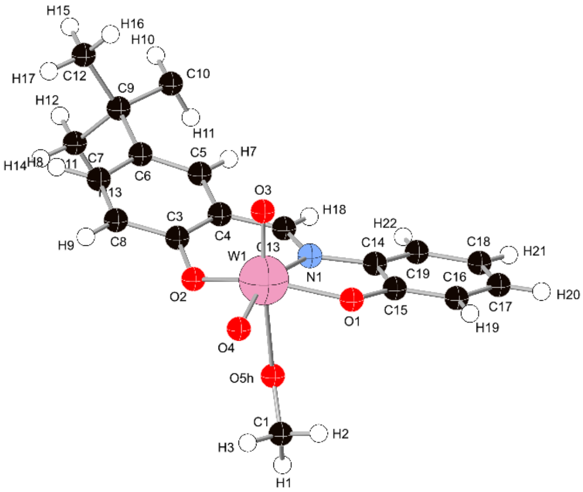

*Figure 2-14: Ball and stick representation of the crystal structure of* ***[WO$_2$L-MeOH]*** *$^{110}$, L representing a SAP ligand bearing the t-Bu group in the para position on the aldehyde ring. A thermal ellipsoid model was not available. Data taken from the literature.*

Crystal structures obtained for **Mo-2**, **Mo-7** and **W-1** confirm the octahedral structure and the binding of the SAP-based ligand and two oxo ligands. The sixth coordination site is occupied by a solvent molecule. The characteristic bond lengths and angles around the metal centre are within the range of previously reported values. A clear distinction has to be made though between the structures of complexes in the solid state discussed in this sub-chapter and their structure in solution during oxygen atom transfer experiments. Analysis of the dissolved complexes by $^1$H NMR spectroscopy is discussed in the following section.

### 2.3.3 $^1$H NMR spectroscopic analysis of the molybdenum and tungsten complexes

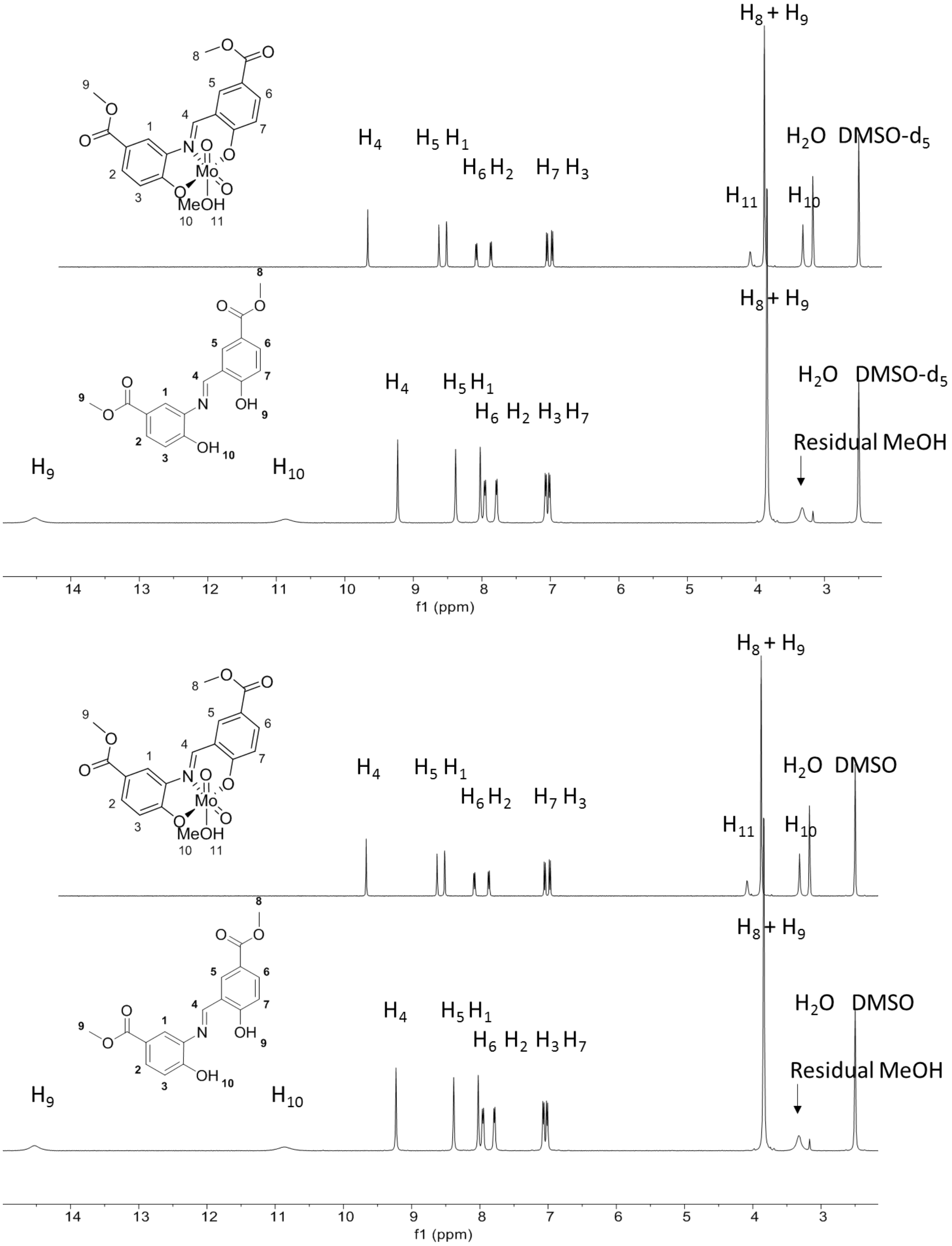

*Figure 2-16: $^{1H}$ NMR spectra of* **L-2** *(bottom) and* ***Mo-2*** *(top) in DMSO-d6.*

Figure 2-16 shows the $^1$H NMR spectra of **L-2** and **Mo-2** in DMSO-$d_6$. The changes upon complexation are evident. First, the two resonances at 11 and 14.8 ppm attributed to the OH groups of the ligand, disappear upon complexation as expected. Secondly, the resonance at 9.23

ppm of the imine proton shifts to 9.66 ppm. As the nitrogen coordinates, electron density of the imine group is transferred to the molybdenum resulting in deshielding of the proton. Thirdly, similar to the imine proton, the aromatic protons shift downfield to varying degrees; the most pronounced shift is observed for H1 and H5 (from 8.03 and 8.38 ppm to 8.51 and 8.62 ppm) probably due to the closer proximity of these atoms to the imine group which after complexation pulls electron density from neighbouring atoms. The resonances of H6 and H2 shift to a lesser extent (from 7.78 and 7.94 to 7.87 and 8.08 ppm), that of H7 only by a small amount and that of H3 similar to H6 and H2 but upfield (from 7.00 and 7.06 to 7.05 and 6.97 ppm). Interestingly, the difference in chemical shift between two resonances of similar protons (e.g. H1 and H5) also decreases upon complexation suggesting that the aromatic rings are affected unequally by the complexation which, as well as the upfield shift of H3, could be a consequence of the intramolecular hydrogen bonds present in the ligand (cf. Figure 2-4 )

The two resonances at 3.16 and 4.13 ppm result from MeOH. Signals of MeOH (solvent during synthesis) were also observed in some of the $^1$H NMR spectra of other complexes; all compounds were dried under reduced pressure prior to characterisation. Integration of the resonances at 3.16 and 4.13 ppm from MeOH and of the imine proton at 9.6 ppm (Figure 2-15) gives values of 3, 4 and 1, respectively, showing that equal amounts of ligand and MeOH are present. It can therefore be assumed that MeOH was incorporated into these complexes, occupying the sixth coordination site (besides the two oxo groups and the tridentate ligand). The incorporation of MeOH or other donor molecules in similar complexes has been reported.[99,111]

When an additional drop of MeOH was added to a sample of **Mo-2** the signals of MeOH increased in intensity but no additional peaks were observed suggesting that the MeOH incorporated into the complex exchanges with the solvent upon dissolution (here DMSO-$d_6$) as the latter is in vast excess and stronger binding. This exchange ensures that NMR characterisation and experiments in solution are not affected by the variation in MeOH content.

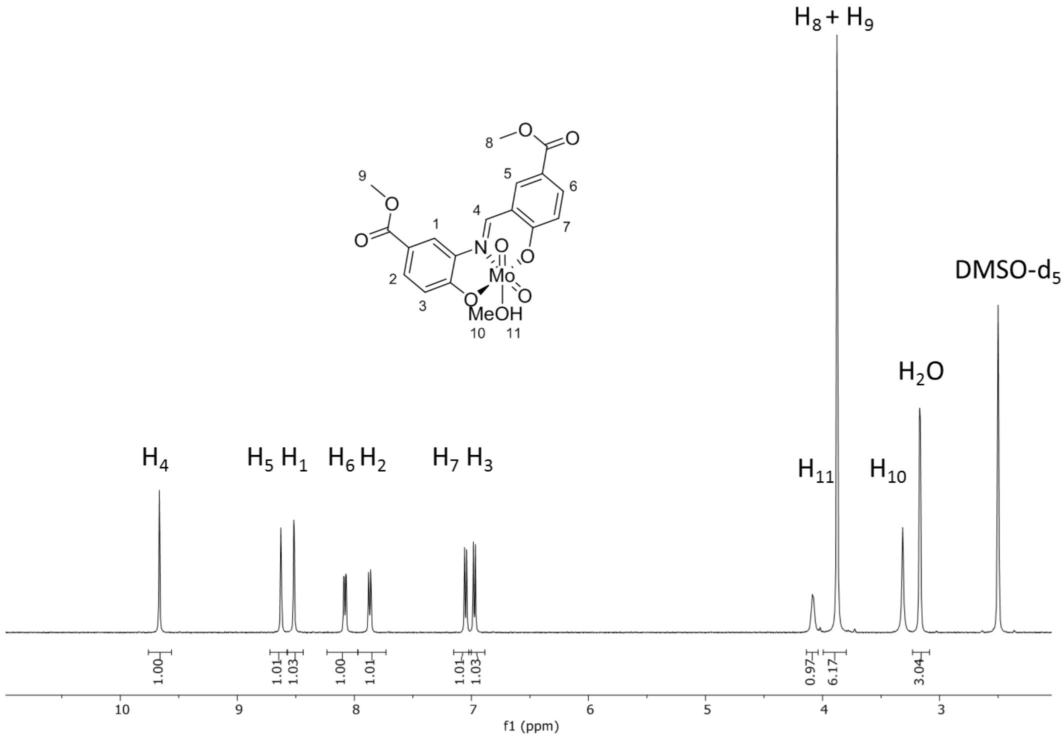

*Figure 2-15: $^1H$ NMR spectrum of **Mo-2** in DMSO-$d_6$.*

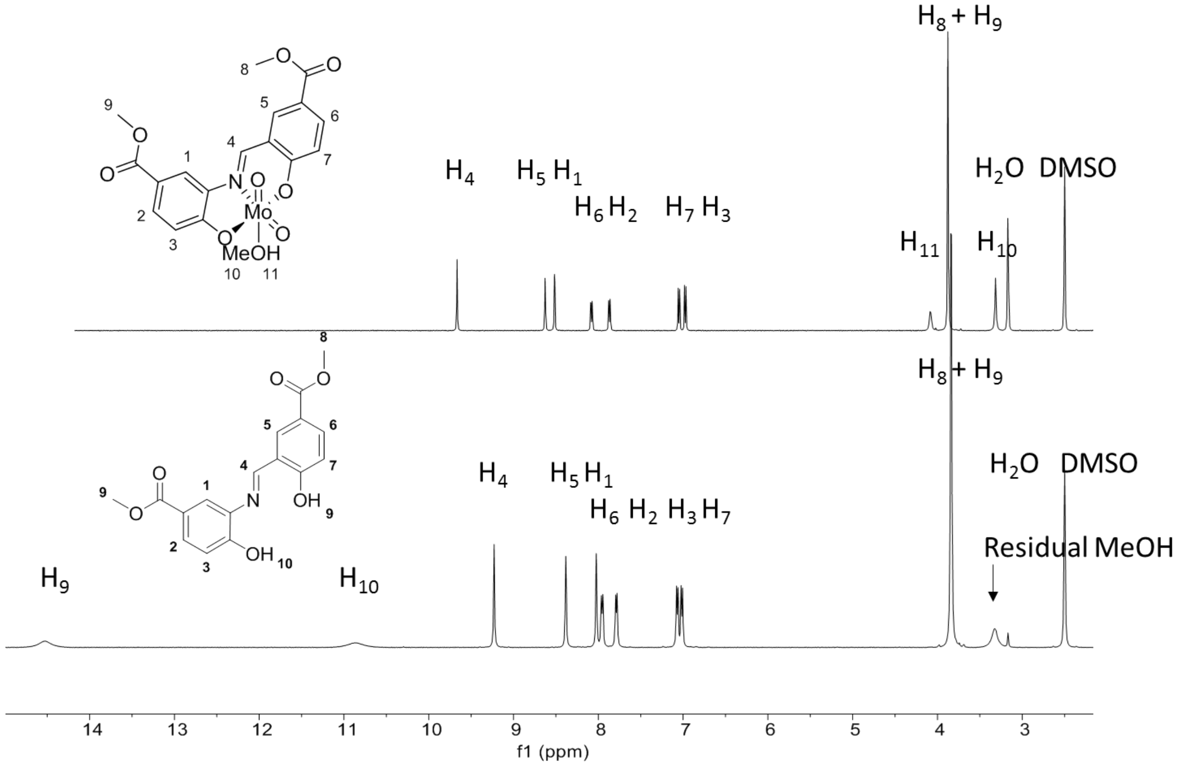

*Figure 2-16: $^1H$ NMR spectra of **L-2** (bottom) and **Mo-2** (top) in DMSO-$d_6$.*

Binding of $[WO_2]^{2+}$ to the SAP ligands resulted in the same changes to the $^1H$ NMR spectrum as observed for $[MoO_2]^{2+}$. Figure 2-17 shows the $^1H$ NMR spectra of **Mo-2** and **W-2** in DSMO-$d_6$. Both spectra are practically identical, except for the resonances at 3.2 and 4.1 ppm which result from MeOH bound to molybdenum that are absent on the spectrum of the tungsten analogue. In addition, there is a small but noticeable difference in chemical shift between the two complexes: all signals of the tungsten complex are shifted slightly downfield by up to 0.05 ppm. The ester protons, being further away and essentially separated by oxygen, are unaffected by the metal centres. The imine proton, however, is unexpectedly insensitive to the change in metal.

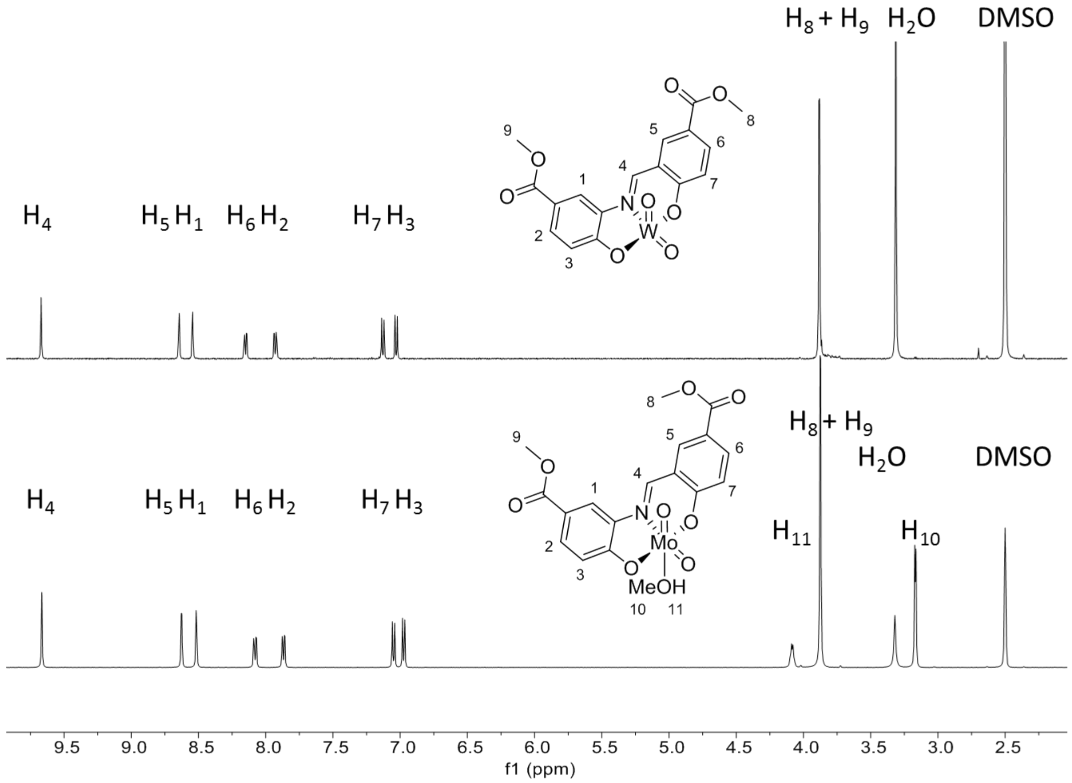

*Figure 2-17: Comparison of $^1H$ NMR spectra of **Mo-2** (bottom) and **W-2** (top) in DMSO-d6.*

### 2.3.3.1 Trends in $^1H$ NMR spectra

A central part of the ligands is the imine group (CH=N) which appears as a singlet in the $^1H$ NMR spectra (see Figure 2-17). As discussed previously the imine proton becomes deshielded upon binding of the nitrogen to the metal. As it is in conjugation to the two aromatic rings, substitution on these rings should affect the chemical shift of the imine proton which allows to study the influence of different substituents.[100,112]

Table 2-4 list the chemical shift of the imine proton of all ligands and complexes and the difference between complex and corresponding ligand, in order of increasing chemical shift of the complexes.

It can be seen that the coordination shift of the imine proton lies between 0.3 and 0.5 ppm. Chemical shifts of the imine proton range from 8.91 to 9.67 ppm for the complexes and 8.63 to 9.24 ppm for the ligands. Using the unsubstituted complex **Mo-1** as a baseline, a trend can be seen: the presence of an amine group lowers the chemical shift whereas all other substituents increase it and the highest increase is seen when two substituents are present.

An increase in chemical shift is seen upon replacing an acid substituent for an ester one (e.g. between **Mo-3** and **Mo-2**) although it is only between 0.01 and 0.03 ppm and, assuming some imprecision in the values obtained from NMR spectra, is not considered significant.

*Table 2-4: The chemical shift of the imine proton (C**H**=N) of the complexes and ligands. [a] Note that the benzene ring is replaced by a naphthalene ring. [b] Unless stated otherwise the substituent is in the ortho position to the phenol group on the al (aldehyde) or am (amine) ring (c.f. Scheme 2-2).*

| Compound | Position [b] | Chemical shift of (C*H*=N) / ppm | | Chemical shift difference / ppm |
|---|---|---|---|---|
| | | Complex | Ligand | |
| **Mo-1**$^{\mathrm{H,H}}$ | / | 9.28 | 8.97 | 0.31 |
| **Mo-2**$^{\mathrm{COOMe,COOMe}}$ | al; am | 9.67 | 9.23 | 0.44 |
| **Mo-3**$^{\mathrm{COOH,COOH}}$ | al; am | 9.63 | 9.21 | 0.42 |
| **Mo-4**$^{\mathrm{COOMe,Et2N}}$ | meta, al; am | 9.10 | 8.68 | 0.41 |
| **Mo-5**$^{\mathrm{COOMe,COOH}}$ | am; al | 9.64 | 9.20 | 0.44 |
| **Mo-6**$^{\mathrm{COOH,COOMe}}$ | al; am | 9.65 | 9.24 | 0.42 |
| **Mo-7**$^{\mathrm{COOH,H}}$ | am | 9.47 | 8.98 | 0.49 |
| **Mo-8**$^{\mathrm{H,COOH}}$ | al | 9.40 | 9.12 | 0.28 |
| **Mo-9**$^{\mathrm{COOMe,H}}$ | am | 9.48 | 9.03 | 0.45 |
| **Mo-10**$^{\mathrm{H,COOMe}}$ | al | 9.43 | 9.14 | 0.29 |
| **Mo-11**$^{\mathrm{COOMe,H}}$ | meta, am | 9.41 | 9.00 | 0.41 |
| **Mo-12**$^{\mathrm{NO2,H}}$ | am | 9.59 | 9.10 | 0.49 |
| **Mo-13**$^{\mathrm{CF3,H}}$ | am | 9.48 | 9.05 | 0.43 |
| **Mo-14**$^{\mathrm{SO2NH2,H}}$ | am | 9.41 | 9.01 | 0.40 |
| **Mo-15**$^{\mathrm{H,ET2N}}$ | meta, al | 8.91 | 8.63 | 0.29 |
| **Mo-16**$^{\mathrm{Naph,H}}$ | / | 9.54 | 9.08 | 0.47 |
| | | | | |
| **W-1**$^{\mathrm{H,H}}$ | / | 9.28 | 8.97 | 0.31 |
| **W-2**$^{\mathrm{COOMe,COOMe}}$ | al; am | 9.67 | 9.23 | 0.44 |
| | | | | |
| Average of **Mo-7-10** | | 9.45 | 9.09 | 0.36 |
| Average of **Mo-2,3,5,6** | | 9.64 | 9.22 | 0.42 |

In order to establish further trends in the chemical shift a way to characterise the substituents and their effect on the ligand is needed. The substituents differ in their electronic properties, some being electron withdrawing others electron donating. They also differ in size, but their steric effect is considered negligible as they are sufficiently distanced from the coordinating imine group. A way to quantify the degree of electron donation / acceptance is the Hammett parameter[113].

Values of the Hammett parameter of the different groups can be found in Table 2-5. From Figure 2-6 it can be seen that the substituents are in the *meta* position with regards to the imine group, except for -NEt$_2$ in **Mo-15** and **Mo-4** and -COOMe in **Mo-11** which are in the *para* position.

*Table 2-5: Hammett parameter of the substituents used in this work.*[113]

| Substituent | $\sigma_{para}$ | $\sigma_{meta}$ |
|---|---|---|
| $NEt_2$ | -0.72 | -0.23 |
| COOH | 0.45 | 0.37 |
| COOMe | 0.45 | 0.37 |
| $CF_3$ | 0.54 | 0.43 |
| $NO_2$ | 0.78 | 0.71 |
| $SO_2NH_2$ | 0.60 | 0.53 |

Two properties of the **SAP**-based ligands, however, are not accounted for in the Hammett parameter: both ester and acid groups have the same value and which of the two phenyl rings the substituent is placed on is also not reflected. Therefore, an average chemical shift was also calculated for mono- and di-substituted acid and ester compounds: 9.44 ppm (mono) and 9.66 ppm (di) (**L/Mo-11**, having a different structure, was excluded).

To determine the electronic effect of the substituents on the complex, the chemical shift of the imine proton was plotted against the Hammett parameter, shown in Figure 2-18. Here, an overall linear trend is observed. However, this is in large due to the three points, that represent the unsubstituted complexes and those with electron donating substituents. The remaining complexes, which bear electron withdrawing substituents, form two clusters and no trend within these is present. Between the mono- and di-substituted complexes containing acid and ester groups the aforementioned shortcoming of the Hammett parameter is still present, although the averages in each group line up well. Only **Mo-11** and **Mo-14** deviate strongly.

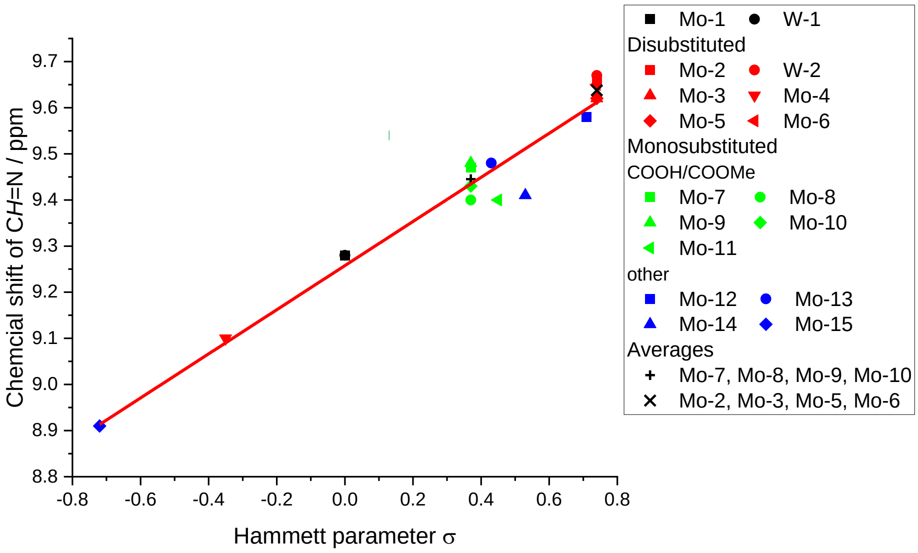

*Figure 2-18: Plot of chemical shift of the imine proton of the molybdenum and tungsten complexes against the Hammett parameter. Values from linear regression: slope = (0.48 ± 0.03) ppm, intercept = (9.26 ± 0.02) ppm, $R^2$ = 0.96.*

The same plot of chemical shift of the imine proton against the Hammett parameter for the ligands is shown in Figure 2-19. It is similar to that of the complexes but shows a greater spread and worse correlation ($R^2$ of only 0.89 compared to 0.96). Substituents have a stronger effect on the imine groups resonance in the complexes (slope of 0.48 compared to 0.39) but differences between ligands and corresponding complexes are mostly due to the complexation leading to a similar downfield shift between all pairs.

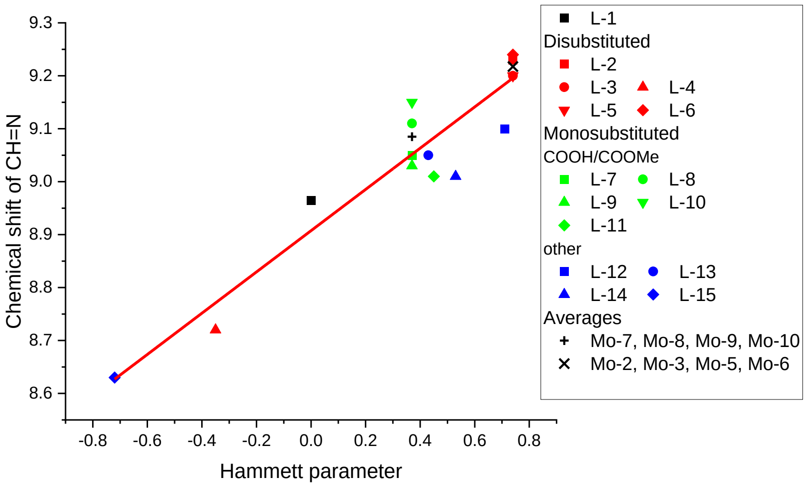

*Figure 2-19: Plot of chemical shift of the imine proton of the ligands against the Hammett parameter. Values from linear regression: slope = (0.39 ± 0.03) ppm, intercept = (8.91 ± 0.02) ppm, $R^2$ = 0.89.*

In conclusion, the complexation of molybdenum and tungsten has been seen in the changes of the resonances of the SAP-based ligands in the $^1$H NMR spectra. The substituents on these ligands led to a shift of the resonance of the imine group, the central feature of the Schiff base. A linear correlation between the shift of the imine group and the Hammett parameter as a measure of the electronic properties of the substituents was found. The nature of the metal centre on the other hand had practically no effect on the $^1$H NMR spectra. A better way of probing the metal centre is IR spectroscopy which analyses the metal oxygen bonds and is discussed below.

### 2.3.4 FTIR spectroscopic analysis of the molybdenum and tungsten complexes

FTIR-ATR spectra of the ligands and complexes were recorded to study the changes upon complexation and confirm the presence of the cis-$MoO_2$-moeity in the complex. The spectra of **L-2**, **Mo-2** and **W-2** are shown and discussed below, while Table 2-6 gives an overview of the most important bands for all complexes.

The spectra of **L-2** and **Mo-2** in the ranges of 400 to 1000 and 1000 to 3600 cm$^{-1}$ are shown in Figure 2-20 and Figure 2-21. Differences in vibration and stretching between ligand and complex would be expected for groups that are involved in the complex formation (the imine and the two phenol groups), as well as those that have been newly introduced (*e.g.* Mo=O, Mo-N). Additionally, the bound ligand is restricted in its movement (*e.g.* the rotation around the C-CHN and CHN-C axes), and inter- and intramolecular hydrogen bonding involving the imine and phenol groups is no longer possible.

The most important bands are found below 1000 cm$^{-1}$ originating from the cis $MoO_2$ moiety. The presence of the two oxide ligands gives rise to two bands, the symmetric and asymmetric stretching of the Mo=O bond at 936 and 909 cm$^{-1}$. In **Mo-1** these are found at 931 and 907 cm$^{-1}$, which is in agreement with previous reports.[105,114,115]

The imine group gives rise to a band around 1650 cm$^{-1}$, the stretching of the C=N bond. In **L-2** it is found at 1621 cm$^{-1}$ but shifts to 1609 cm$^{-1}$ in **Mo-1** upon complexation.

The C=O moieties of the two ester groups are found as two separate bands at 1677 and 1719 cm$^{-1}$ in **L-2** but form a single broad band in **Mo-2** at 1688 cm$^{-1}$.

Deprotonation and binding of the phenol groups leads to the appearance of intense bands in the range of 550 to 650 cm$^{-1}$ (541, 547 and 665 cm$^{-1}$) due to stretching of the metal-$O_{phenol}$-bond.[105,114]

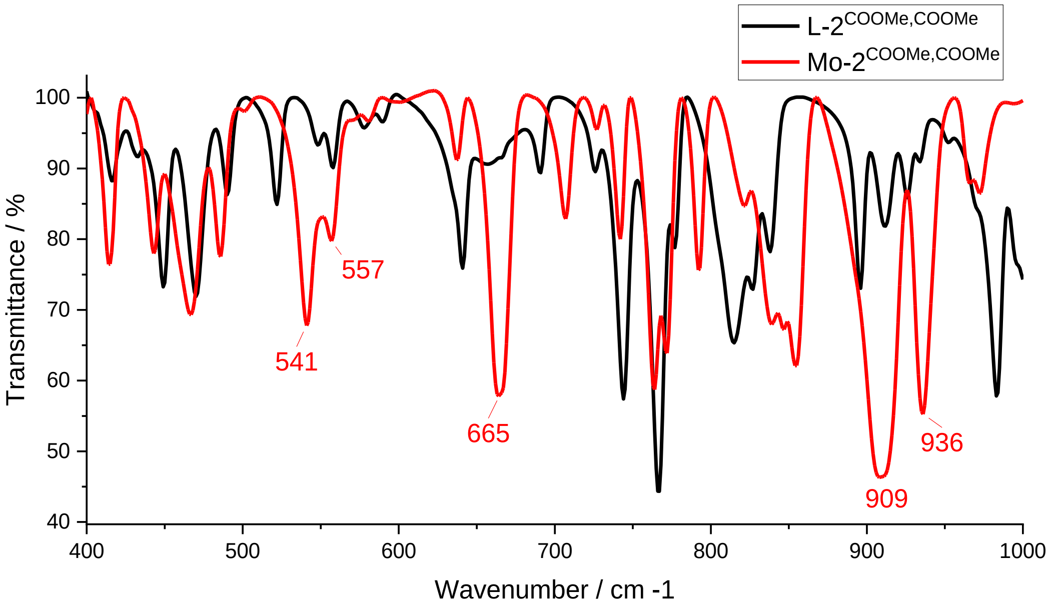

*Figure 2-20: ATR infrared spectra of **L-2** (black) and **Mo-2** (red) in the range of 400 to 1000 cm$^{-1}$.*

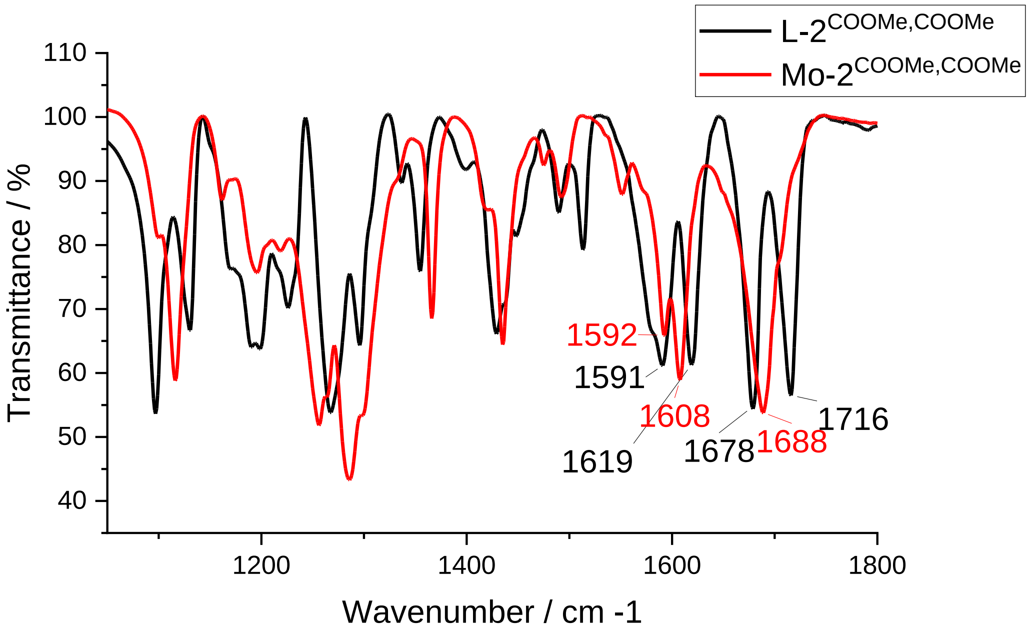

*Figure 2-21: ATR infrared spectra of **L-2** (black) and **Mo-2** (red) in the range of 1000 to 1800 cm$^{-1}$.*

Figure 2-22 shows the IR spectra of **Mo-2** and **W-2** in the range of 1000 to 1800 cm$^{-1}$. The band caused by the stretching of the C=O moieties is shifted by 33 cm$^{-1}$ in **W-2** compared to **Mo-2** (1721 cm$^{-1}$ *vs.* 1688 cm$^{-1}$, possibly due to a difference in structure and hydrogen bonding in the molybdenum complex. See chapter 2.3.5), whereas stretching of the imine group has only shifted by 3 cm$^{-1}$, 1610 cm$^{-1}$ in **W-2** compared to 1607 cm$^{-1}$ in **Mo-2**.

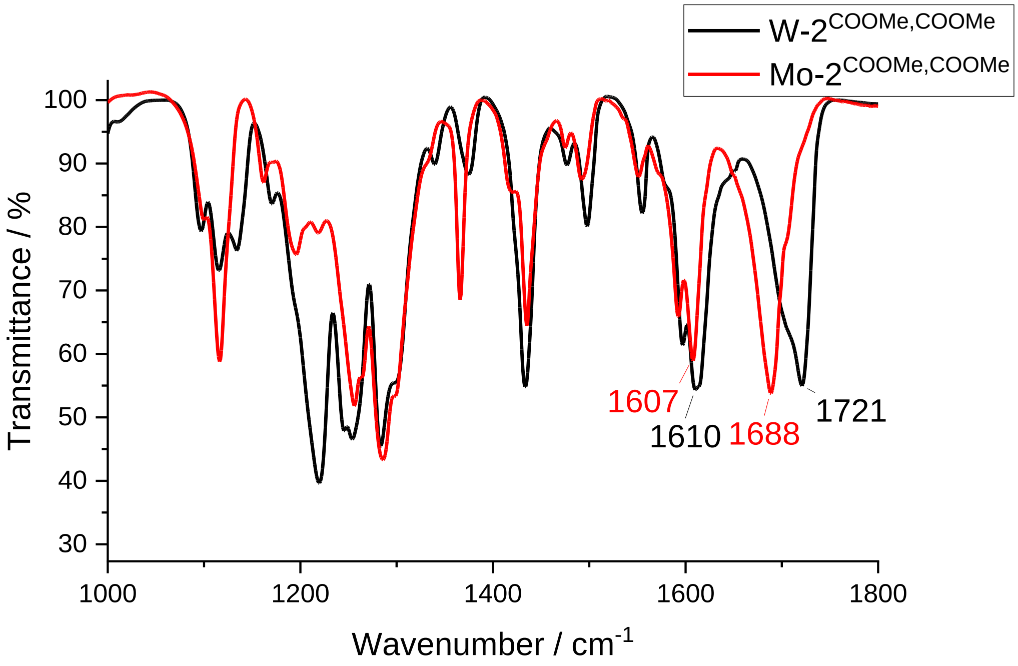

*Figure 2-22: ATR infrared spectra of **W-2** (black) and **Mo-2** (red) in the range of 1000 to 1800 cm$^{-1}$.*

The differences in the metal-oxygen bands between **W-2** and **Mo-2** can been seen from Figure 2-23. The spectrum of **Mo-2** shows two intense bands resulting from the symmetric and asymmetric stretching of the $MoO_2$ core (936 and 910 cm$^{-1}$), the spectrum of **W-2,** however, only has one at 964 cm$^{-1}$. Two more bands with much lower intensity are present in the spectrum of **W-2** at 907 and 935 cm$^{-1}$. In addition, there is also a broad band (or group of bands) at 737 cm$^{-1}$. The bands in **W-2** are indicative of a structural difference compared to **Mo-2** involving bridging W-O-W groups. These differences will be discussed in more details in section 2.3.5.

In both compounds, phenol oxygen donors bound to the metal give rise to additional bands. Two bands are seen in the spectrum of **Mo-2** at 541 and 556 cm$^{-1}$, but only one broader and more intense band in **W-2** at 555 cm$^{-1}$, one more band in each complex is found at 663 (**Mo-2**) and 669 cm$^{-1}$(**W-2**). These differences can be explained by switching the metal centre from molybdenum to tungsten, but also by a difference in structure between the two complexes (cf. section 2.3.5). The higher atomic mass of tungsten should lead to a lower wavenumber of the M=O stretching compared to molybdenum following from a simple analysis using Hook's law (Equation 2-1).[116]

$$\nu \ = \tilde{\nu}\, c = \frac{1}{2\pi c}\sqrt{\frac{\kappa}{\mu}}$$

*Equation 2-1*

with ν = fundamental vibration frequency, $\tilde{\nu}$ = vibration wavenumber, μ = reduced mass, κ = force constant, c = speed of light. However, an increase in bond strength (force constant) would result in a higher wavenumber. It has to be noted, though, that equation 2-1 is based on two atom vibrating, whereas the M=O bands under investigation are due to three atoms. As the bands in **W-2** (and **W-1**) are found at higher wavenumbers, the increase in bond strength must outweigh the increase in atomic mass.

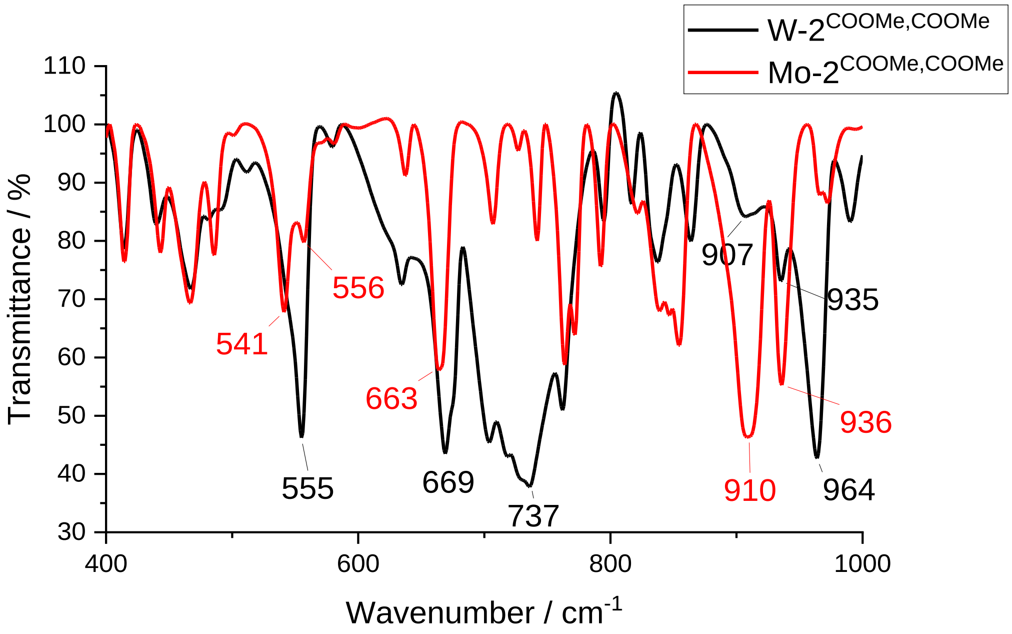

*Figure 2-23: ATR infrared spectra of **W-2** (black) and **Mo-2** (red) in the range of 400 to 1000 cm$^{-1}$.*

Common to all 18 complexes are the bands between 1550 and 1630 cm$^{-1}$. The stretching bands of the C=N group lie above 1600 cm$^{-1}$ and often split into two bands with the second band in some compounds shifted to just below 1600 cm$^{-1}$ (*e.g.* **Mo-3**).[111] One or two stretching bands of the C-O$_{phenol}$ group are found between 1550 and 1590 cm$^{-1}$.[111]

While the bands from C-O$_{phenol}$ groups are found above 1550 cm$^{-1}$, the M-O$_{phenol}$ groups give rise to several intense bands in the ranges of 520 to 550 and 620 to 670 cm$^{-1}$.[105,114]

The ester and acid substituted complexes show intense stretching bands of the C=O group with bands from esters in the range of 1700 to 1720 cm$^{-1}$, and those of acids between 1660 and 1700 cm$^{-1}$. Di-substituted complexes do not always show two bands. **Mo-2** only shows one broad band at 1688 cm$^{-1}$ with a small shoulder at 1707 cm$^{-1}$ and **W-2** a broad band at 1722 cm$^{-1}$ with a shoulder at 1702 cm$^{-1}$.

All complexes display an intense band between 920 and 965 cm$^{-1}$ due to stretching of the M=O group. A second such band is found in most complexes between 875 and 907 cm$^{-1}$ with both bands resulting from the symmetric and asymmetric stretch of the MO$_2$ core. In some complexes this second band is absent, instead a broad band is found around 800 cm$^{-1}$ (Mo) or 735 cm$^{-1}$ (W) which has been assigned to a M-O-M group, *i.e.* two molecules of complex connected by a bridging oxygen.[59,114]

*Table 2-6: Position (in cm$^{-1}$) of characteristic IR bands of the molybdenum and tungsten complexes.* [a] *Symmetric and asymmetric labels do not apply as only one M=O group is present.* [b] *Bands of equal intensity.*

| Compound | CH=N / C-O | C=O | M=O$_{sym}$ | M=O$_{asym}$ | M-O-M | M-O |
|---|---|---|---|---|---|---|
| **Mo-1$^{H,H}$** | 1611, 1600, 1584, 1552 | | 931 | 907 | | 634, 551 , 536 |
| **W-1$^{H,H}$** | 1615, 1602, 1587, 1556 | | 942 [a] | | 734 | 660, 640, 554, 534 |
| **Mo-2$^{COOMe,COOMe}$** | 1609, 1593, 1551 | 1707, 1688 | 936 | 906 | | 542, 558, 664 |
| **W-2$^{COOMe,COOMe}$** | 1616, 1611, 1597 | 1722, 1702 | 964 [a] | | 737 | 669, 554 |
| **Mo-3$^{COOH,COOH}$** | 1607, 1595, 1572 | 1721, 1668 | 945 [a] | | 804 | 555, 539, 641, 664 |
| **Mo-4$^{COOMe,Et2N}$** | 1614, 1585, 1561 | 1716 | 928 | 882 | | 673, 535 |
| **Mo-5$^{COOMe,COOH}$** | 1596, 1608, 1617 | 1682 | 930 | 909 | | 659, 557 |
| **Mo-6$^{COOH,COOMe}$** | 1609, 1592 | 1721, 1670 | 931 | 908 | | 658, 554, 527 |
| **Mo-7$^{COOH,H}$** | 1608, 1592 | 1666 | 932 | 909 | | 672[b], 655[b], 636[b], 526 |
| **Mo-8$^{H,COOH}$** | 1610, 1584 | 1698, 1684 | 923 [a] | | 802 | 663, 651, 561 |
| **Mo-9$^{COOMe,H}$** | 1619, 1602, 1595 | 1713 | 928 | 891 | | 675, 553 |
| **Mo-10$^{H,COOMe}$** | 1609, 1582, 1588 | 1687 | 928 | 904 | | 643, 559, 541 |
| **Mo-11$^{COOMe,H}$** | 1617, 1599 | 1719 | 920 [a] | | 814 | 648, 637, 592 |
| **Mo-12$^{NO2,H}$** | 1611, 1600, 1577 | | 941 [a] | | 796 | 682, 656, 639, 549 |
| **Mo-13$^{CF3,H}$** | 1601 | | 922 [a] | | 801 | 665, 658, 639, 557 |
| **Mo-14$^{SO2NH2,H}$** | 1604, 1584 | | 951 | 910 | | 638, 587, 550 |
| **Mo-15$^{H,ET2N}$** | 1614, 1593, 1567 | | 920 | 887 | | 636, 619, 527 |
| **Mo-16$^{Naph,H}$** | 1623, 1604, 1594 | | 927 | 888, 875 [b] | | 640, 630, 564 |

With regard to OAT, differences in the oxo ligands are of interest. As the band position is linked to the strength of the M=O bond (c.f. Equation 2-1), a trend in the band position could allow rationalisation of OAT discussed in Chapter 3. Due to the difference in structure the complexes with two M=O bands and those with M=O and M-O-M bands are treated separately. The Hammett parameter is used again to quantify the differences in substituents, which are mostly in the para position from the point of view of the phenolate oxygens.

Plots of the wavenumber of Mo=O$_{sym}$ and Mo=O$_{asym}$ and of M=O and Mo-O-Mo, respectively, against the Hammett parameter σ are shown in Figure 2-24 and Figure 2-25. **W-1** and **W-2** are not included because of the different metal centre.

Neither the symmetric nor the asymmetric stretching frequencies show a strong trend, although an increase of the symmetric frequency with the Hammett parameter seems possible. Linear regression yielded poor correlation as evidenced by the $R^2$ values of 0.23 for the symmetric and of 0.36 for the asymmetric stretching frequencies. Interestingly, a higher $R^2$ value was obtained for the asymmetric stretching frequencies despite those appearing more scattered. Correlation in the symmetric frequencies could be slightly improved by treating **Mo-14** as an outlier, yielding an $R^2$ value of 0.54 (blue line in Figure 2-24).

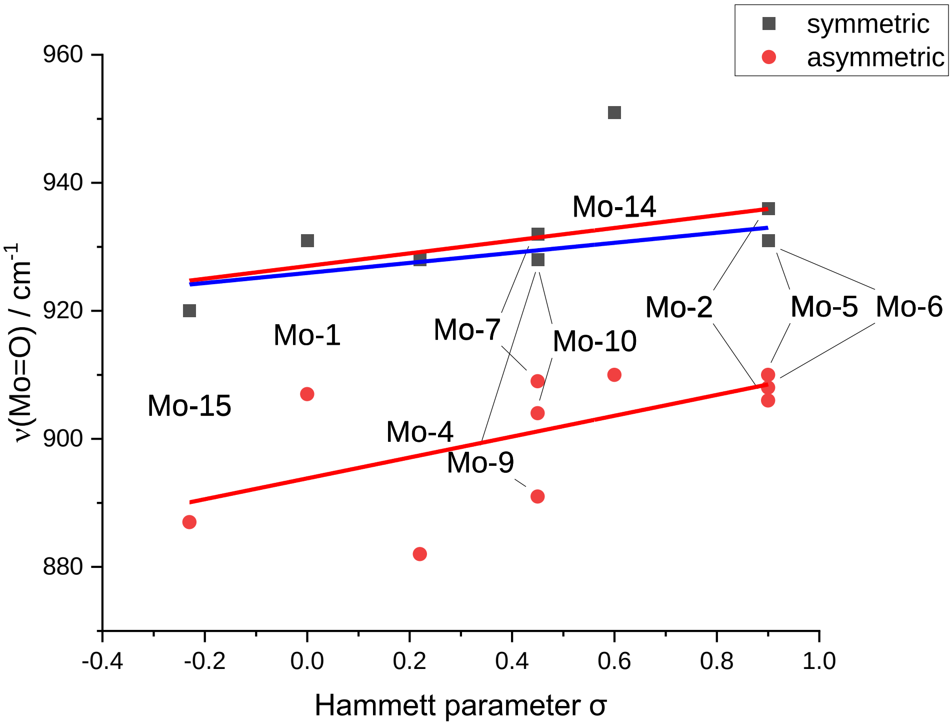

*Figure 2-24: Plot of the symmetric and asymmetric Mo=O stretching frequencies of monomeric **Mo-1, Mo-2, Mo-4, Mo-5, Mo-6, Mo-7, Mo-9, Mo-10, Mo-15** against Hammett parameter. Values of the linear regression: symmetric, red line: slope = (10 ± 6) cm$^{-1}$, intercept = (927 ± 4) cm$^{-1}$, $R^2$ = 0.23; symmetric, **Mo-14** treated as outlier, blue line slope = (8 ± 3) cm$^{-1}$, intercept = (926 ± 2) cm$^{-1}$, $R^2$ = 0.54; asymmetric: slope = (16 ± 7) cm$^{-1}$, intercept = (894 ± 5) cm$^{-1}$, $R^2$ = 0.36.*

The stretching frequencies of the single Mo=O group in the di- or oligomeric complexes **Mo-3, Mo-8, Mo-11, Mo-12,** and **Mo-13** shown in Figure 2-25 increase with σ following a linear dependence, reflected in the much better linear fit ($R^2$ value of 0.94). (Note that there are no two frequencies with the same σ). There are too few data points to show a definite trend in the frequencies of the Mo-O-Mo stretches. They could decrease slightly with σ, but a minimum between 0.6 and 0.8 could also exist.

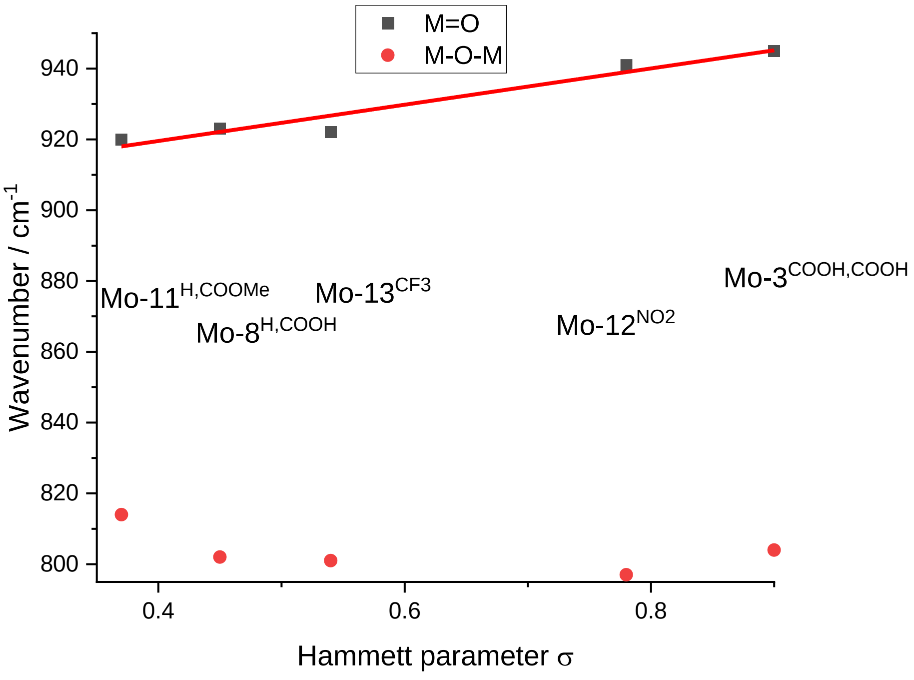

*Figure 2-25: Plot of the Mo=O and Mo-O-O stretching frequencies of di- or oligomeric* ***Mo-3, Mo-8, Mo-11, Mo-12, Mo-13*** *against Hammett parameter. Values of linear regression: slope (52 ± 7) cm$^{-1}$; intercept (899 ± 5) cm$^{-1}$, $R^2$ = 0.94.*

For monomeric and di- or oligomeric complexes an increase of stretching frequency with σ is expected. Electron withdrawing substituents (higher σ) lead to a decrease of electron density on the Mo centre which reduces repulsions with the filled oxygen orbitals allowing for increased Mo=O overlap and hence bond strength. An increased bond strength is reflected in a higher stretching frequency.[89]

Following from the discussion of **Mo-2** and **W-2** involving Hook's law (Equation 2-1) it could be predicted that those compounds with the highest stretching frequencies (and, following from Figure 2-24 and Figure 2-25, higher values in σ) would be the least prone to transferring an oxo ligand because of their higher bond strength. The highest frequency is found in the tungsten complex **W-2,** but the true bond strength is also hidden by the increase in atomic mass. From an earlier discussion it could follow that the bond strength in tungsten is even higher than what the frequency suggests. (see discussion around Equation 2-1). The only other tungsten complex, **W-1**, has a lower stretching frequency, and should therefore have a weaker bond. Within the molybdenum complexes **Mo-14** and **Mo-3** have the highest frequency, the lowest is seen in **Mo-11, Mo-13** and **Mo-15**.

## 2.3.5 Structure of complexes and formation of di- and oligomers

Molybdenum dioxo complexes are usually found to have octahedral geometry.[117] In this geometry, two of the six coordination sites are occupied by the two oxo ligands while the remaining four can be filled by two bidentate ligands, as it is the case in [$MoO_2(acac)_2$]. With a tridentate ligand like SAP, there are three options regarding the sixth site: it can be filled by a solvent or donor molecule, as found in most complexes reported, it could be left vacant[118] or it could be filled by the oxo ligand of a second complex molecule. Mutual sharing of oxo ligands between two molecules would result in a dimeric or even oligomeric structure as shown in Figure 2-26.[98] Note that these dimers are different from the dimers that have been observed during OAT. Here, the dimer contains molybdenum(VI) and two bridging oxygens. During OAT a dimer can form that has molybdenum(V) and only one bridging oxygen.

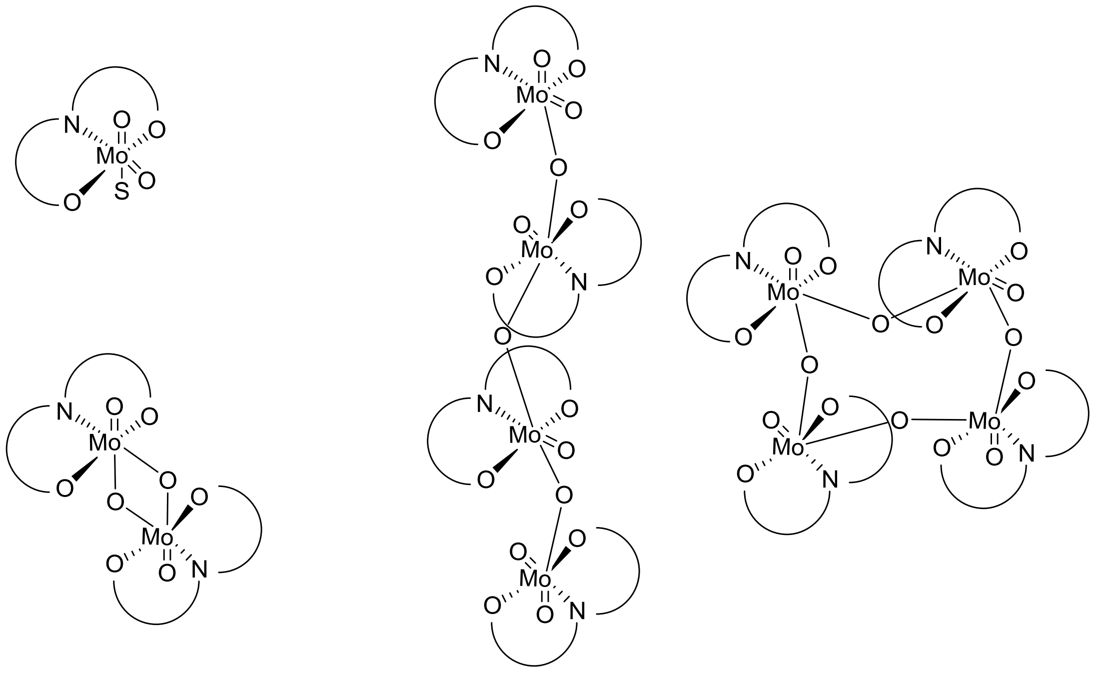

*Figure 2-26: Schematic representation of the geometry of monomeric, dimeric and oligomeric Mo(VI) complexes. S representing a solvent molecule (adapted from [44]).*

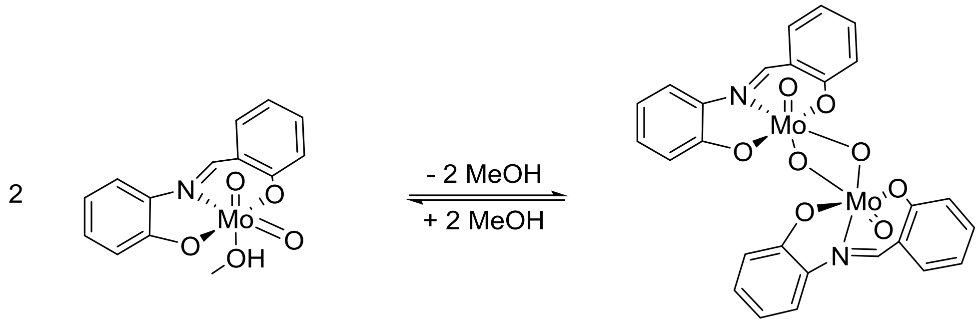

**Mo-1** **Mo-1b**

*Scheme 2-5: Interconversion between the monomeric and dimeric structure of a Mo Schiff base complex.*

As mentioned previously (section 2.3.3), the $^1$H NMR spectra of the synthesised complexes showed the presence of an equimolar quantity of MeOH (with regards to the ligand) and hence incorporation of MeOH into Mo-1, Mo-2, Mo-4, Mo-5, Mo-6, Mo-7, Mo-9, Mo-10, Mo-11, Mo-15, Mo-16. However, the methanol is exchanged for DMSO and therefore is found at a chemical shift that corresponds to free MeOH. Only complexes (**Mo-3, Mo-8, Mo-12, Mo-13, Mo-14, W-1 and W-2**) contain no MeOH. Interestingly, both tungsten complexes are among these MeOH free complexes whereas their molybdenum counter parts contain MeOH. It is unclear why no solvent is found in these complexes as there seems to be no common feature that would explain this behaviour.

As the sixth coordination site is not occupied by a solvent molecule it must remain empty or be occupied by an oxygen from a second molecule of complex resulting in a dimeric or oligomeric structure. The IR data of the complexes in question presented in Table 2-6 clearly points to the later possibility.

The interconversion between the monomeric and dimeric forms of complexes **Mo-1** and **Mo-1-b** (shown in Scheme 2-5), and of related Mo complexes has been reported.[98,119] Loss of solvent from the monomeric form occurred slowly under ambient conditions over time or rapidly under reduced pressure and elevated temperature.[83] Following from these reports, complexes **Mo-1** and **Mo-2** were heated at 200 °C for 1 h.

The IR spectra of **Mo-1** before and after heating are shown in Figure 2-27 in the range of 500 to 1000 cm$^{-1}$. After heating, a new peak at 810 cm$^{-1}$ is seen as well as one at 938 cm$^{-1}$. The former corresponds to Mo-O-Mo while the later corresponds to M=O where now that only one oxide group remains, no distinction between asymmetric and symmetric stretching is present and only one single band is observed. The two original bands above 900 cm$^{-1}$ are still present and due to terminal Mo units of linear chains that still have two oxo ligands (Figure 2-26; The two original bands could also stem from compound still in its original form, although rather unlikely, MeOH may not have escaped from the bulk of larger agglomerates of compound and molecules still containing the solvent were only revealed in the process of recording the IR spectrum).

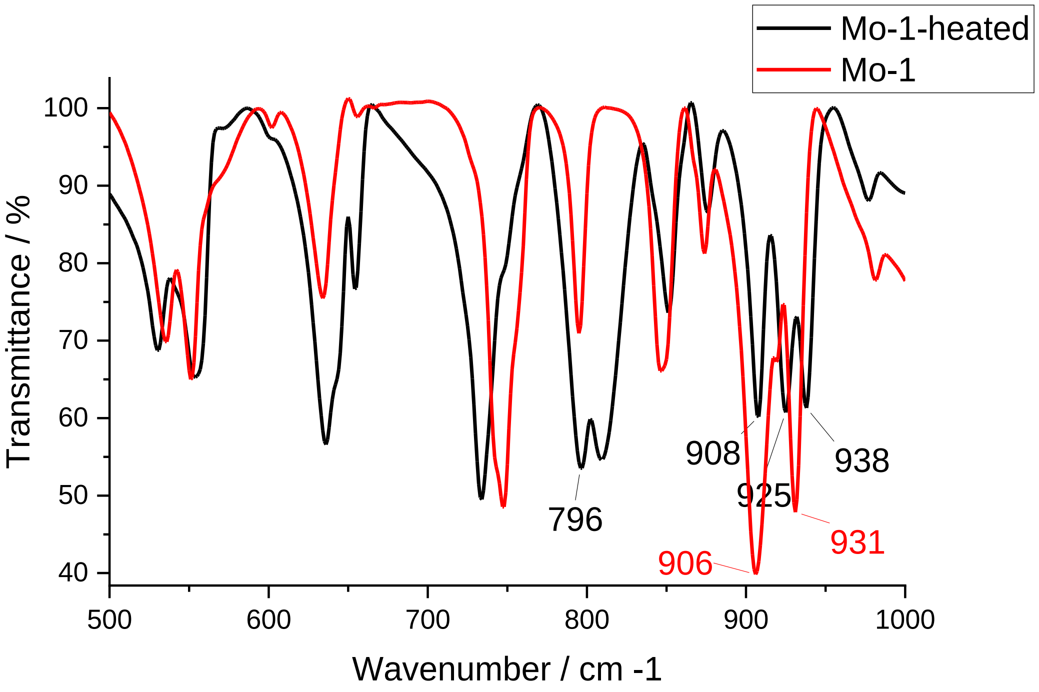

*Figure 2-27: ATR-IR spectra of **Mo-1** (top) and after heating (bottom).*

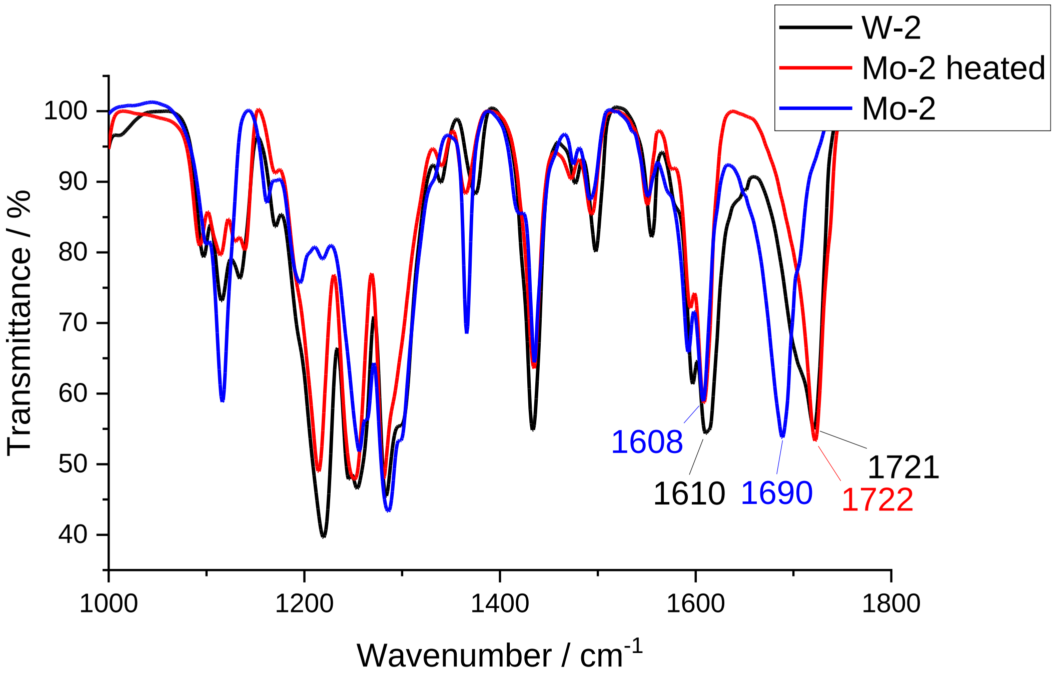

*Figure 2-28: ATR-IR spectra of **W-2, Mo-2** and **Mo-2-heated** in the range of 1000 to 1800 cm$^{-1}$.*

IR spectra of **W-2** and **Mo-2** after the later has been heated to 200 °C for 1 h are shown in Figure 2-28 and Figure 2-29, together with untreated **Mo-2** for comparison (No changes to the IR spectrum were seen when **W-2** was heated). In the range from 1000 cm$^{-1}$ to 1800 cm$^{-1}$, where characteristic bands of the ligand are found – C=O, C=N, C-O – (Figure 2-28) the spectra of the two are now practically identical. Interestingly, the C=O band has shifted to a higher wavenumber after heating, whereas the C=N band remained unaffected. Thus, the change to the Mo coordination sphere has not affected the imine group, whereas the structural rearrangement has led to a change in the ester group. (The crystal structure of **Mo-2** revealed hydrogen bonding involving solvent and one of the ester groups. See 2.3.2).

Only between 400 cm$^{-1}$ and 1000 cm$^{-1}$ are differences visible (Figure 2-29) related to bands involving the metal ligand bond. The M=O band of **W-2** is found at a slightly higher wavenumber compared to **Mo-2-heated** (964 cm$^{-1}$ vs. 948 cm$^{-1}$) both of which are higher than the symmetric stretch of **Mo-2**. The broad band resulting from M-O-M stretching of **W-2** is found at a lower wavenumber (737 cm$^{-1}$ vs. 798 cm$^{-1}$). The M-O$_{phenol}$-bands now coincide, both **W-2** and **Mo-2-heated** showing one broad and intense band at 556 cm$^{-1}$ where **Mo-2** originally had two lower intensity bands. **W-2** and **Mo-2-heated** have additional low intensity bands in the 900 to 950 cm$^{-1}$ region at 907 and 936 cm$^{-1}$ for tungsten and at 924 and 936 (shoulder) cm$^{-1}$ for molybdenum. These bands are possibly due to the presence of $MO_2$ moieties. From Figure 2-26 it can be seen that the linear, oligomeric structure contains terminal $MoO_2$ units. These units are present in much lower number compared to the O-MoO-O units in the linear and other structures, therefore, the corresponding IR-bands show a much lower intensity. The same argument applies to **W-2**.

Given that the two compounds show similar spectra, including the same types of metal bands (M=O and M-O-M, although their positions are shifted) it may be suggested that both **W-2** and **Mo-2-heated** now have the same dimeric or oligomeric structure.

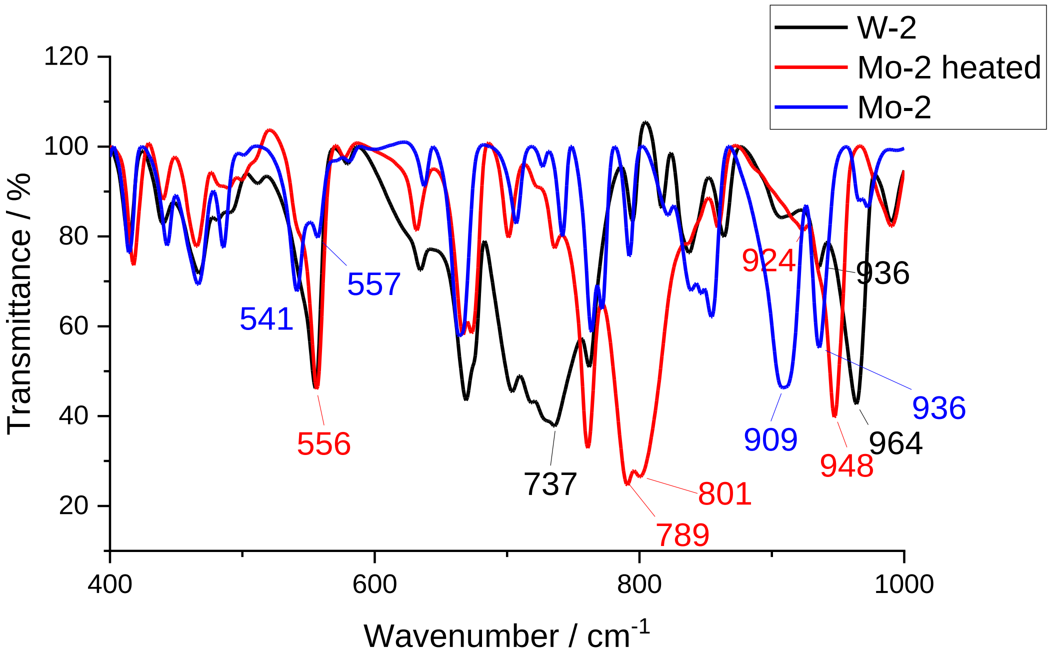

*Figure 2-29: ATR-IR spectra of **W-2, Mo-2** and **Mo-2-heated** in the range of 400 to 1000 cm$^{-1}$.*

The dimeric or oligomeric structure of **Mo-3**, **Mo-8**, **Mo-11**, **Mo-12**, **Mo-13** and **W-1** and **W-2** is only observed in solid form. In solution they are broken up into monomers and the coordination site occupied by a solvent molecule. As a consequence of this process, these complexes were found to dissolve more slowly and showed lower solubility compared to the monomeric complexes. This behaviour was especially pronounced in **W-1** and **W-2** which required strongly coordinating solvents such as DMSO and DMF to obtain concentrated solutions up to 4 mM. Once in solution all complexes are present in monomeric form; therefore, analyses of the dissolved complexes and especially OAT are not affected by this structural difference in the solid state. Interestingly, Mondal *et al.* found that **Mo-1** did not react with catechol to give the reduced [MoO(SAP)(catechol)] complex but the dimeric **Mo-1-heated** did.[120] They attributed this difference in reactivity to a weakening of the oxo ligand in the dimeric complex.

## 2.4 Summary

Several substituted ligands based on SAP were synthesised and characterised by $^1$H and $^{13}$C NMR spectroscopy, FTIR spectroscopy, elemental analysis and mass spectrometry. Molybdenum dioxo complexes of the form [$MoO_2$(L)(MeOH)] and [$MoO_2$(L)] were then made using these ligands. Two dioxo tungsten complexes of the form [$WO_2$(L)] were made with ligands **L-1** and **L-2**. All complexes were characterised by $^1$H and $^{13}$C NMR spectroscopy, mass spectrometry, elemental analysis and FTIR spectroscopy.

Crystal structures of **Mo-2, Mo-7** and **W-1** were obtained. Comparison to known structures of **Mo-1**, **Mo-15** and similar molybdenum and tungsten dioxo complexes revealed no unusual characteristics.

$^1$H NMR spectroscopy of showed a weak linear correlation between the chemical shift of the imine proton of the molybdenum complexes and the Hammett parameter of the substituent. A similar correlation between the symmetrical stretching frequency of the M=O bond and the Hammett parameter was also observed.

Differences in the structure of the as synthesised complexes were studied by $^1$H NMR spectroscopy and ATR-IR spectroscopy. Complexes **Mo-1**, **Mo-2**, **Mo-4**, **Mo-5**, **Mo-6**, **Mo-7**, **Mo-9**, **Mo-10**, **Mo-14**, **Mo-15** and **Mo-16** are of the form of [$MoO_2$(L)(MeOH)] and are monomeric in the solid state whereas **Mo-3**, **Mo-8**, **Mo-11**, **Mo-12**, **Mo-13, W-1** and **W-2** are of the form of [$MO_2$(L)] (M = Mo, W) and form di- or oligomers. The later form could be obtained from the monomeric one by heating, the di- and oligomers can be broken by a sufficiently strong coordinating solvent like DMSO or DMF.

# Chapter 3 Catalytic oxygen atom transfer

## 3.1 Introduction

### 3.1.1 Simplified mechanism of thermal OAT between sulfoxide and phosphine

The generally accepted mechanism for molybdenum catalysed OAT from sulfoxides to phosphines as shown in Scheme 3-1 starts with the nucleophilic attack by the phosphorus electron pair on an empty antibonding Mo=O orbital which weakens the molybdenum oxygen bond. The double bond is eventually broken, and electrons transferred to the metal while a new bond between oxygen and phosphorus is formed. Mo(IV) and phosphine oxide are formed.[121,122] The phosphine oxide dissociates from the metal and a sulfoxide binds. The S=O double bond is broken as the new Mo=O bond forms resulting in the oxidation of Mo and reduction of sulfur. Finally, the newly formed sulfide dissociates closing the cycle.[12]

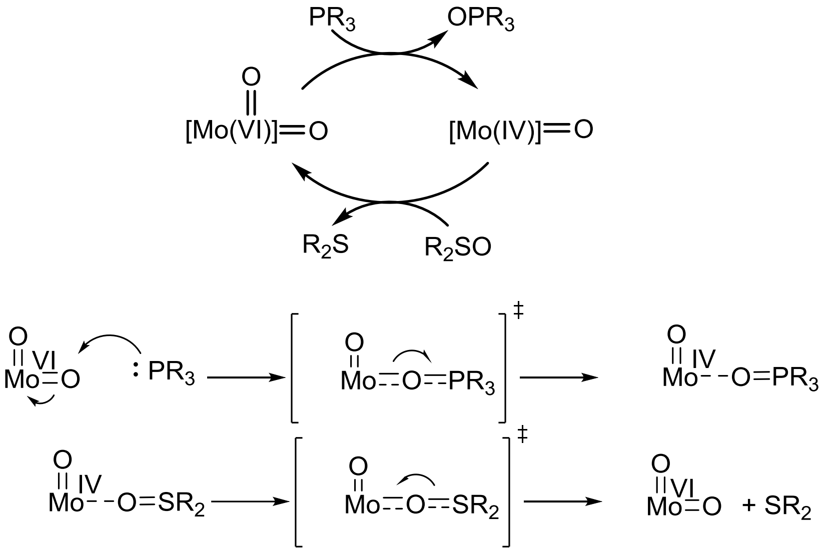

*Scheme 3-1: Generic scheme of OAT from a phosphine to a sulfoxide catalysed by a molybdenum dioxo complex (top) and mechanism of the half cycle reactions (bottom).*

### 3.1.2 Investigation of thermal OAT between sulfoxide and phosphine catalysed by molybdenum dioxo complexes

Almost all OAT reaction with molybdenum or tungsten reported in the literature are performed thermally, at ambient or elevated temperatures (>100 °C). Both stoichiometric and catalytic conditions are employed. Various parameters of the OAT reaction have been investigated in order to establish and improve the mechanistic understanding. Complexes closely modelling the active centres of molybdenum enzymes as well as more synthetic complexes have been studied both experimentally and through calculations. Some of the studies will be briefly presented below.

### 3.1.2.1 Influence of the ligand on thermal OAT between sulfoxide and phosphine catalysed by molybdenum dioxo complexes

Topich and Lyon followed the reduction of molybdenum complexes based on the SSP Schiff base ligand shown in Figure 3-1 with $PEt_2Ph$ in DMF at 30 °C by UV-Vis spectroscopy.[123] The appearance of a band at 465 nm over several hours indicated the formation of the reduced Mo(IV) species.

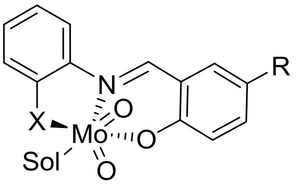

X = O: SAP R = H, Cl, Br, OMe, $NO_2$
X = S: SSP R = H, Cl, Br, OMe
Sol = $H_2O$ DMSO, none

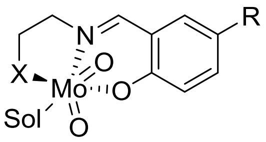

X = O: SAE R = H, Cl, Br, OMe, $NO_2$
X = S: SSE R = H, Cl, Br, OMe
Sol = $H_2O$ DMSO, none

*Figure 3-1: Structures of four sets of molybdenum dioxo complexes based on salicylidene amino phenol (SAP) and – amino ethanol (SAE) ligands studied by Topich and Lyon.* [124,125]

Topich and Lyon also looked at the related complexes with the SAP, SSE and SAE ligands, also shown in Figure 3-1. While the sulfur-containing complexes (SSP and SSE ligands) all performed OAT with $PPhEt_2$, the SAP and SAE systems did not react at “any appreciable rate” even at 60 °C in DMF.[126] For those complexes that reacted, reaction rate constants were obtained which linearly correlated to the Hammett parameter (Figure 3-2).

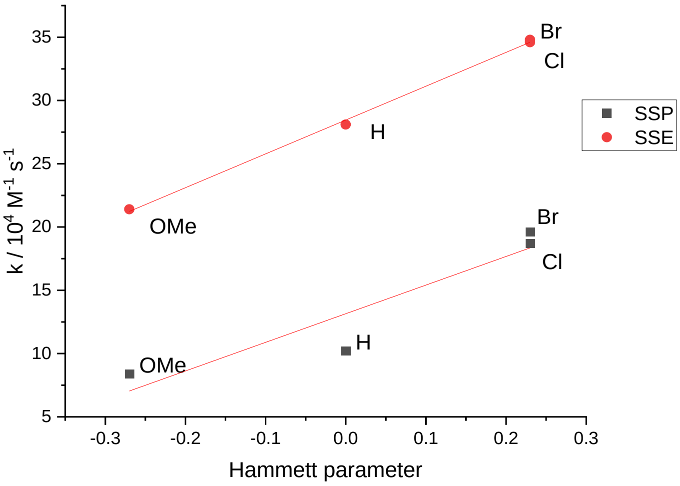

*Figure 3-2: Plot of rate constant against Hammett parameter for the oxidation of $PPhEt_2$ by $[MoO_2(L-X)]$, L = SSP or SSE, X according to labels. Conditions: c([Mo]) = 1 mM, c($PPhEt_2$) >25 mM, DMF, $N_2$, 30 °C (SSP) , 60 °C (SSE). Data taken from Topich and Lyon* [126]

From the rate constants, the Hammett ρ-value was calculated using Equation 3-1, where $k_x$ is the rate constant for substituent X, $\sigma_x$ is the Hammett parameter.

$$\log\frac{k_X}{k_H} = \rho\sigma_X$$

Equation 3-1

Values of 0.42 and 0.74 for $\rho$ were obtained for SSE and SSP complexes, respectively. Both values being positive is consistent with an increase in reaction rate and a mechanism where the energy difference between reactants and transition state is reduced by electron withdrawing groups. The higher values of the SSP complexes shows the better transmission of the substituents effects to the metal centre by the extended π-system.[126]

An improvement in reactivity of Mo complexes by introducing electron withdrawing substituents has been seen in other systems as well. The complexes shown in Figure 3-3 displayed correlation between the reaction rate and Hammett parameter similar to the above example. The positive effect of electron withdrawing substituents on reactivity in the systems shown in Figure 3-1 and Figure 3-3 suggest this is a general feature of molybdenum complex catalysed OAT.

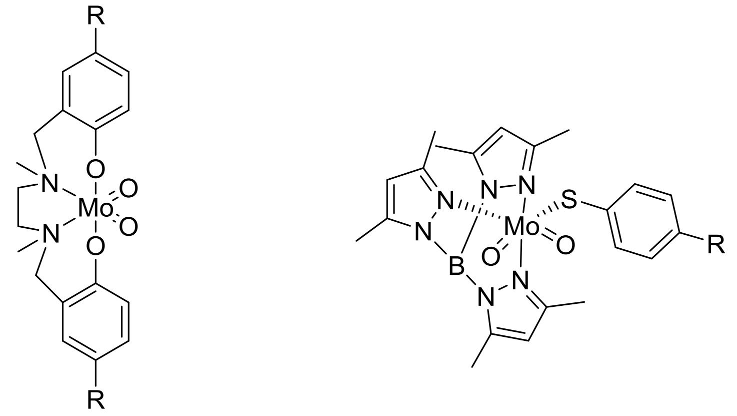

R = H, F, Cl, Br, I, OMe, Me, $NO_2$

R = OMe, Me, H, Cl, $CF_3$

*Figure 3-3: Structures of Mo dioxo complexes used to study the effect of substituents on OAT.*[127,128]

Two conclusions were drawn from the study of complexes employing the SSP, SAP, SSE and SAE ligands (Figure 3-1). First, use of sulfur-based ligands improves the activity of a complex compared to oxygen. Complexes with the sulfur containing SSP and SSE ligands were capable of oxidising $PPhEt_2$ while complexes with SAP and SAE, where the sulfur is replaced by oxygen, were practically inactive. Electrochemical studies showed that sulfur made these complexes more easily reducible.[129] Based on kinetic data and activation parameters, activity of molybdenum complexes with different donor ligands was proposed as follows:[126] $S_4 > N_2S_2 >$ ONS > ONO

Second, as already mentioned in regard to Figure 3-2, an extended π-system on the ligand increases activity of a complex. In the SSE complexes, sulfur and nitrogen are connected by alkyl chain whereas in SSP complexes the two atoms are bound to a benzene ring. The SSP complexes with the extended π-system showed an increased activity by about a factor of 4 compared to the SSE complexes.[126]

These parameters, substituent, donor atom and π-system, cover already some of the main aspects of ligand design. The following section will look into the nature of the phosphine substrate.

### 3.1.2.2 Influence of the phosphine on thermal OAT between sulfoxide and phosphine catalysed by molybdenum dioxo complexes

The influence of the phosphine substrate was studied by Lorber *et al.*[130] Reaction of the complex $[MoO_2(mnt)_2]^{2-}$ ($mnt^{2-}$ = 2,3-disulfanylmaleonitrile dianion (1,2-dicyanoethylenedithiolate)) with different phosphines of the form $PPh_{3-x}Et_x$ (X= 1-3) in MeCN at 25 °C was followed by UV-Vis spectroscopy. Kinetic data was obtained and analysed using equations 3-2 and 3-3

$$k_{obs} = k_1 + k_2 * [PR_3]$$

*Equation 3-2*

$$\log k_2 = a + b * \chi + c * \theta$$

*Equation 3-3*

where $k_x$ are the rate constants, θ is the phosphine's cone angle, χ is the relative σ donor capacity, a the intrinsic reactivity of the complex, and collectively c * θ the steric and b * χ the electronic contribution to the reactivity. Although variation in $k_2$ was small a difference between the phosphines was still seen. Deconvolution of electronic and steric effects using Equation 3-3 revealed a linear dependence on χ but no dependence on θ (Figure 3-4). Lorber and co-workers concluded that the reactivity of phosphines in the reduction of $[MoO_2(mnt)_2]^{2-}$ depends on the basicity of the phosphine in the order $PEt_3 > PEt_2Ph > PEtPh_2 > PPh_3$ and that steric properties of the phosphines seem to be of minor importance.[130]

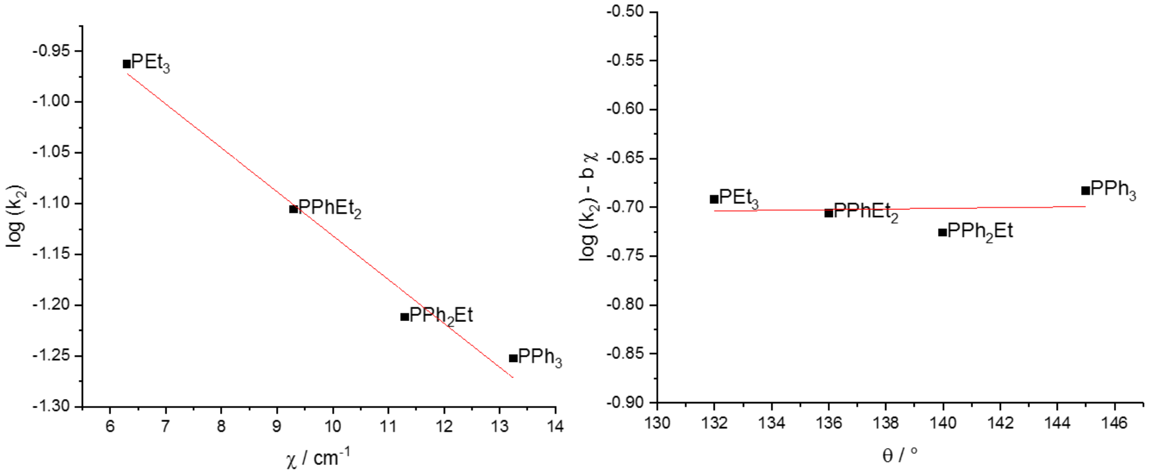

*Figure 3-4: Reaction of $[MoO_2(mnt)_2]^{2-}$ with different phosphines. Left: Correlation between the reaction rate and the electronic parameter χ. Right: Steric profile, no dependence of the cone angle ϑ. Data from Lorber at al.*[130]

### 3.1.2.3 Extending the understanding of the thermal mechanism

**Dissociation of the phosphine oxide**

Scheme 3-1 shows that after the phosphine oxide is formed it has to dissociate from the complex and the available coordination side filled by the sulfoxide or a solvent molecule.

Kail and co-workers have investigated the exchange of the phosphine oxide for a solvent molecule (Scheme 3-2) after reaction of [$MoO_2L(OPh)$] (L = *hydrotris(3-isopropylpyrazol-1-yl)borate*) with $PEt_3$ or $PMePh_2$.[121] Based on calculations a dissociative or dissociate interchange path are both possible. The rate limiting step was found to be the dissociation of the phosphine oxide. Their calculations also suggested a nucleophilic attack by the Mo=O oxygen onto the P-C bond. Importantly, the actual reaction path depends on the solvent and substrate.

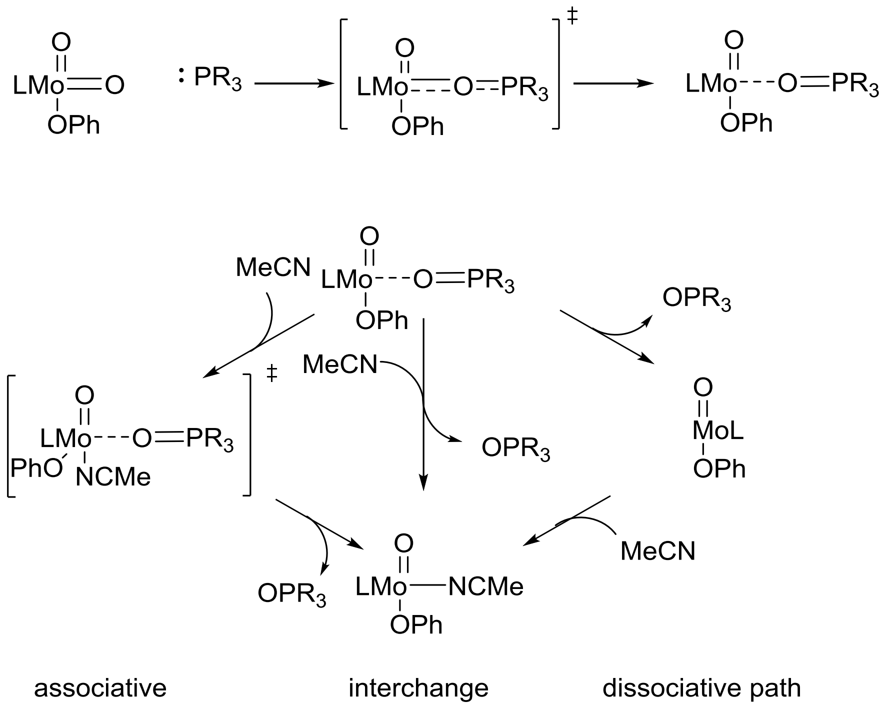

*Scheme 3-2: Pathways for the OAT from [$MoO_2L(OPh)$] (L =* hydrotris(3-isopropylpyrazol-1-yl)borate*) to $PR_3$ (R = $Et_3$, $Ph_2Me$) in MeCN.* [121]

**Potential catalyst deactivation: dimerisation**

At the stage where the phosphine oxide dissociates instead of the binding of solvent or the sulfoxide a third possibility has been observed.

OAT from a molybdenum(VI) complex onto a phosphine formally yields a reduced Mo(IV) species that is then reoxidised by the sulfoxide. But already in the work of Barral *et al.*, the first recognised OAT reaction with molybdenum,[12] it was proposed that Mo(IV) reacts with Mo(VI) following Scheme 3-3 to yield a binuclear Mo(V) species.[131] In their work with Mo dithiocarbamate complexes, the Mo(V) species was detected by UV-Vis spectroscopy both during reduction of the Mo(VI) complex with $PBu_3$ and in the oxidation of the Mo(IV) with $O_2$. Eventually, in each case only the Mo(IV) or Mo(VI) species were obtained showing that the formation of Mo(V) is reversible. Note that these dimers are different from those mentioned in section 2.3.5 which contain molybdenum(VI) and two bridging oxygens.

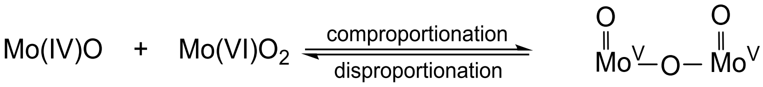

*Scheme 3-3: Formation of dimeric Mo(V) from monomeric Mo(IV) and Mo(VI)*

The formation of Mo(V) has been seen with many different complexes and is not always reversible, nor is a Mo(V) species necessarily catalytically inactive.[132] This process has not been seen in molybdenum enzymes as the molybdenum centres are embedded within the protein and preventing association. Attempts to supress the formation of Mo(V) have been made. Sterically demanding ligands have been shown to prevent dimerisation. For example, the introduction of *iso*-propyl groups on **3-1** shown in Figure 3-5 prevented formation of the Mo(V) dimer. In the reaction with excess $PMe_3$ both **3-1** and **3-2** eventually yielded the reduced Mo(IV) complex, but formation of the Mo(V) dimer intermediate was only observed with **3-1**.[133] Another option is to separate the molybdenum centres by attaching them onto a solid support e.g. a polymer [134], silica[135], or activated carbon.[135]

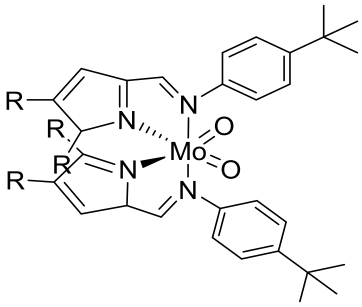

**3-1** R = H
**3-2** R = iPr

*Figure 3-5:Structure of two molybdenum complexes used to study the influence of bulky substituents on dimerization.[133]*

Determining whether Mo(V) is formed or not has proven challenging. It was thought for long time that the sterically demanding phenyl groups as well as the use of sulfur ligands prevents the formation of Mo(V) upon reduction of **3-3**. [136–138] Later studies by Doonan and co-worker showed however that the proposed reduced molybdenum(IV) species was misidentified and was in fact the Mo(V) dimer.[139] The initial identification relied on IR spectroscopy, elemental analysis and UV-Vis spectroscopy. Analysis of this data by Doonan and co-workers revealed inconsistency with the assignment of a Mo(IV) complex, and a newly obtained crystal structure confirmed the reduced form of **3-3** to be the dimer 3-4.

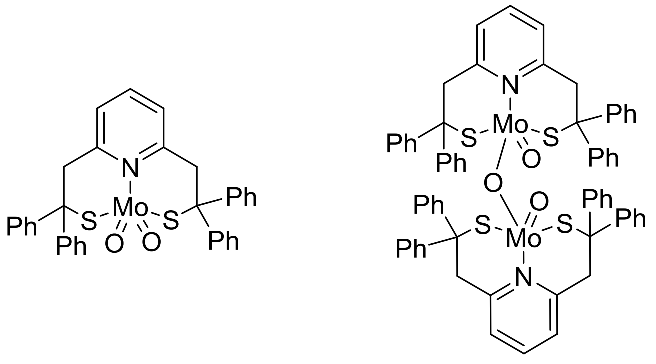

**3-3** **3-4**

*Figure 3-6: **3-3**, a model for the active site of sulfite oxidase designed by Holm and Berg.*[136]

## Molybdenum as a Lewis acid: alternative reaction path

Considering molybdenum(VI) as a Lewis acid makes different reaction pathways possible as the first step of the OAT process involves the coordination of one of the Lewis bases present in the reaction (phosphine, sulfoxide, solvent). Castiñeira Reis *et al.* [140] explored this mechanism computationally based on the work of Sanz *et al.*[141] on [$MoO_2Cl_2(DMF)_2$] reacting with DMSO and $PMe_3$. In the most favourable mechanism (Scheme 3-2), DMSO first coordinates to [$MoO_2Cl_2$] (DMF was considered labile under the experimental conditions, 80 °C, and to have dissociated from molybdenum; only [$MoO_2Cl_2$] was studied to simplify calculations) followed by the nucleophilic attack of the phosphorous on the Mo=O bond. DMS then eliminates, leaving its oxygen atom as the new oxo ligand of molybdenum. Finally, $OPMe_3$ dissociates, yielding the initial molybdenum complex.

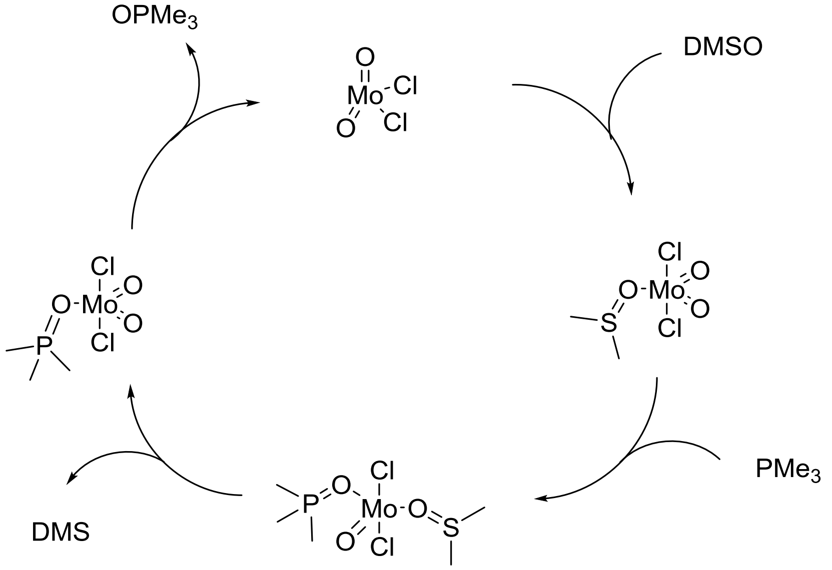

*Scheme 3-4: Proposed mechanism for the OAT from DMSO to $PMe_3$ catalysed by [$MoO_2Cl_2$].*[140]

Although these calculations are based on a simpler model, they are relevant to the SAP based complexes in this work.

In this thesis, OAT has been performed in DMSO (catalyst screening) or acetone (substrate scope and reaction kinetics). The complexes, *e.g.* **Mo-2**, have weakly bound MeOH in the sixth coordination site which can be replaced by the solvent of the OAT reaction, DMSO or acetone. The binding of DMSO could result in the reaction following a path similar to the one proposed above. In acetone, the reaction could follow a mechanism without sulfoxide binding, although sulfoxide is present in 300-fold excess. Both processes could also be taking place in parallel or there could be a transition depending on sulfoxide concentration.

### 3.1.3 Conclusion and chapter aims

At the start of this project many examples of thermal OAT were known, some requiring high temperatures to activate the reaction. Examples of photoactivated OAT, that could use milder conditions were rare and all have disadvantages ranging from preparation of the complex to its performance.

While some parameters like the influence of the ligand have been studied extensively and generalised for molybdenum catalysed OAT, uncertainty in the reaction mechanism as well as high dependence of reaction outcome, like dimerisation, on the complex, solvent and other parameters remains.

The aim of this chapter is to determine the catalytic activity of the synthesised complexes in OAT reactions, study the influence of the different substituents and correlate the electronic, structural and spectroscopic properties to the activity. Further studies on the substrate scope as well as mechanistic investigation will then be performed with the aim to understand the underlying mechanism of photoactivated OAT and differences to the well-known thermal OAT.

## 3.2 Screening of complexes and experimental conditions for OAT between DMSO and $PPh_3$

### 3.2.1 Screening of complexes

Initial screening of the complexes synthesised in this work as an OAT catalyst was undertaken on an NMR scale reacting $PPh_3$ in DMSO-$d_6$ using 1 mM catalyst and 300 mM $PPh_3$.

Irradiation was performed using light at three different wavelengths, 360, 410 and 465 nm. This choice was based on the UV-vis spectra of **Mo-1** and **Mo-2** and the availability of LEDs. **Mo-1** and **Mo-2** show absorption maxima at 421 and 408 nm and 353 and 347 nm, respectively. 465 nm was chosen to excite only one transition as there is significant overlap between the two bands at 360 and 410 nm. (see section 4.2)

$^1H$ NMR spectra were recorded before irradiation and after 3 h. Integration of the signals from the aromatic protons in $PPh_3$ and $OPPh_3$ allowed the conversion to be calculated. The results are shown in Table 3-8 below.

*Table 3-1 Conversion of $PPh_3$ to $OPPh_3$ after 3h, catalysed by [Mo] and ]W}.*

| Complex | Conversion at a wavelength λ in % [b] | | |
|---|---|---|---|
| | 365 nm | 410 nm | 460 nm |
| **Mo-1**$^{H,H}$ | 0 | | |
| **Mo-2**$^{COOMe,COOMe}$ | 69 | 78 | 77 |
| **Mo-3**$^{COOH,COOH}$ | 32 | 35 | 32 |
| **Mo-4**$^{COOMe,Et2N}$ | 0 | | |
| **Mo-5**$^{COOMe,COOH}$ | 52 | 65 | 57 |
| **Mo-6**$^{COOH,COOMe}$ | 32 | 39 | 31 |
| **Mo-7**$^{COOH}$ | 7 | 12 | 12 |
| **Mo-8**$^{H,COOH}$ | 4 | 2 | 2 |
| **Mo-9**$^{COOMe}$ | 30 | 28 | 19 |
| **Mo-10**$^{H,COOMe}$ | 5 | 2 | 2 |
| **Mo-11**$^{COOMe}$ | | 23 | |
| **Mo-12**$^{NO2}$ | | 32 [b] | |
| **Mo-13**$^{CF3}$ | | 25 | |
| **Mo-14**$^{SO2NH2}$ | | 11 | |
| **Mo-15**$^{H,NEt2}$ | 0 | | |
| **Mo-16**$^{Naph}$ | 0 | | |
| **W-1**$^{H,H}$ | 8 | 12 | 10 |
| **W-2**$^{COOMe,COOMe}$ | 62 | 79 | 45 |

In DMSO-$d_6$, under $N_2$, c([Mo])= 1 mM, c($PPh_3$) = 300 mM, irradiation with a light source of the stated wavelength. [a] An uncertainty in the measurement of 3 % is estimated [b] Catalyst deactivation observed, lower conversion obtained from a repeat of the experiment.

The conversion obtained with molybdenum complexes ranged from 0 % to 78 %. The highest conversion was obtained with **Mo-2**. Complexes **Mo-1**, **Mo-4**, **Mo-15** and **Mo-16** were inactive. Conversion obtained with the tungsten complexes ranged from 8 % (**W-1**) to 79 % (**W-2**).

The unsubstituted complex **Mo-1** is known to transfer oxygen to $PEtPh_2$, but not to $PPh_3$.[142] This inactivity could not be overcome under LED irradiation.

Conversion varied with wavelength for individual catalysts although not all complexes were tested at 365 and 460 nm.

A detailed analysis of the results with regard to the aims set out at the beginning of this chapter can be found in section 3.3. In order to facilitate this analysis several control experiments were performed. Reaction between DMSO and $PPh_3$ in the absence of catalyst, both thermal and under irradiation, as well as the thermal reaction in the presence of catalyst; the ligand acting as catalyst or photo sensitizer; the effect of reaction temperature due to thermal heating from the LED, as well as the effect of air and water on the reaction.

To allow meaningful comparison between close results obtained with two complexes a simple statistical analysis was performed.

## 3.2.2 Reproducibility of OAT experiments

The differences in catalyst activity listed in Table 3-8 only accounts to a few percent in some cases (e.g. between **Mo-11** and **Mo-13**). It is therefore important to know the error in those measurements and how much the result can vary. Table 3-2 and Table 3-3 list the conversions measured in several repeat experiments at various points during this project under the same conditions for the reaction of **Mo-2** with $PPh_3$ in DMSO-$d_6$ and of **Mo-2** with $PPh_3$ and **SO-2** (di-*p*-tolyl sulfoxide) in acetone-$d_6$.

*Table 3-2: Conversion of $PPh_3$ to $OPPh_3$ in DMSO-$d_6$ after 3 h catalysed by **Mo-2**.*

| Experiment | Conversion / % |
|---|---|
| 1 | 75 |
| 2 | 77 |
| 3 | 81 |
| 4 | 77 |
| 5 | 76 |
| Mean $x_{avg}$ | 77 |
| Range R | 6 |
| Uncertainty in measurement $\Delta x$ | 3 |

Conditions: c(**Mo-2**) = 1 mM, c($PPh_3$) = 300 mM, in DMSO-$d_6$, $N_2$, irradiation at 410 nm.

*Table 3-3: Conversion of $PPh_3$ to $OPPh_3$ in acetone-$d_6$ after 3 h catalysed by **Mo-2**.*

| | |
|---|---|
| 1 | 46 |
| 2 | 46 |
| 3 | 45 |
| 4 | 47 |
| 5 | 43 |
| 6 | 44 |
| 7 | 45 |
| Mean $x_{avg}$ | 45 |
| Range R | 4 |
| Uncertainty in measurement $\Delta x$ | 2 |

Conditions: c(Mo-2) = 1 mM, c($PPh_3$) = 300 mM, c(**SO-2**) = 300 mM, in acetone-$d_6$, $N_2$, irradiation at 410 nm.

As can be seen the results are fairly consistent, spanning a range of 6 % and 4 %, respectively. These experiments were performed with different batches of **Mo-2** and solvents showing that synthesis of the complex as well as degassing and drying of the solvents was reproducible (see the subsequent sections).

Given the sample sizes of 5 and 7, statistical analysis was done as follows:

$$R = x_{max} - x_{min}$$

*Equation 3-4*

$$\Delta x = R/2$$

*Equation 3-5*

with R = range, Δx = uncertainty in a measurement, N = number of samples.

This gives a range of 6 % and an uncertainty in a measurement of 3 % (reaction in DMSO-$d_6$, Table 3-2) and a range of 4 % and an uncertainty of 2 % (reaction in acetone-$d_6$, Table 3-3), respectively.

Results from the analysis of the data obtained from OAT with **Mo-2** is applied to all other experiments where usually only a single data point was obtained. Particularly, the conversion obtained in all other experiments is assumed to have an uncertainty based on the above calculations.

It follows that the mean conversion obtained in two experiments under similar conditions, $x_{1mean} < x_{2mean}$, *e.g.* between two different complexes, are taken as significantly different if the range of conversion for the two experiments does not overlap, or if the difference of the means is greater than twice the uncertainty, respectively, that is

$$x_{2\,mean} - x_{1\,mean} > 2 * \Delta x$$

*Equation 3-6*

However, except for the two examples listed above, conversions obtained in this work are based on only one experiment and so an individual result does not equal the average. This complicates the use of Equation 3-6. Assuming the uncertainty in a measurement Δx applies, conversion $x_1$ could be greater or smaller than the true average by Δx , *i.e.* $x_{1mean} – \Delta x \leq x_1 \leq x_{1mean} + \Delta x$. The same applies to $x_2$.

There are two extreme cases to be considered when comparing the conversion $x_1 < x_2$ observed in two experiments:

a) $x_1$ is at the lower end of the range, and $x_2$ at the higher end:

$x_{1mean} = x_1 + \Delta x$ and $x_{2mean} = x_2 – \Delta x$, hence $x_{2mean} – x_{1mean} = x_2 - \Delta x - x_1 – \Delta x = x_2 - x_1 - 2 * \Delta x$

which according to Equation 3-6 should be greater than 2 * Δx. It follows that

$x_2 - x_1 > 4\ \Delta x$ for the conversions to be significantly different

b) $x_1$ is at the higher end of the range, and $x_2$ at the lower end.

$x_{1mean} = x_1 - \Delta x$ and $x_{2mean} = x_2 + \Delta x$.

It follows that

$x_2 - x_1 > 0$ for the conversions to be significantly different

Between these two extreme cases, replacing the mean conversion with the measured conversion in Equation 3-6 provides a middle ground for estimating significant differences. The possibility of outliers towards either of the extreme cases should still be considered.

Twice the uncertainty of a measurement amounts to 6 in the case of reactions done in DMSO-$d_6$ (conditions in Table 3-2) and to 4 in the case of reactions done in acetone-$d_6$ (conditions in Table 3-3).

### 3.2.3 OAT between DMSO or di-*p*-tolyl sulfoxide and $PPh_3$ in the absence of catalyst

As a negative control, OAT between sulfoxide and $PPh_3$ in the absence of catalyst was studied under thermal conditions as well as under irradiation with light of 365, 410 and 460 nm wavelength.

In the first experiment, similar to catalyst screening, solutions of 300 mM $PPh_3$ in DMSO-$d_6$ were irradiated at three different wavelengths and $^1H$ NMR spectra recorded after 3 h. A fourth sample was stored in the dark for the same time and analysed; the spectra are shown below.

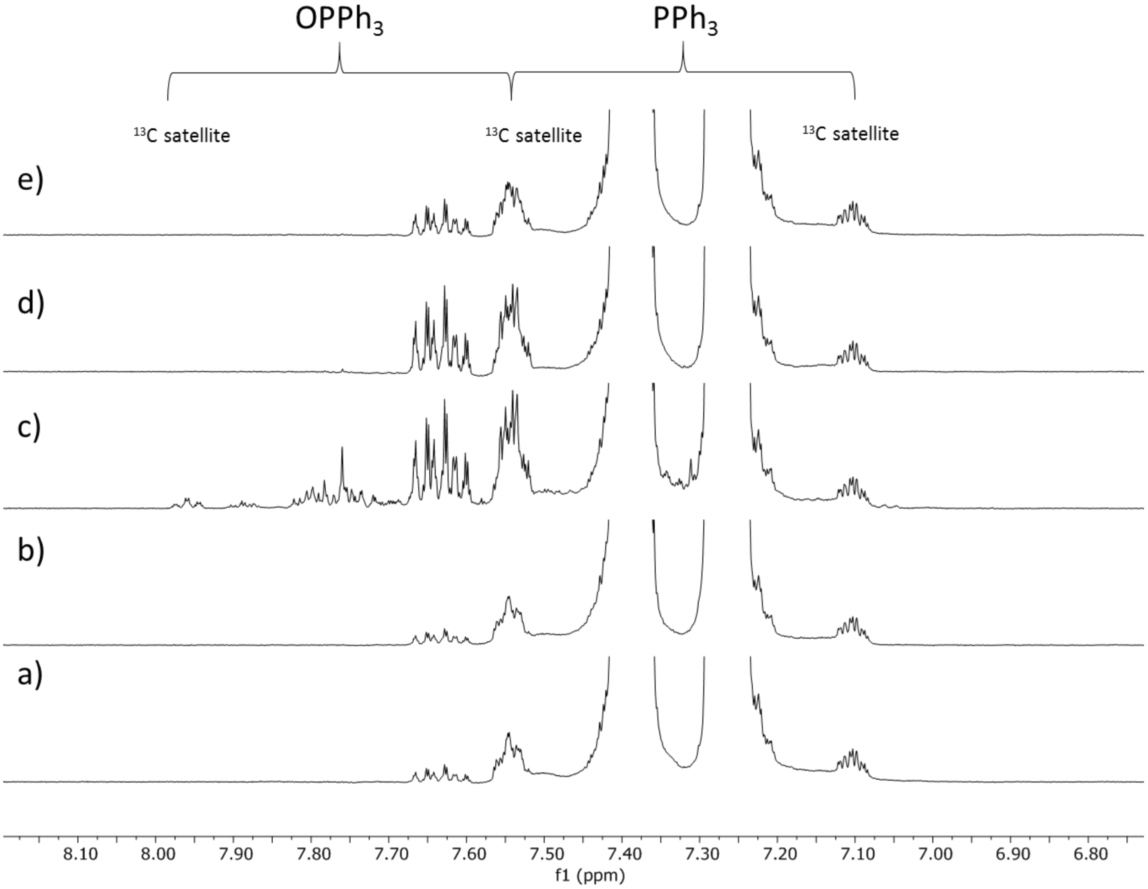

*Figure 3-7: $^1$H NMR spectra in the aromatic region of samples containing 300 mM $PPh_3$ in DMSO-$d_6$. a) as prepared; b) after 3 h , no irradiation; c) after 3 h at 365 nm; d) after 3 h at 410 nm e) after 3 h at 460 nm.*

While the spectra in Figure 3-7 show a noticeable change in the samples that were irradiated for 3 h, especially the sample at 365 nm (spectrum c), the amount of $OPPh_3$ formed is negligible, conversion only amounted to 1-2 %. No change occurred without irradiation.

In the second experiment, OAT was studied on a longer timescale. A sample containing 300 mM di-*p*-tolyl sulfoxide (***SO*-2)** and 300 mM $PPh_3$ in acetone-$d_6$ was irradiated for a total of 48 h at 410 nm. A second sample was stored in the dark. The reaction was monitored over a total of 70 h by $^1$H NMR spectroscopy, shown in Figure 3-8.

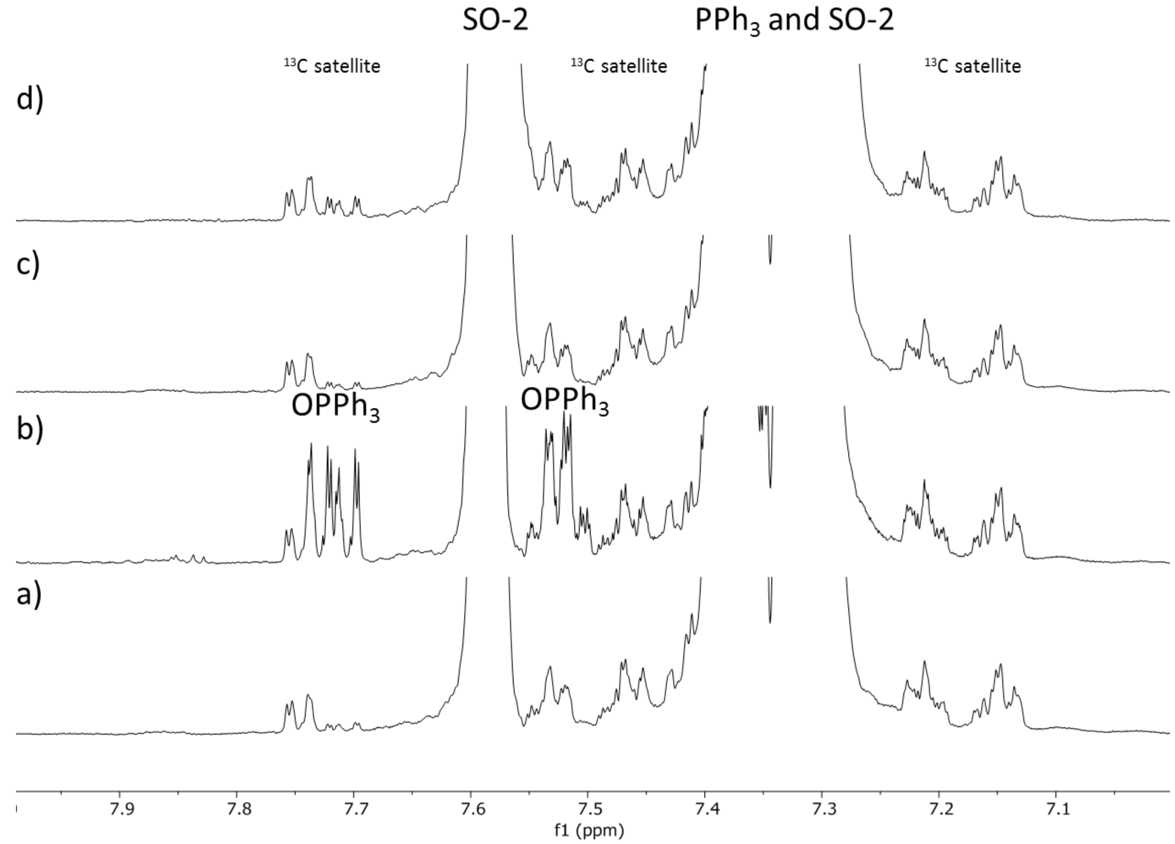

*Figure 3-8: $^1$H NMR spectra of samples containing 300 mM **SO-2** and 300 mM $PPh_3$ in acetone-$d_6$. a) sample 1 as prepared, b) sample 1 after 70 h including 48 h of irradiation at 410 nm, c) sample 2 as prepared, d) sample 2 after 70 h without irradiation.*

The non-irradiated sample remains practically unchanged even after a substantial reaction time of 70 h. The sample irradiated for 48 h on the other hand clearly shows a change but the amount of $OPPh_3$ formed (1 %) is still negligible.

The two experiments presented confirm that the uncatalysed reaction between sulfoxides and $PPh_3$ is negligible and does not affect the study of catalysts.

### 3.2.4 Thermal molybdenum catalysed OAT between *p*-tolyl sulfoxide and $PPh_3$

As presented in the introduction to his chapter, thermal OAT between sulfoxides and phosphines catalysed by molybdenum complexes is well known. It is therefore important to test to what extent the complexes studied in this work are able to catalyse thermal OAT, so that this activity can be separated from photo catalytic activity. Even if the photocatalysed reaction is dominant there could be a significant contribution from the thermal reaction during periods without irradiation, for example between irradiation intervals or during recording of NMR spectra.

A sample containing 1 mM of **Mo-2**, 300 mM of $PPh_3$ and 300 mM of **SO-2** in acetone-$d_6$ under $N_2$ was prepared and monitored by $^1$H NMR spectroscopy over 70 h. $^1$H NMR spectra recorded at the start and after 70 h are shown in Figure 3-9. No changes were observed, particularly, no formation of phosphine oxide and sulfide or decomposition of **Mo-2.**

Similar control experiments were also performed with **Mo-2, W-1** and **W-2** in DMSO-$d_6$ over 3 h. No changes were observed. Thus, thermal OAT at room temperature catalysed by molybdenum or tungsten complexes does not appear to take place, OAT observed in this work consequently results from photoactivation.

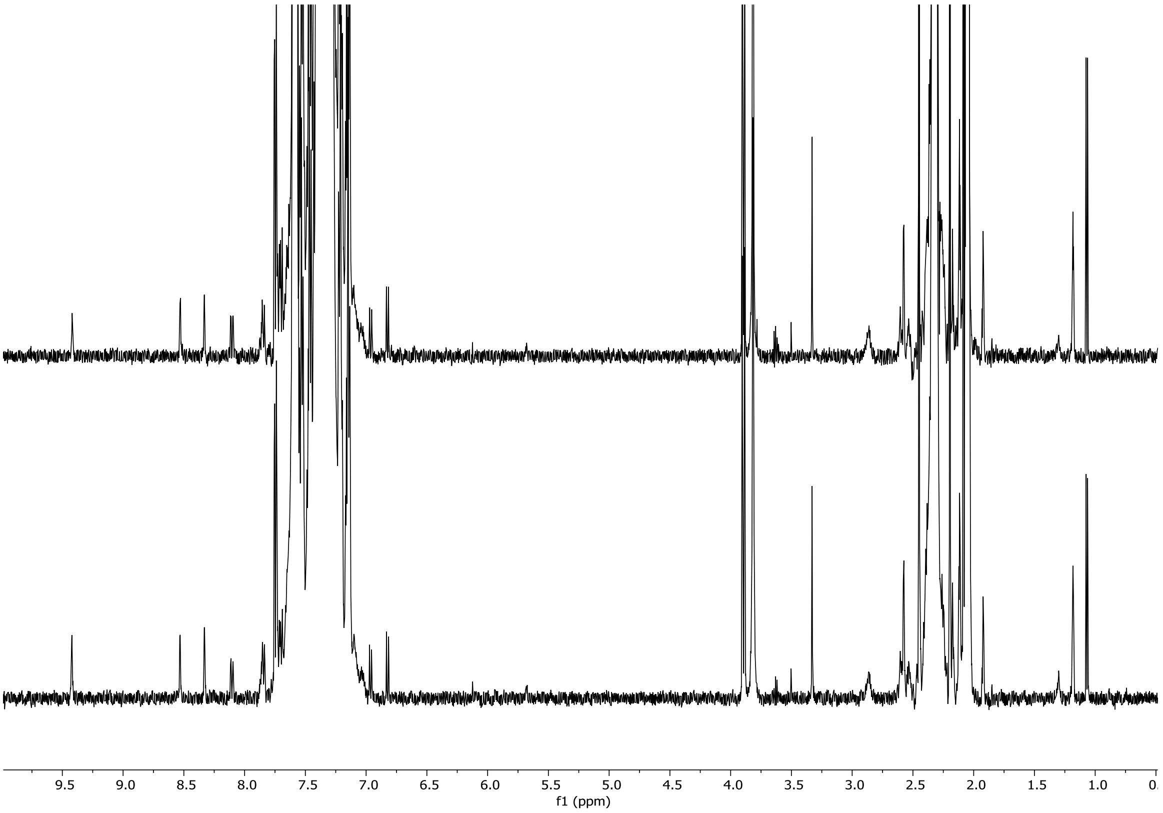

*Figure 3-9: $^1H$ NMR spectra of a sample containing 300 mM $PPh_3$, 300 mM **SO-2** and 1 mM **Mo-2** in acetone-$d_6$ as prepared (bottom) and after 70 h, without irradiation (top).*

## 3.2.5 Ligand catalysed OAT between DMSO and $PPh_3$

To confirm that the OAT activity is due to the molybdenum complex and not just due to the ligand, experiments analogous to those described in section 3.2.1 were performed with ligands **L-1, L-2** and **L-3** instead of the corresponding molybdenum complexes. Conversion of $PPh_3$ to $OPPh_3$ after 3 h is reported and discussed below.

*Table 3-4: Conversion of $PPh_3$ to $OPPh_3$ after 3 h of irradiation in the presence of ligands* ***L-1***, ***L-2*** *and* ***L-3*** *and complexes* ***Mo-1***, ***Mo-2*** *and* ***Mo-3***.

| Compound | Conversion [a] at a wavelength λ in % | | |
|---|---|---|---|
| | 365 nm | 410 nm | 465 nm |
| **L-1**$^{H,H}$ | 0 | 0 | 0 |
| **L-2**$^{COOMe,COOMe}$ | 0 | 6 | 7 |
| **L-3**$^{COOH,COOH}$ | 0 | 2 | 3 |
| **Mo-1**$^{H,H}$ | 0 | 0 | 0 |
| **Mo-2**$^{COOMe,COOMe}$ | 69 | 78 | 77 |
| **Mo-3**$^{COOH,COOH}$ | 32 | 35 | 32 |

c(**L-X/Mo-X**) = 1 mM, c($PPh_3$) = 300 mM, DSMO-$d_6$, $N_2$. [a] An uncertainty in the measurement of 3 % can be assumed.

No conversion was observed in the samples with **L-1** added. Only the sample at 365 nm had changed, its colour had gone from pale yellow to orange and in the $^1$H NMR spectrum, the resonances due to the two phenolic protons and the imine proton had disappeared, and some signals in the aromatic region had disappeared (at 6.95 and 7.00 ppm) while new ones had appeared (three groups of signals at 7.75, 7.8 and 7.95 ppm).

All three samples with **L-2** added changed colour from yellow to orange with the sample at 365 nm having the darkest colour. Again, no phosphine oxide was detected at 365 nm. Noticeable amounts, however, were detected at 410 and 460 nm, 6 and 7 % respectively. The $^1$H spectra of all three samples showed shifting of the signals, the resonances due to the imine group proton moved downfield, whilst the aromatic signals moved upfield; the shift is highest in the 365 nm sample.

Only small amounts of oxidised phosphine were detected at 410 and 460 nm in the samples with **L-3** added. No phosphine oxide was detected at 365 nm, instead shifting and broadening of the ligand signals suggest degradation of the ligand. The samples colour also changed from yellow to dark orange.

When the **SAP**-based ligands **L-1, L-2** and **L-3** were used instead of the metal complexes, a small amount of $OPPh_3$ formed in some cases. Similarly, to the complexes, **L-1** was inactive, and **L-2** showed higher conversion than **L-3**. In all cases there were signs of side reactions (changes in colour, changes in the NMR spectra). Hydrolysis of the imine bond, as well as isomerisation of the double bond are possible reactions but no evidence for their occurrence was found. Hydrolysis of the ligands produces an aldehyde, whose characteristic signal was not seen in the $^1$H NMR spectrum. The complete absence of resonances above 8 ppm in the sample containing L-1 and irradiated at 365 nm is surprising as it suggests the absence of any aldehyde, imine or phenol groups and degradation further than hydrolysis of the imine bond.

Only 3 % conversion of phosphine was observed in the samples containing **L-2** which is comparable to the amount observed in the uncatalyzed reaction between $PPh_3$ and sulfoxide (section 3.2.3) and therefore cannot account for the complex catalysed data. In samples containing **L-3** conversion of phosphine amounted to 7 % corresponding to 11 % of the amount obtained with the corresponding molybdenum complex under the same conditions, which is significant. However, this activity of the ligands occurred at the cost of their degradation and should not be relevant in the reaction of complexes, where no degradation was observed.

## 3.2.6 Temperature dependence of molybdenum-catalysed OAT between DMSO and $PPh_3$

On the irradiation it was noticed that the NMR tubes became warm due to the heat being produced by the circuitry within the reactor.

The temperature inside an NMR tube was monitored by an immersed probe during irradiation over 1 h which stabilised at 43-45°C.

In a control experiment the effect of the heating was studied. 1 mM of **Mo-2**, 300 mM of $PPh_3$ in DMSO-$d_6$ was heated in a water bath at 45 °C for 1 h. No change was observed. The activity of complexes is therefore due to the irradiation not the increased temperature although the latter could have an additional benefit compared to irradiation at room temperature.

## 3.2.7 Influence of water on molybdenum-catalysed OAT between p-tolyl sulfoxide and $PPh_3$

Performing reactions in water rather than an organic solvent is advantageous from a green chemistry perspective. However, not all catalytic systems tolerate water (if solubility is not an issue already). To study the stability of the molybdenum complexes in water OAT from *para*-tolyl sulfoxide (**SO-2**) to $PPh_3$ was performed with added water. The conversion measured in this experiment is listed in Table 3-5 together with results from experiments without added water.

*Table 3-5: Conversion of $PPh_3$ to $OPPh_3$ after intervals of irradiation for three OAT experiments.*

| Experiment | 1<br>with added water | 2<br>no water added | 3<br>no water added |
|---|---|---|---|
| Total duration of irradiation / h | Conversion [a] / % | | |
| 3 | 41 | 43 | 46 |
| 5 | 48 | 55 | |
| 9 | 56 | | 71 |

Conditions: c(**Mo-2**) = 1 mM, c($PPh_3$) = 300 mM, c(**SO-2**) = 300 mM, c($H_2O$) = 50 mM (concentration of additional $H_2O$ in experiment 1), acetone-$d_6$, $N_2$, irradiation at 410 nm. [a] An uncertainty in the measurement of 3 % can be assumed.

After the first 3 h interval of irradiation the conversion in the presence of water is not significantly different from that in the water free experiments. After a total of 5 h, but especially after a total of 9 h of irradiation, the addition of water has led to a decreased conversion by 7 and 15 %, respectively. The decrease in conversion shows that the reaction is affected by a 50 mM concentration water, either through inhibition or decomposition of the catalyst. The $^1H$ NMR spectra in the region of 6 to 10 ppm (Figure 3-10) show changes to the catalyst after irradiation, a new resonance appears at 9.15 ppm while signals in the aromatic region shift and become weaker. The signals in the topmost spectrum, after a total irradiation time of 9 h, are also much weaker almost disappearing in the background.

One conceivable way of catalyst decomposition is through hydrolysis of the imine bond (the back reaction of the Schiff base synthesis, see scheme 2-2, chapter 2). The resulting aldehyde should have a resonance at around 10 ppm which was not observed. It is not clear however, where this resonance would be expected if the aldehyde is still bound to the metal. Additional reactions under the experimental conditions are possible, water could bind to the complex (replacing solvent) yielding the aqua or, after further deprotonation, the hydroxide complex.

Although its exact role is not known, the presence of (large) volumes of water negatively effects OAT using the complexes studied.

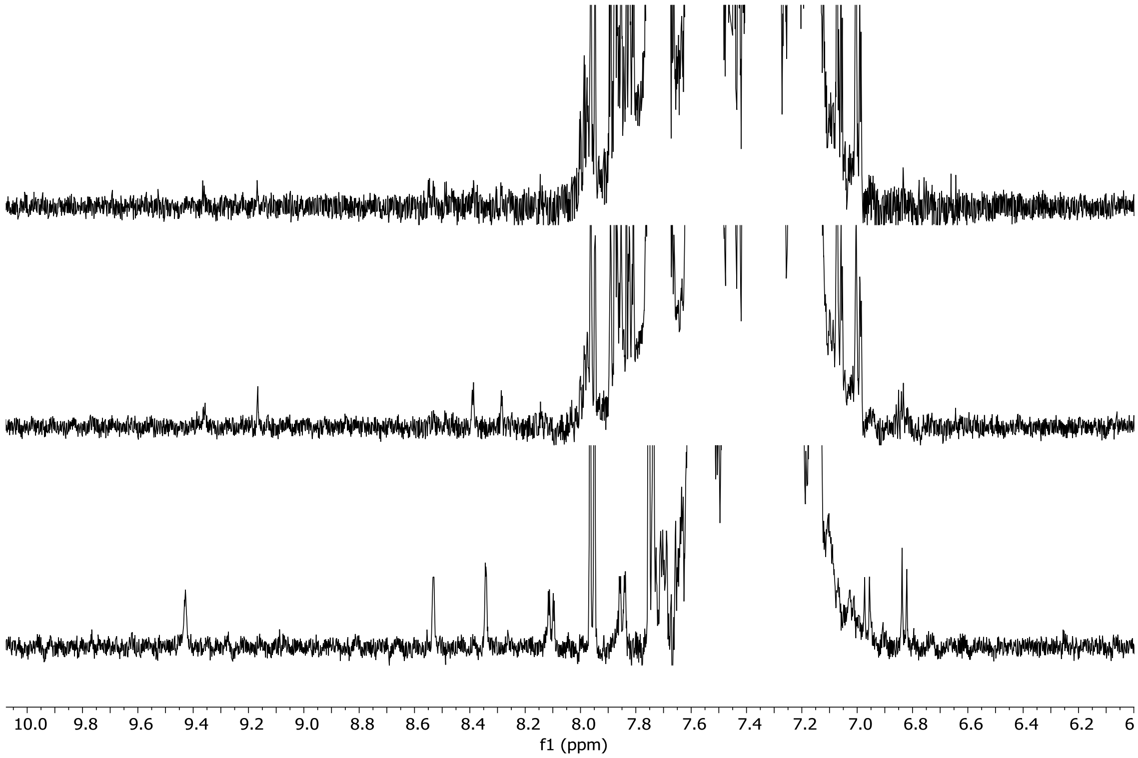

*Figure 3-10: $^1$H NMR spectra in acetone-$d_6$ of OAT between $PPh_3$ and **SO-2** catalysed by **Mo-2** in the presence of water before irradiation (bottom), after 5 h of irradiation (middle) and after 9 h of irradiation (top). Conditions: c(**Mo-2**) = 1 mM, c($PPh_3$) = 300 mM, c(**SO-2**) = 300 mM, c($H_2O$) = 50 mM, acetone-$d_6$, $N_2$, irradiation at 410 nm.*

## 3.2.8 Influence of air on molybdenum catalysed OAT between DMSO and $PPh_3$

Although $O_2$ (air) would be a readily available oxygen source for OAT, the presence of oxygen presents an issue for the work in this project as explained below.

The reduction of sulfoxides, or other substrates, constitutes a main application of OAT. The reduction of oxygen through direct reaction with the phosphine or via the catalyst as a competing reaction is therefore undesirable in these studies. In mechanistic studies the potential formation of peroxo-complexes would introduce another mechanism of oxidation. Having a second mechanistic path in parallel complicates the mechanistic studies and could also lead to formation of undesired side products. Oxygen also needs to be excluded from the sample when half cycle experiments are performed, different sulfoxides are studied, or the concentration of the oxygen source needs to be varied.

Samples were prepared under air and OAT performed to determine the effect of the presence of oxygen. The first experiment used excess DMSO-$d_6$, while the second one employed 300 mM **SO-2** in acetone-$d_6$.

Table 3-6 lists the conversion calculated for the experiment with **SO-2** in acetone-$d_6$. Conversion was calculated for the reduction of **SO-2** and the oxidation of $PPh_3$. It should be noted that the statistical analysis performed earlier considered at repetitions of an experiment, and not the agreement between the conversion of $PPh_3$ to $OPPh_3$ and sulfoxide to sulfide within the same sample. In the absence of any experimental error such as an oxygen leak, conversion of phosphine and conversion of sulfoxide generally differed by 0.5 %, in some cases up to 2 %.

A difference of 9 % between reduction and oxidation was seen in the sample containing **Mo-2** and considered to be significant, meaning that some of the $OPPh_3$ contains oxygen not originating from the sulfoxide but from molecular oxygen (and ignoring the 1 mM $OPPh_3$ where the oxygen stems from the catalyst). Whether the OAT from molecular oxygen to $OPPh_3$ was catalysed by **Mo-2** or not has not been determined. The conversion of 4 % in the catalyst free sample might suggest that **Mo-2** is not required, but this amount is not significant in comparison to the metal complex catalysed reaction.

*Table 3-6: Conversion of **SO-2** and $PPh_3$ after 3 h for samples prepared under air, one containing no catalyst and on containing 1 mM **Mo-2**.*

| | Catalyst | | No catalyst | |
|---|---|---|---|---|
| | $C_{14}H_{14}SO$ to $C_{14}H_{14}S$ | $PPh_3$ to $OPPh_3$ | $C_{14}H_{14}SO$ to $C_{14}H_{14}S$ | $PPh_3$ to $OPPh_3$ |
| Conversion [a] / % | 41 | 50 | 0 | 4 |

Conditions: c(**SO-2**) = 300 mM, c($PPh_3$) = 300 mM, acetone-$d_6$. [a] An uncertainty in the measurement of 3 % can be assumed

Conversions calculated in the experiment with excess DMSO-$d_6$ are shown in Table 3-7. Two sets of samples, one with and one without complex, were irradiated twice, at 365 or 460 nm, and also one sample each which was not irradiated at all. The samples that were not irradiated showed only negligible conversion.

The sample containing **Mo-2** gave conversions of 92 % (365 nm) and 87 % (460 nm) after 3 hours. The sample only contained 150 mM of $PPh_3$, comparison to results in Table 3-8 where samples were under $N_2$, are therefore difficult to make.

The effect of oxygen is evident in the samples without catalyst. Conversions of 16 and 20 %, respectively, were recorded after a total of 45 h including 3 h of irradiation which is a significant amount, much higher than in the relevant control experiments under $N_2$ (chapter 3.2.3) and could easily complicate data analysis.

In the sample irradiated at 460 nm conversion only occurred during the second cycle of irradiation and the subsequent storage time. In the second sample conversion occurred almost exclusively when the sample was not irradiated which would suggest that oxidation is independent of irradiation and slow, and therefore was only noticeable after the longer storage times. The two samples containing **Mo-2** did not show this inconsistent behaviour, oxidation of $PPh_3$ only occurred while the sample was being irradiated.

*Table 3-7: Conversion of $PPh_3$ to $OPPh_3$ at different points in time for samples prepared under air, one containing no catalyst and one containing 1 mM* ***Mo-2****.*

| Time / h | Time of irradiation / h | Conversion [a] / % | | | | | |
|---|---|---|---|---|---|---|---|
| | | Catalyst | | | No catalyst | | |
| | | 365 nm | 460 nm | dark | 365 nm | 460 nm | dark |
| 2 | 1 | 50 | 43 | 0 | 2 | 2 | 0 |
| 21 | 1 | 51 | 44 | 0 | 10 | 2 | 1 |
| 24 | 3 | 92 | 87 | 1 | 12 | 10 | 1 |
| 45 | 3 | 92 | 87 | 1 | 16 | 20 | 2 |

Conditions: c($PPh_3$) = 150 mM, DMSO-$d_6$, irradiation with light sources of the wavelength given or no irradiation at all. [a] An uncertainty in the measurement of 3 % can be assumed

Interestingly, the solubility of oxygen in DMSO and acetone is quite different: 0.33 mM in DMSO and 2.37 mM in acetone.[143] In both cases, the concentration of dissolved oxygen is much lower than the concentration of substrates used in OAT, so that oxygen has to be constantly supplied from the reaction headspace. Given that the liquid-gas surface is small compared to the volume of liquid the availability of oxygen is limited which could explain why high conversion was only observed after 21 h in the two samples no containing **Mo-2**.

While the exact processes are unclear, the experiments under oxygen certainly show that the exclusion of oxygen is necessary to achieve OAT exclusively from sulfoxides and to provide controlled conditions that allow for reproducible results. Use of molecular oxygen for OAT is still feasible, but more work is needed to account for the issues discussed.

### 3.2.9 Summary

The molybdenum and tungsten complexes synthesised were screened. To allow for meaningful analysis, several control experiments and a simple statistical analysis were performed. For all the conversions obtained throughout this work an uncertainty of 2 % (acetone-$d_6$) and 3 % (DMSO-$d_6$), respectively, will be estimated depending on the solvent used.

Control experiments revealed that OAT in the absence of catalyst, as well as thermal OAT in the presence of catalyst is not significant for the study of photoactivated catalysed OAT using the complexes described in this thesis. Residual oxygen and water have been shown to be competitive for OAT under controlled conditions.

With these parameters considered the data from the catalyst screening can be analysed.

## 3.3 Molybdenum and tungsten catalysed OAT between DMSO and $PPh_3$

The results from the screening of complexes are listed again in the table below and will be discussed in more detail with regard to the design choices presented in chapter 2.

*Table 3-8 Conversion of $PPh_3$ to $OPPh_3$ after 3h, catalysed by [Mo] and ]W}.*

| Complex | Conversion$^b$ at a wavelength λ in % | | |
|---|---|---|---|
| | 365 nm | 410 nm | 460 nm |
| **Mo-1**$^{\mathbf{H,H}}$ | 0 | | |
| **Mo-2**$^{\mathbf{COOMe,COOMe}}$ | 69 | 78 | 77 |
| **Mo-3**$^{\mathbf{COOH,COOH}}$ | 32 | 35 | 32 |
| **Mo-4**$^{\mathbf{COOMe,Et2N}}$ | 0 | | |
| **Mo-5**$^{\mathbf{COOMe,COOH}}$ | 52 | 65 | 57 |
| **Mo-6**$^{\mathbf{COOH,COOMe}}$ | 32 | 39 | 31 |
| **Mo-7**$^{\mathbf{COOH}}$ | 7 | 12 | 12 |
| **Mo-8**$^{\mathbf{H,COOH}}$ | 4 | 2 | 2 |
| **Mo-9**$^{\mathbf{COOMe}}$ | 30 | 28 | 19 |
| **Mo-10**$^{\mathbf{H,COOMe}}$ | 5 | 2 | 2 |
| **Mo-11**$^{\mathbf{COOMe}}$ | | 23 | |
| **Mo-12**$^{\mathbf{NO2}}$ | | 32 | |
| **Mo-13**$^{\mathbf{CF3}}$ | | 25 | |
| **Mo-14**$^{\mathbf{SO2NH2}}$ | | 11 | |
| **Mo-15**$^{\mathbf{H,NEt2}}$ | 0 | | |
| **Mo-16**$^{\mathbf{Naph}}$ | 0 | | |
| **W-1**$^{\mathbf{H,H}}$ | 8 | 12 | 10 |
| **W-2**$^{\mathbf{COOMe,COOMe}}$ | 62 | 79 | 45 |

In DMSO-$d_6$, under $N_2$, c([Mo])= 1 mM, c($PPh_3$) = 300 mM, irradiation with a light source of the stated wavelength. $^a$ Catalyst deactivation observed, lower conversion obtained from a repeat of the experiment. $^b$ An uncertainty in the measurement of 3 % is estimated.

### 3.3.1 The influence of electron withdrawing and electron donating substituents on photoactivated OAT catalysed by molybdenum and tungsten complexes

A positive correlation between electron withdrawing groups and catalyst activity is well established for thermal OAT (c.f. introduction to this chapter).[126–128] Substituents with different degrees of electron withdrawing or donating ability were therefore added to the **SAP**-based complex to test if similar correlation also applies to photoactivated OAT.

The Hammett parameter σ was used to quantify the electron withdrawing or donating capacity of the substituents (c.f. table 2-5, in chapter 2). For a given substituent σ takes different values if the substituent is in the *meta*- or *para*-position. The acid group in **Mo-7** is in the para position with regard to the phenol group and in the meta position with regard to the imine group. As both imine and phenol convey the electronic properties onto the metal centre, both positional considerations are valid. Two plots of the conversion against the Hammett parameter where therefore drawn accounting for the two options (Figure 3-11).

In both plots, a linear correlation between Hammett parameter and conversion is not observed, in contrast to reported thermal OAT. There is however an approximate non-linear correlation, the conversion increases as σ increases, *i.e.* - the more electron withdrawing the substituents become. In addition, there needs to be a net electron withdrawing effect acting on the metal centre of $\sigma > 0$ or $\sigma > 0.3$, respectively, depending on if σ is in regard to the phenol or imine group.

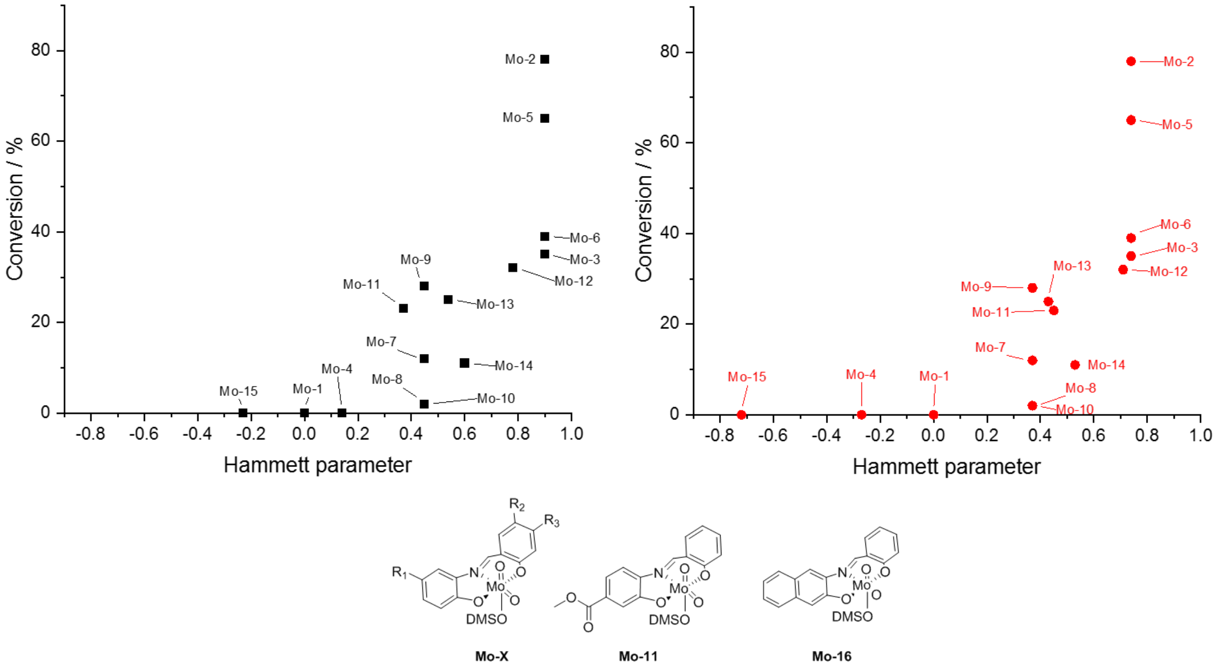

| $R_1$ | $R_2$ | $R_3$ | X |
|---|---|---|---|
| H | H | H | 1 |
| COOMe | COOMe | H | 2 |
| COOH | COOH | H | 3 |
| COOMe | H | NEt$_2$ | 4 |
| COOMe | COOH | H | 5 |
| COOH | COOMe | H | 6 |
| COOH | H | H | 7 |

| $R_1$ | $R_2$ | $R_3$ | X |
|---|---|---|---|
| COOH | H | H | 8 |
| COOMe | H | H | 9 |
| H | COOMe | H | 10 |
| NO$_2$ | H | H | 12 |
| CF$_3$ | H | H | 13 |
| SO$_2$NH$_2$ | H | H | 14 |
| COOMe | H | NEt$_2$ | 15 |

*Figure 3-11: Plot of conversion after 3 h ($OPPh_3$ / $PPh_3$) against Hammett parameter (top) and structures of complexes (bottom). Top left: substituent position para to phenol groups, top right: substituent position meta to imine group. In DMSO-$d_6$, under $N_2$, c([Mo])= 1 mM, c($PPh_3$) = 300 mM, irradiation at 410 nm.* ***Mo-16*** *has not been considered due to its different structure.*

Despite having the same Hammett parameter, the ester substituent led to higher activity than the acid as seen between **Mo-9** and **Mo-7**. Similarly, **Mo-7** and **Mo-8** both contain the carboxylic acid substituent, but in the former the substituent is on the amine ring whereas in the later it is on the aldehyde ring.

The lack of a clear linear correlation between the conversion and the Hammett parameter, as well as the shortcomings mentioned above, could mean that the latter is not suited to describe the electronic properties of the complexes. Indeed, one shortcoming of the Hammett parameter is that resonance effects are not accounted for. Improved Hammett parameters $\sigma_p^+$ and $\sigma_p^-$ were developed that take into account the ability of substituents to delocalise negative or positive charge.[113]

The plot in Figure 3-11 included all complexes except **Mo-16** due to its different structure which does not follow the pattern of substitution of the other complexes. However, excluding additionally **Mo-4, Mo-8, Mo-10** and **Mo-15,** an interesting trend appears. From Figure 3-12 a linear correlation is much more evident. Although **Mo-2**, **Mo-5** and **Mo-9** do not fit in, it appears that their catalytic activity is much higher than what would be expected from their Hammett parameter. Interestingly these three contain the ester substituent on the amine ring.

Complexes **Mo-4, Mo-8, Mo-10** and **Mo-15** could be excluded for the following reasons: Conversion obtained with **Mo-8** and **Mo-10** was only 2 % at 410 nm which is not significantly different from **Mo-1**. In addition, they contain their substituent on the aldehyde ring which, as discussed earlier, has much less effect on the catalytic activity. As conversion cannot be lower than zero, inclusion of complexes **Mo-4** and **Mo-15** is less helpful. Their true data points would need a negative conversion to match their negative Hammett parameter to align with a linear trend.

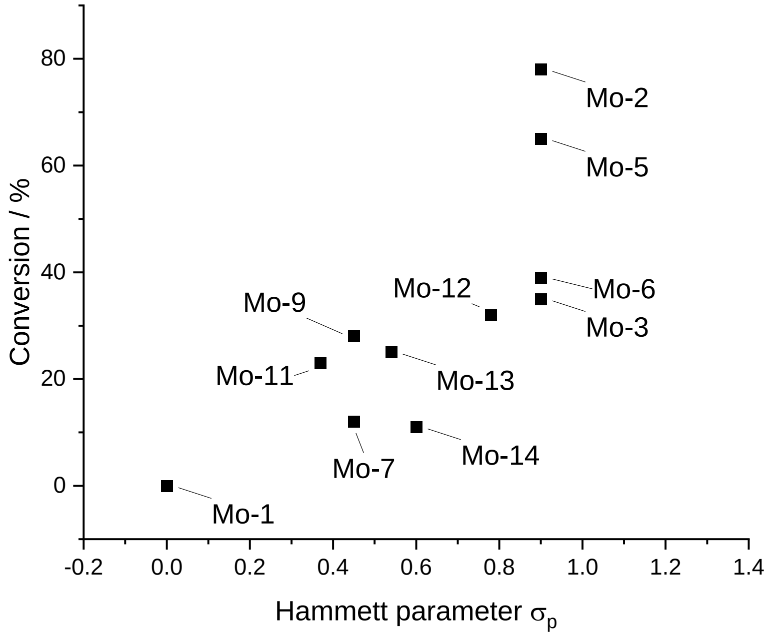

*Figure 3-12: Modified plot of conversion after 3 h ($OPPh_3$ / $PPh_3$) against Hammett parameter, substituent position para to phenol groups. In DMSO-$d_6$, under $N_2$, c([Mo])= 1 mM, c($PPh_3$) = 300 mM, irradiation at 410 nm. Complexes **Mo-4, Mo-8, Mo-10, Mo-15** and **Mo-16** have been omitted.*

An additional comment has to be made in regard to the acid substituents in **Mo-3**, **Mo-5**, **Mo-6 Mo-7** and **Mo-8**. So far it has been assumed that the acid groups are protonated in solution, which is not necessarily the case. The degree of deprotonation in DMSO is not known and the acidity of these groups, their $pK_a$ values, on the relevant complexes has not been measured. To get an estimate for the degree of deprotonation, benzoic acid will be used as a reference for which the $pK_a$ values is 4.2 in water and 11.1 in DMSO.[144]

The degree of deprotonation α can be obtained from Equation 3-7, where $c_0$ is the initial concentration of the acid. $[H_3O^+]$ is obtained from the equilibrium constant $K_a$ where $[HA] = c_0$ is assumed.

$$\alpha = \frac{[H_3O^+]}{c_0}$$

*Equation 3-7*

$$K_a = \frac{[H_3O^+] * [A^-]}{[HA]}$$

*Equation 3-8*

At an initial concentration of 1 mM, $\alpha < 1$ % in DMSO (which confirms the above assumption to be correct). In contrast 22 % of benzoic acid would be deprotonated in water. Benzoic acid is a very simple model. The conjugation on the ligands used in this work would stabilize the negative charge of a deprotonated acid group as would additional electron withdrawing groups like acids or esters in the case of the disubstituted ligands **L-3**, **L-5** and **L-6**. Complexation to molybdenum decreases the electron density on the ligand, as shown by the downfield shift of resonances in the $^1$H NMR spectrum (section 2.3.3), and therefore also stabilises the negative charge. Whether these effects are strong enough to lead to significant deprotonation of complexes is not clear, a substantial increase in acidity to a $pK_a < 4$ would be needed.

The above discussion considered the complexes (and the benzoic acid reference) to be the only compound dissolved in DMSO. During OAT however, phosphines are also present (and as OAT progresses, increasing amounts of phosphine oxide and DMS). The $pK_a$ value of $HPPh_3^+$, the conjugated acid of $PPh_3$, is 8.8 in MeCN whereas for benzoic acid it is 21.5 which clearly shows that benzoic acid would not be deprotonated by $PPh_3$.[144] Values in DMSO were not available but the trend is assumed to be the same given the large difference in $pK_a$ values.

The complexes themselves also contain the imine and oxo groups that could deprotonate the acids. Given that signals of protonated oxo or imine groups were not observed in the $^1$H NMR spectra of the complexes or ligands it seems unlikely that these sites are basic enough.

Based on the above analysis carboxylic acid substituents are probably protonated. However, the effect of excitation and subsequent processes that could lead to deprotonation have not been considered.

The electronic properties of the deprotonated acid are different from the protonated one, the negative charge makes this group more electron donating. This change is reflected in the Hammett parameter which takes a value of 0.0 for $COO^-$, from 0.45 for COOH, making this substituent essentially the same as not having a substituent at all. Clearly, that is not reflective of the reactivity.

The values of the improved Hammett parameter were obtained using substituted phenol and aniline , instead of benzoic acid like in the original Hammett parameter. Upon deprotonation the negative charge on the oxygen or nitrogen can be delocalised on the aromatic ring and the substituent resulting in an increased stabilisation by substituents with mesomeric effects that was not seen in the original work with benzoic acid.[113]

$\sigma_p^-$ values of the improved Hammett parameter for acid and ester substituents are listed in Table 3-9. This new value is higher than the previously used value for the ester / acid substituents in all cases. **Mo-2**, **Mo-3**, **Mo-5, Mo-6, Mo-7** and **Mo-9** contain acid or ester groups and so their corresponding Hammett parameters change.

*Table 3-9: Modified and normal Hammett parameters of acid and ester groups.*[113]

| Substituent | Modified Hammett parameter $\sigma_p^-$ | Hammett parameter $\sigma_p$ |
|---|---|---|
| COOH | 0.77 | 0.45 |
| $COO^-$ | 0.31 | 0.0 |
| COOMe | 0.64 | 0.45 |

Two plots of conversion against the modified Hammett parameter are shown in Figure 3-13, for protonated and deprotonated acid groups, respectively. A linear increase of conversion with the modified Hammett parameter is now more clearly seen in both cases, in line with findings on thermal OAT mentioned previously. A better correlation is obtained when the acid groups are assumed to be deprotonated which is in contrast to the above discussion on the degree of deprotonation but could be a result of photo excitation which was not accounted for in the discussion.

Regarding the plot including deprotonated acid groups, **Mo-14** is an outlier and the issue of distinguishing ring positions still remains as seen between **Mo-5** and **Mo-6**.

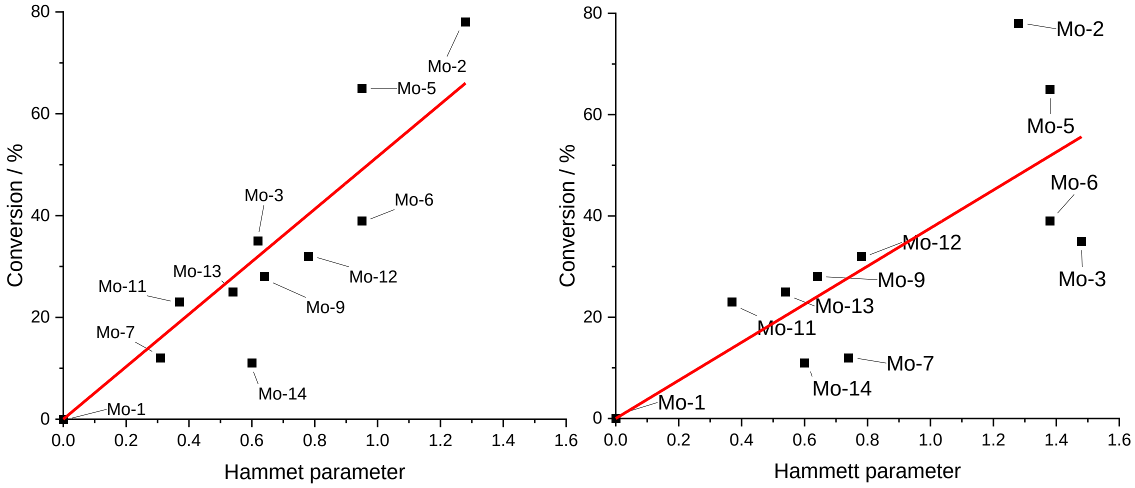

*Figure 3-13: Modified version of Figure 3-12 using the improved Hammett parameter $\sigma_p^-$ for the ester and acid substituents. Acid groups deprotonated (left, intercept set to 0, slope = (52 ± 4) %, $R^2 = 0.94$) and protonated (right, intercept set to 0, slope = (38 ± 5 ) %, $R^2 = 0.87$).*

Modified Hammett parameters have been calculated for $CF_3$, $NO_2$ and $SO_2NH_2$ substituents and the corresponding plots are shown in

Figure 3-14. Correlation has not improved compared to Figure 3-13 which suggests that the conjugation which the modified Hammett parameter accounts for is stronger with acid or ester substituents. The better correlation between conversion and the improved Hammett parameter when the ability of the ester and acid substituents to delocalise electron density is accounted for suggests that during catalysis substantial negative charge builds up on the complex and is stabilised by these substituent leading to higher conversion. This could occur in a transition state (e.g. after nucleophilic attack by the phosphine), but could also include the reduced, electron richer Mo(IV) (see Scheme 3-1 and Scheme 3-2)

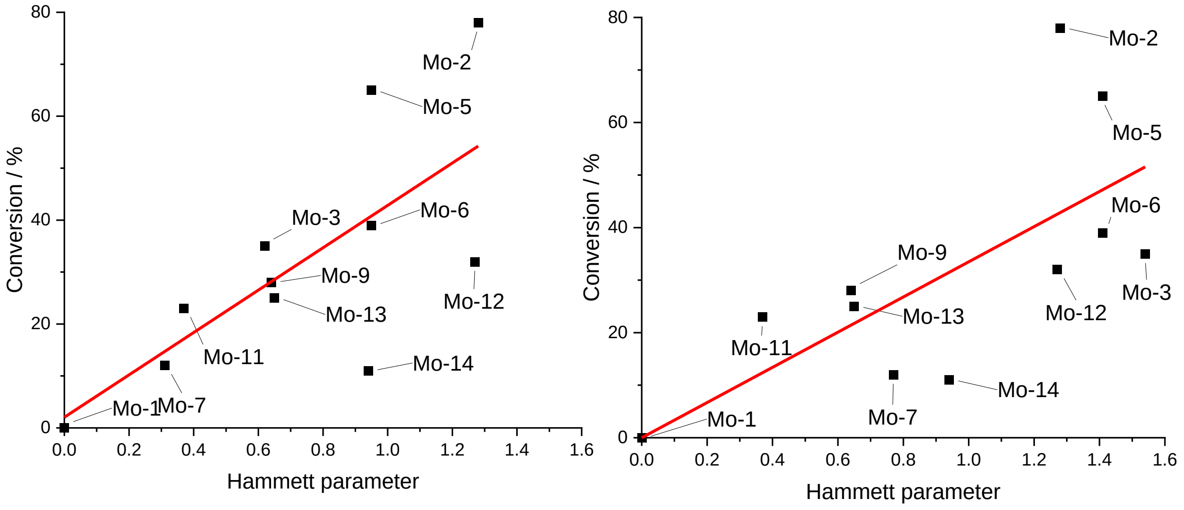

*Figure 3-14: Modified version of Figure 3-12 using the improved Hammett parameter $\sigma_p^-$ for all substituents. Acid groups deprotonated (left, intercept set to 0, slope = (33 ± 5) %, $R^2 = 0.83$) and protonated (right, intercept set to 0, slope = (43 ± 6 ) %, $R^2 = 0.84$).*

Although use of the modified Hammett parameter allows to quantify the effect of substituents, additional effects on OAT activity are still be present. This is especially important, as the OAT process is light activated and the excited state species are not the same as the complexes in their ground state for which the Hammett parameters were determined. The weak activity of, and lack of difference between **Mo-8** and **Mo-10** as well as the difference in activity between **Mo-5** and **Mo-6** show that effects not accounted for by the Hammett parameter are still present, particularly a greater importance of the amine ring compared to the aldehyde.

### 3.3.2 The influence of substituent position on photoactivated OAT catalysed by molybdenum and tungsten complexes

Regarding the effect of substituent position, two cases have to be distinguished: the same substituent in the *para* or *meta* position on the same phenol ring, or the same substituent in the para position on different phenol rings (Figure 3-15).

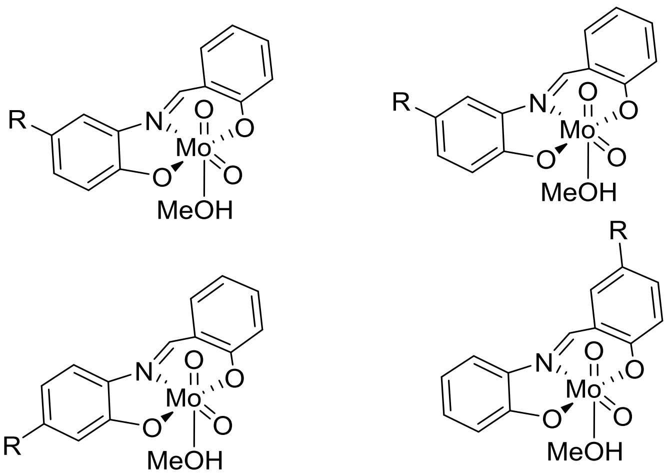

*Figure 3-15: Two cases of different substituent positions: para or meta position on the same phenol ring (left) and para position on different phenol ring (right). Positions are assigned with regard to the phenol oxygen.*

**Mo-11** and **Mo-9** fall into the first category. For **Mo-11** the conversion was 23 % and for **Mo-9** 28 %. Given the uncertainty in these results a difference of 5 % is considered to be insignificant and the position of the substituent, in this case the ester group, has no influence on the activity.

Comparing substituents on different phenol rings a more pronounced effect can be seen. Between **Mo-9** and **Mo-10** for example, the complex where the substituent is found on the amine ring (**Mo-9**) showed a much higher conversion than that where it is on the aldehyde ring (**Mo-10**): 30 %, compared to 5 %. The same applies to the two acid-substituted complex **Mo-7** and **Mo-8** and the mixed acid/ester-substituted complexes **Mo-5** and **Mo-6**.

From the structure of **Mo-1** it can be seen that this complex is symmetrical, if the C=N group is ignored, meaning the positions in which substituents are introduced are equivalent: both are in the para position to phenol oxygens, which are mutually trans. This pseudosymmetry is evident from the crystal structures where complexes **Mo-2** and **W-2** which have symmetrical substitution, show significant disorder due to the existence of enantiomers only occurring because the imine group introduces a small asymmetry. **Mo-7** does not show such disorder due to its substitution pattern.

It follows that the imine group distinguishes the two aromatic rings. Out of the above-mentioned pairs of complexes the more active complex, e.g. **Mo-9**, the substituent was introduced on the amine ring and is closer to the imine nitrogen which in turn conveys the electron withdrawing effect on to the metal.

To what extent the electronic effects are conveyed through the nitrogen or the phenolic oxygens is unclear. Also, the crystal structures of **Mo-1**, **Mo-2**, **Mo-7** and **Mo-15** showed that the SAP ligand is not planar with dihedral angles of 4 to 14 ° between the aromatic rings. This non-planarity could reduce the orbital alignment and the conjugation between the imine group and the two aromatic rings which could result in reduce transfer of electronic effects from the aldehyde ring to the nitrogen. To what extend the crystal structure reflects the situation in solution is unclear.

## 3.3.3 The influence of wavelength on photoactivated OAT catalysed by molybdenum and tungsten complexes

OAT was carried out under excitation sources of different wavelength (365, 410 and 460 nm) with the acid and ester substituted complexes and the tungsten complexes.

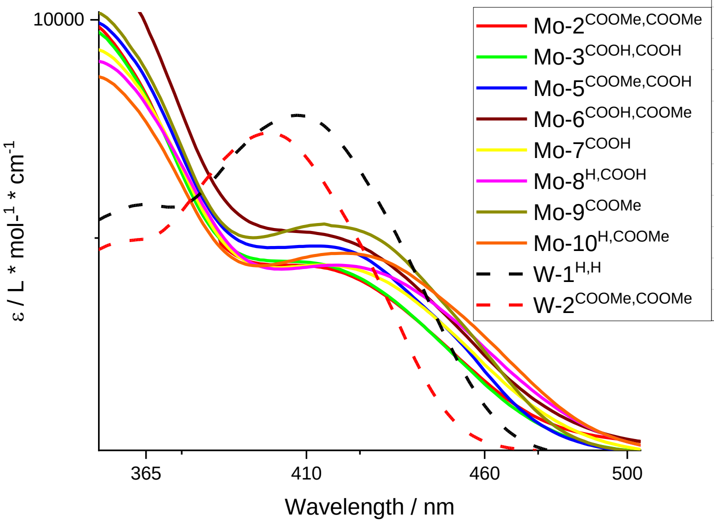

| | Conversion / % at λ / n | | |
|---|---|---|---|
| | 365 | 410 | 460 |
| Mo-2$^{COOMe,COOMe}$ | 69 | 78 | 77 |
| Mo-3$^{COOH,COOH}$ | 32 | 35 | 32 |
| Mo-5$^{COOMe,COOH}$ | 52 | 65 | 57 |
| Mo-6$^{COOH,COOMe}$ | 32 | 39 | 31 |
| Mo-7$^{COOH}$ | 7 | 12 | 12 |
| Mo-8$^{H,COOH}$ | 4 | 2 | 2 |
| Mo-9$^{COOMe}$ | 30 | 28 | 19 |
| Mo-10$^{H,COOMe}$ | 5 | 2 | 2 |
| W-1$^{H,H}$ | 8 | 12 | 12 |
| W-2$^{COOMe,COOMe}$ | 62 | 79 | 45 |

*Figure 3-16: UV-Vis spectra of the complexes containing acid and ester groups at 0.05 mM in DMSO and conversion of $PPh_3$ to $OPPh_3$ after 3 h. In DMSO-$d_6$, under $N_2$, c([Mo])= 1 mM, c($PPh_3$) = 300 mM, irradiation with a light source of the stated wavelength. An uncertainty in the conversions of 3 % is estimated.*

Changing the wavelength of the light source between 365, 410 and 460 nm barely affected the activity of the complexes. In fact, a clear effect was only observed when **W-2** was used. The highest activity (79 %) was observed using the 410 nm light source. Activity dropped to 62 % at 365 nm and dropped even more to 45 % at 460 nm.

Otherwise, the change in conversion with wavelength might only be seen as significant based on the analysis in 3.2.2 in three cases with molybdenum complexes: a difference of 13 % between

**Mo-5** at 410 nm and 365 nm, a difference of 11 % between **Mo-9** at 365 nm and 460 nm and a difference of 9 % between **Mo-2** at 410 nm and 365 nm.

All molybdenum complexes showed an increase in absorbance from 460 nm to 410 nm to 365 nm. This, however, only has an effect if the reaction is not limited by the intensity of the excitation source. The insensitivity to the exciting wavelength could indicate that the same or a very similar chemically-relevant excited state or reactive intermediate is being accessed using the wavelengths studied. Alternatively, the reaction could be limited by a thermally activated process subsequent to a photolytic step. These possibilities are considered later in this and the following chapter.

Based on initial studies a wavelength of 410 nm was used for further experiments as it yielded the highest activity overall.

### 3.3.4 The influence of acidic protons on photoactivated OAT catalysed by molybdenum and tungsten complexes

The ester-containing complexes were made in order to investigate the role of the acidic proton, for example whether inter- or intramolecular protonation of the substrates or complexes is relevant. It was found however, that the acidic proton is not needed for the OAT to occur. The activity seen with **Mo-12** and **Mo-13** (32 and 25 %) which both do not contain an acidic proton but yielded much higher conversion than their acid analogue (**Mo-7**, 12 %) also confirms this.

An acidic proton may even be hindering the reaction as complexes where the acid groups were esterified showed increased activity (e.g. **Mo-7**: 12 %, **Mo-9**: 25 %). The electronic properties of the two substituents, the ester and the acid, are the same based on the Hammett parameter[113] which excludes a purely electronic effect.

### 3.3.5 The influence of the electronic absorption and emission on photoactivated OAT catalysed by molybdenum and tungsten complexes

**Mo-16** with the extended πsystem was intended to provide a catalyst with increased absorbance in the visible region. While this increase in absorbance was confirmed by spectroscopic data (Figure 3-17) the complete inactivity of **Mo-16** showed that simply increasing absorbance is not beneficial.

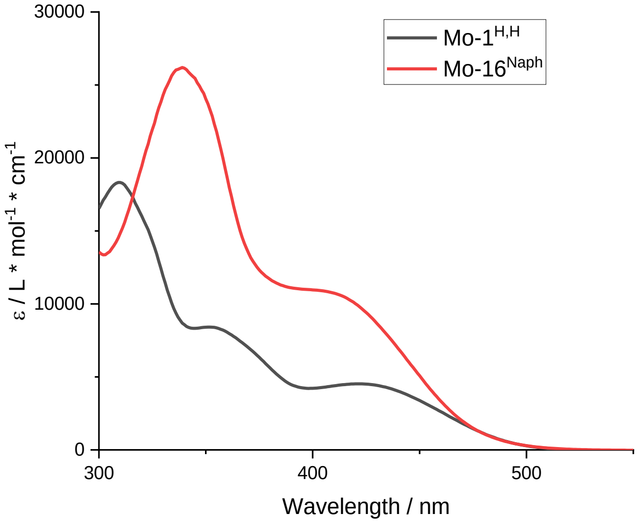

*Figure 3-17: UV-vis spectra of **Mo-1** and **Mo-16** at 0.05 mM in DMSO.*

The amine group -$NEt_2$ was used to modify the emissive properties of a complex to test if complex activity was linked to emissivity. Neeraj *et al.* showed that the introduction of the $NEt_2$ group increased emissivity of **L-15** compared to **L-1**.[145] The combination of an acceptor group with the amine donor was also found to increase emissivity in related salen type Schiff bases shown in Figure 3-19.[146] **Mo-4** contains both an electron acceptor (COOMe) and an electron donor ($NEt_2$). Spectroscopic properties of **Mo-4,** which is the most emissive complex, and **Mo-15,** which only showed very weak emissivity, are shown in Figure 3-18 together with **Mo-1** and **Mo-2.** Further spectroscopic analysis can be found in sections 4.2 and 4.3.

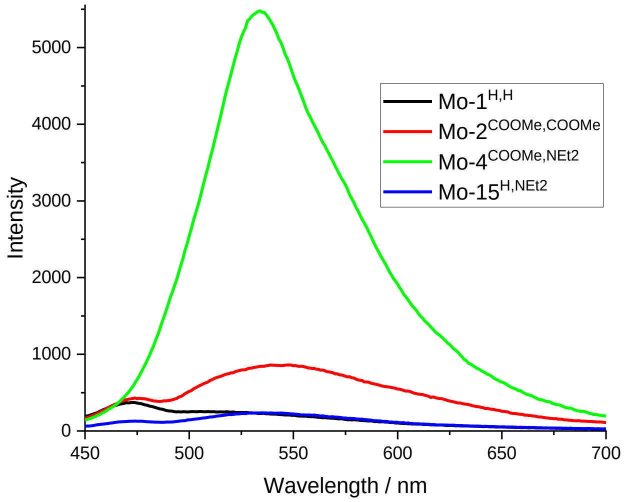

*Figure 3-18: Emission spectra of **Mo-1, Mo-2, Mo-4** and **Mo-15** at 0.05 mM in acetone under $N_2$, $\lambda_{ex}$ = 410 nm.*

Both **Mo-4** and **Mo-15** were inactive which suggests that emissivity is not the key property in determining the activity of a complex.

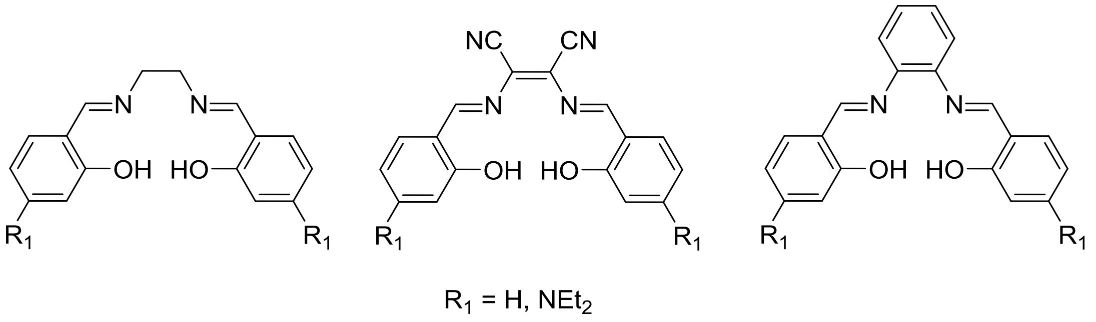

Figure 3-19: Structures of salen type ligands used to study the effect of electron donor- / acceptor-groups on emissivity.[146]

### 3.3.6 The influence of the metal centre on photoactivated OAT catalysed by molybdenum and tungsten complexes

Molybdenum and tungsten have similar properties and can be interchanged in some cases in enzymes.[147–149] Differences between the two metals in OAT have been studied. Holm and Yu did not observe any reaction between the tungsten complexes **W-1** and [$WO_2$(tBu-**L1**)] (Figure 3-20) and various phosphines (including $PPh_3$), even at temperatures > 100 °C and over 24 h whereas the molybdenum analogues reacted. [110]

In contrast, Arumuganathan *et al.* observed a significantly faster reaction with the tungsten complex [$WO_2Cl$(L-ONN)] (Figure 3-20).[150] The reaction with 10 eq. of $PMe_3$ was completed after only 30 min using the tungsten complex compared to 16 h with the molybdenum analogue.

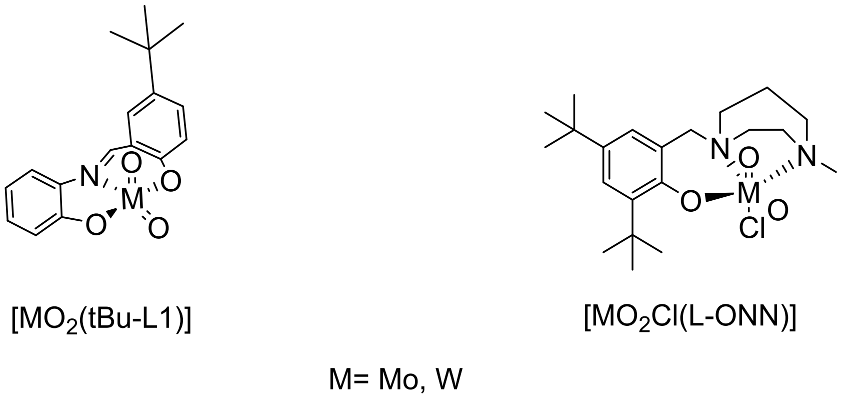

Figure 3-20: Structures of two molybdenum and tungsten complexes studied by Holm and Yu (left) [110], and Arumuganathan et al. (right). [150]

The two pairs of Mo/W complexes studied in this work (**Mo-1** and **W-1**; **Mo-2** and **W-2**) only differ in the metal centre but are otherwise structurally identical. The structural differences in the solid state of these four complexes (the molybdenum complexes are monomeric whereas the tungsten complexes are di- or oligomeric, see section 2.3.1 and 2.3.5) are nullified once in solution.

Figure 3-21 shows the conversion obtained with the four molybdenum and tungsten complexes and their UV-Vis absorbance at different wavelengths.

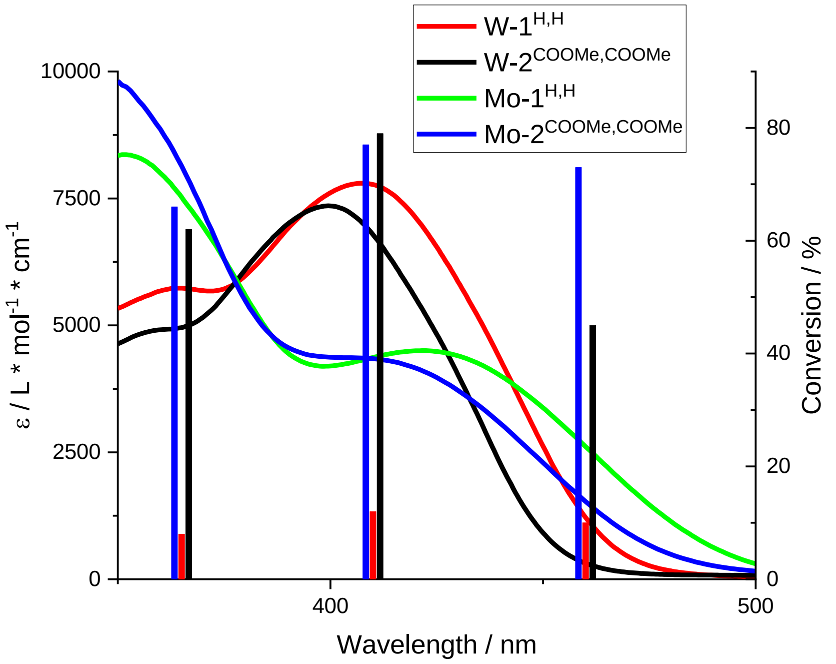

*Figure 3-21: A plot of the UV-Vis extinction coefficient and conversion, respectively, against wavelength for* ***Mo-1, Mo-2, W-1*** *and* ***W-2****. UV-Vis data recorded from 0.1 mM solutions in DMSO. Conversion of $PPh_3$ to $OPPh_3$ after 3 h, c([catalyst]) = 1 mM, c($PPh_3$) = 300 mM, DMSO-$d_6$, $N_2$. Note that no conversion was observed with* ***Mo-1****.*

The unsubstituted molybdenum complex **Mo-1** was inactive whereas the tungsten analogue **W-1** gave a conversion of around 10 %.

**W-2** and **Mo-2** showed similar activity except when irradiated at 460 nm where the tungsten complex was much less active, possibly due to lower absorbance (ε = 1600 L * mol$^{-1}$ * cm$^{-1}$ for **Mo-2** and 300 L * mol$^{-1}$ * cm$^{-1}$ for **W-2**). At 365 nm both **Mo-2** and **W-2** showed similar activity despite higher absorption by **Mo-2**. In section 3.3.3 it was hypothesised that reactivity could be limited by the amount of light available to the complexes. The amount of light available could be higher than absorption for **W-2** at 460 nm resulting in lower activity compared to **Mo-2**. **W-1** which showed no wavelength dependence has an absorptivity similar to **Mo-2** at 460 nm.

In addition, the nature of the transition that is excited could have an effect. There is substantial overlap between the two bands at 365 and 410 nm, so that light sources with those wavelengths excite two transitions at once, to varying degrees. Only the 460 nm light source excites specifically one transition. (see section 4.2 for further discussion of the electronic absorption of the complexes).

It is interesting to note that for **Mo-1** and **W-1, W-1** shows higher activity, whereas **Mo-2** and **W-2** show similar activity at 365 and 410 nm but **Mo-2** shows more activity at 465 nm. Arumuganathan *et al.* hypothesised a change in mechanism going from Mo to W.[150] The reaction of the molybdenum complex proceeds via the reduced Mo(IV) intermediate which is reoxidised by

DMSO. Because of larger relativistic effects in tungsten compared to molybdenum the tungsten 5d orbital is more destabilised than the molybdenum 4d orbital which leads to a preference of the M(VI) over the M(IV) state. Hence, the tungsten complex is more difficult to reduce.[151] This affects the reaction mechanism of OAT which then occurs in a concerted manner (Scheme 3-5). This hypothesis is corroborated by the inactivity of the tungsten complex and $PPh_3$ in the absence of DMSO and the tendency of tungsten to form seven coordinate complexes; dissociation of one arm of the ONN ligand would allow for the intermediate to retain hexa-coordination.

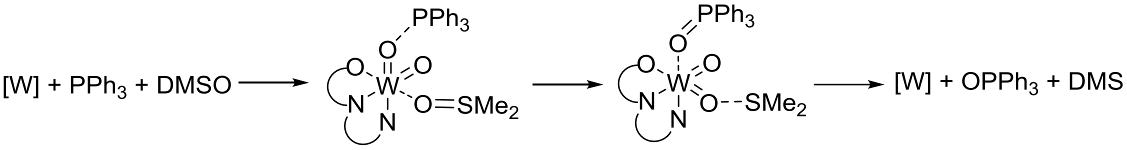

*Scheme 3-5: Hypothesised mechanism for the reaction of [MoO₂Cl(L-ONN)] with PPh₃ and DMSO showing the coordination of both substrates in the intermediates.*

Based on the absorption spectra the reasons for the observed differences between Mo and W analogues are not clear. Chapter 4 describes further studies, in particular excited state lifetime measurements to possibly understand the observed reactivity differences.

### 3.3.7 Correlation between M=O Vibrational frequency and activity in photoactivated OAT catalysed by molybdenum and tungsten complexes

As discussed (section 2.3.5), a stronger M=O bond is reflected by a higher wavenumber of the symmetric and asymmetric stretching bands of the $MO_2$-moiety.

Topich and Bachert, after studying several Mo complexes based on substituted SAP and SAE ligands and their mono substituted thiol analogues [$(MoO_2(L)(DMF))$], L shown in Figure 3-22) found a correlation between the frequency of the asymmetric stretch vibration of the dioxo ligand and the reactivity of the complex towards OAT onto $PEtPh_2$.[89] Reactive complexes showed a $\nu_{asym}$ (Mo=O) between 899 and 902 cm$^{-1}$ in DMF whereas the corresponding frequencies for unreactive complexes were observed between 906 and 916 cm$^{-1}$.

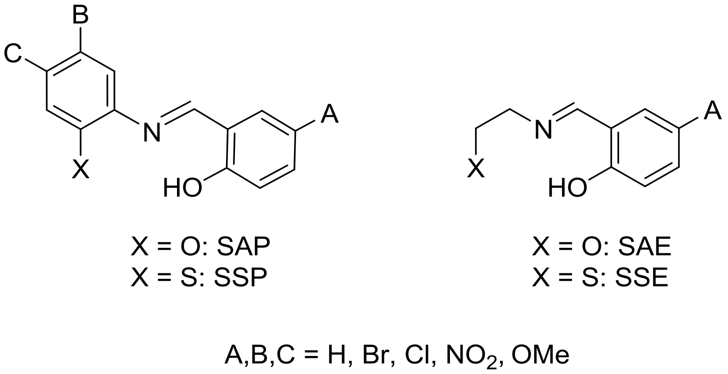

*Figure 3-22: Structures of the substituted SAP, SSP, SSE and SAE ligands*

A plot of the conversion at 410 nm from Table 3-8 against ν (Mo=O) is shown in Figure 3-23 together with the structures of the complexes in DMSO at the start of OAT. Complexes **Mo-3, Mo-8, Mo-11, Mo-12** and **Mo-13** were not included due to their different solid state structures and hence Mo=O bands (see section 2.3.5)

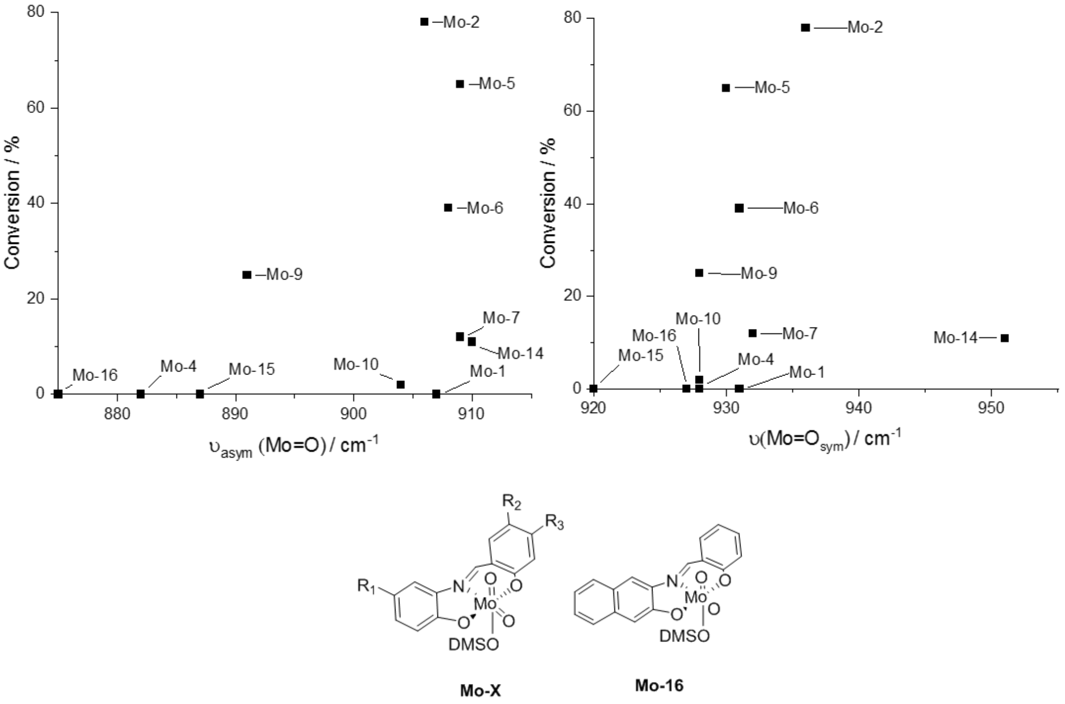

| $R_1$ | $R_2$ | $R_3$ | X |
|---|---|---|---|
| H | H | H | 1 |
| COOMe | COOMe | H | 2 |
| COOMe | H | $NEt_2$ | 4 |
| COOMe | COOH | H | 5 |
| COOH | COOMe | H | 6 |

| $R_1$ | $R_2$ | $R_3$ | X |
|---|---|---|---|
| COOH | H | H | 7 |
| COOMe | H | H | 9 |
| H | COOMe | H | 10 |
| $SO_2NH_2$ | H | H | 14 |
| COOMe | H | $NEt_2$ | 15 |

*Figure 3-23: Plot of conversion after 3 h ($OPPh_3$ / $PPh_3$) against $v_{asym}$ (Mo=O) (top left) and against $v_{sym}$ (Mo=O) (top right);in DMSO-$d_6$, under $N_2$, c([Mo] )= 1 mM, c($PPh_3$) = 300 mM, irradiation at 410 nm. Structures of complexes in DMSO as prepared for OAT.*

There is poor correlation between conversion and both symmetric and asymmetric stretching frequency. However, there appears to be a cut off frequency in the frequency of the asymmetric stretch: below 890 $cm^{-1}$ complexes are inactive. **Mo-1**, having a band at 907, would be an outlier. Except for **Mo-9**, all active complexes are found between 905 and 910 $cm^{-1}$ which is in contrast to the aforementioned findings of Topich and Bachert (although the difference in IR measurement, ATR *vs*. solution, could play a role). In the frequency of the symmetric stretch a cut off frequency appears to exist around 928 $cm^{-1}$ with **Mo-1** and **Mo-4** being outliers.

In section 2.3.4 the band position of the Mo=O stretch of the complexes was discussed. It was hypothesised that those complexes with the highest stretching frequency should show less activity as their stronger Mo=O bonds make them less prone to OAT. However, as Figure 3-23 shows, the highest activity is in fact seen in those complexes with higher stretching frequency. This suggests that the correlation between ground state strength of the Mo=O bond, and photo-induced activity is more complex and that the Mo=O bond strength is not a defining feature for photo-induced OAT as is observed in thermally activated OAT.

### 3.3.8 Summary

Screening of the complexes showed **Mo-2** and **W-2** to be the most active catalyst, **Mo-1**, **Mo-4**, **Mo-15** and **Mo-16** were inactive. Activity of the complexes was linearly correlated with the Hammett parameter, taking into account conjugation effects in acid and ester substituents. Electron withdrawing substituents favour OAT. A strong dependence on the aromatic ring the substituent is attached to was also observed. OAT with light sources of different wavelength revealed no strong wavelength dependence and suggested limitation of the reactions by the amount of light available to the catalysts.

## 3.4 Exploring the substrate scope of OAT - sulfoxides

Catalyst regeneration requires the transfer of oxygen from an oxygen source. So far in this project DMSO has been used for this purpose which resulted in the formation of dimethylsulfide as a by-product. However, the synthesis of sulfides from sulfoxides is a potentially useful reaction. Sulfide groups are found in pharmaceuticals, for example, and OAT could in the future provide an alternative tool in the synthesis of these compounds from sulfoxides or more usefully sulfones. [152]

To explore the substrate scope and to gain further insight into the mechanism, a selection of other sulfoxides was tested under OAT conditions. In addition, employing sulfoxides that are more easily reduced could also accelerate the OAT reaction, in cases where this is the rate limiting step.

In order to allow OAT with different sulfoxides to be comparable, a known quantity must be used. Instead of being in vast excess, sulfoxides were used in equimolar ratio compared to the phosphine (300-fold excess compared to the catalyst).

The selection of sulfoxides contained aliphatic and aromatic sulfoxides and heterocycles. Electron withdrawing and electron donating groups as well as hydrogen bond donors and acceptor containing aromatic sulfoxides were also selected. The structures of the selected sulfoxides are shown below:

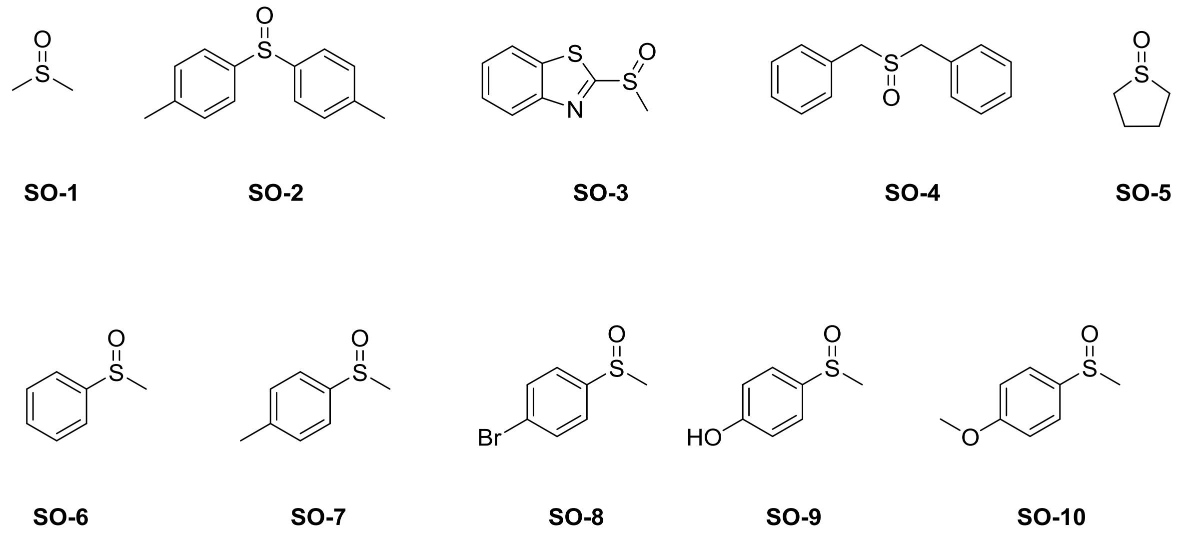

**SO-1** **SO-2** **SO-3** **SO-4** **SO-5**

**SO-6** **SO-7** **SO-8** **SO-9** **SO-10**

*Figure 3-24: Structure of sulfoxides used in this work.*

OAT was performed using sulfoxides **SO-1** to **SO-10** under the following conditions: catalyst, **Mo-2** (1 mM), PPh$_3$ (300 mM), sulfoxide (300 mM) in acetone-d$_6$, irradiation at 410 nm.

The conversion observed after three hours is listed in Table 3-10.

*Table 3-10: OAT with various sulfoxides, conversion after 3 h.*

| Sulfoxide | Conversion[a] of sulfoxide to sulfide / % | Conversion[a] of PPh$_3$ to OPPh$_3$ / % |
|---|---|---|
| **SO-1** | 14 | 20 |
| **SO-2** | 46 | 46 |
| **SO-3** | 28 | 29 |
| **SO-4** | 21 | [b] |
| **SO-5** | 47 | 54 |
| **SO-6** | 35 (36[c]) | [b] |
| **SO-7** | 44 (46[c]) | 41 (42[c]) |
| **SO-8** | 36 | 39 |
| **SO-9** | 4 | 2 |
| **SO-10** | 46 | 45 |

Condition: c(**Mo-2**) = 1 mM, c(PPh$_3$) = 300 mM, c(**SO-X**) = 300 mM, acetone-d$_6$, N$_2$,irradiation at 410 nm. [a] An uncertainty in the measurement of 2 % is assumed. [b] Determination not possible due to signal overlap. [c] Results from a repeat of the experiment

There is generally good agreement between the amount of sulfoxide reduction and the amount of PPh$_3$ oxidation confirming OAT. Conversions for both processes deviate in the reactions with **SO-1** and **SO-5,** by 6 and 7 %, respectively. The statistical discussion in section 3.2.2 only looked at the reproducibility and uncertainty of separate experiments, not the agreement between the observed reduction and oxidation within a single sample. Based on the overall good agreement, it seems reasonable to conclude that the difference in conversion in the reactions with **SO-1** and **SO-5** is not just due to uncertainty in the measurement.

Reduction of **SO-1** yields dimethyl sulfide which is a volatile liquid (boiling point of 37 °C)[153] and can escape into the head space of the NMR tube where it will not be detected by the NMR spectrometer. Hence, the amount of sulfide measured is lower than the amount produced. Similarly, reduction of **SO-5** yields the volatile[154] tetrahydrothiophene and gassing out of solution of the product could also occur.

The conversion obtained with **SO-1** (20 %) was lower than the conversion obtained previously, where it was in excess (78 %, Table 3-8 ). Conversion could be increased by replacing one or both methyl groups of DMSO and introducing aromatic systems.

The aromatic system needs to be directly bound to sulfur as **SO-4,** which contains two distal aromatic rings, showed the same conversion as **SO-1** (Since the conversion of $PPh_3$ to $OPPh_3$ could not be determined in this case, it is assumed that this conversion corresponds to the measured conversion of **SO-4** to **S-4**). This suggests that increased steric demand, or any π- π-interaction with the metal complex ligand do not significantly affect the reaction.

However, when the aromatic ring is bound directly to sulfur two-fold higher conversion compared to **SO-1** were obtained as shown by **SO-2, SO-6, SO-7, SO-8** and **SO-10**. **SO-3** containing an aromatic heterocycle gave a slightly higher conversion than **SO-1** and **SO-4**. The effect of this heterocycle is weaker than that of a tolyl group in **SO-7**. However, going from one to two aromatic rings had no cumulative effect as shown by the identical conversion observed with **SO-2** and **SO-7**.

Interestingly, **SO-5** showed the highest conversion despite containing no aromatic rings, but as a cyclic sulfoxide is unique in this series suggesting ring strain could support OAT from the sulfoxide to the Mo(IV) complex.

The result with **SO-9** was also intriguing. The presence of the OH group must be interfering with the sulfoxide reduction as activity is restored when the oxygen is methylated (**SO-10**). Further investigation of the OH group has been undertaken and results can be found in section 3.4.1.

**SO-2** had yielded the highest conversion of the sulfoxides tested early on (**SO-1, SO-2, SO-3**) and was used for further studies discussed in chapters 3.5 and 3.6 . It was also easiest to handle and available in sufficient quantity.

OAT from **SO-2** was also continued to97 %. Reaction time and conversion are listed in the table below (Table 3-11).

*Table 3-11: Conversion of $PPh_3$ to $OPPh_3$ and time of irradiation for OAT from* ***SO-2****.*

| Time of irradiation / h | Conversion[a] / % |
|---|---|
| 3 | 46 |
| 9 | 71 |
| 24 | 90 |
| 48 | 97 |

c(**Mo-2**) = 1 mM, c($PPh_3$) = 300 mM, c(**SO-2**) = 300 mM, acetone-$d_6$, $N_2$,irradiation at 410 nm . [a] An uncertainty in the measurement of 3 % is estimated.

The reaction slows down significantly as it progresses, especially during the last 24 h interval only a 7 % increase in conversion was obtained. It is worth to note that the reaction was unstirred (as are all OAT reactions in this work) and hence the reaction rate may be limited by diffusion; Although mixing occurred from handling the sample during NMR recording and the heating of the sample from the bottom in the photoreactor could have resulted in convectional mixing.

### 3.4.1 Influence of phenol on OAT between di-*para*-tolyl sulfoxide and $PPh_3$

Following from the low conversion of **SO-9** it seemed that the presence of OH groups interferes with OAT. To further test this hypothesis, OAT was performed with added phenol: 1 mM of **Mo-2**, 300 mM of $PPh_3$, 300 mM of **SO-2** and 100 mM of phenol.

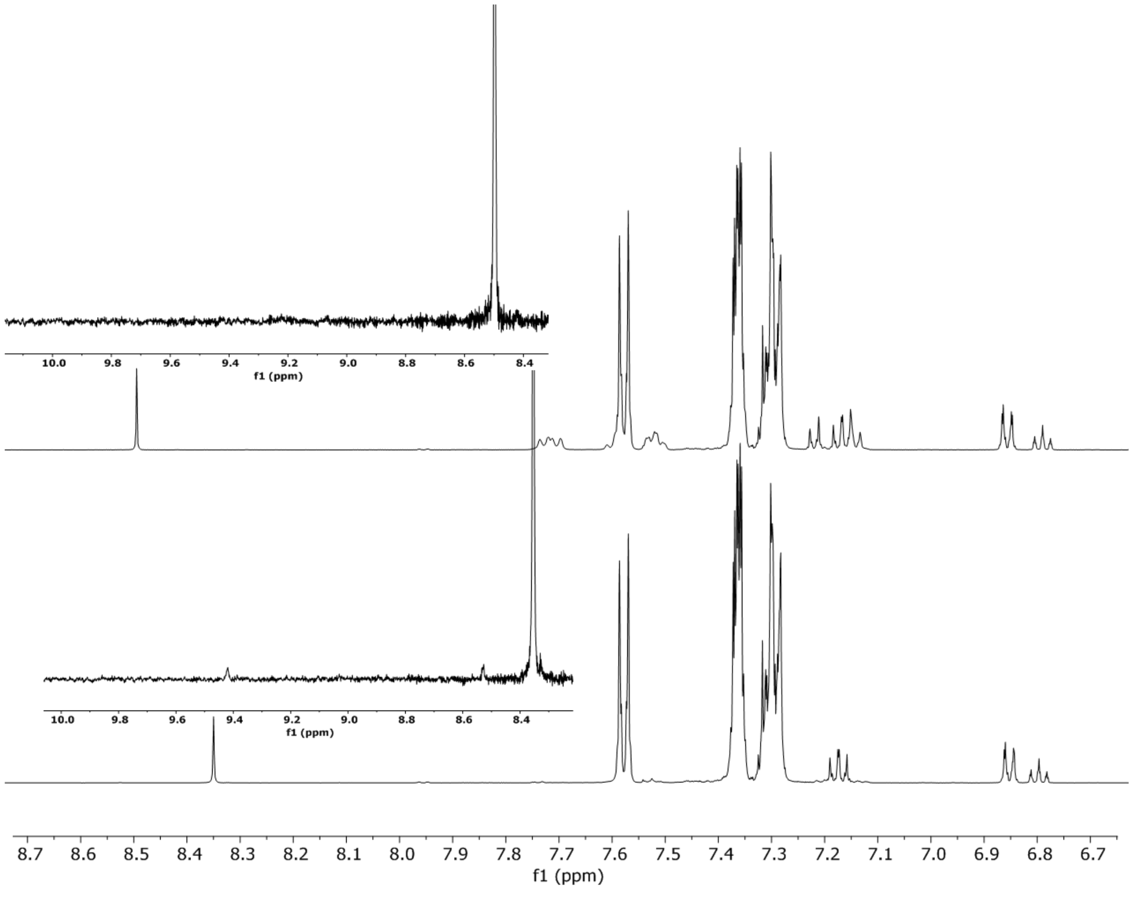

*Figure 3-25: $^1H$ NMR spectra of the OAT reaction in the presence of phenol after 3 h (top) and as prepared (bottom). Conditions: c(**Mo-2**) = 1 mM, c($PPh_3$) = 300 mM, c(**SO-2**) = 300 mM, c(phenol) = 100 mM, acetone-$d_6$, $N_2$, irradiation at 410 nm.*

After 3 hours of irradiation at 410 nm a conversion of only 12 % was seen (compared to 45 % in experiments without phenol) confirming the hypothesis that phenolic hydroxyl groups retard the OAT reaction. From the $^1H$ NMR spectra shown in Figure 3-25 before and after irradiation, the only noticeable differences are a shift of the resonance of the OH proton of phenol by 0.15 ppm (from 8.35 to 8.5 ppm), and the disappearance of the resonances from the complex (9.4 and 8.5 ppm). In the $^1$H NMR of phenol (Figure 3-26), the OH proton resonates at 8.22 ppm, whereas in the reaction sample it is found at 8.35 ppm before and at 8.5 ppm after irradiation. Similarly, a small shift is seen in the resonances of the aromatic protons.

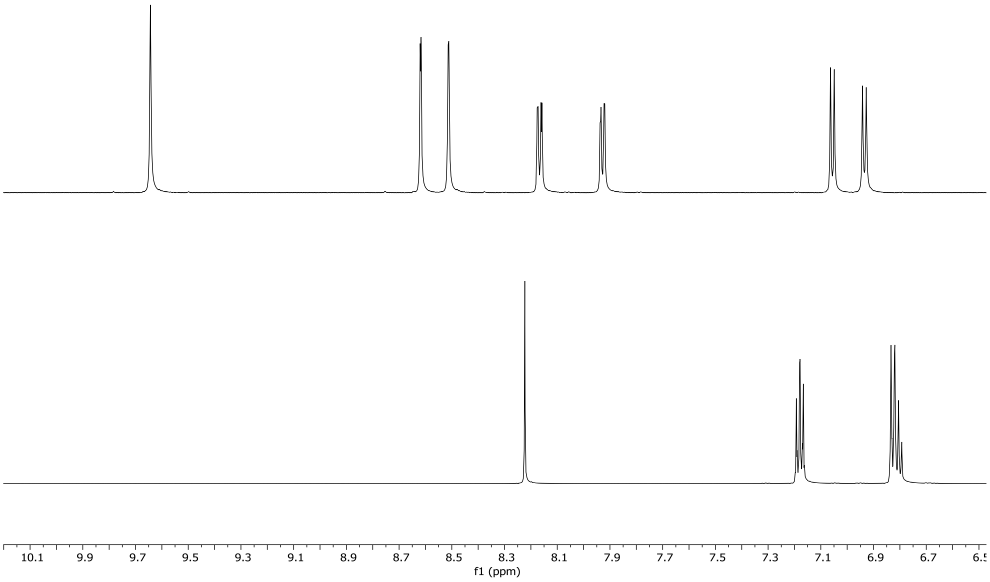

*Figure 3-26: $^1$H NMR spectra of **Mo-2** (top) and phenol (bottom) in acetone-$d_6$ in the range of 6.5 to 10 ppm.*

A mixture of **Mo-2** and phenol, without the OAT substrates $PPh_3$ and **SO-2**, was irradiated for 3 h. $^1$H NMR spectra before and after irradiation are shown in Figure 3-27. In contrast to the OAT experiment (Figure 3-25), a shift in the resonance form the phenolic proton was not observed, some weak new resonances around 8.3, 7.3 and 6.9 ppm are did appear, however. These new resonances were not seen in the spectra of the OAT reaction due to strong signals of phosphine and sulfoxide species.

From OAT with **SO-9** and **SO-10** it is clear that the phenol group interferes with OAT. The shift of the resonances of the phenolic proton in the OAT experiment (Figure 3-25) but lack thereof in the experiment without substrates (Figure 3-27) suggest an interaction between phenol and **SO-2, S-2**, $PPh_3$ or $OPPh_3$. The loss in reactivity when phenol was added requires some form of interaction with the catalyst. Interaction with molybdenum is evidenced by the disappearance of resonances of **Mo-2** in the NMR spectrum of the reaction with added phenol and by the appearance of new resonances in the spectrum of the reaction between **Mo-2** and phenol (Figure 3-25 and Figure 3-27).

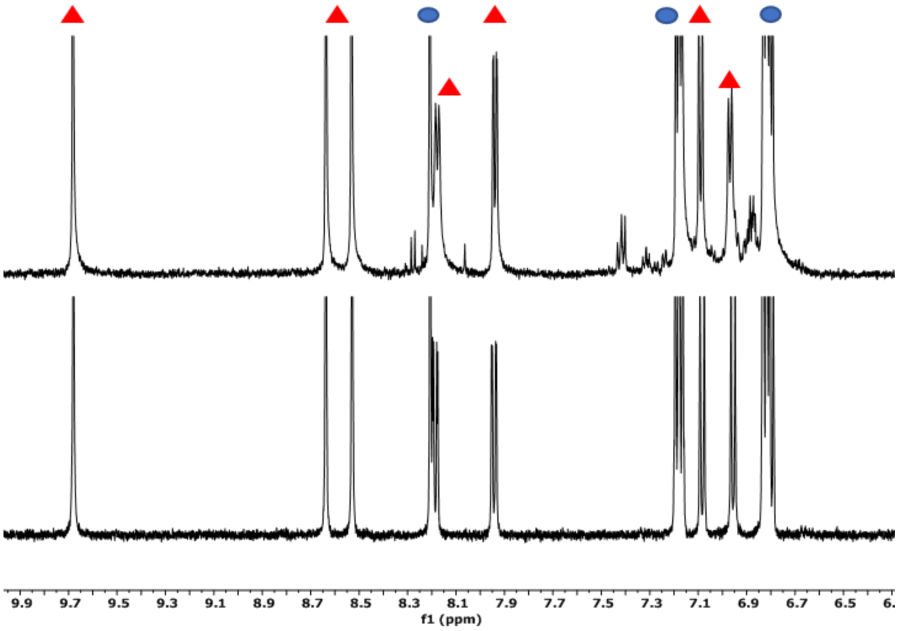

*Figure 3-27: $^{1}$H NMR spectra of a mixture of **Mo-2** and phenol in acetone-$d_6$ before (bottom) and after 24 h irradiation (top). Resonances of **Mo-2** are marked with red triangles, those of phenol with blue circles. Condition: c(**Mo-2**) = 3 mM, c(phenol) = 15 mM, acetone-$d_6$, $N_2$, irradiation at 410 nm.*

### 3.4.2 Summary

Exploring the scope of sulfoxides revealed that direct attachment of an aromatic ring to sulfur is beneficial however high conversion was also achieved with the aliphatic sulfoxide **SO-5.** More important, it was found the presence of an OH group on the substrate or as an additive to the reaction is detrimental. The mechanism by which the OH group interferes remains unclear.

## 3.5 Exploring the substrate scope of OAT - phosphines

Triphenylphosphine, PPh$_3$, is commonly used as a substrate in OAT. Although other more active phosphines like PMe$_3$ have found use as well. To explore the substrate scope and to find possible links to the mechanism, a selection of other phosphines was tested under OAT conditions.

Replacement of one or two phenyl groups of PPh$_3$ by methyl groups reduces steric demand and increases electron density on the phosphorus atom. Alkyl phosphines were generally found to be more active than PPh$_3$ (see section 3.1). The electronic properties of PPh$_3$ were modified with electron donating and electron withdrawing substituents on the phenyl rings.

Their structures are shown in Figure 3-28.

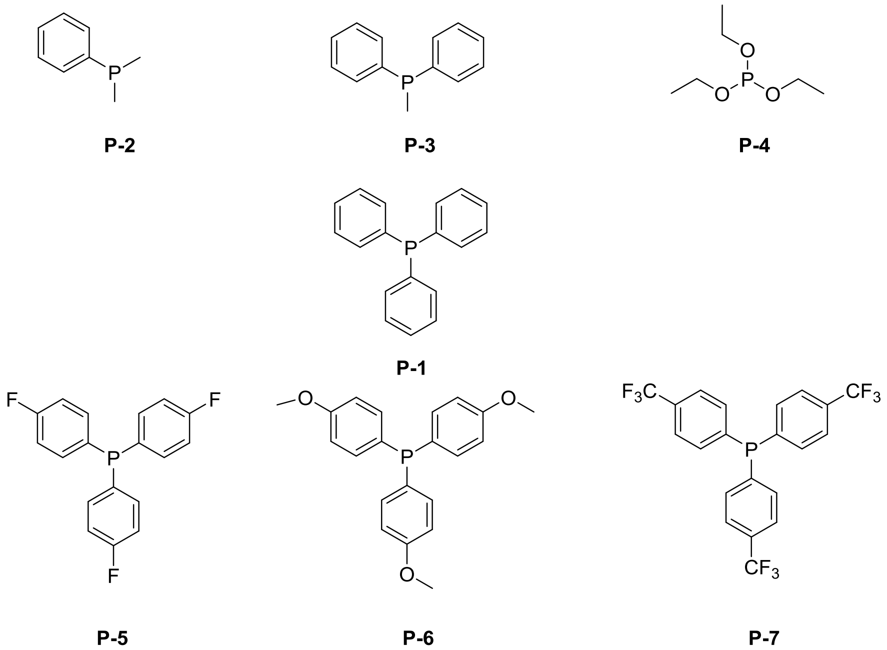

*Figure 3-28: Structure of phosphines studied in this work.*

OAT was performed using phosphines **P-1** to **P-7** under the following conditions: catalyst, **Mo-2**, 1 mM; phosphine , 300 mM; sulfoxide DMSO or **SO-2**, 300 mM; in acetone-d$_6$; irradiation at 410 nm.

The conversion observed after three hours is listed in Table 3-12 and Table 3-14.

Around two times higher conversion was observed with **P-2** and **P-3** compared to PPh$_3$ and almost no conversion with **P-4**.

Alkyl and alkoxy phosphines are more basic and more active in thermal OAT.[130] Between **P-2** and **P-3** only 9 % difference was observed which can probably be regarded as significant. **P-2** with two methyl groups is more basic and should be more active than **P-3,** but this is not the case. The almost complete loss in activity from **P-1** to **P-4** was also unexpected.

Steric demand decreases in the order **P-1** > **P-3** > **P-2** > **P-4** whereas the electronic parameter (Table 3-13) follows a similar order, except that **P-4** > **P-1 > P-3** > **P-2.** The observed conversion is, however, not reflected by either of the two parameters.

*Table 3-12: Conversion of $PR_3$ to $OPR_3$ after 3 h for different combinations of phosphine and sulfoxide.*

| Phosphine | Sulfoxide | Conversion[a] / % |
|---|---|---|
| P-1 | SO-1 | 18 |
| P-2 | SO-1 | 35 |
| P-3 | SO-1 | 44 |
| | | |
| P-1 | SO-2 | 45 |
| P-4 | SO-2 | 3 |

c(**Mo-2**) = 1 mM, c($PR_3$) = 300 mM, c(sulfoxide) = 300 mM, acetone-$d_6$, $N_2$,irradiation at 410 nm. [a] An uncertainty in the measurement of 2 % is estimated.

*Table 3-13: Steric and electronic parameters for phosphines used in this work.* [155]

| Phosphine | Steric parameter θ / ° | Electronic parameter ν / $cm^{-1}$ |
|---|---|---|
| P-1 $PPh_3$ | 145 | 2068.9 |
| P-2 $PMe_2Ph$ | 122 | 2065.3 |
| P-3 $PMePh_2$ | 136 | 2067.0 |
| P-4 $P(OEt)_3$ | 109 | 2076.3 |
| P-5 $P(p\text{-}C_6H_4F)_3$ | 145 (assumed) | 2071.3 |
| P-6 $P(p\text{-}C_6H_4OMe)_3$ | 145 (assumed) | 2058.3 |
| P-7 $P(p\text{-}C_6H_4CF_3)_3$ | 145 (assumed) | / |

Use of substituted $PPh_3$ derivative **P-5, P-6** and **P-7** did not increase conversion. Introduction of the $CF_3$-group (**P-7**) had no significant effect, whereas the fluoro and methoxy group led to a decrease in conversion. Steric effects are most likely no relevant as the substituents are introduced in the *para* position on the phenyl ring, away from the phosphorus atom. Both the electronic parameter according to Tolman and the Hammett parameter (Table 3-13 and Table 3-14) show the **P-6** as more electron donating than **P-1** and **P-7** and **P-5** as more electron withdrawing, although to different degrees. This trend is, however, not reflected in the conversion.

*Table 3-14: Conversion of $PR_3$ to $OPR_3$ after 3 h for substituted triphenyl phosphines and Hammett parameter for these substituents in para position.*[113]

| Phosphine | Sulfoxide | Conversion[a] / % | $\sigma_p$ |
|---|---|---|---|
| **P-1** $PPh_3$ | **SO-2** | 45 | 0 |
| **P-5** P(4-Fluorophenyl)$_3$ | **SO-2** | 14 | 0.06 |
| **P-7** P(4-Trifluoromethyl phenyl)$_3$ | **SO-2** | 41 | 0.54 |
| **P-6** P(4-Methoxyphenyl)$_3$ | **SO-2** | 32 | -0.27 |

Conditions: c(**Mo-2**) = 1 mM, c($PR_3$) = 300 mM, c(**SO-2**) = 300 mM, acetone-$d_6$, $N_2$,irradiation at 410 nm. [a] An uncertainty in the measurement of 3 % is estimated.

Although conversion could be improved using **P-3** instead of **P-1** the underlying reason could not be determined. In contrast to literature presented in section 3.1a correlation between conversion and electronic properties was not observed. An influence of steric properties was also not observed, in agreement with the literature.

Similar to observations relating to the metal complexes described above, these data also indicate that there is no clear correlation between ground state effects and the rate of the reaction.

## 3.6 Kinetic analysis of molybdenum-catalysed OAT between sulfoxides and $PPh_3$

An analysis of reaction kinetics can allow determination of a rate limiting step and provide information on the underlying mechanism.[156] Photochemical reactions are, however, more difficult to analyse than their thermal counterparts due to added complexity from the absorbance of a photon by the photo active species and subsequent excitation and relaxation processes.

Several experiments employing different conditions were carried out where the initial concentration of sulfoxide, phosphine or catalyst were varied while keeping the other two constant. Table 3-15 gives an overview on the relevant parameters. The data from these experiments is analysed separately but interpretation is more useful with the combined results (see 3.6.4)

*Table 3-15: Summary of kinetic experiments: parameter under investigation (varied), nature of substrates, concentration of species not investigated and solvents used.*

| Experiment | c(**Mo-2**) /mM | c($PPh_3$) / mM | Sulfoxide | c(sulfoxide) /mM | solvent |
|---|---|---|---|---|---|
| 1 | 1 | varied | DMSO-$d_6$ | excess | DMSO-$d_6$ |
| 2 | 1 | varied | **SO-2** | 150 | acetone-$d_6$ |
| | | | | | |
| 3 | 1 | 300 | **SO-1** | varied | acetone-$d_6$ |
| 4 | 1 | 300 | **SO-2** | varied | acetone-$d_6$ |
| | | | | | |
| 5 | varied | 300 | DMSO-$d_6$ | excess | DMSO-$d_6$ |
| 6 | varied | 300 | **SO-2** | 300 | acetone-$d_6$ |

The data obtained in these experiments in the form of conversion of phosphine over time was then analysed using Variable Time Normalisation Analysis (VTNA).[157–160] VTNA provides a simpler way of determining the reaction order of reactants. Conventionally, reaction rates are obtained by having all but one reactant in excess so that their concentration stays essentially constant (pseudo first order condition). This has the disadvantage that all experiments have to be repeated for each species under study. The condition of having all other reactants in excess is not only different from the typical reaction conditions it is also not always possible due to, for example, limited solubility. VTNA only needs a minimum of one data set per parameter that is changed from the default conditions.

Instead of the common conversion vs. time plot, VTNA uses a different quantity on the x axis:

For substrates:

$$x = \int_{t=0}^{t=n} [A]^{\alpha}\, dt \; = \sum\nolimits_{i=1}^{n} \left( \frac{[A]_i \; - \; [A]_{i-1}}{2} \right)^{\alpha} \; (t_i - t_{i-1}) = \sum [A]^{\alpha}\, \Delta t$$

*Equation 3-9*

For the catalyst:

$$x = \int_{t=0}^{t=n} [cat]^{\gamma}\, dt \; = \sum\nolimits_{i=1}^{n} \left( \frac{[cat]_i \; - \; [cat]_{i-1}}{2} \right)^{\gamma} \; (t_i - t_{i-1}) = \sum [cat]^{\gamma}\, \Delta t$$

*Equation 3-10*

which can be simplified if the concentration of catalyst remains constant during the reaction to give

$$x = t\; [cat]^{\gamma}$$

*Equation 3-11*

t = time, [A] = concentration of substrate and [cat] = concentration of the catalyst, α and γ = the order in substrate and catalyst, respectively.

If the order is 0, x simply equals t for both substrates and catalyst and the usual concentration vs. time plot is obtained.

### 3.6.1 OAT at varied phosphine concentration

To study the effect of the phosphine two sets of experiments were carried out, one in DMSO-$d_6$ the other one in acetone-$d_6$ with **SO-2**.

In the first set of experiments the concentration of $PPh_3$ was varied from 50 to 100 to 200 mM while catalyst concentration was kept at 1 mM. DMSO being the solvent was in excess. A plot of concentration of $OPPh_3$ vs. time that includes several datapoints between 0 and 3 h is shown in Figure 3-29.

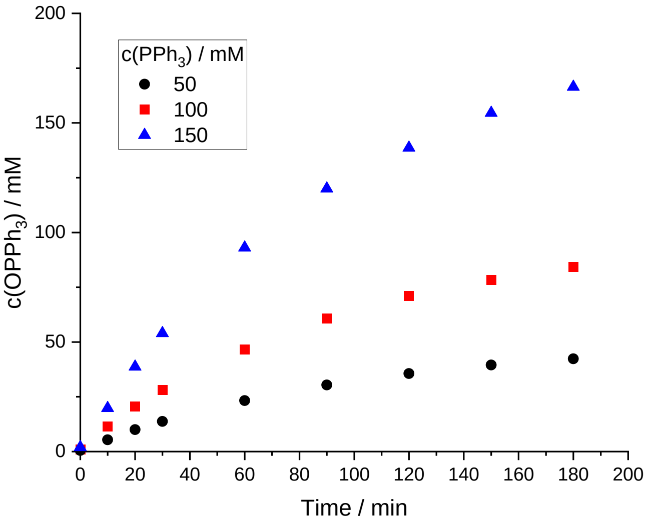

*Figure 3-29: Plot of concentration of OPPh$_3$ vs. time for the oxidation PPh$_3$ at various concentrations of PPh$_3$. Conditions: 1 mM **Mo-1**, in DMSO-d$_6$, N$_2$ atmosphere, irradiation at 410 nm.*

It can be seen that at any time point in Figure 3-29 that the relative concentrations of the Ph$_3$PO product reflect the relative concentration of PPh$_3$ at t = 0. It follows that the reaction rate depends linearly on the concentration of PPh$_3$.

In the second set of experiments acetone was used instead of DMSO and the sulfoxide, now **SO-2**, was no longer in excess. Concentrations of PPh$_3$ of 150 and 300 mM were used while the catalyst concentration was kept at 1 mM. A plot of concentration of OPPh$_3$ vs. time that includes several datapoints between 0 and 4 h is shown in Figure 3-30.

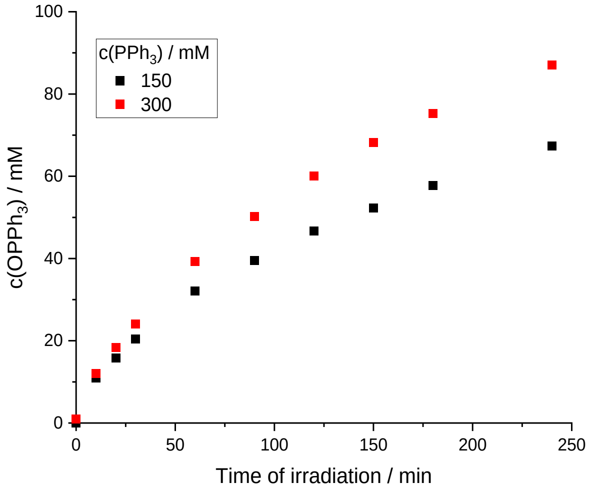

*Figure 3-30: Plot of concentration of OPPh$_3$ vs. time for the oxidation PPh$_3$ at various concentrations of PPh$_3$. Conditions: 1 mM **Mo-1**, 300 mM **SO-2** in acetone-d$_6$, N$_2$ atmosphere, irradiation at 410 nm.*

From the plot in Figure 3-30 a correlation between the concentrations of the product $OPPh_3$ and the initial concentration is not obvious which is where VTNA can provide additional information.

VTNA, as presented in the introduction to this section, is a less commonly used method to calculate the reaction order in a reactant using visual determination of data point overlap. The data from Figure 3-29 provides a good opportunity to compare the result obtained via VTNA with the result obtained conventionally in this simple case.

Figure 3-31 shows the VTNA plots based on the data from Figure 3-29 employing Equation 3-9. To show how the overlap of the datapoints depends on the order in phosphine, three plots with different reactant order (0, 1 and 2) are compared. With a reaction order of 1 good overlap is obtained confirming that 1 is the order that the reaction rate depends on the concentration of phosphine which agrees with what was already seen from the concentration vs. time plot. An order of 1 in phosphine concentration suggests that under these conditions the rate equation contains one molecule of phosphine.

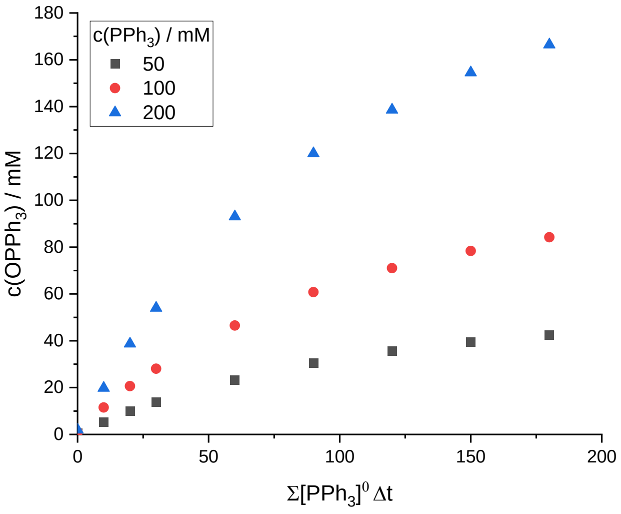

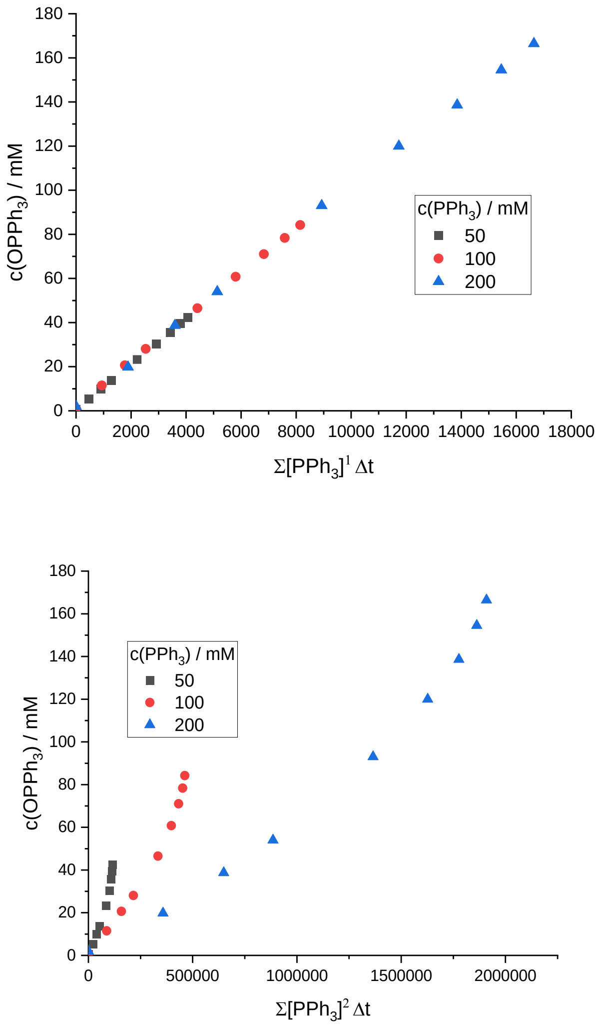

*Figure 3-31: VTNA plots for the oxidation of PPh$_3$ with different orders in PPh$_3$ , 0, 1 and 2. Alignment of all data points is only observed when the reactant order is set to 1 (middle). Reaction conditions: c(PPh$_3$) = 50 , 100 and 300 mM, c(**Mo-2**) = 1 mM, in DMSO-d$_6$, under N$_2$, irradiation at 410 nm.*

For the second set of experiments, VTNA of the data from Figure 3-30 gave the best overlap of data points for a reaction order of 0.5 (Figure 3-32).

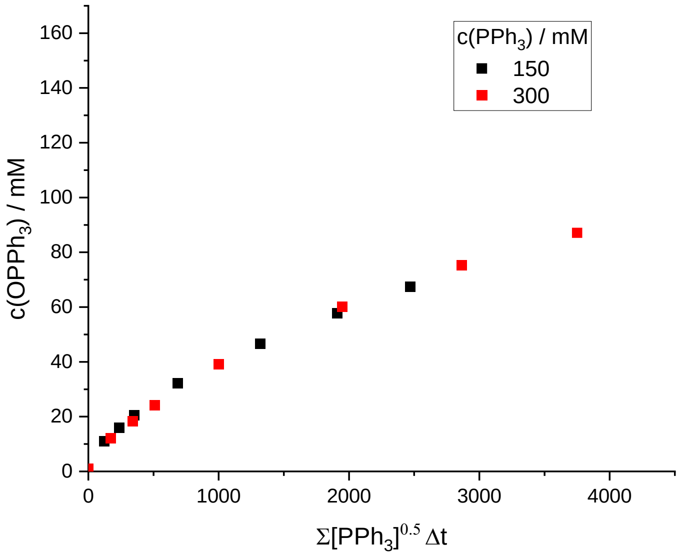

*Figure 3-32: VTNA plot for different amounts of PPh$_3$.*

The reaction order of phosphine determined by the two sets of experiments was calculated to be 1 in DMSO-d$_6$, and 0.5 in acetone-d$_6$.

This difference could suggest a difference in the mechanism. When the reaction is performed in DMSO, the sulphide needed for regeneration is already part of the complex at the beginning of the reaction as it is present in vast excess (being the solvent) and occupies the sixth coordination site on the complex. In contrast, most of these sites will be occupied by acetone when it is the solvent. In DMSO, a more concerted reaction could be possible where oxidation of the phosphine and regeneration of the complex take place simultaneously (see also Scheme 3-4).

### 3.6.2 OAT at varied sulfoxide concentration

To study the effect of the sulfoxide two sets of experiments were performed in acetone-d$_6$. The first set used concentrations of 50, 100 and 200 mM of DMSO, the second one used concentrations of 150 and 300 mM of **SO-2**. The plots of concentration of OPPh$_3$ vs. time that include several datapoints between 0 and 4 h for the two sets of experiments are shown in Figure 3-33 and Figure 3-34.

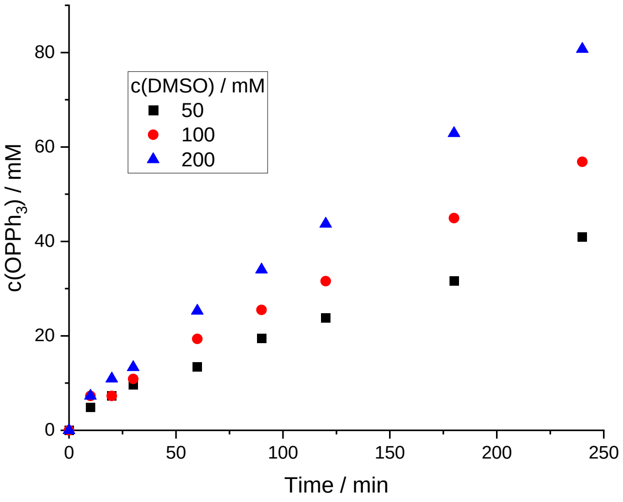

*Figure 3-33: Plot of concentration of $OPPh_3$ vs. time for the oxidation $PPh_3$ at various concentrations of DMSO. Conditions: 1 mM* ***Mo-1****, 300 mM $PPh_3$ in acetone-$d_6$, $N_2$ atmosphere, irradiation at 410 nm.*

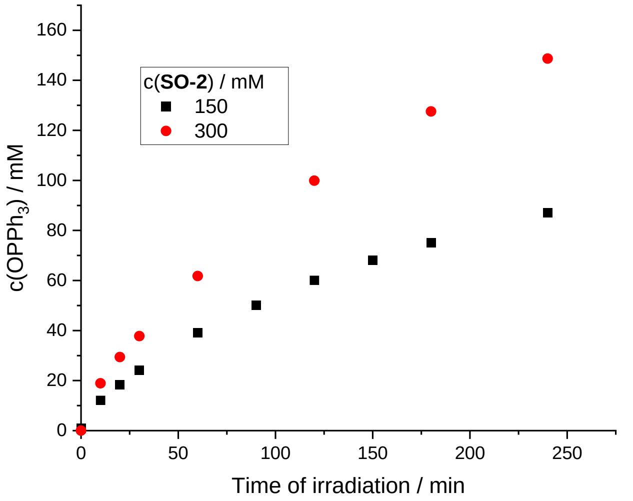

*Figure 3-34: Plot of concentration of $OPPh_3$ vs. time for the oxidation $PPh_3$ at various concentrations of* ***SO-2****. Conditions: 1 mM* ***Mo-1****, 300 mM $PPh_3$ in acetone-$d_6$, $N_2$ atmosphere, irradiation at 410 nm.*

In both cases a higher concentration of product $OPPh_3$ is obtained when the initial concentrations of DMSO or **SO-2** are increased. The exact correlation is determined by VTNA, the plot for DMSO shown in Figure 3-35 and the plots for **SO-2** in Figure 3-36.

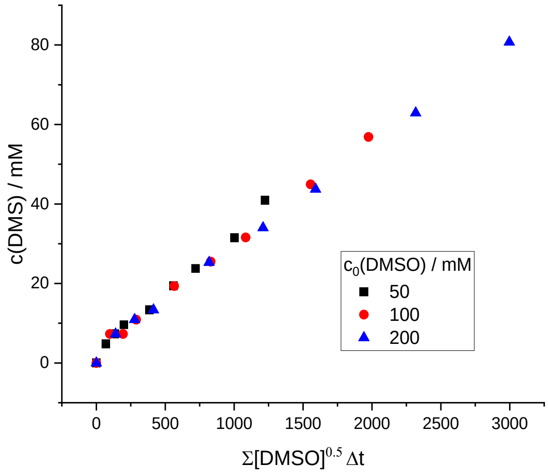

*Figure 3-35: VTNA plot for different amounts of DMSO.*

The best alignment for DMSO is found for an order of 0.5, although some deviations are still present.

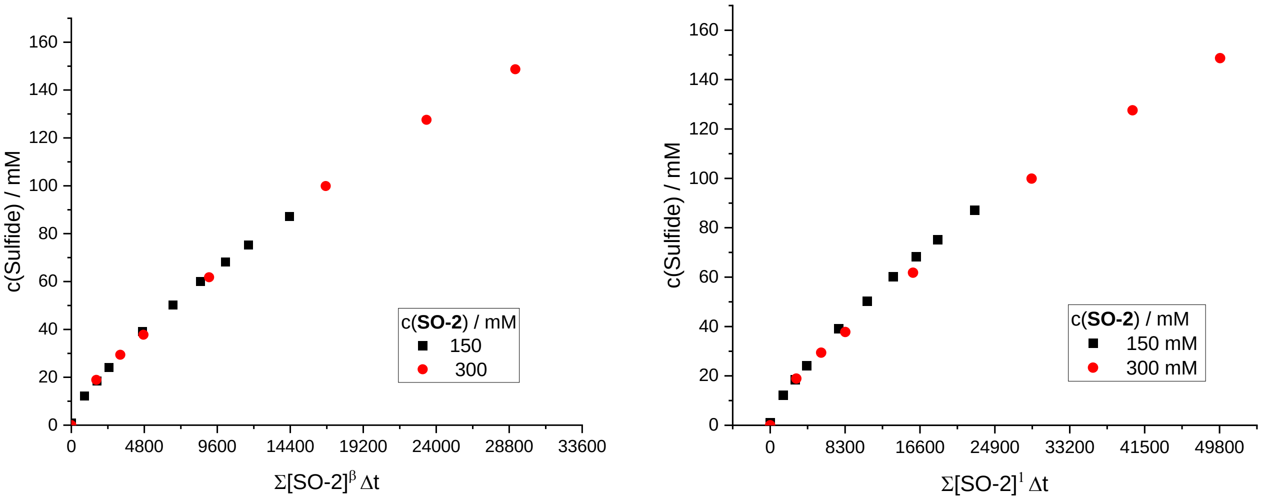

*Figure 3-36: VTNA plots for different amounts of **SO-2**, reactant order of 0.9 (left) and 1 (right).*

The best overlap of data points was obtained for a reaction order of 0.9, although the difference to an order of 1.0 is minimal.

A reaction order of 0.5 was obtained for DMSO and an order of 0.9 for **SO-2**. Reaction conditions were identical for both sulfoxides. This difference is again suggestive of a difference in the mechanism similar to the previous section.

### 3.6.3 OAT at varied catalyst concentration

Catalyst concentration was varied to study its influence on the conversion of phosphine and to find the optimal catalyst concentration. Two sets of experiments were performed, in DMSO-$d_6$ and in acetone-$d_6$.

In the first set of experiments the catalyst concentration was varied between 0.01 and 3 mM. The exact concentrations tested and conversions obtained are summarised in Table 3-16.

*Table 3-16: Concentration of $OPPh_3$ at different catalyst concentrations.*

| Time of Irradiation / h | Concentration[a] of $OPPh_3$ in mM at c([**Mo-2**]) | | | | |
|---|---|---|---|---|---|
| | 3 mM | 1 mM | 0.5 mM | 0.1 mM | 0.01 mM |
| 3 | 228 | 225 | 219 | | |
| | | | | | |
| 2 | | 207 | 189 | 105 | |
| 4 | | 273 | 240 | 111 | |
| 6 | | 291 | 246 | 117 | |
| | | | | | |
| 3 | | 243 | | 129 | 30 |
| 6 | | 288 | | 132 | 42 |
| 10 | | 288 | | 132 | 48 |

Conditions: 300 mM $PPh_3$, DMSO-$d_6$, under $N_2$, irradiation at 410 nm. [a] An uncertainty in the measurement of 6 mM is estimated.

First, catalyst concentrations of 3, 1 and 0.5 mM were tested. Surprisingly, no significant difference in the concentration of the product $OPPh_3$ was observed.

The so-called inner filter effect, where molecules at the centre of the sample are effectively shielded from the light by molecules around them, could play a role here. There is only a certain number of catalyst molecules that can absorb light at a time. Above this threshold concentration additional molecules do not contribute to the reaction as the limit of catalyst molecules that can be exited at a moment has been reached.

Catalyst concentrations of 1, 0.5, 0.1 and 0.01 mM were employed next to test for the inner-filter effect and potentially determine a threshold concentration. In all cases, a lower conversion was obtained when catalyst concentration was reduced.

A more important observation can be made when conversion rates are compared before and after the first measurement (at 2 hours and 3 hours respectively). Taking, for example, the second entry at 1 mM concentration, a concentration of 207 mM is achieved in the first two hours with a further increase to 273 and 291 mM, respectively, in the following two intervals of 2 hours each. As the reaction proceeds, substrates are being used up which decreases their concentration and thereby lowers reaction rate. However, at lower catalyst concentration, especially at 0.1 mM and less, concentration increases by a mere 6 mM in the hours following the recording of the first data point. Given that the reaction had not even reached 50 % conversion, this drop in conversion rate indicates catalyst deactivation.

Catalyst deactivation could be due to hydrolysis of the imine bond by residual water, which is present in all samples, but this process might be slow and at higher concentrations there is enough complex left to continuously catalyse the reaction. Alternatively, dissociation of the ligand, rearrangement or aggregation of catalyst could be occurring. Evidence for either of those pathways has not be found

$^1$H NMR spectra of the samples showed disappearance and shifting of the signals of the complex, but no signal of an aldehyde which would be the product of hydrolysis or other species.

VTNA was not performed as there was not enough good quality data. At catalyst concentrations below 1 mM, deactivation / decomposition of catalyst is occurring that would require the concentration of active catalyst to be known in order to perform this analysis. Above a concentration of 1 mM the only available data point indicates no change to catalyst activity with increased concentration. Because these results were very unclear no further experiments under these conditions were performed. Instead OAT was studied in acetone with **SO-2** and $PPh_3$ where a slower reaction rate was expected (c.f. section) allowing to observe the effects of substrates and catalyst on the reaction rate.

In the second set of experiments acetone-$d_6$ was used as the solvent and the catalyst concentration was varied between 0.3 and 8 mM. Each concentration was tested twice. Exact concentrations of **Mo-2** tested, and conversions obtained are summarised in Table 3-17, the concentration of the phosphine oxide over time is shown in Figure 3-37.

*Table 3-17: Concentration of $OPPh_3$ after 3 h at different concentrations of* ***Mo-2.***

| Concentration of **Mo-2** / mM | Concentration [a] of $OPPh_3$ / mM | |
|---|---|---|
| | Experiment 1 | Experiment 2 |
| 0.3 | 110 | 111 |
| 0.5 | 115 | 118 |
| 0.8 | 120 | 136 |
| 1 | 128 | 135 |
| 3 | 95 | 92 |
| 5 | 79 | 83 |
| 8 | 72 | 71 |

Conditions: 300 mM $PPh_3$, 300 mM **SO-2,** acetone-$d_6$, $N_2$, irradiation for 3 h at 410 nm. [a] An uncertainty in the measurement of 6 mM is estimated.

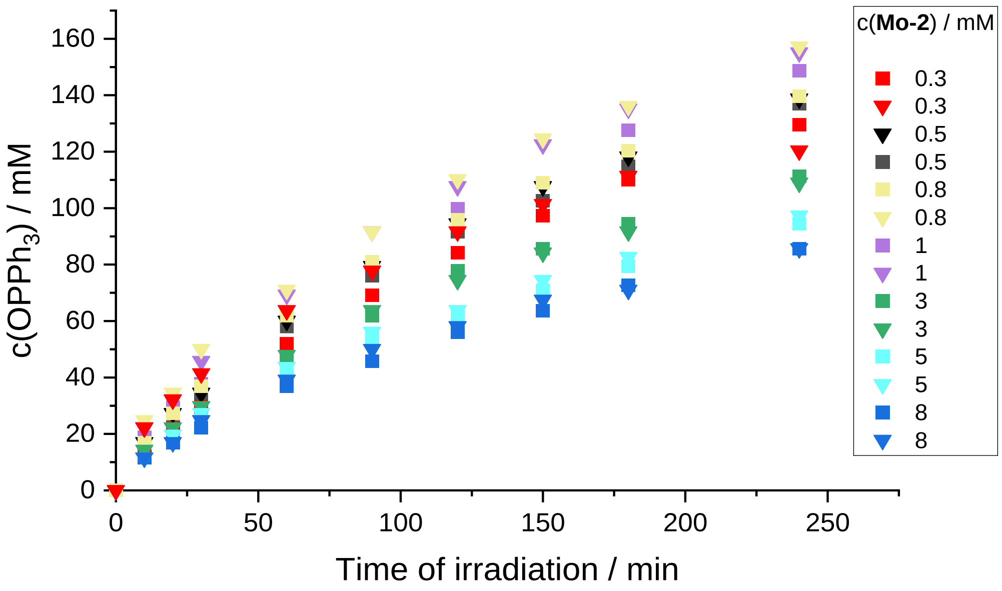

*Figure 3-37: Plot of concentration of OPPh$_3$ vs. time at different concentrations of* ***Mo-2****. In acetone-d$_6$, under N$_2$, excitation wavelength of 410 nm, concentration of PPh$_3$ = 300 mM, concentration of* ***SO-2*** *= 300 mM. An uncertainty in the measurement of 6 mM is estimated.*

Interestingly, the concentration versus time plot shows that the highest conversion of phosphine to phosphine oxide is obtained at catalyst concentrations of 0.8 and 1 mM. These are also the concentrations at which there is more variability between experiments 1 and 2. At all other concentrations the difference in the results from the two repeats is insignificant.

The correlation between catalyst concentration and reaction rate becomes clearer when the concentration of product OPPh$_3$ is viewed as a function of catalyst concentration. Concentration of OPPh$_3$ after 2, 3 and 4 h *vs.* initial concentration of catalyst is plotted in Figure 3-38.

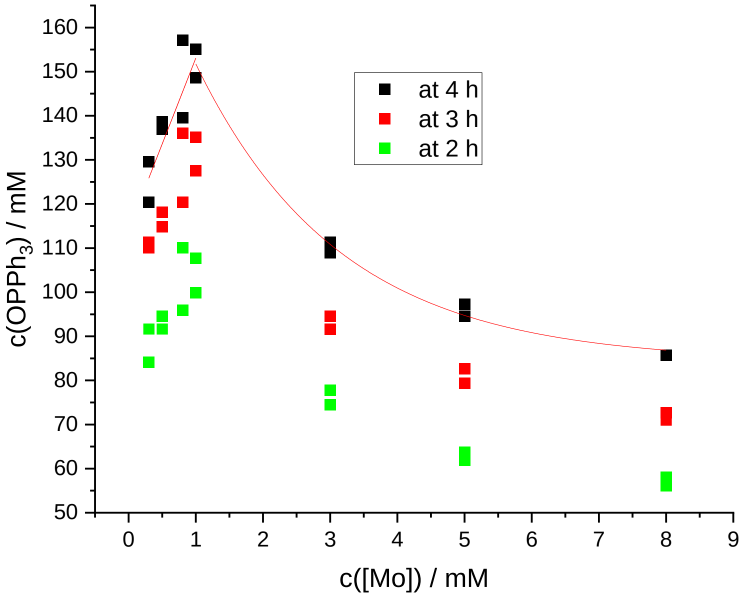

*Figure 3-38: Plot of the concentration of OPPh$_3$ against initial catalyst concentration after 2, 3 and 4 h. with linear fitting of the data after 4 h and at catalyst concentrations ≤ 1 mM and single exponential fitting at concentrations ≥ 1 mM, respectively. In acetone-d$_6$, under N$_2$, excitation wavelength of 410 nm, catalyst* ***Mo-2****, concentration of PPh$_3$ = 300 mM, concentration of* ***SO-2*** *= 300 mM. R$^2$ values: 0.73 (linear fit) and 0.99 (exponential).*

From this plot, a correlation between initial concentration of catalyst and conversion is evident. Maximum conversion appears to be reached with a catalyst concentration of 1 mM. Whilst the approximately linear increase of conversion with concentration up to 1 mM is intuitively expected, the exponential decrease above 1 mM is rather unexpected. Concentration dependent dimerisation and inner-filter effect could contribute to these observations. Experiments in DMSO suggest catalyst deactivation, but the difference between solvents is more pronounced than for the substrates.

### 3.6.4 Summary and discussion of the kinetic analyses

Table 3-18 summarises the experimental conditions and calculated reaction orders.

*Table 3-18: Overview on kinetic experiments: parameter under investigation (varied), nature of substrates, concentration of species not investigated and solvents used.*

| c(**Mo-2**) /mM | c($PPh_3$) / mM | Sulfoxide | c(sulfoxide) /mM | solvent | Reactant order |
|---|---|---|---|---|---|
| 1 | varied | DMSO-$d_6$ | excess | DMSO-$d_6$ | 1 |
| 1 | varied | **SO-2** | 150 | acetone-$d_6$ | 0.5 |
| | | | | | |
| 1 | 300 | DMSO | varied | acetone-$d_6$ | 0.5 |
| 1 | 300 | **SO-2** | varied | acetone-$d_6$ | 0.9-1.0 |
| | | | | | |
| varied | 300 | DMSO-$d_6$ | excess | DMSO-$d_6$ | / [a] |
| varied | 300 | **SO-2** | 300 | acetone-$d_6$ | / [b] |

[a] Catalyst deactivation at lower concentrations. [b] Linear increase of rate with catalyst concentration < 1 mM, exponential decrease at concentrations > 1 mM.

Reaction order in substrates changed depending on the solvent. Although there is no clear rate law under the conditions studied, it seems clear that both the phosphine and sulfoxide are present and that neither phosphine oxidation nor DMSO reduction dominate the rate of reaction. A strong dependence was also seen in the correlation between catalyst concentration and conversion.

The insensitivity of the reaction in DMSO-$d_6$ to changes in catalyst concentration, apart from catalyst deactivation, suggests the reaction to be limited by a different parameter (*e.g.* the amount of light that can be absorbed.

In the literature of thermal OAT the reaction order in substrates is reported as being 1 for phosphines and also for sulfoxides although focus has been on the first half of the catalytic cycle. For example, Whiteoak *et al.* reported an order of 1 in $PPh_3$ in the reaction with Mo salan complexes encountered earlier (Figure 3-5) in DMSO. Topich and Lyon also reported an order of 1 in $PEtPh_2$ in DMF using SSP and SSE based systems (Figure 3-3). Examples including tungsten complex reported the same order.[150,161,162]

The question whether the reaction order in a photochemical reaction has any meaning, has been raised. Logan has argued that only quantum yield is a meaningful parameter to describe photochemical reactions.[163] Hippler on the other hand argued that the elementary steps that compose a photochemical reaction do have defined molecularity and reaction order.[164] A reply from Toby criticised Hippler analysis, prompting the latter to a follow-up comment.[165] Photochemical reactions clearly pose some issues regarding their treatment.

Despite this dispute, reaction order (determination) continues to be applied to photochemical systems. Kaphan and co-workers used VTNA to determine reaction orders in the reduction of cyclohexanone with formate, photocatalysed by an iridium complex and to identify a change in active catalyst speciation.[166]

## 3.7 Stoichiometric reaction between Mo-2, W-2 and $PPh_3$

The difference in OAT activity between complexes studied in this work cannot be fully rationalised based on the data presented so far. Based on the kinetic analysis there also seems to be a strong dependence on the solvent and sulfoxide used. Stoichiometric reactions between complexes and $PPh_3$ could provide additional insights by focussing on the first half of the catalytic cycle, the reduction of the complex by $PPh_3$. Analysis of the reduced intermediate could show if dimerisation or other reactions take place which could affect activity.

### 3.7.1 Analysis by ATR-IR spectroscopy of the stoichiometric reaction between , Mo-2, W-2 and $PPh_3$

The reaction mixtures contained **Mo-2** and 1 equivalent of $PPh_3$ in acetone-$d_6$ or **W-2** and 5 equivalents of $PPh_3$ in a 1:1- mixture of acetone-$d_6$ and DMF-$d_7$, as **W-2** is not sufficiently soluble in acetone. After irradiation at 410 nm for 16 h, the solvent was removed under reduced pressure and the solids analysed by ATR-IR spectroscopy. Analysis of the results will focus on the wavenumber range of 400 to 1000 $cm^{-1}$ where the characteristic bands involving the metal oxo centre are found. ATR-IR spectra of $PPh_3$ and $OPPh_3$ are shown in Figure 3-39.

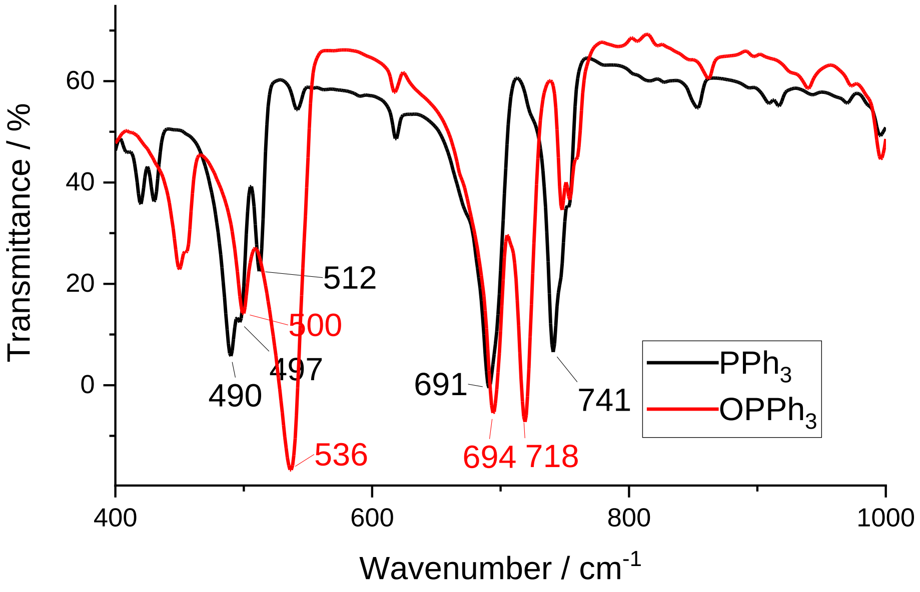

*Figure 3-39: ATR-IR spectra of $PPh_3$ and $OPPh_3$ in the range of 400 to 1000 $cm^{-1}$.*

The spectrum of the reaction mixture containing equal amounts of **Mo-2** and $PPh_3$ is shown in Figure 3-40. In the region of 900 to 950 $cm^{-1}$ where the Mo=O stretching bands are found a single intense and broad band is seen in the reaction mixture at 939 $cm^{-1}$. The unreacted (as synthesised) **Mo-2** however shows two ($\nu_{sym}$(Mo=O) = 936 and $\nu_{asym}$(Mo=O) = 909 $cm^{-1}$). The presence of only one band signifies that only one oxo ligand is present. The loss of one of the oxo ligands is expected during OAT, however, both Mo(IV) as well as Mo(V) species could have formed.

From the bands around 700 $cm^{-1}$ it can be seen that the phosphine has been oxidised. The intense band at 724 $cm^{-1}$ is characteristic of $OPPh_3$ (718 $cm^{-1}$ in $OPPh_3$). Bands found in $PPh_3$ but not $OPPh_3$ overlap with bands of **Mo-2** (743 $cm^{-1}$, 490 $cm^{-1}$), but from their intensities and from the bands in the region between 480 and 500 $cm^{-1}$ the amount of $PPh_3$ present seems to be small.

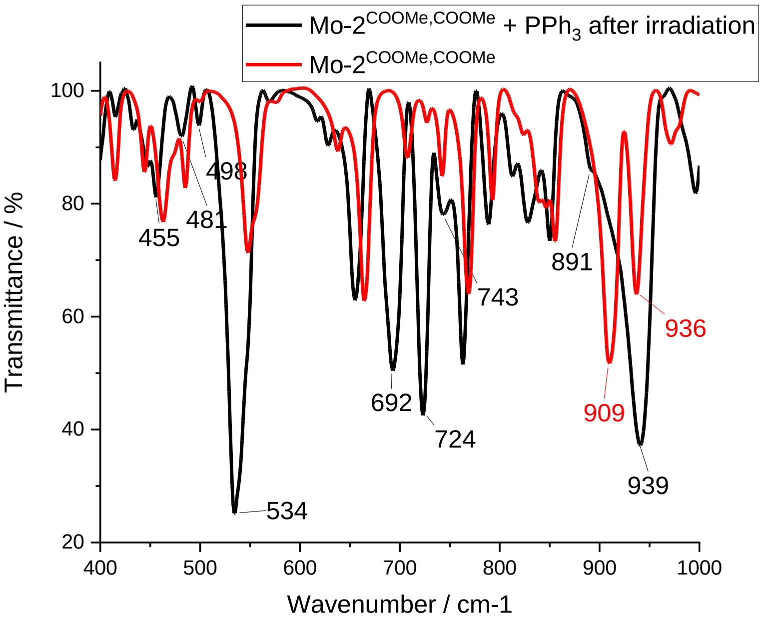

*Figure 3-40: ATR-IR spectra of the solid obtained from the reaction mixture of* ***Mo-2*** *and* $PPh_3$ *after irradiation and of pure* ***Mo-2*** *in the range of 400 to 1000* $cm^{-1}$*.*

The IR spectrum of the solid obtained in the analogous reaction with **W-2**, together with the spectrum of as synthesised **W-2** are shown in Figure 3-41. Note that **W-2** is in its di- or oligomeric form (see chapter 2.3.6).

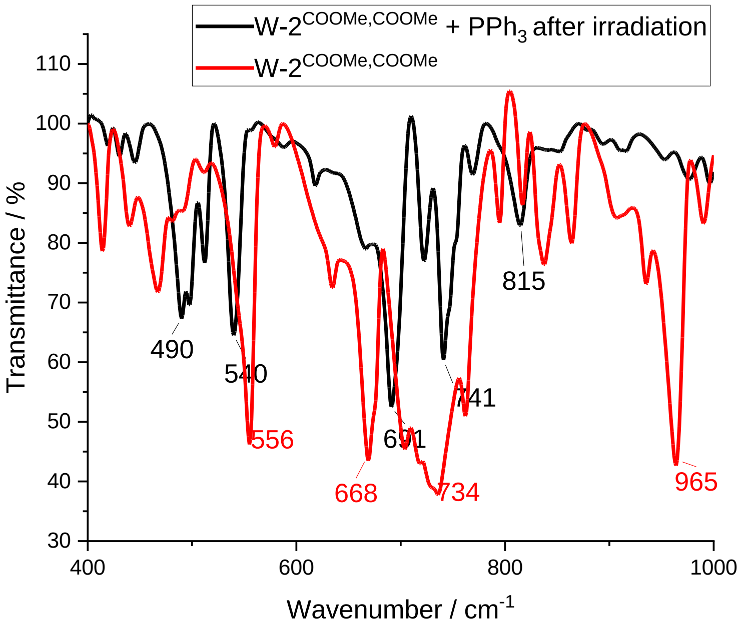

*Figure 3-41: ATR-IR spectra of the reaction mixture of* ***W-2*** *with PPh$_3$ after irradiation in the range of 400 to 1000 cm$^{-1}$ and of* ***W-2****.*

The sample shows characteristic bands of PPh$_3$ and OPPh$_3$, some of them shifted by up to 5 cm$^{-1}$ (c.f. Figure 3-39). The absence of strong bands above 900 cm$^{-1}$ suggest that no W=O groups are present. However, a band at 815 cm$^{-1}$ could be due to a decomposition product containing tungsten.

From IR spectroscopy it appears that **Mo-2** has transferred one of its oxo ligands and **W-2** has performed OAT, but decomposition occurred afterwards, possibly due to DMF which was added to the tungsten samples to increase solubility.

### 3.7.2 Analysis by $^1$H and $^{31}$P NMR spectroscopy of the stoichiometric reaction between Mo-2, W-2 and PPh$_3$

Reaction mixtures containing **Mo-2** or **W-2** and 5 equivalents (1 in the case of **Mo-2**) of PPh$_3$ in acetone-d$_6$ (**Mo-2**), or a 1:1- mixture of acetone-d$_6$ and DMF-d$_7$, as **W-2** is not sufficiently soluble in acetone**,** were irradiated at 410 nm for 16 h and analysed by $^1$H and $^{31}$P NMR spectroscopy.

The $^1$H NMR spectra of a mixture of **Mo-2** and PPh$_3$ in equimolar amounts in acetone-d$_6$ are shown in Figure 3-42 as prepared and after irradiation overnight.

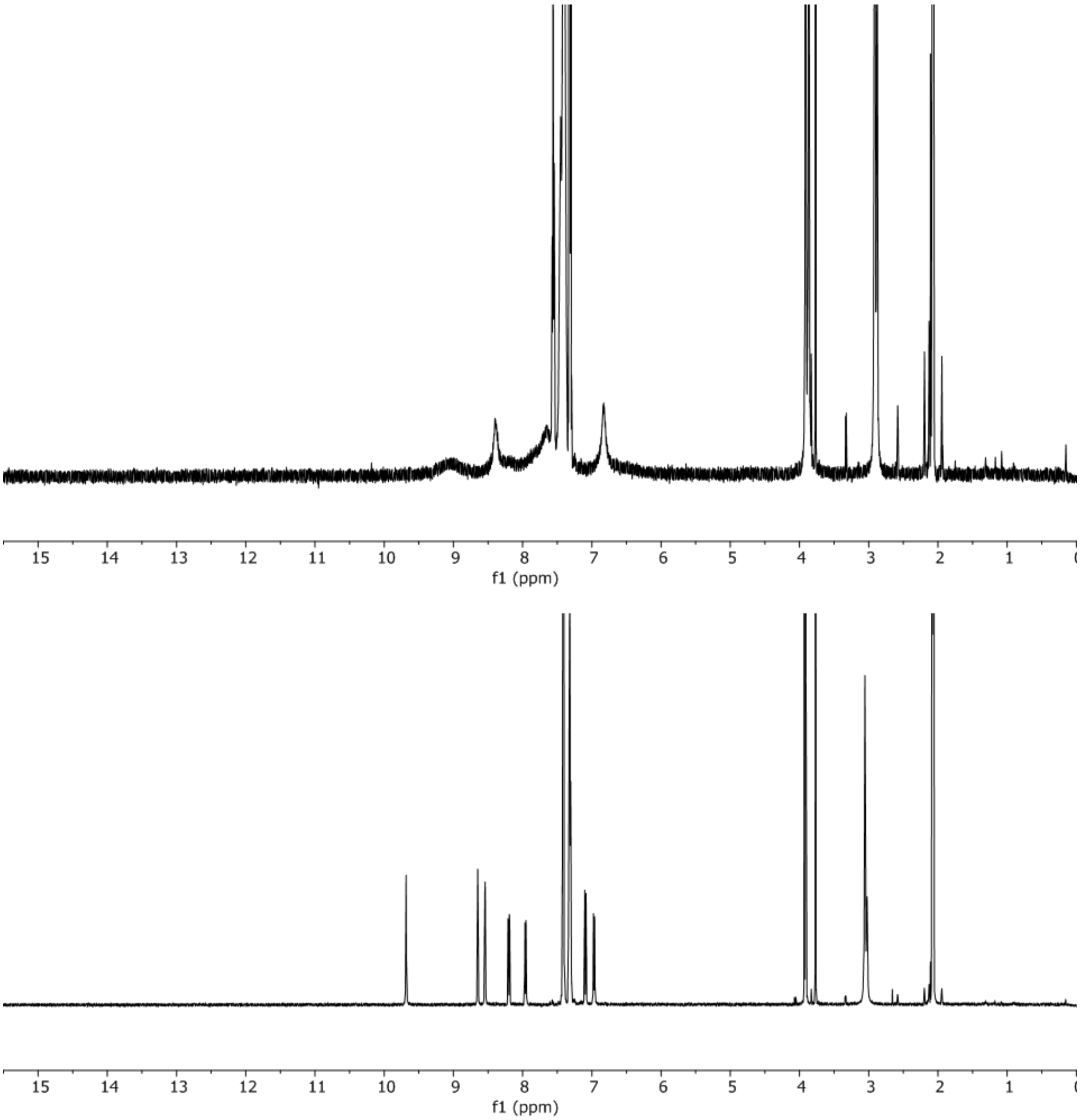

*Figure 3-42: $^1$H NMR spectra of a solution containing equimolar amounts of* ***Mo-2*** *and $PPh_3$ in acetone-$d_6$ under $N_2$ as prepared (bottom) and after irradiation for 16 h at 410 nm (top).*

The difference upon irradiation is significant. The resonances of the aromatic protons and the imine have disappeared. Instead several broad and low intensity signals appear between 6.5 and 9.5 ppm. Signals at 7.3 and 7.4 ppm show the presence of free $PPh_3$. The later signals overlaps with additional resonances which together with a distorted triplet at 7.55 and a very broad signal at 7.70 ppm are in the chemical shift range expected for $OPPh_3$. Interestingly, the resonances from the two ester groups are still clearly visible. The $^{31}$P NMR spectrum of this sample in the range of -240 to 140 ppm only showed one signal at -5.6 ppm assigned to free $PPh_3$.

The resonances or lack thereof in the $^1$H NMR spectrum points to the presence of a paramagnetic species. A paramagnetic molybdenum centre, having unpaired electrons, would strongly affect the NMR signal of atoms close to it while the ones further away are little affected. This may explain the absence of resonances of the aromatic protons which are fairly close to molybdenum (or the conjugated π-system that transfers effects on the metal) while the protons on the ester groups are further away. Some of the signal belonging to $OPPh_3$ are distorted and broadened which could be due to binding to the paramagnetic molybdenum.

The $^1H$ NMR spectra of the mixture of **W-2** with $PPh_3$ (1:5) in acetone-$d_6$ / DMF-$d_7$ (1:1) as prepared and after irradiation overnight are shown in Figure 3-43. $^{31}P$ NMR showed the formation of $OPPh_3$.

Many new signals appear after irradiation in the $^1H$ NMR spectrum. Those with high intensity around 7.5 ppm belong to newly formed $OPPh_3$. Additional signals with lower intensity are attributed to the tungsten complex or fragments and decomposition products thereof. The singlets above 8.5 ppm are likely ligand detached from the metal centre (signal of the imine at 9 ppm) or hydrolysis products (signals of aldehyde and OH group between 10 and 11 ppm, Figure 3-43). In addition, the region around 3.8 ppm where the signals of the two methyl groups are found becomes much more complex after irradiation suggesting formation of several decomposition products.

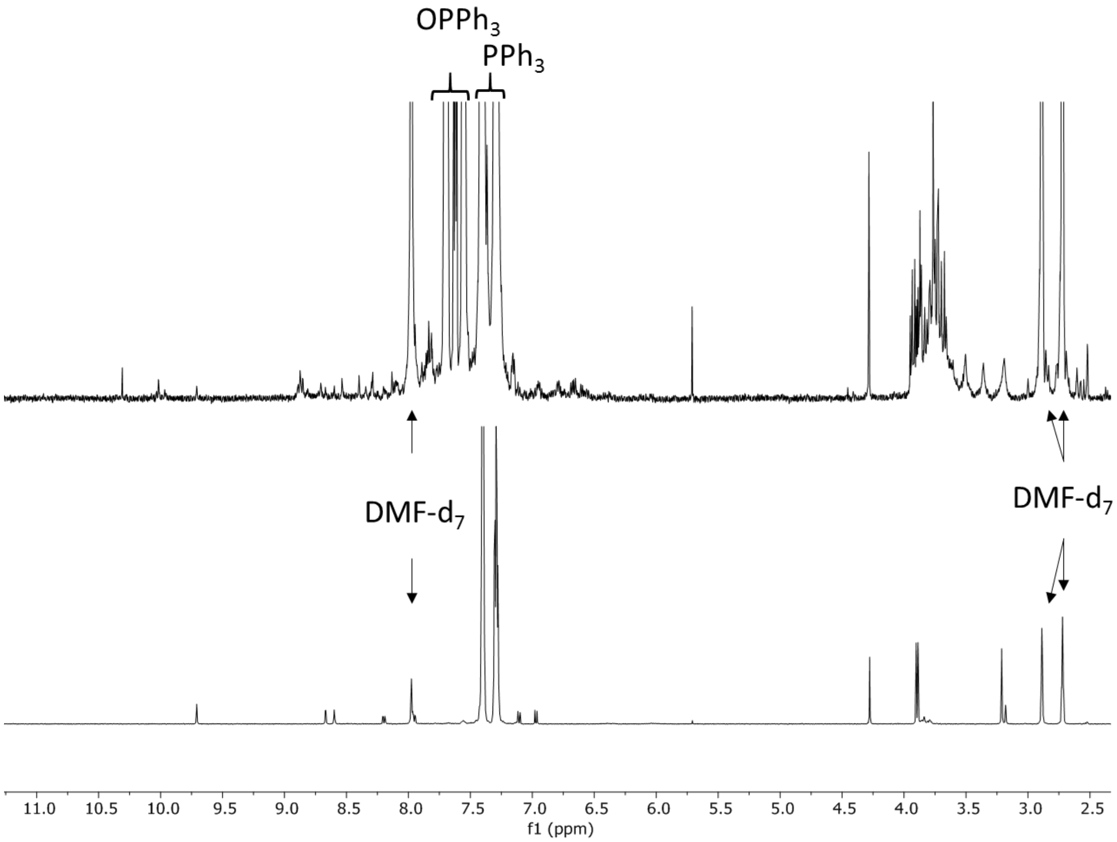

*Figure 3-43: $^1H$ NMR spectra of a 1:5 mixture of **W-2** and $PPh_3$ in acetone-$d_6$ / DMF-$d_7$ (1:1) under $N_2$ before (bottom) and after (top) irradiation at 410 nm for 20 h.*

### Electronic configuration of reduced molybdenum

The molybdenum and tungsten complexes contain the $MO_2$-core (M = Mo, W) where the metal is formally in the +6 oxidation state, M(VI), and is a $d^0$ cation. Upon OAT the metal formally gains two electrons and is reduced to M(IV) which is $d^2$. Through comproportionation between M(IV) and M(VI) two M(V) $d_1$ cations could form.

Hence, during catalysed OAT a reaction mixture could contain $d^2$, $d^1$ and $d^0$ cations. d electrons are relevant in UV-Vis spectroscopy as they can give raise to weak d-d transition and make MLCT transitions possible.[167] In NMR spectroscopy it is important whether unpaired electrons are present as these electrons complicate the analysis of NMR spectra.[168]

In $d^2$ Mo(IV) the two electrons can be paired occupying a single molecular orbital (singlet configuration) or unpaired occupying different molecular orbitals (triplet configuration). The configuration that is lower in energy will be favoured. Pietsch and Hall have calculated the energy difference between singlet and triplet for the model complex $[MoO_2(NH_3)_2(SH)_2]$. The triplet configuration was favoured by only 1 kcal/mol. The authors assumed the calculated OAT to $PMe_3$ to yield the singlet configuration as the triplet configuration cannot be accessed due to different symmetries of the singlet and triplet states surfaces.[122] Kail *et al.* also concluded that the triplet state is not important in OAT of $[MoO_2(L)OPh]$ (L = hydrotris(3-isopropylpyrazol-1-yl)borate)) to $PEt_3$ or $PPh_2Me$, based on calculations and the lack of experimental evidence for the triplet configuration.[121]

Mo(V) only has one unpaired electron. However, in OAT Mo(V) is thought to always form oxygen bridged dimers (see Scheme 3-3). In these dimers, orbitals from the two metals and the bridging oxygen form three-centre delocalised molecular orbitals. The bonding and nonbonding orbitals are filled by the two unpaired electrons from each metal and two electrons from the bridging oxygen which gives rise to a diamagnetic molecule.[117,169] Diamagnetism is found in virtually all dimeric Mo(V) species.[170]

Based on the above discussion, in this work a diamagnetic molybdenum species would be the most likely result of OAT. However, the $^1H$ NMR spectrum of **Mo-2** after reaction with $PPh_3$ (Figure 3-42) suggest the presence of a paramagnetic species which would suggest Mo(IV) in the triplet configuration. Additional experiments, *e.g.* EPR spectroscopic measurements, are needed to confirm the formation of paramagnetic Mo(IV).

The $^{31}P$ NMR spectrum of **W-2** shows formation of $OPPh_3$ but the $^1H$ NMR spectrum suggests decomposition of the complex in line with the IR spectroscopic results (Figure 3-41).

## 3.7.3 Analysis by UV-Vis spectroscopy of the stoichiometric reaction between Mo-2, W-2 and $PPh_3$

Reaction mixtures containing **Mo-2** and 1 equivalent of $PPh_3$ in acetone-$d_6$ or 5 equivalents in MeCN-$d_3$ and **W-2** and 5 equivalents of $PPh_3$ in a 1:1- mixture of acetone-$d_6$ and DMF-$d_7$, as **W-2** is not sufficiently soluble in acetone**,** were irradiated at 410 nm for 16 h and analysed by UV-Vis spectroscopy. Note that $PPh_3$ and $OPPh_3$ only absorb light of a wavelength < 330 nm.

Figure 3-44 shows the UV-vis spectra of **Mo-2** after irradiation in the presence of $PPh_3$ in acetone-$d_6$ and MeCN-$d_3$. After irradiation, both samples had gone from yellow solutions to dark green ones. In both solvents there is one main band at 431 nm in acetone and at 422 nm in MeCN in the reaction mixture which is red shifted by 21 nm and 10 nm. The difference in absorbance before and after irradiation is much higher in acetone than in MeCN. This could be due to the reaction having progressed further in acetone or due to the different solvent and higher concentration of $PPh_3$. It also has to be noted that the MeCN sample had very fine particles suspended in it which could have affected the measurement.

Absorbance of the main band continues in to the 700 to 750 nm region in both samples with a clear but broad peak in MeCN at 610 nm. A new band is consistent with the presence of d-d transitions in reduced molybdenum, but these are possible in Mo(IV) as well as Mo(V).

The perceived green colour of the irradiated sample would correspond to absorbance of red light and a band around 620 to 700 nm. Absorbance in that region is relatively weak, in MeCN there is a band centred at 620; the main band is around 450 nm in both solvents. A band in the range of 580 to 620 nm would be perceived as blue, whereas around 450 nm it would be perceived as orange (430 to 490 nm). However, this concept of complementary colours (colour absorbed <-> colour perceived) is not suitable when two bands in the visible region exist.[167]

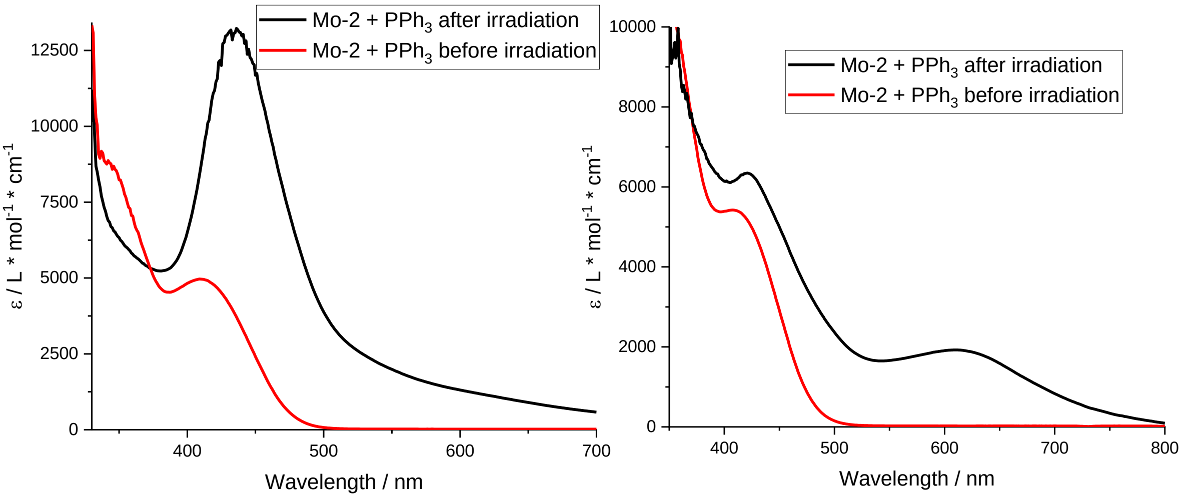

*Figure 3-44: UV-Vis spectra of the reaction mixtures of **Mo-2** with $PPh_3$ in acetone-$d_6$ (0.3 mM, 1 eq $PPh_3$, left) before and after, and in MeCN-$d_3$ (0.3 mM, 5 eq $PPh_3$, right) before and after irradiation at 410 nm for 16 h.*

The UV-Vis spectrum of **W-2** after irradiation in the presence of $PPh_3$ is shown in Figure 3-45. The sample changed colour from a yellow solution to an orange-brown solution after irradiation. One absorption band is seen at 468 nm red shifted by 69 nm.

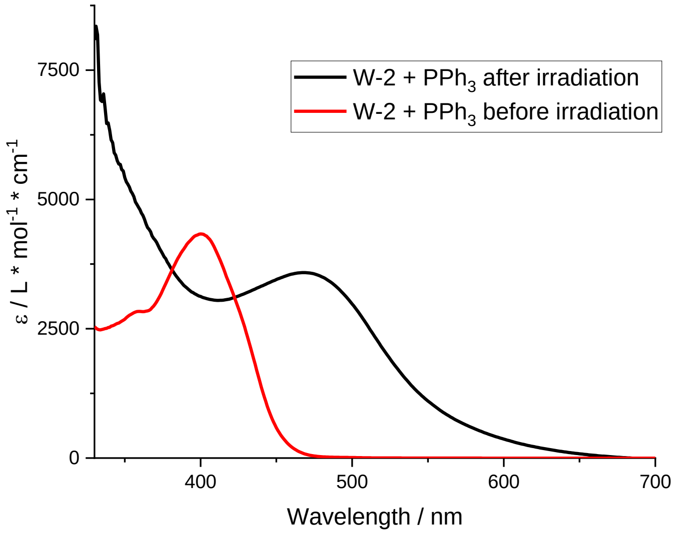

*Figure 3-45: UV-Vis spectra of reaction mixture of* ***W-2*** *with* $PPh_3$ *in DMF/acetone at a concentration of 0.4 mM before and after irradiation at 410 for 16 h.*

The spectra of **Mo-2** in acetone and **W-2** after irradiation are quite similar, both only showing one broad band that continues up to 700 nm or 650 nm, respectively. In **Mo-2** this band is much more intense compared to the spectrum before irradiation whereas in **W-2** it is less intense compared to the spectrum before irradiation.

Reduction of **Mo-2** and **W-2** with $PPh_3$ yield Mo (IV) or (V) and W (IV) or (V) which possess d electrons. Additional bands due to the presence of d electrons are possible, although particularly d-d transitions would be quite weak due to them being formally forbidden.[167] An additional transition is only seen in **Mo-2** in MeCN, but they could be hidden under or overlapping with the main band in **Mo-2** in acetone and in **W-2**. Whether the spectral features are due to the metal (IV) or (V) state could not be determined.

Differences between **Mo-2** and **W-2** are expected due to the d orbitals in **W-2** laying higher in energy and the difference in solvents used, but IR and NMR spectroscopy had also shown degradation of the tungsten sample.

### 3.7.4 Analysis by LIFDI-Mass spectrometry of the stoichiometric reaction between Mo-2, W-2 and $PPh_3$

Reaction mixtures containing **Mo-2** or **W-2** and 1 and 5 equivalents of $PPh_3$ for **Mo-2** and **W-2**, respectively, in acetone-$d_6$ (**Mo-2**), or a 1:1- mixture of acetone-$d_6$ and DMF-$d_7$, as **W-2** is not sufficiently soluble in acetone**,** were irradiated at 410 nm for 16 h and analysed by LIFDI-MS. LIFDI or liquid injection field desorption ionisation is a soft ionisation technique by an electric field that minimises fragmentation of the analyte.[171]

The LIFDI-mass spectrum obtained in the experiment with **Mo-2** is shown in Figure 3-46, with potential structures corresponding to the observed m/z values in Figure 3-47. Several groups of signals are seen. (Additional spectra zooming in on the individual group of signals as well as mass accuracy calculations can be found in the appendix).

The peak at 278 was identified as $OPPh_3$, the expected product of OAT. All other signals contain molybdenum based on their isotope pattern (see appendix). The most intense one with an m/z of 456.9693 was identified as unreacted **Mo-2** having lost the bound MeOH. Close to it is a much less intense signal of an m/z of 440.9721, which corresponds to a reduced Mo(IV) mono-oxo complex, [MoO(**L-2**)].

The peak at 719.0598 corresponds to [$MoO_2$(**L-2**)($PPh_3$)] but two structures are conceivable. One corresponding to unreacted **Mo-2** with $PPh_3$ bound the other one corresponding to reduced mono oxo **Mo(IV)-2** with $OPPh_3$ bound where one oxo ligand has been transferred to the phosphine to form phosphine oxide. Binding of $PPh_3$ has not been observed in a control sample containing $PPh_3$ and **Mo-2** that was not irradiated. Binding of phosphine oxide after OAT agrees with the mechanism discussed in section 3.1.2.3 where the newly formed oxide stays bound to molybdenum until replaced by solvent.

At an m/z of 735.0546 $OPPh_3$ bound to **Mo-2** was identified.

Finally, the peak at 893.9444 can be attributed to a species of the formula $[MoOL\text{-}2]_2O$. This is the molybdenum(V) dimer. Note that this peak at 893.9444 is the most intense peak for $[MoOL\text{-}2]_2O$ but the values calculated in Figure 3-47 (obtained from Chem Draw) and Figure A-3-6 (obtained from the mass spectrometer) have a higher m/z due to this value being based on isotopes with lower abundance. The isotope patterns measured around 894 and the pattern calculated for [MoO(**L-2**)]$_2$O (Figure A-3-6) match exactly.

It has to be noted that the detection of the species discussed above does not necessarily prove their existence in the reaction mixture during OAT. Their formation only under the conditions of the mass spectrometer cannot be excluded.

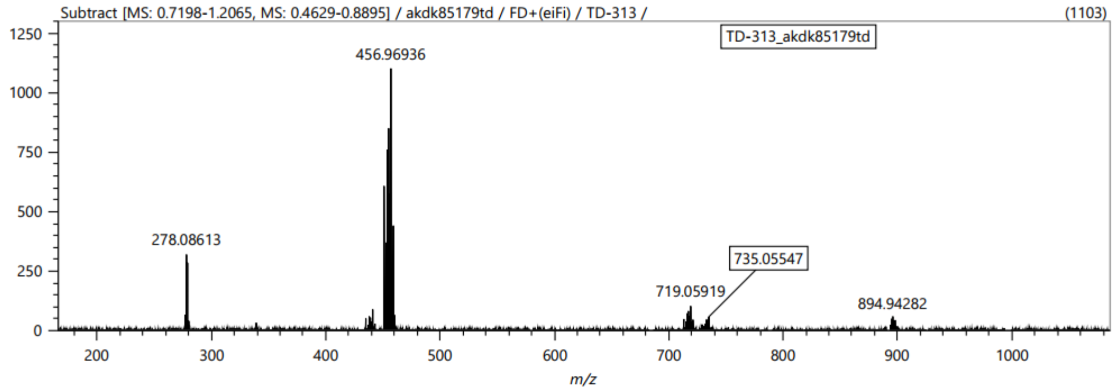

*Figure 3-46: LIFDI-mass spectrum of a mixture of* ***Mo-2*** *and* $PPh_3$ *in acetone-*$d_6$ *after irradiation at 410 nm for16 h. Note that peak at 894.94 does not have the highest intensity in that group, the peak at 893.94 has the highest intensity. A zoomed in spectrum can be found in the appendix.*

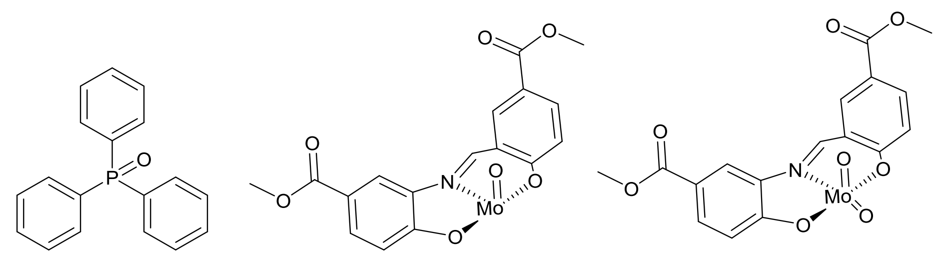

Chemical Formula: $C_{18}H_{15}OP$
Exact Mass: 278,0861

Chemical Formula: $C_{17}H_{13}MoNO_7$
Exact Mass: 440,9746
Mo(IV)

Chemical Formula: $C_{17}H_{13}MoNO_8$
Exact Mass: 456,9695
Mo(VI)

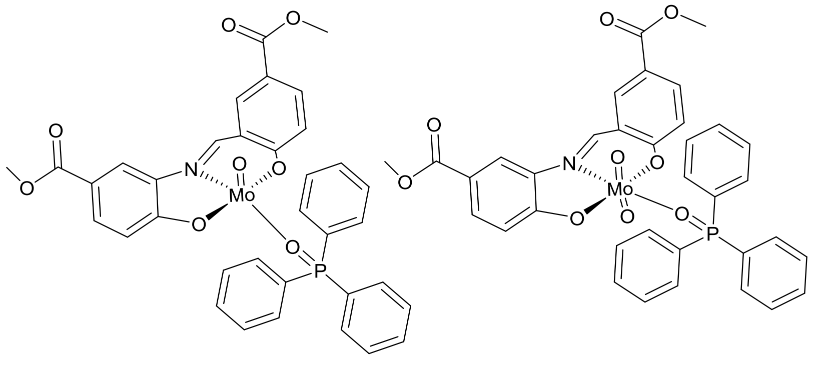

Chemical Formula: $C_{35}H_{28}MoNO_8P$
Exact Mass: 719,0607
Mo(IV)

Chemical Formula: $C_{35}H_{28}MoNO_8P$
Exact Mass: 719,0607
Mo(VI)

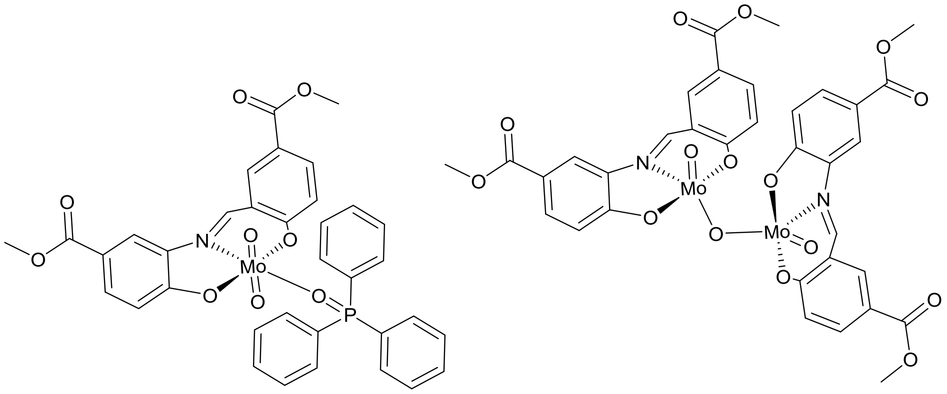

Chemical Formula: $C_{35}H_{28}MoNO_9P$
Exact Mass: 735,0556
Mo(VI)

Chemical Formula: $C_{34}H_{26}Mo_2N_2O_{15}$
Exact Mass: 897,9441
Mo(V)

*Figure 3-47: Structure and calculated mass ($^{98}$Mo, single positive charge) of species identified from the mass spectrum in Figure 3-46.*

The mass spectrum of the reaction with **W-2** (Figure 3-48) only showed one m/z signal with a tungsten isotope pattern which matched **W-2** as prepared. The additional signals in the spectrum are considered impurities not related to the reaction. $^1$H NMR and UV-Vis spectroscopy have shown formation of new species containing tungsten or fragments of the ligand. Clearly, these species could not be detected by mass spectrometry, and are perhaps anionic tungstate species that cannot be observed in these MS experiments.

As said earlier, the species detected by mass spectrometry have not necessarily formed during OAT. Equally, species formed during OAT may not be detected by mass spectrometry.

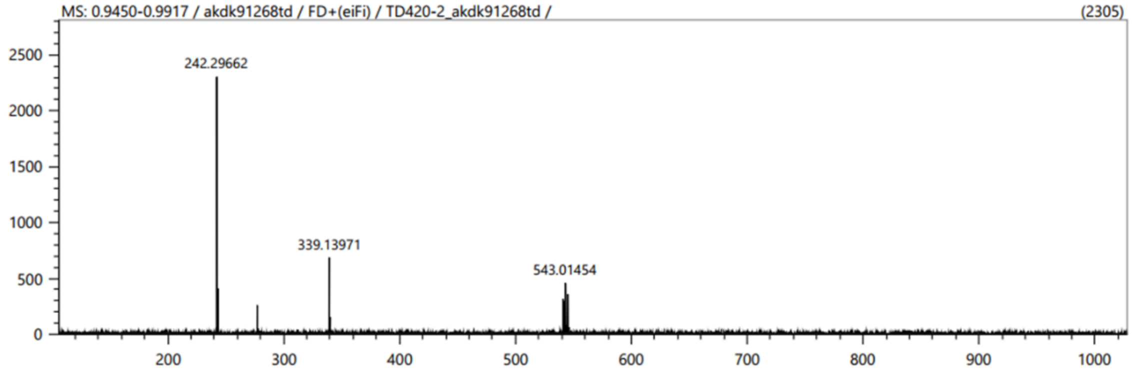

*Figure 3-48: LIFDI-mass spectrum of a mixture of **W-2** (top) and $PPh_3$ in acetone-$d_6$ under $N_2$ after irradiation at 410 nm for 16 h.*

### 3.7.5 Conclusion of the stoichiometric reaction between Mo-2, W-2 and $PPh_3$

Reaction mixtures containing **Mo-2**or **W-2** and 5 equivalents (1 in the case of **Mo-2**) in acetone-$d_6$ (**Mo-2**), or a 1:1- mixture of acetone-$d_6$ and DMF-$d_7$ (**W-2**) were irradiated at 410 nm for 16 h and analysed by ATR-IR spectroscopy, $^1$H NMR spectroscopy, UV-Vis spectroscopy, LIFDI-Mass spectrometry.

Both **Mo-2** and **W-2** reacted with $PPh_3$ to form $OPPh_3$.

**Mo-2** reacted similar to what would have been predicted based on observations in previous reactions. IR spectroscopy (Figure 3-40) showed the transfer of one oxo ligand but did not suggest dimerisation. $^1$H NMR spectroscopy (Figure 3-42) suggested formation of a paramagnetic species consistent with formation of Mo(IV). Mass spectrometry (Figure 3-46) detected Mo(IV), Mo(V) and Mo(VI) species although it is not clear that these species were also present in the reaction mixture. Overall, the data suggest the formation of Mo(IV) in triplet electronic configuration. Formation of a mixture of molybdenum species, possibly dominated by Mo(IV) cannot be excluded.

Although **W-2** did perform OAT no W=O bands were observed in the expected region in the IR spectrum (Figure 3-41) and $^1$H NMR data (Figure 3-43) showed decomposition although no decomposition products were identified.

In future experiments, the stoichiometric reaction could be performed in the same solvent for both molybdenum and tungsten complexes so that results for both complexes are comparable. Solution IR would allow immediate, or even *in situ*, characterisation of samples and avoid removal of solvent under reduced pressure which could have affected the samples. A shorter reaction time to prevent decomposition of **W-2** would also be beneficial.

## 3.8 Stoichiometric reaction between Mo-2, W-2 and $PPh_3$ followed by exposure to air

Following the work in the previous section which investigated reduction of the dioxo complexes, the second half of a catalytic cycle in the OAT reaction was subsequently studied. In these studies, the complex was first reduced with phosphine in the absence of an oxygen source. The reaction mixture was then exposed to air and subsequent catalyst regeneration was monitored.

The ability to use oxygen or air to regenerate the catalyst was noted when a sample containing reduced **Mo-2** catalyst was transferred into a cuvette for UV-Vis measurements (section 3.7.3) and within a couple of minutes had changed its colour from dark green back to yellow.

The effect of exposure to air of reaction mixtures containing the reduced complexes **Mo-2** and **W-2** will be discussed subsequently.

The UV-Vis spectra of **Mo-2** (Figure 3-49) shows a significant change over time, the intense band at 431 nm decreases and blue shift. Absorbance up to 800 nm decreases until no absorbance is observed above 500 nm resulting in a spectrum that takes the same form as that of unreacted **Mo-2**.

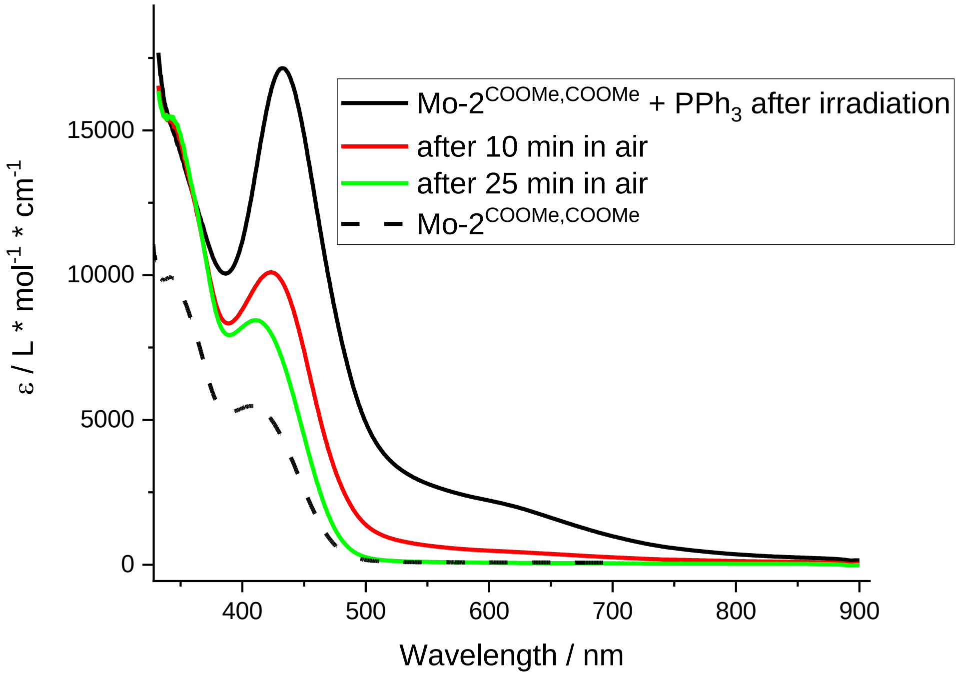

*Figure 3-49: UV-Vis spectra of the reaction mixtures of* ***Mo-2*** *with* $PPh_3$ *in acetone-*$d_6$ *(1 mM) after irradiation at 410 for 16 h (black) and 10 min (red) and 25 min (green) after the reaction mixture had been exposed to air, and of pure* ***Mo-2*** *in the same solvents at a concentration of 0.1 mM (dashed line).*

Regeneration of reduced **Mo-2** by oxygen was also followed by $^1$H NMR spectroscopy (Figure 3-50). As seen before (section 3.7), the resonances of the complex broaden and partially disappear after irradiation of **Mo-2** in the presence of $PPh_3$ and additional resonances of $OPPh_3$ can be seen. After the samples had been exposed to air the resonances of the complex sharpened and reappeared overtime. There is, however, still some broadening present, especially of the imine proton resonance at 9.4 ppm, and the signals are shifted upfield compared to the sample as prepared (*e.g.* the imine proton by 0.3 ppm from 9.7 ppm).

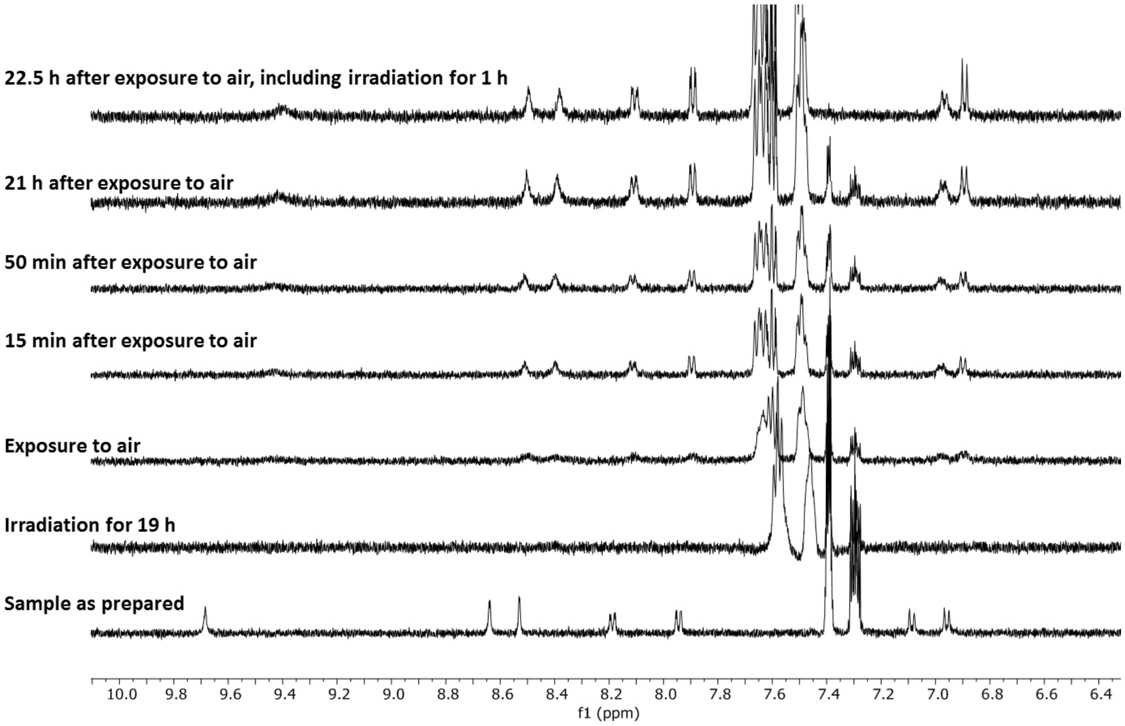

*Figure 3-50: $^1$H NMR spectra in the range of 6.4 to 10 ppm of a mixture of **Mo-2** and $PPh_3$ in acetone-$d_6$ over time. Conditions: 1 mM **Mo-2**, 1 mM $PPh_3$, acetone-$d_6$, $N_2$, irradiation at 410 nm.*

The difference between the $^1$H NMR spectra of the as prepared sample and of the regenerated sample points to the regenerated complex and **Mo-2** being different. Addition of $O_2$ to Mo(IV) results in complexes with different electron distribution: [$Mo^{IV}(O_2)$], [$Mo^{V}(O_2)$] or [$Mo^{VI}(O_2)$], the dioxygen, superoxo, or peroxo complex, respectively. The downfield shift of the $^1$H NMR resonances indicates stronger electron withdrawing effect of the molybdenum centre consistent with its oxidation with the signal broadening possibly due to the formation of more than one species. Dioxygen complexes of oxo molybdenum generally take the form of the peroxo complex where the $O_2^{2-}$ ligand is an $\eta_2$-binding π-donor that acts like an oxo ligand and is found mutually *cis* to the oxo ligand.[172] The result is a pentagonal bi-pyramidal structure which is shown for the re-oxidised **Mo-2** in Figure 3-51. The strong resemblance of the UV-vis and NMR spectra of **Mo-2** and the re-oxidised **Mo-2** follow from the similarity between the oxo and peroxo ligands and hence between the two complexes**.** The reoxidation of Mo(IV) complexes by dioxygen and formation of a Mo(VI)-peroxo complex has been reported. [70,173,174]

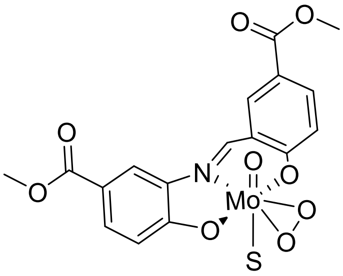

*Figure 3-51: Possible structure of **Mo-2** after reduction with PPh₃ and re-oxidation with O₂.*

Figure 3-52 shows the UV-Vis absorption spectra of **W-2** after irradiation in the presence of $PPh_3$ and 20 min after the sample had been exposed to air and after 25 h. The spectrum changes little, the band at 492 nm is still present but absorbance below 450 and above 550 nm decreases. The lack of change in the UV-Vis spectra supports the observations by IR and NMR in previous sections that the tungsten complex reacted differently from **Mo-2** and had decomposed irreversibly.

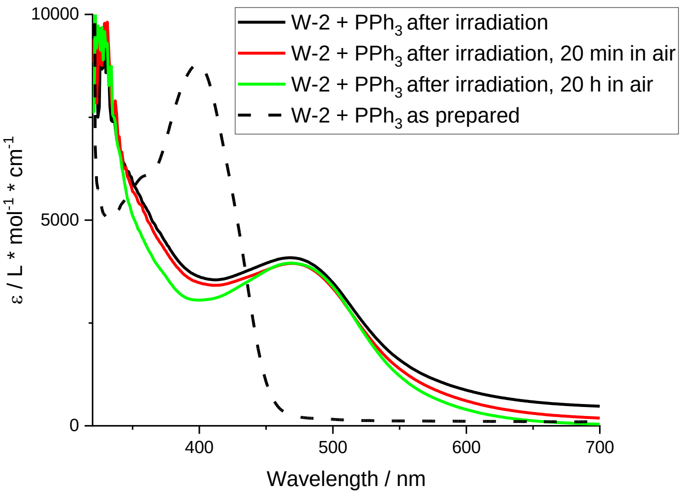

*Figure 3-52: UV-Vis spectra of the reaction mixtures of **W-2** with $PPh_3$ in DMF/acetone at a concentration of 0.4 mM after irradiation at 410 for 18 h, after 20 min under air and after overnight storage under air (solid lines), and of pure **W-2** in the same solvents at a concentration of 0.1 mM (dashed lines).*

Exposure to air of **Mo-2** and **W-2** after irradiation gave different results. UV-Vis data of **Mo-2** showed that the changes on irradiation are reversible but $^1$H NMR spectra showed that the initial state of the complex was not completely restored. **W-2**, however, did not change in air as it had probably decomposed.

## 3.9 Summary

All complexes, 16 containing Mo and two containing W, were screened for their ability to photocatalyse OAT from $PPh_3$ to DMSO. The highest activity was observed with **Mo-2** and **W-2**, 78 % after 3 h, and no activity with **Mo-1**, **Mo-4**, **Mo-15** and M**o-16**. Activity of other complexes ranged from 2 to 65 %.

A clear dependence on the wavelength of the light source used was not seen. Complexes with modified spectral properties (**Mo-4**, **Mo-15** and **Mo-16**) were inactive.

A correlation between electronic properties of the substituents and activity of the complexes was found. Activity increased linearly with the Hammett parameter when the acid substituents is assumed to be deprotonated and both acid and ester substituent have their Hammett parameter modified to account for conjugation. A strong dependence on the aromatic ring that bears the substituent was observed, substituents on the amine ring had a much stronger effect on activity than their counterparts on the aldehyde ring.

It was found that presence of a larger volume of water as well as aromatic OH groups, in the form of phenol or as substituent on a sulfoxide, inhibit OAT.

Sulfoxides other than DMSO can be used as substrates. All tested sulfoxides were found to be more active than DMSO, except **SO-9** which contains the aforementioned phenol substituent. An aromatic system as a substituent to the sulfoxide appeared to be beneficial, but modification of these aromatic groups had no effect. The highest conversion was obtained with **SO-2**, **SO-5**, **SO-7** and **SO-10** of which **SO-5**, interestingly, is the only aliphatic sulfoxide. With **SO-2**, OAT was continued until completion, 97 % conversion was achieved after a total of 48 h of irradiation.

Different phosphines were explored as well. Conversion could be improved by replacing one or two of the phenyl groups in $PPh_3$ with a methyl substituent. Substitution of the phenyl groups on the other hand did not affect conversion or decreased it. Using $P(OEt)_3$ resulted in almost no conversion.

The kinetics of OAT catalysed by **Mo-2** were studied between DMSO or **SO-2** and $PPh_3$ in DMSO or acetone, respectively. The reaction order of the substrates was found to be dependent on the solvent and the sulfoxide.

In DMSO the reaction was unaffected by changes in the catalyst concentration. In acetone, however, conversion was found to increase linearly with catalyst concentration < 1 mM and decreased exponentially for concentrations > 1 mM.

The stoichiometric reaction of **Mo-2** with $PPh_3$ in the absence of sulfoxide or any other oxygen source yielded a reduced Mo species which had transferred one of its oxo groups. Although the reduced species was not identified it is likely to be Mo(IV). Small amounts of other reduced Mo species, particularly the dimer could also be present. In the stoichiometric reaction of **W-2** with $PPh_3$ OAT also occurred, but the complex decomposed.

Exposure of the reduced **Mo-2** species to air resulted in re-oxidation, likely yielding the **Mo-2** peroxo-complex.

A more detailed analysis of the results from this chapter in regard of a potential mechanism can be found in section 5.1, which includes the results from the spectroscopic studies in chapter 4.

# Chapter 4 Spectroscopic investigations

## 4.1 Introduction

The photophysical properties of a potential photocatalyst are an important aspect of their study. The electronic structure of a catalyst determines what light source is suitable to initiate the photoreaction. Many different sources are available, from the sun with a broad spectral output that varies with time and location, which is free and “green”, to a fixed wavelength LED or LASER source with adjustable power output.

As the use of molybdenum and tungsten complexes for photocatalysed OAT is rare in the literature, the spectroscopic characterisation of these complexes is usually limited to UV-Vis spectroscopy and rarely looks for correlations between complexes.

Spectroscopic studies on Schiff bases and their complexes with metals other than molybdenum and tungsten are common mainly due to the use of Schiff bases as chemo sensors.[77,78] These examples are difficult to compare to the complexes discussed in this work due to different ligand features that affect the spectroscopic properties. The use of metals other than molybdenum and tungsten even with ligands similar to the SAP-system can also yield complexes with vastly different characteristics, for example when d-d or metal-to-ligand charge transfer (MLCT) transitions are present.

The examples of photoactivated catalysis shown in chapter 3 for which extensive characterisation has been done (e.g. the dyad **3-7**) are mostly too different from the complexes in this work to allow for meaningful comparison. The tungsten complex **3-8** and more so its unsubstituted analogue **4-1** (Figure 4-1) resemble the complexes in this work although only **3-8** has been reported to be a potential photo catalyst for OAT (see chapter 3.1.3).[67]

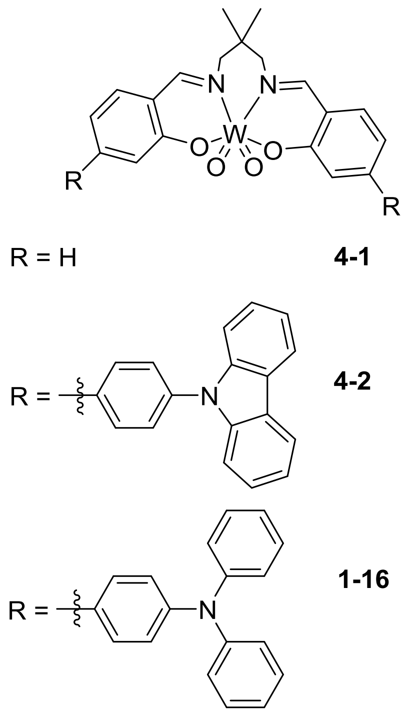

**4-1**

**4-2**

**1-16**

*Figure 4-1: Structure of related, spectroscopically characterised tungsten dioxo complexes.*

**1-16** and the related tungsten complexes **4-1** and **4-2** were characterised spectroscopically (Table 4-1).

*Table 4-1:Spectroscopic data of the tungsten complexes **2-8**, **4-1** and **4-2**. Taken from Yu et al.*[67]

| | Absorption | | Emission |
|---|---|---|---|
| | λ / nm, (ε / $10^3$ $mol^{-1}$ $dm^3$ $cm^{-1}$) | Character | $\lambda_{em}$ / nm (τ / µs) |
| **1-16** | 407 (34.6), 297 (43.7) | ILCT; LMCT | 608 (4.6) |
| **4-1** | 402 (5.5), 299 (18.2) | IL; LMCT | 582 (83.6) |
| **4-2** | 420 (sh, 10.6), 365 (sh, 25.0), 341 (31.9), 327 (30.4), 292 (49.8) | IL; LMCT | 553 (74.9) |

Data recorded in $CH_2Cl_2$, $\lambda_{ex}$ = 355 nm

As mentioned, only **3-8** was used in OAT. The light source used had a wavelength of 365 nm. On moving to 450 nm the conversion dropped from 52 to 15 % in the oxidation of indanol. Based on the UV-Vis data, at 450 nm only the intra ligand charge transfer (ILCT) transition was excited into whereas at 365 due to band overlap the LMCT band will be excited to some extent. In decatungstates, the LMCT state initiates hydrogen atom abstractions (HAT),[175,176] whereas in the reaction with 3-**8** an ILCT is thought to be the reactive state that the LMCT converts to.[67]

All three complexes **3-8**, **4-1** and **4-2** were tested in photo catalysed C-B bond formation from aryl chlorides and $B_2Pin_2$ (bis(pinacolato) diboron) with light of 410 nm wavelength. **3-8** gave the highest product yield, 89 % compared to 30 % with **4-1** and 14 % with **4-2**, but these differences were not explicitly discussed by Yu and coworkers. The spectroscopic data implies the nature of the excited state to be the main reason for the different activity, **3-8** having an ILCT transition whereas **4-1** and **4-2** have intra ligand (IL) transitions. Absorbance at 410 nm differs between complexes but does not correlate with activity, neither do excited sate lifetimes. The borylation is thought to start with reductive quenching of the exited tungsten complex by the bromide. However, **3-8** showed the lowest oxidation potential in the excited state of the three complexes.

As the mechanisms of both reactions, the OAT and the borylation, are not fully understood, it is possible that the observed differences are due to steps in the catalytic cycle not related to these spectroscopic characteristics.

### 4.1.1 Chapter aims

Almost all ligands and complexes were synthesised as yellow to orange solids and yielded yellow solutions. In the following sections the electronic absorption spectra of the complexes will be discussed. The effect of substituent on optical properties will be described and these properties linked to OAT activity. Emissivity and excited state lifetimes of selected complexes with and without phosphine and sulfoxide substrates were measured and differences between these complexes, particularly in regard to the OAT studies of chapter 3, described.

## 4.2 UV-Vis spectra of the synthesised complexes

Prior to performing catalysis, UV-Vis absorbance spectra were recorded for all of the complexes. Based on the band maxima observed the wavelength of the LEDs for the custom-made photochemistry set-up used for OAT experiments in chapter 3 were chosen.

### 4.2.1 UV-Vis spectra of L-1 and Mo-1 and assignment of transitions

The UV-Vis absorption spectra of 0.1 mM solutions of **L-1** and **Mo-1** in DMSO are shown in Figure 4-2. The spectrum of **L-1** is dominated by an intense band at 357 nm, a second band is found at 272 nm. A third band at 443 nm is barely visible at this concentration. A small amount (~1 %) of **L-1** exists as the Z-keto isomer (Scheme 4-1) and gives rise to this weak band.[177] The spectrum of **Mo-1** shows one intense band at 309 nm and two less intense ones at 352 nm and 421 nm. Both spectra agree with reported data.[124,178,179]

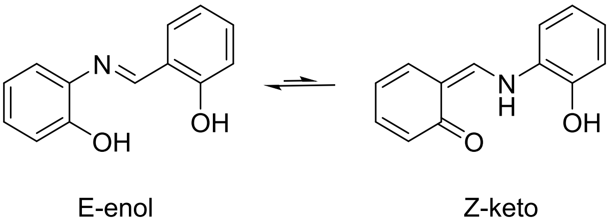

*Scheme 4-1: Keto-enol isomerism of **L-1**.*

**L-1** and **Mo-1** are known in the literature and their spectral properties have been studied. Assignments of the observed transitions were made and are listed in Table 4-2. The charge transfer (CT) transition at 357 nm in **L-1** involves the imine group.[180] Upon complexation, electron density from the imine nitrogen is transferred to the metal hence the change observed in the UV-Vis spectrum for **Mo-1**. A new band due to charge transfer from the phenol oxygen into empty d orbitals of the metal (ligand to metal charge transfer, LMCT) is observed at 422 nm upon complexation.[181] Thus, the bands at 443 nm in **L-1** and at 422 nm in **Mo-1** result from different transitions. This transition in **L-1** (n -> π*) is not possible in **Mo-1** as the free electron pair of the nitrogen it originates from is no longer available.

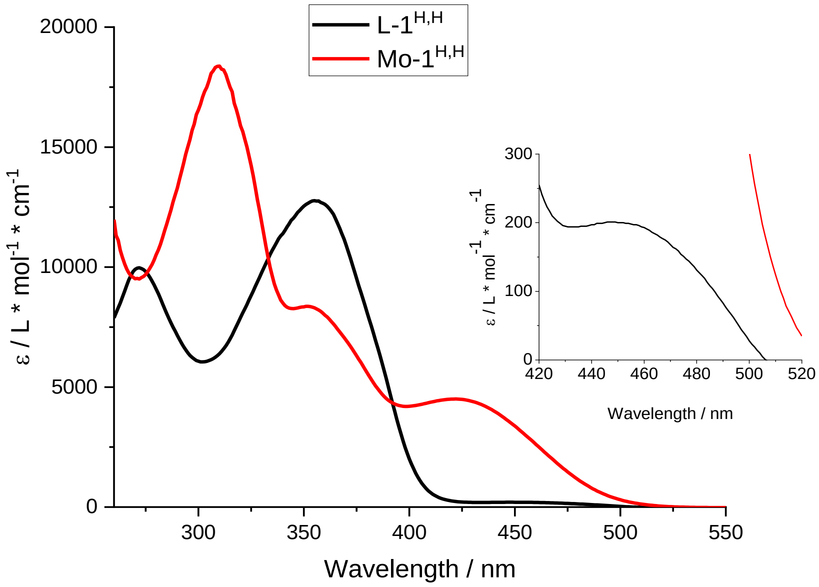

*Figure 4-2: UV-Vis spectra of **L-1** and **Mo-1** at 0.1 mM in DMSO. Insert showing a very weak band in **L-1** between 420 and 500 nm.*

*Table 4-2: Bands in UV-Vis spectra of **L-1** and **Mo-1** and their attribution to electronic transitions. n, π and π* referring to nonbonding orbital, π orbital and π* orbital, respectively .*

| | $\lambda_{max}$ / nm | ε / mol * L$^{-1}$ * cm$^{-1}$ | Transition |
|---|---|---|---|
| **L-1** | 272 | 9800 | π to π* [178,179] |
| | 357 | 14900 | π to π* CT, amine ring and imine group to aldehyde ring [180] |
| | 443 | 260 | n to π* [179] |
| | | | |
| **Mo-1** | 309 | 18400 | π to π* |
| | 352 | 7800 | π to π*, C=N |
| | 422 | 4500 | LMCT [181] |

### 4.2.2 Influence of different substituents on the UV-Vis spectrum of molybdenum complexes

The influence of the substituent on the electronic absorption spectra was studied in DMSO. Figure 4-3 shows the UV-Vis spectra recorded of the sixteen Mo-complexes synthesised in this work.

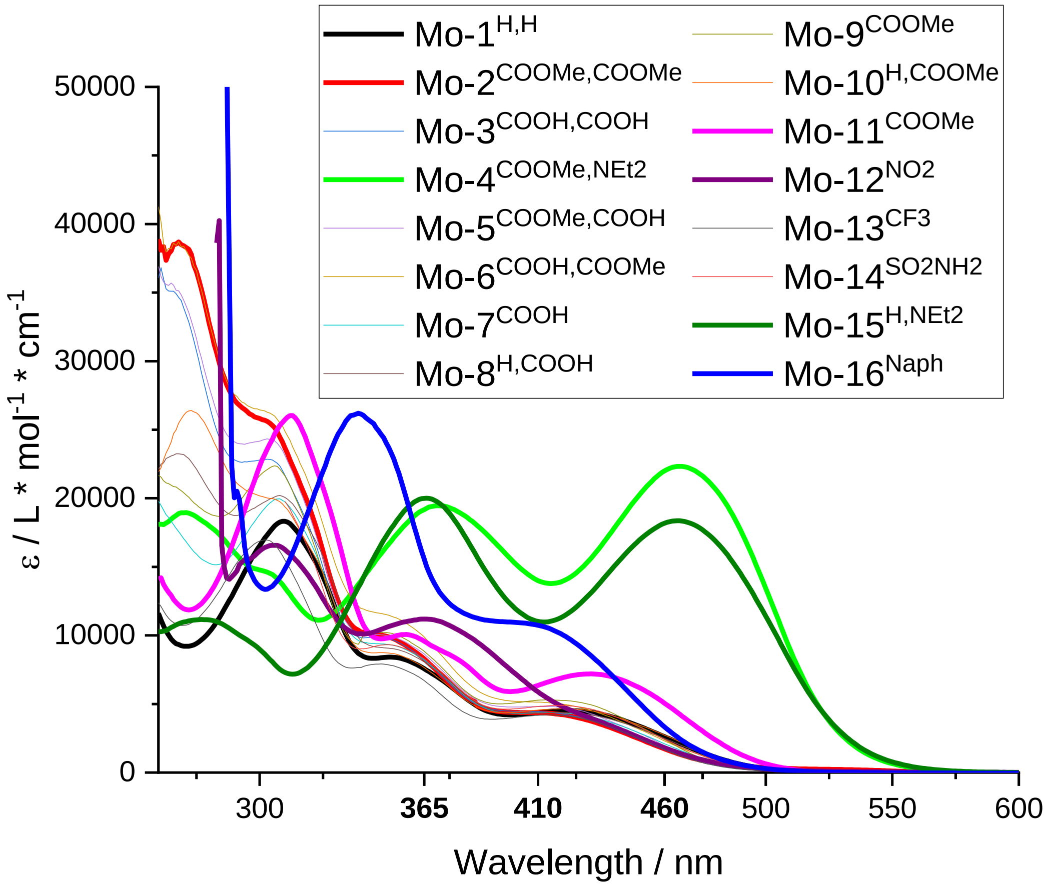

*Figure 4-3: UV-Vis spectra of molybdenum complexes in DMSO at a concentration of 0.05 mM. Wavelengths used in photocatalysis, 365, 410 and 460 nm, are marked in bold. Spectra of **Mo-1** and **Mo-2,** as reference, and spectra that are significantly different are highlighted in bold.*

The spectra of most complexes are similar especially above 330 nm. Between the ester and acid substituted complexes the nature and position of the substituent has little effect on the band position and intensities. Complexes **Mo-4, Mo-11, Mo-12, Mo-15** and **Mo-16** strongly differ in band position and intensity. The band maxima for the two lowest energy transitions of all complexes are listed in Table 4-3.

*Table 4-3: UV-Vis spectra of the molybdenum complexes: max wavelength of the two lowest energy bands and extinction coefficients.*

| | $\lambda$ / nm | $\varepsilon$ / L * mol$^{-1}$ * cm$^{-1}$ | $\lambda$ / nm | $\varepsilon$ / L * mol$^{-1}$ * cm$^{-1}$ |
|---|---|---|---|---|
| **Mo-1**$^{\text{H,H}}$ | 422 | 4500 | 352 | 7800 |
| **Mo-2**$^{\text{COOMe,COOMe}}$ | 409 | 4500 | 347 | 10000 |
| **Mo-3**$^{\text{COOH,COOH}}$ | 406 | 4200 | 345 | 2500 |
| **Mo-4**$^{\text{COOMe,Et2N}}$ | 466 | 22000 | 370 | 19500 |
| **Mo-5**$^{\text{COOMe,COOH}}$ | 415 | 3500 | 348 | 10300 |
| **Mo-6**$^{\text{COOH,COOMe}}$ | 412 | 5100 | 347 | 11200 |
| **Mo-7**$^{\text{COOH}}$ | 414 | 4700 | 351 | 10300 |
| **Mo-8**$^{\text{H,COOH}}$ | 418 | 4300 | 352 | 9000 |
| **Mo-9**$^{\text{COOMe}}$ | 415 | 4700 | 349 | 10200 |
| **Mo-10**$^{\text{H,COOMe}}$ | 421 | 4400 | 351 | 9300 |
| **Mo-11**$^{\text{COOMe}}$ | 431 | 7300 | 358 [b] | 10200 |
| **Mo-12**$^{\text{NO2}}$ | 430 to 450 [a] | | 365 | 13100 |
| **Mo-13**$^{\text{CF3}}$ | 414 | 4200 | 348 | 7900 |
| **Mo-14**$^{\text{SO2NH2}}$ | 419 | 4900 | 351 | 9700 |
| **Mo-15**$^{\text{H,NEt2}}$ | 465 | 18300 | 366 | 20200 |
| **Mo-16**$^{\text{Naph}}$ | 403 | 11700 | 339 | 28800 |

Due to broadness and shape of bands, determination of the exact maxima is ambiguous [a] barely visible shoulder. [b] additional shoulder at 378 nm.

It can be seen that the band around 350 nm varies between 346 and 352 nm in most complexes. Only **Mo-4**, **Mo-12, Mo-15** and **Mo-16** lay outside this range at 370, 365, 366 and 339 nm, respectively. Above 400 nm most maxima lay between 404 and 422 nm. **Mo-4**, **Mo-12** and **Mo-15** show higher maxima of 466, 440 and 465 nm. Both bands of **Mo-11** also lay outside of the usual range, but not as far.

From Figure 4-3 and Table 4-3 it appears that **Mo-4**, **Mo-15** and **Mo-16** are significantly different from the other complexes. The two lowest energy transitions in **Mo-4** and **Mo-15** are substantially red shifted and display a much higher extinction coefficient. In **Mo-16** both transitions are blue shifted but still show a higher extinction coefficient. The amine substituent and naphthalene ring present additional chromophores with transitions overlapping with the LMCT and π to π* transitions.

**Mo-4, Mo-15** and **Mo-16** were synthesised to study the effect of spectroscopic properties on OAT (see chapter 3.3.5). The extended π system of **Mo-16** has led to an increase in absorbance and at the same time a blue shift of the two lowest energy transitions. In contrast, a red shift was thought to be more beneficial as this would shift absorbance further into the visible region which corresponds to a lower energy and allows for better use of “green” sources like sunlight. A strong red shift of the two lowest energy transitions was indeed observed with **Mo-4** and **Mo-15.**

The nitro substituent in **Mo-12** appears to only produce an overlapping transition at 366 nm. The band at 440 nm is shifted but the low extinction coefficient suggests that the LMCT is still present but weakened as a new transition overlapping with the LMCT band would show as a combined band with higher absorbance.

**Mo-11** displays a small red shift with only the LMCT band having an extinction coefficient that is higher compared to most other complexes. As only the substituent position differs between **Mo-11** and **Mo-9** no new transitions can be introduced. The ester group is in the *para* position in **Mo-9** and the *meta* position in **Mo-11** and therefore both the LMCT transition that involves the phenolates as well as the π to π* transition that involves the imine group are affected from this change in substituent position.

Excitation of complexes during OAT experiments was done at 365, 410 and 460 nm (see Figure 4-3). This corresponds to excitation of the π to π* CT at 365 nm or the LMCT at 410 and 460 nm for most complexes. All complexes showed some extent of overlap of the two bands resulting in excitation of both bands to different degrees which might explain the lack of a clear correlation between the activity of the complexes and the excitation wavelength (see chapter 3.3.3). The existence of additional strongly absorbing bands in **Mo-4**, **Mo-15** and **Mo-16** that overlap with the LMCT and π to π* CT bands could result in absorbed light primarily or even exclusively exciting these transitions. **L-15** for example has been reported to have a strong absorbance around 410 - 420 nm due to either π to π * transition[145], or n to π* transition of the imine group.[182] Neither of the three complexes with modified spectroscopic properties catalysed OAT from DMSO to $PPh_3$ which suggests that the transitions that are being excited are different from those in active complexes and are not sufficient to active the molybdenum centre.

A trend in the band maxima of the complexes is not obvious from Table 4-3. The band maxima of the LMCT transitions were therefore plotted against the improved Hammett parameter *[113]* $\sigma_p^-$ taking into account the ability of substituents to delocalise negative charge (see also Section 3.3.2), shown in Figure 4-4. **Mo-4, Mo-11, Mo-12, Mo-15** and **Mo-16** were not considered.

A weak correlation is found, the wavelength of the LMCT band decreases with the Hammett parameter. This Correlation agrees with the work of Topich who reported a linear decrease of the wavelength of the LMCT transition maxima with the Hammett parameter for bromo, nitro and methoxy substituted [$MoO_2$(SAP)] and [$MoO_2$(SAE)] (c.f. Figure 3-1, Section 3.1.1).*[124]* However, the unsubstituted [$MoO_2$(SAP)] and [$MoO_2$(SAE)] did not fit in this trend.

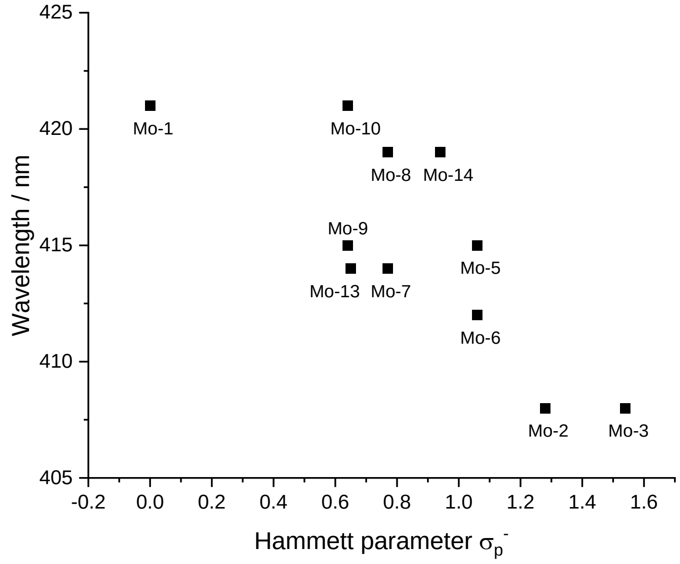

*Figure 4-4: Plot of max. wavelength against improved Hammett parameter $\sigma_{p}$- for the LMCT transition of the molybdenum complexes. Acid groups are assumed to be protonated.*

A plot of conversion of $PPh_3$ to $OPPh_3$ from Section 3.3 against the wavelength of the LMCT band (Figure 4-5) also shows a weak correlation where the conversion increases with the energy difference between ground and excited state.

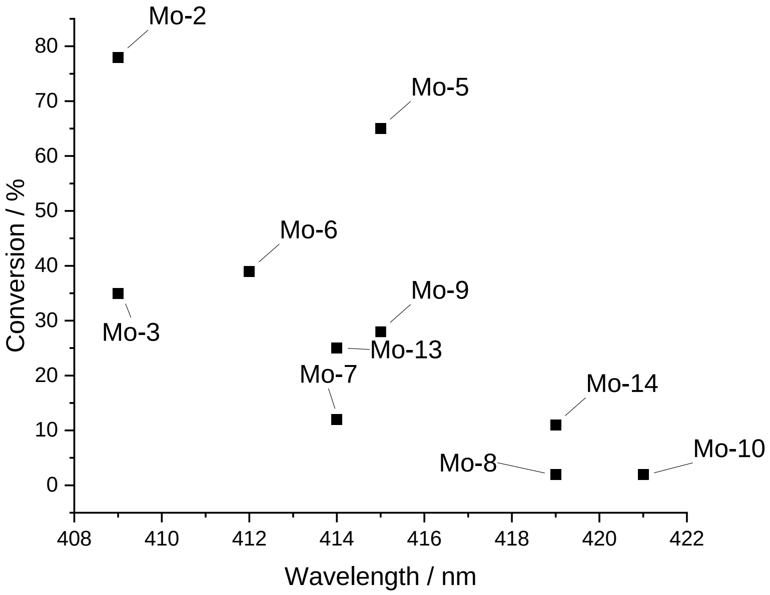

*Figure 4-5: Plot of the conversion of $PPh_3$ to $OPPh_3$ against $\lambda_{max}$ of LMCT band.*

### 4.2.3 Influence of solvents on the UV-Vis spectrum of Mo-2

The influence of the solvent on the electronic absorption was studied with the most active OAT catalyst **Mo-2** in acetone, DMSO, MeCN and MeOH. The UV-Vis spectra are shown in Figure 4-6 while Table 4-4 shows the position and intensity of the band maxima. Due to the absorbance of the solvents the spectral range recorded varied.

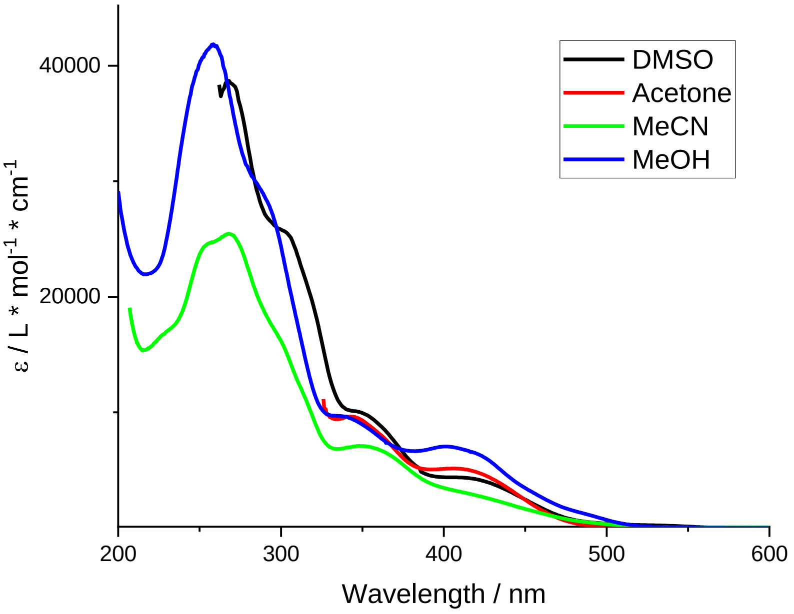

*Figure 4-6: UV-Vis absorbance spectra of **Mo-2** in different solvents at a concentration of 0.05 mM.*

Overall, changing the solvent affects band intensity and position.

Only small differences are seen above ~330 nm and particularly between DMSO and acetone these can be regarded as negligible. This is important as these two solvents were used for the OAT experiments discussed in chapter 3. Below 330 nm differences are mostly between MeCN and MeOH where the spectrum in MeCN shows more features but has a lower intensity.

Solvent polarity decreases from MeOH (0.762) to MeCN (0.460) and DMSO (0.444), which are similar, to acetone (0.355) based on the empirical $E_T^N$ parameter; all solvents can act as hydrogen bond acceptor but only MeOH can also donate hydrogen bonds.[183] Neither the band position nor the extinction coefficient correlates with the solvent polarity, but in MeOH for the first three bands, λ and ε always take the extreme values between the four solvents.

An effect of solvent polarity on both the LMCT and ligand-based CT band would be expected as the charge transfer leads to changes in polarity of the excited state, but the solvents used in this work are too similar to yield marked differences. MeOH as the only solvent capable of hydrogen bond donation shows a more pronounced effect. In MeOH both CT bands are shifted more to lower wavelength than in the other solvents. The higher energy corresponding to a destabilised excited state or more stabilised ground state.[184]

*Table 4-4: UV-Vis spectroscopy of* ***Mo-2****, band maxima and extinction coefficient in different solvents.*

| Solvent | λ / nm | ε / L * mol$^{-1}$ * cm$^{-1}$ | Assignment |
|---|---|---|---|
| DMSO | 409 | 4400 | LMCT |
| Acetone | 406 | 5300 | |
| MeOH | 401 | 5900 | |
| MeCN | 400-450 [b] | / | |
| | | | |
| MeCN | 349 | 6800 | π to π*, C=N, CT |
| Acetone | 344 | 8000 | |
| DMSO | 347 | 10500 | |
| MeOH | 338 | 9700 | |
| | | | |
| MeCN | 317 | 11400 | π to π* |
| DMSO | 306 | 25200 | |
| MeCN | 298 [a] | 17500 | |
| MeOH | 291 [a] | 28000 | |
| | | | |
| MeCN | 269 | 27200 | |
| DMSO | 269 | 35500 | |
| MeOH | 259 | 42400 | |
| MeCN | 253 | 25500 | |
| MeCN | 228 [a] | 16300 | |

c(**Mo-2**) = 0.05 mM. [a] shoulder. [b] very weak shoulder with undefined maximum

### 4.2.4 Influence of the metal on the UV-Vis spectra of complex with ligands L-1 and L-2

The effect of the metal centre on electronic absorption was studied between **Mo-1**, and **W-1** and **Mo-2** and **W-2.** UV-Vis spectra in DMSO are shown in Figure 4-7, band maxima and absorbances in Table 4-5.

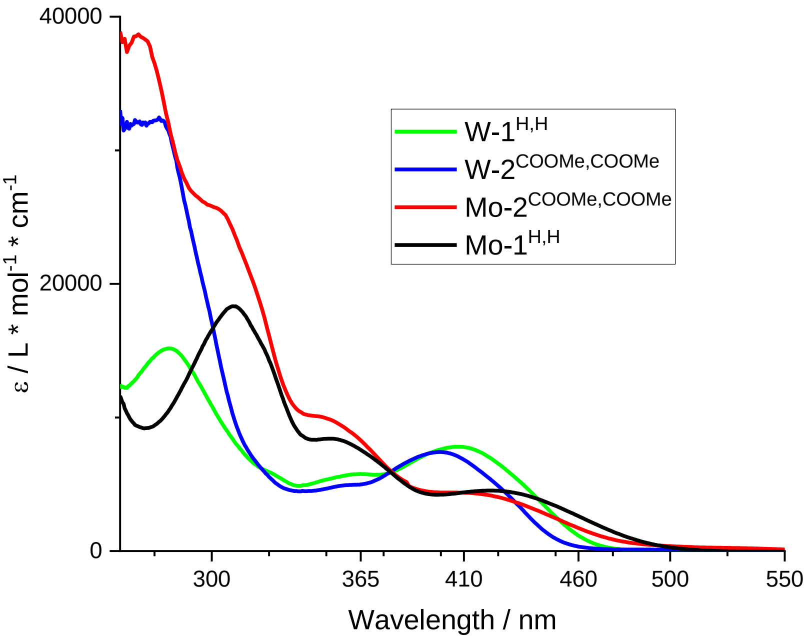

*Figure 4-7:UV-Vis spectra of **Mo-1, Mo-2, W-1** and **W-2** at a concentration of 0.05 mM in DMSO.*

Complexes of the same metal have very similar spectra. The band lowest in energy, the LMCT band around 400 nm, and the one highest in energy, around 300 nm are both substantially blue shifted in **W-1** and **W-2** compared to **Mo-1** and **Mo-2**, whereas the band around 350 nm is red shifted. The ester substituents in **Mo-2** and **W-2** equally led to a blue shift of the band maxima compared to **Mo-1** and **W-1**. The band maxima and extinction coefficients for **W-1** are consistent with reported data in DMF.[110]

As the band around 350 nm is ligand centred the nature of the metal has only a weak influence on this transition. In the LMCT however, charge is transferred into the metal d orbitals. The 4d orbitals of molybdenum are lower in energy than the 5d orbitals of tungsten which leads to the LMCT bands shifting to higher energy in the tungsten complexes compared to molybdenum.

Regarding the nature of the transitions in the tungsten complexes, so far it was assumed that the lowest and second lowest transitions are still of LMCT and CT character. The results from the fluorescence measurements suggest however, that the LMCT band in the tungsten complexes is found at much lower wavelength (see chapter 3.3.4).

*Table 4-5: UV-Vis spectroscopy of **Mo-1**, **Mo-2**, **W-1** and **W-2**, band maxima and extinction coefficients of the two lowest energy transitions.*

| Complex | λ / nm | ε / L * mol$^{-1}$ * cm$^{-1}$ | λ / nm | ε / L * mol$^{-1}$ * cm$^{-1}$ |
|---|---|---|---|---|
| **Mo-1$^{H,H}$** | 352 | 7808 | 422 | 4500 |
| **Mo-2$^{COOMe,COOMe}$** | 347 | 10000 | 409 | 4400 |
| **W-1$^{H,H}$** | 362 | 5600 | 407 | 7100 |
| **W-2$^{COOMe,COOMe}$** | 359 | 6300 | 400 | 7000 |

The wavelengths of the light used in OAT (365, 410 nm) do not coincide with the band maxima of the four complexes but the corresponding transitions are still being excited. The absorbance at these wavelengths is similar for complexes of the same metal with the absorbance of the π to π* CT transition in the molybdenum complexes being higher and the absorbance of the LMCT transition lower compared to the bands in tungsten in the same region. The result of the OAT experiments in Section 3.3.6 suggested that the effect of this difference in absorbance on catalytic conversion is, however, negligible. The much lower absorbance of **W-2** only seemed to have had an effect at 460 nm as activity was significantly lower compared to **Mo-2.** Both complexes were similarly active at 365 and 410 nm.

### 4.2.5 Summary

UV-Vis spectra of all synthesised complexes were recorded and analysed. Spectral properties were similar with small shifts in band position and absorbance for most complexes. **Mo-4**, **Mo-15** and **Mo-16** show substantially shifted and more intense bands due to the amine and naphthalene chromophores. A shift in position and change in intensity were also observed on replacing molybdenum with tungsten. With regard to photoactivated OAT, these differences seem to be of minor importance, except for **Mo-4**, **Mo-15** and **Mo-16**. These complexes were inactive, possibly because light is absorbed by the additional transitions due to the chromophores that do not activate the molybdenum centre.

In the following section, the properties of the excited state of some of the complexes in the form of emissivity and lifetime measurements will be described.

## 4.3 Fluorescence spectroscopy of ligands and complexes

As UV-Vis spectroscopy had shown no clear differences between complexes that could explain the differences in OAT activity, further spectroscopic studies on the emissivity of complexes were done. In contrast to UV-Vis spectroscopy which provides information on the ground state, fluorescence spectroscopy provides information on the excited states.

The emissivity of complexes was recorded in DMSO or acetone. Spectra of pure DMSO and acetone are shown in Figure 4-8.

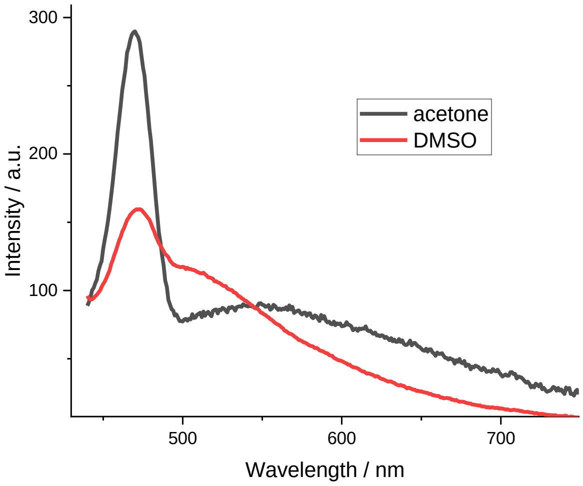

*Figure 4-8: Emission background from acetone and DMSO. $\lambda_{ex}$ = 410 nm.*

Both spectra show a small and intense band and a weak but broad band.

The intense band at 470 (acetone) and 472 nm (DMSO) is due to Raman scattering, whereas the broad band is due to the use of a cut-off filter (λ < 430 nm) to minimise signal from scattering.

Raman scattering is a phenomenon inherent to these types of experiments where the incident light is scattered inelastically by solvent molecules. Photons loose energy in this process resulting in detection of light at a higher wavelength than that of the incident light. The loss in energy is on the order of 3000 wavenumbers. The position of Raman bands shifts with the excitation wavelength and can be calculated as follows:

$$\lambda_{Raman} = \frac{1}{\frac{1}{\lambda_{ex}} - \tilde{\nu} * 10^{-7}}$$

*Equation 4-1*

where $\lambda_{ex}$ is the wavelength of excitation, $\tilde{\nu}$ is the wavenumber of the Raman shift. At an excitation wavelength of 410 nm a Raman band appears around 470 nm.

The Raman band is present in all spectra shown subsequently but can be hidden under very intense emission bands.

## 4.3.1 Fluorescence spectroscopy of L-1, L-2 and L-4 and Mo-1, Mo-2 and Mo-4 in acetone

Emissivity of three ligands was measured in acetone. Emission spectra of **L-1**, **L-2** and **L-4** are shown in Figure 4-9 together with the corresponding molybdenum complexes.

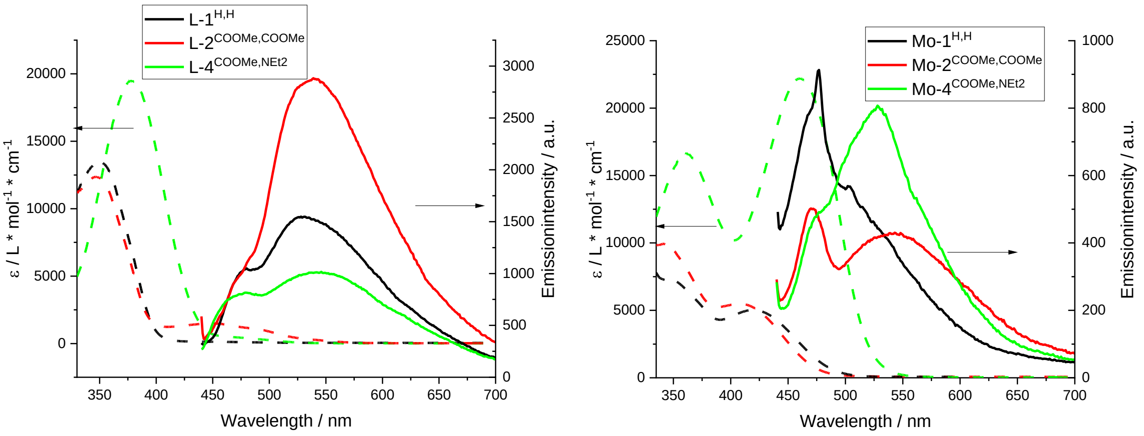

*Figure 4-9: Absorption (dashed lines) and emission (solid lines) spectra of **L-1, L-2, L-4** (left) and **Mo-1, Mo-2, Mo-4** (right) in acetone. Absorption spectra were recorded at a concentration of 0.1 mM. Emission spectra were recorded under $N_2$ with samples having an absorbance of 0.1 at the excitation wavelength $\lambda_{ex}$ = 410 nm.*

Compared to **L-1** ($\lambda_{em}$ = 530 nm), the emission bands in **L-2** (539 nm) and **L-4** (546 nm) are red shifted. Emission from **L-2** is more intense whereas from **L-4** it is less intense than **L-1**. All three ligands show a higher intensity than the corresponding complexes. The low emissivity of **L-4** was unexpected as this ligand was designed to have a high emissivity through the combination of electron donating and electron withdrawing subsitutents.[146]

In general, an imine group can provide a path for non-radiative deactivation of excited states through rapid cis-trans isomerisation.[145] Molecules incorporating an imine group therefore are often non-fluorescent. Isomerisation involves the free electron pair of the nitrogen and can be inhibited through hydrogen bonding.[145] This is the case in **SAP**-based ligands (Scheme 4-2).

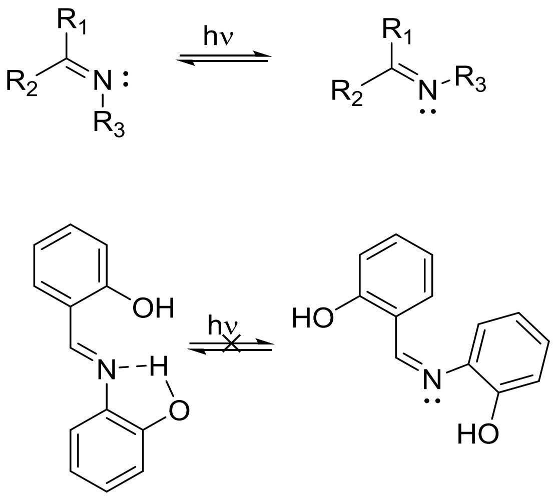

*Scheme 4-2: Light induced isomerisation of an imine group (top) and prevention of isomerisation by hydrogen bonding in **L-1** (bottom).*

In complexes, the bonding of nitrogen to the metal via its free electron pair equally prevents isomerisation.[185]

The bonding to the metal also prevents proton transfer that would lead to the formation of the keto isomer (Figure 4-10). Klinhom *et al.* observed two emission bands at 420 and 547 nm after excitation of a solution of **L-1** in MeCN at 350 nm.[186] They attributed the first band to emission from the $S_1$ to the $S_0$ state, while the second one results from the keto form (Figure 4-10) after excited state intramolecular proton transfer (ESIPT).

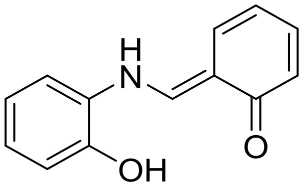

*Figure 4-10: Keto form of **L-1**.*

Due to the possibility of isomerisation of the imine double bond, keto-enol tautomerism and isomerisation of the double bond in the keto form, in the ground and excited state, spectroscopic properties of SAP Schiff bases are rather complex.[177,186] While some of these changes can lead to non-radiative relaxation, the keto form is actually more emissive than the enol. After complexation, these isomerisations are no longer possible and the rigid structure of the complex should also prevent conformational changes. Some of the non-emissive relaxation pathways are inhibited, as is the emissive keto form. The weak fluorescence observed for the complexes, could also be due to electron density being drawn from the ligand as it binds to the metal as well as *via* LMCT transfer upon excitation.

It follows that emission is mainly ligand based and weak emission after excitation at 410 nm is due to ligand-based transitions which overlap with higher absorbance LMCT bands. Emission from free ligand that is present in low concentration in an equilibrium with the complex is also possible.

Kurapati *et al.* have made similar observations with ligand **4-3** and complex **4-4** (Figure 4-11).[187] Both ligand and complex were similarly emissive when excited at 390 nm, the lowest energy ligand based transition. No emission was observed when the LMCT band was excited.

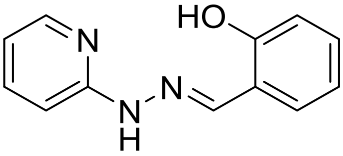

**4-3**

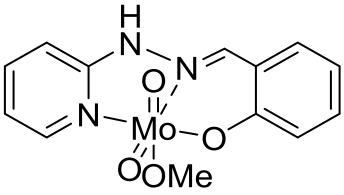

**4-4**

*Figure 4-11: Structure of the hydrazono ligand and molybdenum complex thereof studied by Kurapati et al.* [187]

## 4.3.2 Fluorescence spectroscopy of Mo-1, Mo-2, Mo-4, Mo-9, Mo-12, Mo-13, Mo-15 and Mo-16 in acetone

The emissivity of **Mo-1**, **Mo-2**, **Mo-4**, **Mo-9**, **Mo-12**, **Mo-13**, **Mo-15** and **Mo-16** was recorded in acetone at 0.05 mM. The spectra are shown in Figure 4-12.

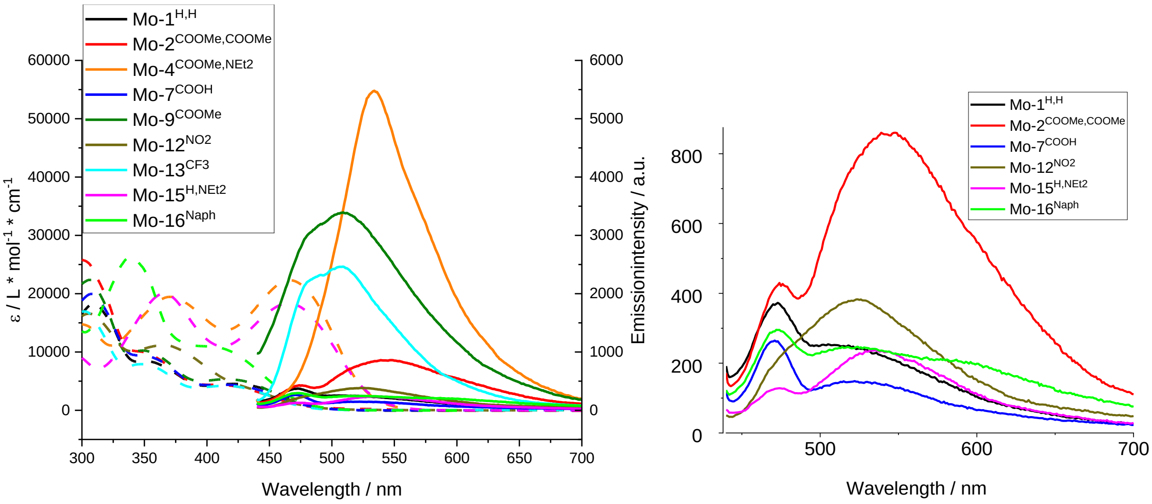

*Figure 4-12: Emission spectra of **Mo-1, Mo-2, Mo-4, Mo-9, Mo-12, Mo-13, Mo-15, Mo-16** at 0.05 mM in acetone under $N_2$. λex = 410 nm.*

Emission intensity varied drastically and there is also a shift in the position of the emission band. Band positions are listed in Table 4-6.

*Table 4-6: Emission wavelength of several complexes in acetone.*

| | $\lambda_{em}$ / nm |
|---|---|
| **Mo-1$^{H,H}$** | / |
| **Mo-2$^{COOMe,COOMe}$** | 544 |
| **Mo-4$^{COOMe,NEt2}$** | 534 |
| **Mo-7$^{COOH}$** | / |
| **Mo-9$^{COOMe}$** | 509 |
| **Mo-12$^{NO2}$** | 525 |
| **Mo-13$^{CF3}$** | 507 |
| **Mo-15$^{NEt2}$** | 537 |
| **Mo-16$^{Naph}$** | 523 |
| | 593 |

$\lambda_{ex}$ = 410 nm, acetone, $N_2$

**Mo-1** and **Mo-7** appear to be non-emissive or only weakly emissive. The highest intensity was recorded for **Mo-4**, which, similar to UV-Vis spectroscopy, is due to the push-pull effect of the combined ester and amine substituents. **Mo-16** is the only complex displaying two emission bands, although both are very weak, with the band at 593 nm having the highest wavelength of all complexes. This red shift of the emission wavelength is consistent with an extended π system.[146] The third complex designed to have modified spectroscopic properties is **Mo-15**, which does show a red shifted emission band compared to **Mo-1** but only similar intensity. From the UV-Vis spectra in section 4.2.2 it seemed that all three complexes, **Mo-4, Mo-15** and **Mo-16**, have strong ligand-based bands at the excitation wavelength and therefore a different excited state with different relaxation paths is possible.

The fourth highest emission wavelength is observed with **Mo-2**. Interestingly, where **Mo-7** is non-emissive, **Mo-9** shows the second highest emissivity. The corresponding ligand **L-7** has been reported to be emissive with a band around 525 nm stemming from the zwitterionic species.[93] In **Mo-7,** however, formation of a zwitterion is less likely due to the nitrogen as the most basic centre being involved in binding to the metal.

The amine group -$NEt_2$ was used to modify the emissive properties of a complex to test if catalytic activity was linked to emissivity. Neeraj *et al.* showed that the introduction of the $NEt_2$ group increased emissivity of **L-15** compared to **L-1**.[145] The combination of an acceptor group with the amine donor was also found to increase emissivity in related salen type Schiff bases.[146] Neeraj *et al.* also observed dual emission bands from **L-15** and **L-15** bound to $Al^{3+}$ at 471 and 498 nm in water after excitation at 419 nm due to the $NEt_2$ group. The band in **Mo-15** is redshifted compared to that of the reported free ligand, in part due to complexation and use of a different solvent. A second weak band could be hidden under the Raman band.

From this and the previous section it seems that the observed emission is only due to ligand-based transitions. In most complexes this band overlaps with the more emissive LMCT band leading to low excitation of the emissive band. In strongly emissive complexes, e.g. **Mo-4**, additional chromophores could give rise to an emissive ligand band with higher absorbance. Additional transitions and emissive states could also be present, possibly overlapping with other bands. Conclusive results will require more measurements, at different excitation wavelength and possibly in different solvents and of all ligands. Computational studies to identify transitions and geometries would also be helpful.

**Mo-15** was catalytically inactive but showed the strongest emissivity whereas **Mo-2**, the most active complex, only showed medium emissivity, behind **Mo-4, Mo-9** and **Mo-13.** In these complexes the electron withdrawing group on the amine ring could result in a difference in electron density between the two rings that might be beneficial to emissivity, whereas in **Mo-2** no such effect is found due to its symmetrical substitution. **Mo-12,** with its $NO_2$ group on the amine ring, however, showed lower emissivity than **Mo-2**. It appears that emissivity and catalytical activity are not linked, although the effect of the different substituents on emissivity, and absorbance, is not understood yet.

### 4.3.3 Fluorescence spectroscopy of L-2 and Mo-2 in acetone in the presence of $PPh_3$ and DMSO

After the initial screening experiments with ligands and complexes the effect of substrates on emissivity was studied.

Figure 4-13 shows the emission spectra of **L-2** and **Mo-2** in acetone with successive addition of $PPh_3$ and DMSO.

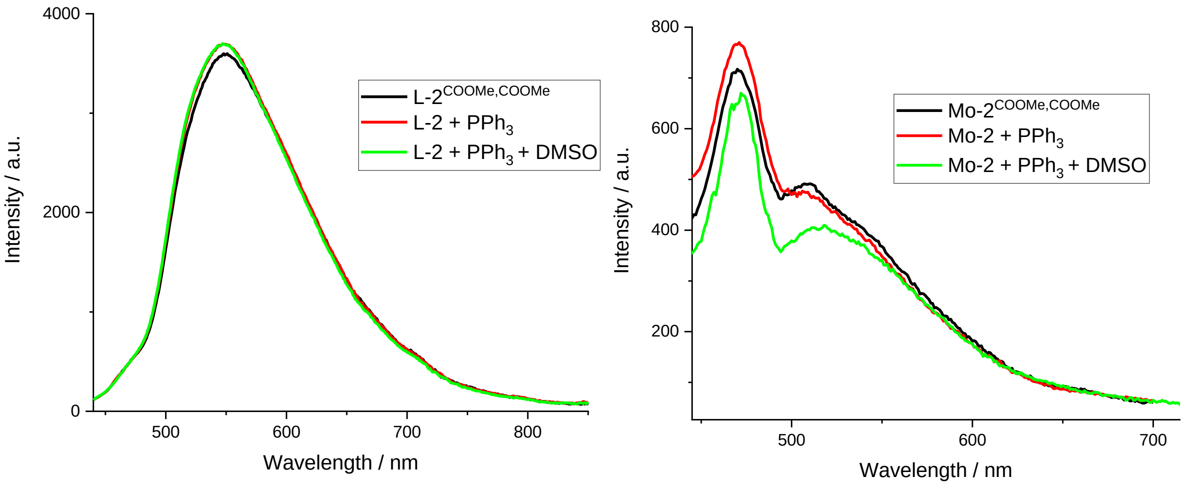

*Figure 4-13: Emission spectra in acetone of 0.02 mM **L-2** with and without 6.5 mM $PPh_3$ or 5 M DMSO added (left) and of 0.02 mM **Mo-2** with and without 6.5 mM $PPh_3$ or 5 M DMSO added (left). $\lambda_{ex}$ = 410 nm, spectra have been adjusted for absorbance at 410 nm, 0.07 (left) and 0.14 (right).*

The position and intensity of the emission band of **L-2** are unaffected by the presence of $PPh_3$ or DMSO which suggests that the excited state that ultimately emits light is unaffected by the presence of $PPh_3$ or DMSO. Whether any interaction at all takes place cannot be determined from the data, but DMSO and acetone are too similar to see marked differences.

The emission spectra of **Mo-2** without and with $PPh_3$ present are similar. In the former case a small peak can be seen around 510 nm but could be due to noise. Both spectra are however slightly different from the solvent spectrum shown in Figure 4-8. Emission, if present, is only very weak but was observed at higher concentration ( Figure 4-12). Only when DMSO is present in addition to $PPh_3$ is emission clearly observed. The overall intensity of the spectrum below 550 nm is lower compared to the two other spectra, but a clear peak is seen at 520 nm.

As discussed in the previous sections, emissivity is likely due to ligand-based transitions but interaction of the complex with DMSO or $PPh_3$ could still effect theses transitions. Even if no effect of $PPh_3$ or DMSO on the free ligand was observed, interaction with the metal centre can affect the electron density of the ligand. In addition, if one of the coordinating groups of the ligand or the entire ligand (temporarily) unbinds, these additives could instead coordinate and stabilise the metal. The less restricted or free ligand could then be emissive.

Some interaction of $PPh_3$ with **Mo-2** would not be unexpected (*c.f.* thermal OAT between $PPh_3$ and Mo complexes in Section 3.1.2. The nature of interaction, whether would $PPh_3$ occupies the sixth coordination site of molybdenum or interacts with one of the oxo ligands, is not known. In this work, DMSO has been found to be a better solvent for molybdenum complexes than acetone and for $PPh_3$, strong binding to molybdenum complexes has been reported.[114] The existence of different species of the form [$MoO_2$(**L-2**)D] (D = DMSO, $PPh_3$, acetone) in solution seems likely.

### 4.3.4 Fluorescence spectroscopy of Mo-1, Mo-2, W-1 and W-2 in DMSO in the presence or absence of $PPh_3$ and $OPPh_3$

The effect of the metal centre on emissivity has been studied in DMSO by comparing the spectra of **Mo-1** and **W-1** as well as **Mo-2** and **W-2**. In addition, the effect of species relevant to OAT has been investigated by measuring emissivity of these complexes after addition of $PPh_3$ or $OPPh_3$. The emission spectra of **Mo-1** and **Mo-2** in the absence and presence of $PPh_3$ or $OPPh_3$ are shown in Figure 4-14, those of **W-1** and **W-2** in Figure 4-15.

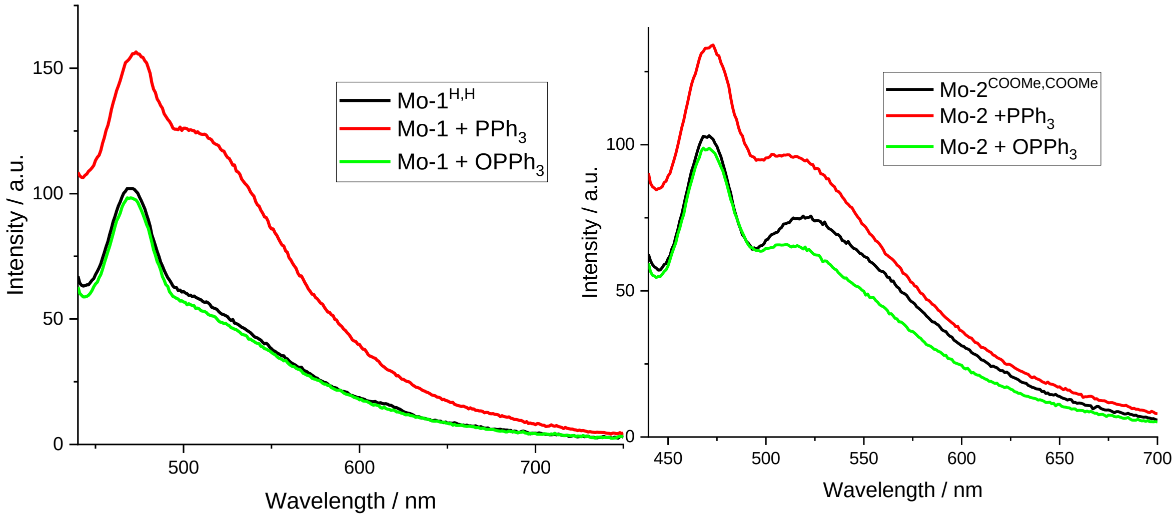

*Figure 4-14: Emission spectra of **Mo-1** (0.022 mM, left) and **Mo-2** (0.015 mM, right) in DMSO with and without 300 equivalents of PPh$_3$ or OPPh$_3$ added. Absorbance of 0.07 at $\lambda_{ex}$ = 410 nm.*

The emission from **Mo-1** and **Mo-2** is very weak. Compared to the solvent background (Figure 4-8) it seems that only the sample of **Mo-2** containing no additive shows significant emission with a maximum at 522 nm. Whether the sample of **Mo-2** containing PPh$_3$ is emissive or not is not clear. Emission from these two sample would be consistent with results from the previous sections. Concentrations are, however, lower, resulting in even weaker fluorescence.

The emission spectra of **W-1** and **W-2** are shown in Figure 4-15. In contrast to their molybdenum analogues, both tungsten complexes are highly emissive and unaffected by the presence of PPh$_3$ or OPPh$_3$. The emission band in **W-2** is found at 516 nm whereas in **W-1** it is redshifted to 547 nm and has a lower intensity.

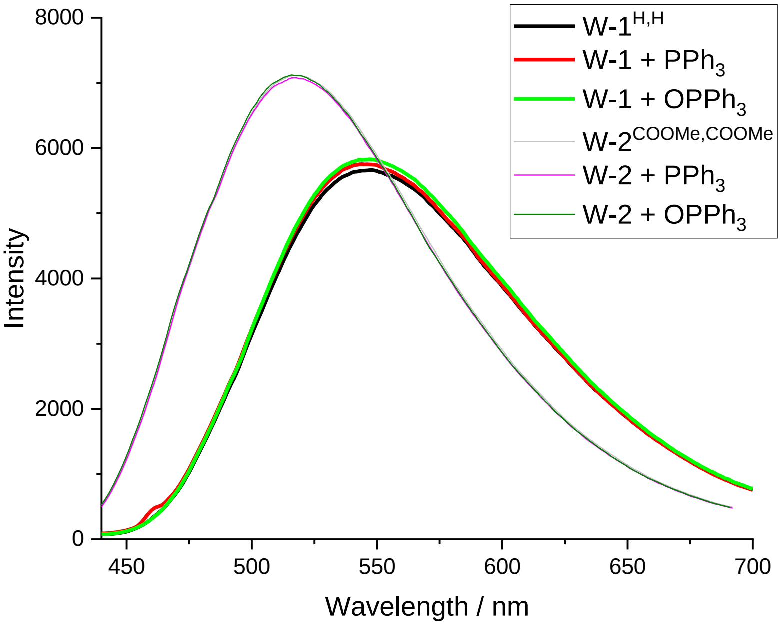

*Figure 4-15: Emission spectra of* ***W-1*** *(0.18 mM, absorbance of 0.14) and* ***W-2*** *(0.15 mM, absorbance of 0.13) in DMSO with or without 300 equivalents of PPh$_3$ or OPPh$_3$ added. $\lambda_{ex}$ = 410 nm.*

In the *tert*-butyl substituted complex **4-6 (**Figure 4-16) the emission band is found at 573 nm.[188] Although, emission of **4-6** was recorded in MeOH and a solvent dependence of the band position exists, it seems reasonable to conclude that electron donating substituents lead to a redshift while electron withdrawing substituents lead to a blue shift of the band position, similar to the findings for Mo complexes (chapter 4.3.2).

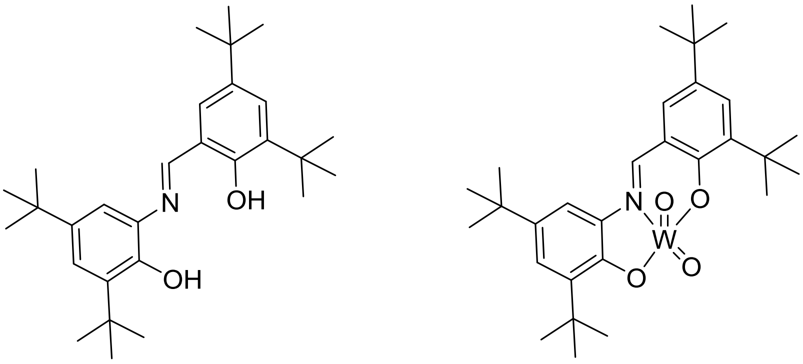

*Figure 4-16: Structure of the tert-butyl substituted SAP ligand* ***4-5*** *(left) and tungsten complex* ***4-6*** *(right).*

Emissivity of the tungsten complex **4-6** was studied by Wang *et al.* together with the corresponding ligand **4-5**.[188] The ligand **4-5** only showed a weak emission band at 550 nm upon excitation at 425 nm whereas **4-6** was highly emissive with a band centred at 573 nm. Calculations of the geometries **4-5** and **4-6** in the ground and excited state showed that the ligand experiences substantial twisting upon excitation, the dihedral angle between the two aromatic rings increases from 37 to 76 °. The coordination to tungsten restricts the movement of the ligand and the geometry of **4-6** changes less drastically upon excitation (14 ° to 20 °). The higher rigidity of **4-6** results in less energy relaxation and hence a higher emissivity than in the ligand. These findings agree with those by Petkov *et al.* regarding excited state twisting leading to non-radiative decay in **L-1.**[177]

While the high emissivity of **W-1** and **W-2** in this work follows the findings of Wang *et al*., the argument based on geometry alone cannot explain differences between the two metals.

From the UV-Vis spectrum in Figure 4-7 it can be seen that the assumed LMCT band (the band lowest in energy) in the tungsten complexes shows higher absorbance than in the molybdenum complexes but this might in fact be due to the ligand based band around 350 nm which is much broader compared to molybdenum complexes. Higher absorbance of this ligand-based band at the excitation wavelength of 410 nm would allow to excite more of the emissive bands and thus lead to higher emission intensity. The difference between **Mo-2** and **W-2** is on the order of 100-fold and seems too high to be based purely on absorbance of different bands. However, in **4-6** the LMCT band was calculated to be at 230 nm which is substantially higher in energy than in the molybdenum complexes.[188]

Similar differences between molybdenum and tungsten complexes were also observed in different ligand systems. Ramos *et al.* reported a substantial increase in emission upon complexation of a quinoline ligand to tungsten but only a slight increase upon complexation to molybdenum. They attributed this difference to the position of LMCT excited states which constitute path for non-radiative relaxation. In the molybdenum complex, the LMCT band overlaps with the lowest energy ligand based transition, while in the tungsten complex it is situated at higher energy, higher than the ligand based transition and thus does not provide a non-radiative relaxation pathway.[189]

If the LMCT band in **W-1** and **W-2** is similarly high in energy, the question rises what the nature of the lower energy bands are, and more importantly, it would follow that comparison of spectroscopic properties between molybdenum and tungsten complexes in this project are less useful.

Both tungsten complexes catalyse OAT, with **W-2** being as active as **Mo-2**, and **W-1** far less active. **Mo-1** is much less emissive than the two tungsten complexes which suggests again that there is not link between activity and emissivity. As emissivity seems to be due to ligand-based transitions, it could be that catalytic activity on the other hand is due to the LMCT transition hence the two do not correlate. The overlap of bands in the UV-Vis spectra hides this separation, a clear wavelength dependence was not observed in OAT (chapter 3.3.3).

### 4.3.5 Conclusions

Emission spectroscopy has shown that ligands **L-1**, **L-2** and **L-4** are much more emissive than the corresponding molybdenum complexes. The emissivity of complexes in acetone also vastly differed. **Mo-1** and **Mo-7** were non-emissive whereas **Mo-4** showed the highest emissivity, in line with its design, having an electron donating and an electron withdrawing substituent. Although, emission wavelength increases with the Hammett parameter, this correlation is weak and more importantly, no correlation with OAT activity is seen.

Comparison of **Mo-1**, **Mo-2**, **W-1** and **W-2** in DMSO showed the tungsten complexes to be much more emissive than their molybdenum counterparts. They were also unaffected by additives, $PPh_3$ or $OPPh_3$. **Mo-1** and **Mo-2** were practically non-emissive except for **Mo-2** in the presence of $PPh_3$.

The combined results so far suggest that emissivity is actually due to ligand-based transitions centred around 350 nm. Complexation to molybdenum hinders this ligand-based emission, whereas tungsten does not reduce or even enhances it (a direct comparison between ligand and tungsten complex under identical condition was not done).

## 4.4 Measurement of the excited state lifetimes of Mo-1, Mo-2 and W-1, W-22

Excited state lifetimes of **Mo-1**, **Mo-2**, **W-1** and **W-2** were measured in DMSO in the presence or absence of $PPh_3$ or $OPPh_3$. Excited state lifetimes of **Mo-2** and **L-2** were also recorded in acetone, with successive addition of $PPh_3$ and DMSO.

Excited state lifetimes were measured by time-correlated single-photon counting on an Edinburgh Instruments FLS980 spectrometer in DMSO. Samples were deaerated and put under nitrogen. Excitation was done at 473 nm which should only excite the LMCT band according to UV-Vis characterisation. Although most OAT experiments in this work were done with light of 410 nm wavelength, catalytic activity was also observed at 460 nm which sufficiently close to 473 nm. Sample concentrations giving a UV-Vis absorbance of 0.1 were chosen.

The obtained emission decay curves were fitted using one exponential using the software provided with the instrument. The process of data fitting is explained in more detail in section 4.4.1.

### 4.4.1 Time-resolved luminescence of Mo-2 and L-2 in acetone

The emission decay profiles of **Mo-2** and **L-2** in acetone are shown in Figure 4-17 and the calculated lifetimes in Table 4-8.

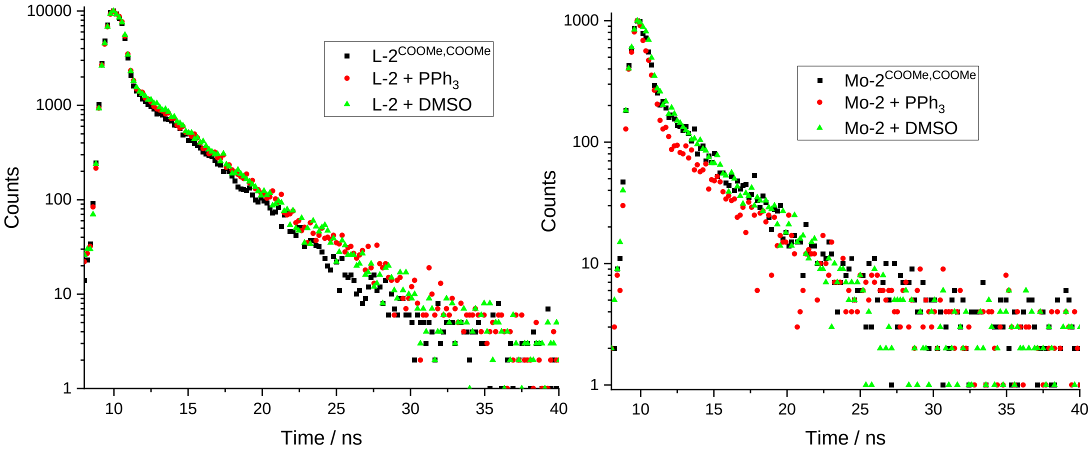

*Figure 4-17: Emission decay profiles obtained at 550 nm, $\lambda_{ex}$ = 473 nm, under nitrogen for a 0.012 mM solution of* ***L-2*** *(left), and 0.020 mM solution of* ***Mo-2*** *(right), containing 10 equivalents of PPh$_3$, 0.5 M DMSO or no additive.*

The decay profiles were fitted with exponential curves of the form shown in Equation 4-2. The linear portion of the profile was identified (around 10 to 25 ns for the profiles in Figure 4-17) and fitting performed on this interval. Single, double and triple exponential fitting was tested.

$$Fit = A + B_1 * exp\left({}^{-t}/_{\tau_1}\right) + B_2 * exp\left({}^{-t}/_{\tau_2}\right) + \ldots.$$

*Equation 4-2*

However, use of more than two exponentials did not provide meaningful results.

Single and double exponential fitting of pure **L-2** and **Mo-2** are shown in Figure 4-18. The relevant results of the fitting are given in Table 4-7.

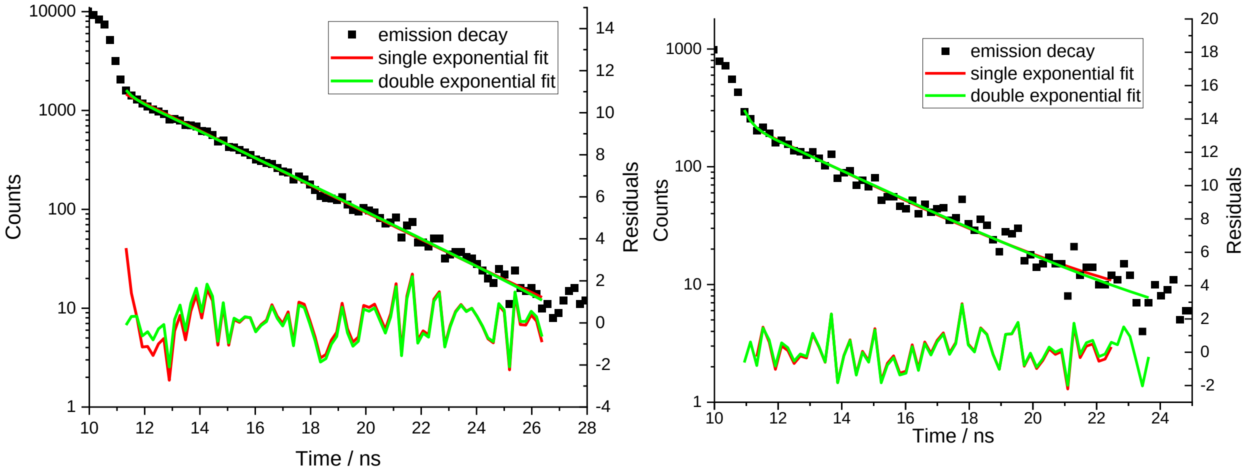

*Figure 4-18: Emission decay profiles of **L-2** and **Mo-2** with single and double exponential fitting curves and residuals.*

*Table 4-7: Results from single and double exponential fitting as shown in Figure 4-18.*

| | $\tau_1$ / ns | standard deviation | Relative contribution / % | $\tau_2$ / ns | standard deviation | Relative contribution / % | $X^2$ (goodness of fit) |
|---|---|---|---|---|---|---|---|
| **L-2** | | | | 3.2 | 0.03 | | 1.456 |
| | 0.2 | 0.01 | 2 | 3.23 | 0.05 | 98 | 0.879 |
| **Mo-2** | | | | 3.2 | 0.17 | | 1.065 |
| | 0.2 | 0.05 | 11 | 3.4 | 0.17 | 89 | 1.091 |

From Figure 4-18 it can be seen that the addition of a second exponential did not improve the fitting as both curves are practically identical in both cases. This is confirmed by the corresponding values, given in Table 4-7. For **L-2** the additional exponential results in an additional very short lived component of only 0.2 ns, which is lower than the spectrometers operational range, and only contributes 2 % to the total decay profile. $\tau_2$ is essentially unchanged. In the case of **Mo-2** a similar, short lived component is added but with a higher contribution. Note in Figure 4-18 that the interval had be slightly increased in order to obtain a meaningful fit.

Since using more than one exponential did not improve the fitting of the decay profiles only single exponential fitting was performed in subsequent experiments.

The lifetimes obtained from the decay profiles of **L-2** and **Mo-2** with and without added $PPh_3$ or DMSO (Figure 4-17) are shown in Table 4-8

.

*Table 4-8: Excited state lifetimes of **L-2** and **Mo-2** in acetone.*

| | Excited state lifetime / ns at $\lambda_{em}$ |
|---|---|
| | 550 nm |
| **L-2** | 3.2 ± 0.03 (1.5) |
| + $PPh_3$ | 3.3 ± 0.04 (1.3) |
| + DMSO | 3.3 ± 0.05 (1.5) |
| **Mo-2** | 3.2 ± 0.17(1.1) |
| + $PPh_3$ | 3.4 ± 0.7 (0.95) |
| + DMSO | 3.4 ± 0.17 (0.9) |

$\lambda_{ex}$ = 472 nm, in acetone, under $N_2$. $\chi^2$ values (goodness of fit) are given in brackets

The decay profiles of **L-2** and **Mo-2** do not significantly change upon addition of either $PPh_3$ or DMSO. The calculated lifetimes are identical within error within the sets of ligand or complex but also between **L-2** and **Mo-2**. The insensitivity of the ligand to additives is consistent with findings in previous sections. From the UV-Vis spectra (Figure 4-9 and section 4.2.1), it can be seen that different transitions should be excited into, LMCT in **Mo-2** and n to π* in **L-2**. No overlap with other bands occurs at the excitation wavelength of 473 nm.

From section 4.3 it seemed that emission is due to ligand-based transitions. As mentioned, time-resolved luminescence was measured after excitation at 473 nm. At this wavelength, only the band belonging to the Z-keto isomer of the Schiff base should be excited which, in **L-1**, was found to be emissive.[177] In the samples with **Mo-2** the keto isomer can only occur in the free ligand that could be present in equilibrium with the complex. Emission only resulting from this isomer would explain the within error identical results obtained with **L-2** and **Mo-2.**

## 4.4.2 Time-resolved luminescence of Mo-1 and Mo-2 in DMSO

Emission decay profiles of **Mo-1** are shown in Figure 4-19, those of **Mo-2** in Figure 4-20 with the lifetimes obtained from fitting shown in Table 4-9.

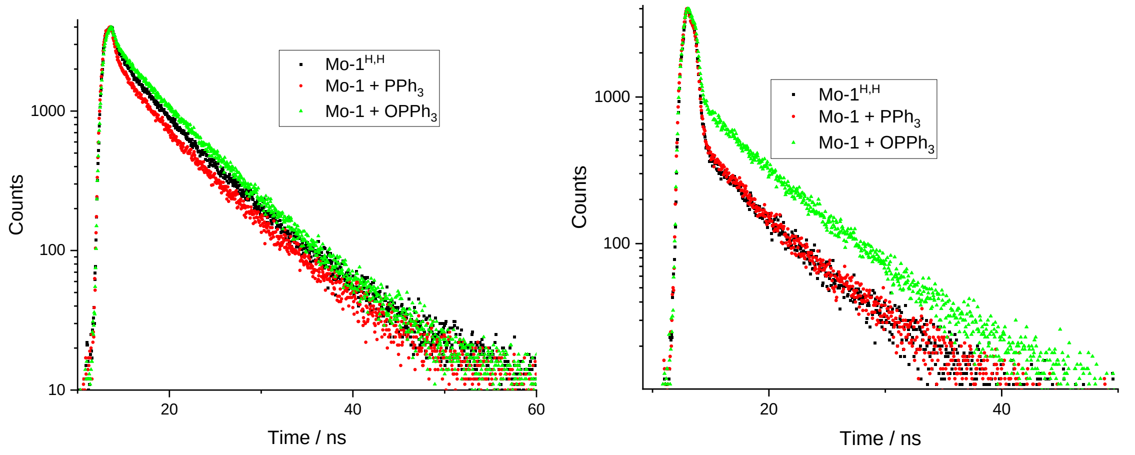

*Figure 4-19: Emission decay profiles obtained at 525 nm (left) and 550 nm (right), λex = 473 nm, under nitrogen for a 0.056 mM solution of Mo-1, containing 300 equivalents of PPh₃, 300 equivalents of OPPh₃ or no additive.*

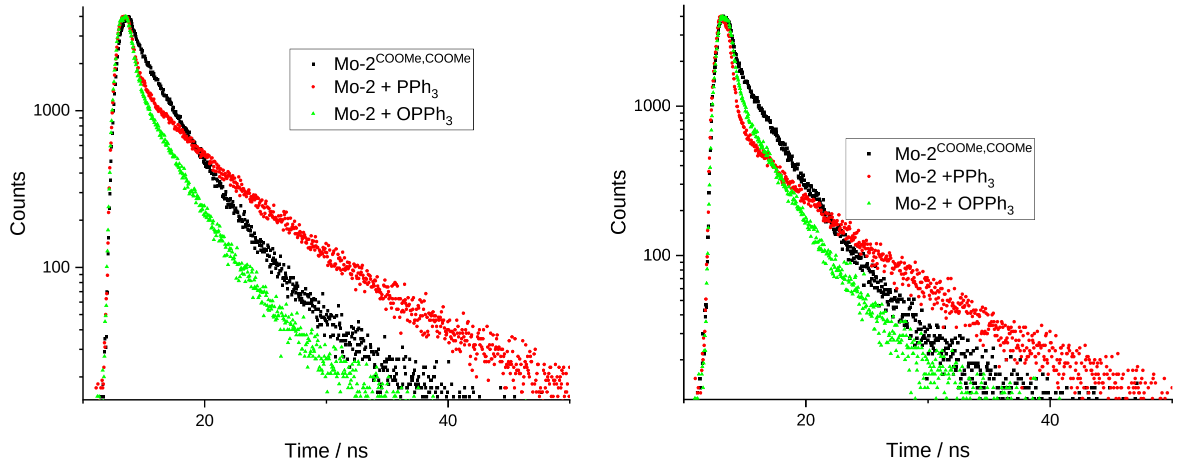

*Figure 4-20: Emission decay profiles obtained at 525 nm (left) and 550 nm (right), $\lambda_{ex}$ = 473 nm under nitrogen for a 0.013 mM solution of **Mo-2**, containing 300 equivalents of PPh$_3$, 300 equivalents of OPPh$_3$ or no additive.*

The emission decay profiles for both complexes at 525 nm are very similar as are the profiles at 550 nm, notably they have a similar slope, i.e. decay rate is equal. The profile of the sample of

Mo-1 with added $OPPh_3$ and those of **Mo-2** in the presence of $PPh_3$ differ from the two other cases in each set. The decaying part of the profile of **Mo-1** + $OPPh_3$ appears however, to be still parallel to those of **Mo-1** and **Mo-1** + $PPh_3$ meaning that decay rates are similar.

The obtained lifetimes reflect these similarities. The addition of $PPh_3$ to **Mo-1** has no effect on the lifetimes. The addition of $OPPh_3$ seemingly increases the lifetimes both at 525 and 550 nm but this difference of 0.7 and 0.8 ns is likely insignificant.

In contrast, **Mo-2** in the presence of $PPh_3$ differs from the two other cases. The calculated excited state lifetimes of **Mo-2** are identical at 525 and 550 nm and identical within error to the lifetimes in the presence of $PPh_3$. When $PPh_3$ is added to **Mo-2**, however, the excited state lifetimes increase by around 2 ns.

All calculated lifetimes fall within the range of 2.7 to 6 ns with those of **Mo-2** being on average shorter than those of **Mo-1**. No reason that would explain why **Mo-1** was found to be inactive whereas **Mo-2** was active in the OAT catalyst screening experiments in section 3.2 are apparent.

The lifetimes obtained for **Mo-2** in DMSO are comparable to those obtained in acetone in the previous section excepted for when $PPh_3$ was added. Even if emission is only ligand based, differences were still seen between complexes (see chapter 4.3.2), hence differences in the excited state lifetimes are plausible.

An argument could be made that these differences are insignificant. Lifetimes and differences are on the order of ns which is close to the lower end of the detection limit of the spectrometer. The goodness of the fit could also be improved ($\chi^2$ values are ideally close to 1).[190]

*Table 4-9: Excited state lifetimes of* ***Mo-1*** *and* ***Mo-2*** *in DMSO.*

| | Excited state lifetime / ns at $\lambda_{em}$ | |
|---|---|---|
| | 525 nm | 550 nm |
| **Mo-1** | 5.3 ± 0.02 (2.6) | 4.8 ± 0.06 (1.4) |
| + $PPh_3$ | 5.3 ± 0.02 (2.3) | 4.7 ± 0.06 (1.2) |
| + $OPPh_3$ | 6.0 ± 0.02 (1.7) | 5.6 ± 0.04 (1.3) |
| | | |
| **Mo-2** | 3.1 ± 0.01 (1.8) | 3.1 ± 0.01 (1.7) |
| $PPh_3$ | 5.2 ± 0.03 (1.7) | 4.8 ± 0.05 (1.6) |
| $OPPh_3$ | 2.8 ± 0.01 (4.0) | 2.7 ± 0.02 (3.6) |

$\lambda_{ex}$ = 472 nm, in DMSO, under $N_2$. $\chi^2$ values (goodness of fit) are given in brackets

### 4.4.3 Time-resolved luminescence of W-1 and W-2

Emission decay profiles of **W-1** and **W-2** in DMSO with and without added $PPh_3$ or $OPPh_3$ are shown in Figure 4-21 and Figure 4-22 respectively, with the lifetimes obtained from fitting shown in Table 4-10.

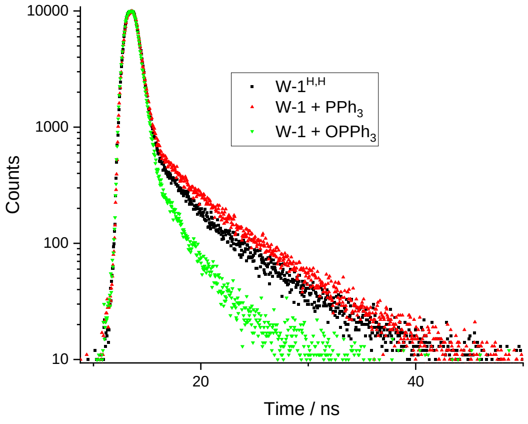

*Figure 4-21: Emission decay profiles obtained at 545 nm, $\lambda_{ex}$ = 473 nm under nitrogen of a 0.32 mM solution of **W-1**, containing 300 equivalents of $PPh_3$, 300 equivalents of $OPPh_3$ or no additive.*

The emission decay profiles of **W-1** and **W-1** in the presence of $PPh_3$ are similar. The profile of **W-1** in the presence of $OPPh_3$ is different, the decay rate higher. In the case of **W-2**, in contrast, the decay profiles of **W-2** and **W-2** in the presence of $OPPh_3$ are identical, but that of **W-2** in the presence of $PPh_3$ is different.

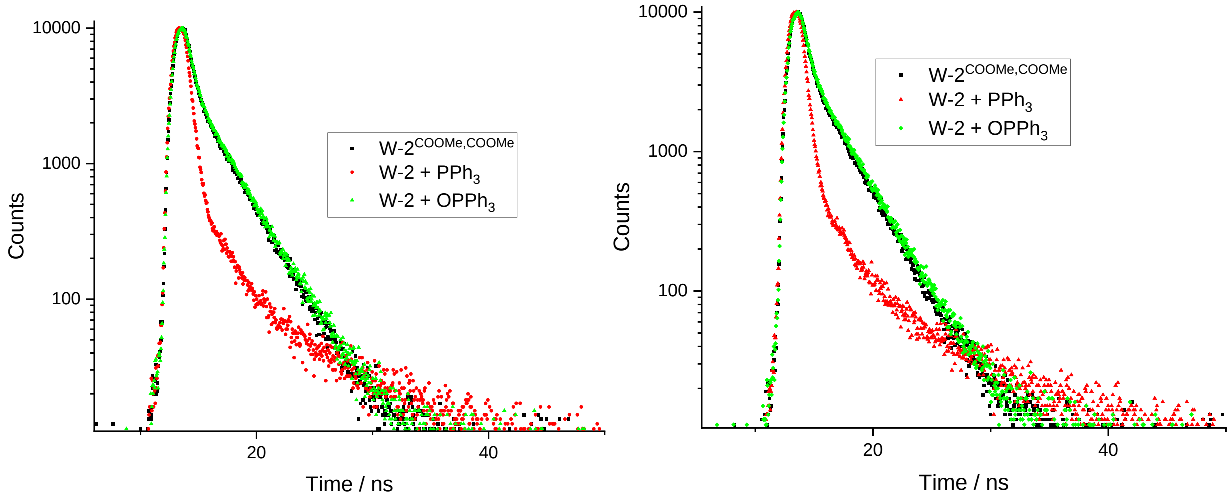

*Figure 4-22: Emission decay profiles obtained at 525 nm (left) and 545 nm (right), $\lambda_{ex}$ = 473 nm under nitrogen of a 1.71 mM solution of **W-2**, containing 300 equivalents of $PPh_3$, 300 equivalents of $OPPh_3$ or no additive.*

The lifetime calculated for **W-2** are within error identical and unaffected by additives. The lifetimes of **W-1** are slightly longer, by ~1.5 ns, with the exception of the sample containing $OPPh_3$ which has lifetime 2 ns shorter similar to the samples of **W-2**.

*Table 4-10: Excited state lifetimes of **W-1** and **W-2** in DMSO.*

| | Excited state lifetime / ns at $\lambda_{em}$ | |
|---|---|---|
| | 525 nm | 545 nm |
| **W-1** | | 4.2 ± 0.05 (1.3) |
| + $PPh_3$ | | 4.8 ± 0.06 (1.2) |
| + $OPPh_3$ | | 2.4 ± 0.05 (1.2) |
| **W-2** | 2.7 ± 0.01 (1.2) | 2.8 ± 0.01 (0.9) |
| + $PPh_3$ | 2.7 ± 0.06 (1.2) | 3.2 ± 0.04 (1.5) |
| + $OPPh_3$ | 2.8 ± 0.01 (1.1) | 2.8 ± 0.01 (1.9) |

$\lambda_{ex}$ = 472 nm, in DMSO, under $N_2$. $\chi^2$ values (goodness of fit) are given in brackets

Similar to the previous section, these differences could be insignificant, although the fitting of the decay curves for the tungsten complexes is much better compared to the molybdenum complexes ($\chi^2$ values are close to 1).

### 4.4.4 Conclusions

Excited state lifetimes obtained for **Mo-1**, **Mo-2**, **L-2**, **W-1** and **W-2** were in the range of 2 to 6 ns. Data on similar SAP based complexes is not available, but the values calculated for **L-2**, **Mo-1** and **Mo-2** are comparable to those for a dithiocarbazate ligand (3 ns) and corresponding molybdenum complex (4 ns) reported by Pramanik *et al.*[191] The excited states of the **4-1**, **4-2** and **2-8** discussed in the introduction to this chapter are, however, much longer lived (10 to 100 μs) than those of **W-1** and **W-2.**

Lifetimes of **Mo-2** and **L-2** in acetone were identical within error and not affected by addition of $PPh_3$ and DMSO (3.2 to 3.4 ns).

Overall, the lifetimes of **Mo-1** in DMSO were on the upper end of the range, followed by **W-1**, whereas **Mo-2** and **W-2** had shorter lifetimes. There could be an influence of the substituent, however, the differences are so small that their significance is questionable.

Importantly, no difference in the lifetimes between the four complexes, on themselves or with added $PPh_3$ or $OPPh_3$, was seen that would correlate with OAT where **Mo-1** was inactive, **W-1** showed low activity and **Mo-1** and **W-2** showed similarly high activity.

Excited state lifetimes need to be sufficiently long to allow a reaction to occur. Diffusion occurs on the nanosecond time scale in most solvents.[192] The lifetimes calculated for **Mo-1**, **Mo-2**, **W-1** and **W-2** are on the lower end of this scale. There is no evidence for a significant ground state interaction between any of the complexes studied and $PPh_3$ indicating that the photoreaction proceeds through a transient encounter between a complex and $PPh_3$. This may also partially account for reaction times on the hour timescale. A longer excited state lifetime does not necessarily lead to an increase in overall rate or conversion if the exited state species is not involved in the rate determining step as is the case for example in the trifluoromethylation of quinoline catalysed by different polypyridyl iridium(III) complexes.[193] Furthermore, in the absence of a clear long-lived excited state the short-lived emissive states studied using time resolved spectroscopy may not be chemically relevant. It also has to be considered that the excited state that is involved in catalysis is not necessarily emissive.

## 4.5 Summary

UV-Vis characterisation has been carried out of the molybdenum and tungsten complexes synthesised in this work. Emissivity of some complexes (**Mo-1, Mo-2, Mo-4, Mo-9, Mo-12, Mo-13, Mo-15** and **Mo-16**) and ligands (**L-1**, **L-2** and **L-4**) has been measured. For ligand **L-2** and complexes **Mo-1**, **Mo-2**, **W-1** and **W-2** emissivity and excited state lifetimes were recorded and the effect of substrates relevant to OAT, $PPh_3$ and $OPPh_3$, on these characteristics studied.

Differences in the UV-Vis spectra due to substituents were unexpectedly small with the exception of complexes bearing additional chromophores, **Mo-4, Mo15** and **Mo-16**. These chromophores give raise to new bands that overlap with the LMCT band. Having higher absorbance these bands are preferentially excited into which could be the reason for their catalytical inactivity. A shift in position and change in intensity were also observed on replacing molybdenum with tungsten

The emissivity of complexes varies drastically. Molybdenum complexes are less emissive than their corresponding ligands and tungsten complexes were much more emissive than their molybdenum counterparts. A weak correlation with the Hammett parameter was observed, but no correlation with OAT activity. Analysis of the fluorescence experiments suggested that emission is due to ligand based transitions and that the nature of transitions in tungsten complexes could be very different from the molybdenum ones.

Lastly, excited state lifetimes of **L-2** and **Mo-1**, **Mo-2**, **W-1** and **W-2** were found to be in the range of 2 to 6 ns. Some small differences were observed between complexes and depending on addition of $PPh_3$ or $OPPh_3$ , but these differences could be insignificant. Importantly, the lifetimes do not correlate with the OAT activity of the complexes.

# Chapter 5 Conclusions and future work

In this work several substituted ligands based on SAP were synthesised and characterised by $^1$H and $^{13}$C NMR spectroscopy, FTIR spectroscopy, elemental analysis and mass spectrometry. These ligands were then coordinated to the molybdenum dioxo ($MoO_2^{2+}$) core yielding complexes of the form [$MoO_2$(L)(MeOH)] and [$MoO_2$(L)]. Two dioxo tungsten complexes of the form [$WO_2$(L)] were made with ligands **L-1** and **L-2**. All complexes were characterised by $^1$H and $^{13}$C NMR spectroscopy, mass spectrometry, elemental analysis and FTIR spectroscopy. Crystal structures were obtained of **Mo-2, Mo-7** and **W-1**. Characterisation data of the new complexes were similar to those of SAP-based complexes reported in literature.

The effects of substituents on the SAP backbone were studied by $^1$H NMR and ATR-IR spectroscopy. A weak linear correlation between the chemical shift of the imine proton of the molybdenum complexes and the Hammett parameter of the substituent as well as between the symmetrical stretching frequency of the M=O bond and the Hammett parameter were found.

Differences between the complexes in the solid state were observed: **Mo-1**, **Mo-2**, **Mo-4**, **Mo-5**, **Mo-6**, **Mo-7**, **Mo-9**, **Mo-10**, **Mo-14**, **Mo-15** and **Mo-16** are of the form of [$MoO_2$(L)(MeOH)] and are monomeric whereas **Mo-3**, **Mo-8**, **Mo-11**, **Mo-12**, **Mo-13, W-1** and **W-2** are of the form of [$MO_2$(L)] (M = Mo, W) and form di- or oligomers. The later form could be obtained from the monomeric one by heating, while the di- and oligomers could be broken up into monomers by addition of a suitable solvent, MeOH or strongly coordinating solvent, such as DMSO or DMF.

In addition to the above-mentioned characterisation, the synthesised complexes were also characterised with regard to their intended role as photoactivated OAT catalysts. UV-Vis spectra were recorded of all complexes while emissivity and excited state lifetimes were only measured of selected complexes.

UV-Vis spectra were unexpectedly similar, except for complexes **Mo-4**, **Mo-15** and **Mo-16** which contain additional chromophores. Theses chromophores gave raise to new strong bands that overlap with the LMCT band, the lowest energy transition found around 420 nm in molybdenum complexes. The nature of transitions in the tungsten complexes was assumed similar to those in molybdenum, but emission spectroscopy and excited state lifetime measurements suggest marked differences, with an LMCT transition of higher energy in the tungsten complexes.

Emission bands were observed around 500 to 590 nm of selected complexes and ligands after excitation at 410 nm. The molybdenum complexes were found to be less emissive than the corresponding ligands with some being non-emissive, while tungsten complexes were substantially more emissive than their molybdenum analogues. Emission around 525 to 550 nm occurred after excitation of **L-2, Mo-1**, **Mo-2**, **W-1** and **W-2** at 473 nm and the lifetimes of the corresponding excited states were found to be in the range of 2 to 6 ns. The presence of $PPh_3$ or $OPPh_3$ had small effects on emissivity and lifetimes but differences between lifetimes were considered insignificant.

The combined spectroscopic experiments suggested that emission occurred from intra-ligand transitions and that there could be a marked difference between processes in the excited state between tungsten and molybdenum complexes and between different molybdenum complexes. More work is needed to fully understand these processes including varying the reaction conditions under which emissivity and lifetimes were recorded, use of different solvents and excitation wavelength, as well as analysing other complexes and corresponding ligands.

Computational work to calculate differences in energy and geometry between states would greatly help analysis.

The potential of the molybdenum and tungsten complexes to act as photoactivated OAT catalysts was assessed using $PPh_3$ as the oxygen acceptor and DMSO as the donor and solvent of the reaction. Solutions of the respective complex and phosphine in DMSO were irradiated for 3 h at 410 nm and conversion of the phosphine determined by $^1H$ NMR spectroscopy. Complexes **Mo-1**, **Mo-4**, **Mo-15** and **Mo-16** were inactive while the highest activity was observed for **Mo-2** and **W-2**. A weak linear correlation between the Hammett parameter of the substituent and the conversion were observed in line with the trend observed in thermal OAT that electron withdrawing groups are beneficial to catalytic activity. The Hammett parameter had to be modified for acid and ester groups to account for electron delocalisation.

Catalytic activity was not only influenced by the electron withdrawing capacity of substituents, but also depended strongly on whether a substituent was located on the former amine aromatic ring or the aldehyde ring but not on the position on a given aromatic ring. This could be due to the electronic communication between the two aromatic rings as well as between ligand and metal during excitation.

The screening of catalytic activity of all complexes had revealed **Mo-2** to be the most active complex. Further catalytic studies were therefore carried out with this complex.

First, several other phosphine and sulfoxide substrates were tested. While faster conversion was observed using $PPh_2Me$ and $PPhMe_2$ instead of $PPh_3$ and amongst others, di-*p*-tolyl sulfoxide instead of DMSO in acetone, no clear trend was observed using substituted $PPh_3$ or between different sulfoxides. Interestingly, it was found that aromatic OH groups hinder OAT, but the exact reason for this behaviour was not determined.

Second, studies of the underlying mechanism in photoactivated OAT were carried out.

A stoichiometric reaction of **Mo-2** with $PPh_3$ was performed in order to analyse the reduced molybdenum complex and identify whether comproportionation and dimerisation, as reported for some molybdenum complexes in thermal OAT, occurred.

Analysis of a solution of **Mo-2** and $PPh_3$ in acetone that was irradiated at 410 nm over night by $^1H$ NMR spectroscopy, UV-Vis spectroscopy, LIFDI mass spectrometry and ATIR analysis of the residue after removal of the solvent suggested the formation of (primarily) monomeric Mo(IV), but the Mo(V) dimer was also detected by mass spectrometry. Similar analysis of **W-2** was inconclusive as decomposition of the complex occurred after OAT. In the future, modification of the reaction conditions to allow tungsten complexes to be studied, as well as study of other molybdenum complexes could provide additional insights. Further information on the reduced species could be obtained from EPR spectroscopy, distinguishing between Mo(V) / Mo(IV) in the singlet / triplet state. Ultimately, a crystal structure of the reduced complex could prove the presence of the reduced species in the +4 or +5 oxidation state.

Analysis of the kinetics of the reaction between **Mo-2**, $PPh_3$ and sulfoxide in DMSO or acetone using VTNA revealed a strong dependence on the solvent and an unexpected dependence of reaction rate on catalyst concentration: at concentrations below 1 mM the rate increased linearly with catalyst concentration while above 1 mM it decreased exponentially.

## 5.1 Possible mechanism of photo activated OAT

Large parts of this project focused on investigating the mechanism behind photo activated OAT. The following is a summary of the results relevant to the mechanism:

- OAT requires light activation (section 3.2.4)
- **Mo-1**, **Mo-4**, **Mo-15** and **Mo-16** are inactive (section 3.2.1)
- No correlation between activity and wavelength (section 3.3.3). Excitation at 365 and 410 nm excites both the ligand centred transition and the LMCT transition, at 460 nm only the latter is excited.
- Electron withdrawing substituent is required, linear increase in activity with the Hammett parameter, better correlation with improved Hammett parameter of acid and ester substituents (section 3.3.1)
- Reaction orders (section 3.6.4):
    - In acetone: 0.5 for $PPh_3$; 0.5 for DMSO, but 1 for **SO-2**; **Mo-2:** linear increase below 1 mM, exponential decrease above 1 mM
    - In DMSO: 1 for $PPh_3$; **Mo-2**: no increased activity above 1 mM, deactivation at lower concentration
- Stoichiometric reaction of **Mo-2** with $PPh_3$ most likely generates Mo(IV) (section 3.7.5)
- Ligand centred transition at 365 nm, LMCT at 410 nm (section 4.2.1)
- Similar UV-Vis spectra for most complexes (**Mo-2, Mo-3, Mo-5, Mo-6, Mo-7, Mo-8, Mo-9, Mo-13)**, but different activity (section 4.2.2)

Possible mechanisms of photo activated OAT will be presented subsequently after some general considerations and their agreement with the above results discussed.

In all cases the reaction starts with absorption of light by the complex. The absence of a clear effect of the excitation wavelength (365, 410 or 460 nm) suggests that the same excited state is ultimately generated from which the reaction proceeds, or that due to band overlap the lowest energy transition (LMCT) is excited in all cases and initiates the OAT. The difference in absorption between the three wavelengths did not affect the reaction. The reaction could be limited by the intensity of the excitation source or the rate limiting step could be different from this excitation step. Complexes containing additional chromophores (**Mo-4, Mo-14, Mo-16**) were inactive possibly due to transitions involving these chromophores having much stronger absorbance but leading to inactive excited states.

The correlation between the (improved) Hammett parameter and the catalytic activity suggests an electron density increase which is stabilised by the electron withdrawing substituent. Electron density is increased on the metal centre upon reduction to Mo(IV) but stabilisation could also be important at other points during reaction.

Regarding formation of dimerised Mo(V), the results from the stoichiometric reaction between **Mo-2** and $PPh_3$ suggest this process to only have a minor contribution if it is at all present. Its occurrence may depend on the solvent and substrates used and even the complex. Dimerisation could even contribute to the difference in activity if it occurs different degrees between the complexes tested and lowers the concentration of active catalyst. Since the mechanistic work was mostly done using only **Mo-2** and no indication of dimerisation was seen during complex screening, it will not be considered in the mechanism.

In the simplest mechanism of photo activated OAT, the complex only functions as a sensitizer and activates either $PPh_3$ or the sulfoxide with the OAT only occurring between the two substrates. Such a mechanism, where oxygen atom donor and acceptor directly transfer oxygen without involvement of a metal complex was proposed as a possible pathway in the dehydrogenation with the tungsten complex **1-16** (see section 1.4.3).[67] In the present work the stoichiometric reaction between **Mo-2** and $PPh_3$ (see section 3.7) yielded $OPPh_3$ and the reduced Mo complex that had lost one of its oxo ligands, showing that photo activated OAT proceeds via the metal complex, as is the case in thermal OAT.

The second possible mechanism parallels the thermal reaction but starts with excitation of the molybdenum complex (Scheme 5-1). Only the photo activated complex is then attacked by the phosphine to yield phosphine oxide and the reduced molybdenum complex. Additional activation of the reduced Mo(IV) before reoxidation by the sulfoxide is also possible but was not studied in this work.

Excitation of the complex results in a LMCT transition which increases the electron density on the metal centre. This would weaken the Mo=O bond through population of the Mo=O* antibonding orbital.

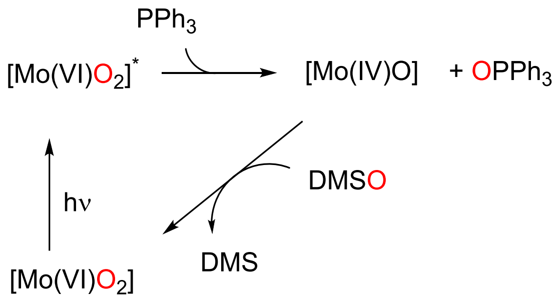

*Scheme 5-1: Potential, simple mechanism for photoactivated OAT from DMSO to $PPh_3$.*

This mechanism is consistent with the results of the stoichiometric reaction. In the thermal reaction the increase in activity due to electron withdrawing substituents has been explained as these substituents lowering the electron density on the $[MoO_2]$ core which facilitates the nucleophilic attack of the phosphine.[125] This explanation is contradictory to the electron density increase due to the LMCT and might not apply to the photo activated reaction. The strong dependence of the ring the substituent is attached to could also point to this conclusion. In addition, stabilisation of the increased electron density on the [MoO] core in the reduced Mo(IV) by electron withdrawing substituents could play a role.

A shortcoming of this mechanism is its simplicity in that it cannot explain the results of the kinetic analysis where a strong dependence of the solvent, sulfoxide and catalyst concentration was observed and the order in reactants was also different from those observed in thermal reactions.

A third possibility of a mechanism is based on work by Clarke *et al.* on the photoactivated OAT from DMSO to $PPh_3$ catalysed by iridium complexes (Scheme 5-2).[194] In this reaction, where OAT does not involve a metal complex, the excited iridium catalyst is reductively quenched by $PPh_3$ producing a phosphine radical cation which then reacts with the sulfoxide to give the phosphine oxide and a sulfide radical. This sulfide radical can either react with the reduced $[Ir^{2+}]$ and the catalytic cycle starts again, or it can react with fresh $PPh_3$ to propagate the radical chain.

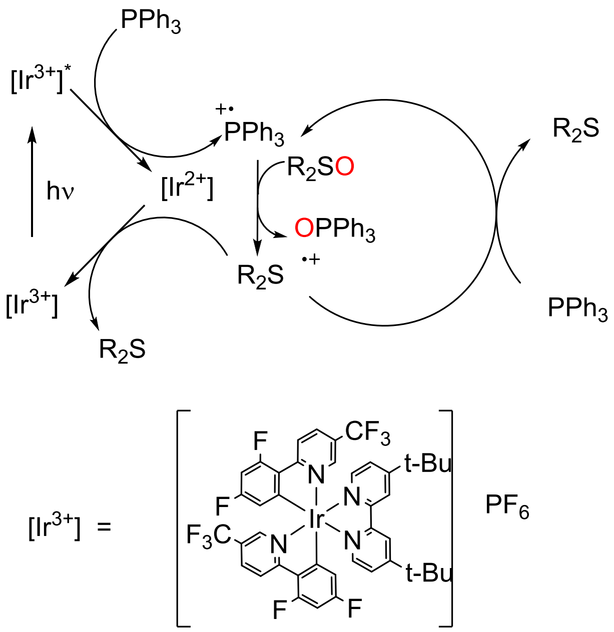

*Scheme 5-2: Suggested mechanism for photoactivated OAT between $PPh_3$ and $R_2SO$ catalysed by an iridium complex. Adapted from Clarke et al.* [194]

Based on the above examples, an alternative mechanism for the OAT system studied in this work is proposed in Scheme 5-3.

The first step is the excitation of the molybdenum complex **5-2**. This would then be followed by reductive quenching of the excited state by the phosphine yielding the phosphine radical cation **5-6** and the negatively charged complex **5-4** where the electron could be located on the metal giving Mo(V) or on the ligand. Radical cation **5-6** is then attacking the oxo ligand of the electron rich **5-4** giving the phosphine oxide and transferring a second electron onto molybdenum to give the reduced Mo(IV). Regeneration of **5-5** with DMSO would follow the conventional thermal OAT mechanism.

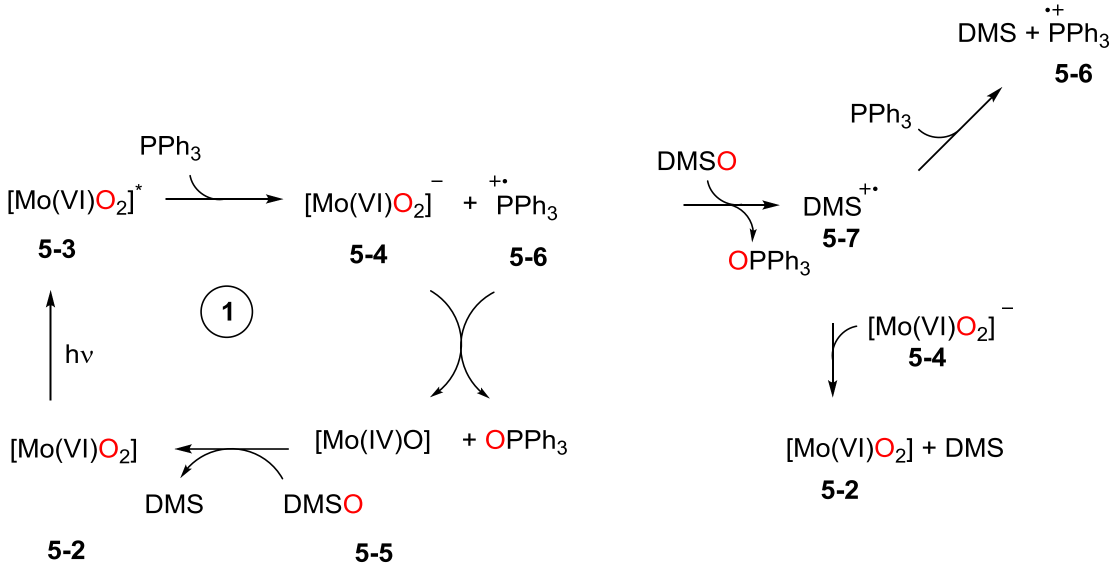

*Scheme 5-3: Potential mechanism for photoactivated OAT from DMSO to $PPh_3$ including two pathways with and without direct involvement of the molybdenum complex in the OAT.*

The mechanism thus far (marked with 1 in Scheme 5-3) is very similar to the thermal mechanism and the first possible mechanism present above (Scheme 5-1). However, additional paths are possible after the reductive quenching step. As shown, **5-6** can also react with DMSO directly**,** which could be bond to the complex or a free solvent molecule, giving the sulfur based radical cation **5-7** and phosphine oxide. **5-7** in turn could react with fresh $PPh_3$ propagating a radical chain, or with **5-4** closing the catalytic cycle.

In addition to the pathways shown in Scheme 5-3 further branches of the mechanism are possible. **5-4** and **5-6** reacting after quenching do not necessarily have to be the same molecules between which quenching occurred. Reaction of **5-4** with $PPh_3$ or **5-6** with **5-2** cannot be excluded either. Whether all these possible pathways are followed, and which one is dominant will depend on several factors, one being concentration of the species involved which could explain the results of the kinetic analysis in chapter 3.6.

Most complexes (**Mo-2, Mo-3, Mo-5, Mo-6, Mo-7, Mo-8, Mo-9, Mo-13**) showed very similar UV-vis spectra around 410 nm (absorbance and position of the LMCT band) meaning that they have a similar difference in energy between ground and excited state. Higher activity of some complexes could then be due to the ground state lower in energy which after excitation of one electron can be more easily reductively quenched by the $PPh_3$ (Scheme 5-3).

This mechanism, in contrast to the previous possibility, is more complex due to the possible pathways introduced by the presence of radicals. Due to this complexity the resultant rate laws are likely too complex for the kinetic analysis and obtained reaction orders which would rule out this mechanism.

The two possible mechanisms presented in Scheme 5-1 and Scheme 5-3 would be practically identical without the additional pathways in the latter with the reaction between $PPh_3$ and 5-3 involving electron transfer (followed by transfer of $O^-$). But neither of the two can explain the results obtained in this work. Additional modifications of the mechanism presented or a completely new one are needed. It also seems likely that more than one mechanism or mechanistic pathways could be involved, depending on the reaction conditions. Based on the kinetic analysis (section 3.6), a strong effect of the solvent (DMSO *vs.* acetone) and the nature of the sulfoxide (DMSO *vs.* **SO-2**) was observed. The changes in reactant order suggest a change in the mechanism. Additionally, the catalyst seemed to affect the reaction rate in different ways depending on its concentration which could be due to different mechanisms or pathways dominating depending on the concentration.

In this regard, the chromium complex **5-1** is an interesting example. It catalyses the oxidation of sulfides by PhIO (Scheme 5-4), which, although different from the examples in this work, still constitutes OAT based on the overall reaction R-S-R' + PhIO -> R-SO-R' + PhI.

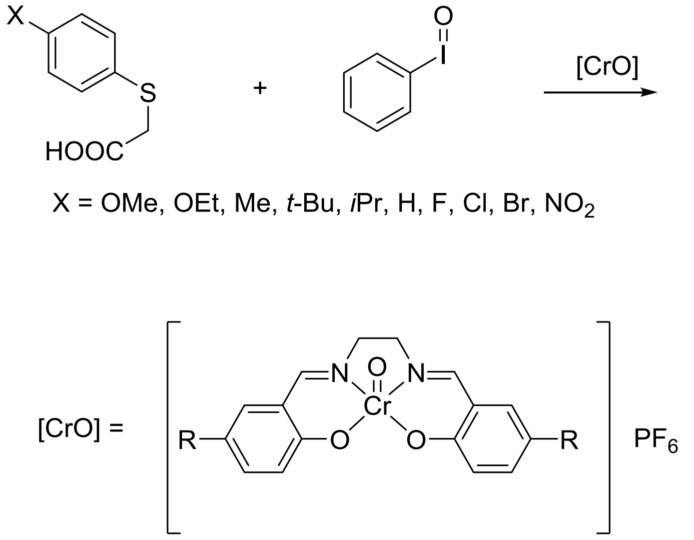

**5-1**

*Scheme 5-4: Oxidation of sulfide catalysed by a chromium oxo complex.* [195]

Subramaniam and co-workers have studied this system and found that the mechanism depended on the sulfide.[195] Oxidation of electron poor sulfides (X is an electron withdrawing group) followed a conventional OAT mechanism, where the sulfide attacks the oxo ligand yielding the sulfoxide and Cr(III).

Oxidation of electron richer sulfides (X is an electron donating group) however proceeded by a single electron transfer from the sulfide to chromium yielding Cr(IV) and a cationic sulfide radical which then attacked the oxo ligand producing the sulfoxide and Cr(III) as well. In both cases, **5-1** is regenerated from the Cr(III) species by PhIO.

## 5.2 Future work

It is clear that more work is needed to eventually find the mechanism(s) that govern photo activated OAT in these compounds.

In the stoichiometric reaction between **Mo-2** and $PPh_3$ isolation of the reduced molybdenum species would improve its analysis. A crystal structure would provide final prove of its nature. Better conditions need to be found for the reaction of **W-2** with $PPh_3$ where decomposition of the tungsten complex occurs under current conditions.

Measurements of emissivity and excited state lifetimes could be extended to include more complexes and ligands, as well as conditions, *e.g.* solvents, with the aim to identify possible trends between complexes and better understand the processes in the excited state. These measurements would also benefit from computational work to determine energy levels, structures and the nature of electronic transitions.

OAT in the presence of radical traps or EPR analysis could be used to determine the presence of radical species as suggested in the previous section. EPR spectroscopy could be used to determine the presence of radical species. A phosphine-based radical would be a strong indication for the proposed mechanism while molybdenum-based radicals could also stem from reduced molybdenum as found in the conventional mechanism. A DMS-based radical would also support existence of the additional pathways without direct involvement of the complex.

Involvement of radical species in the reaction could also be evidenced by addition of radical quenchers such as TEMPO (2,2,6,6-Tetramethyl-1-piperidinyloxy) that react with the radicals generated during reaction thus stopping the reaction. The product of this quenching can be identified allowing determination of the radical species present during reaction.

Apart from investigations of the mechanism, future work could focus more on the substrate scope and potential applications of photoactivated OAT with molybdenum and tungsten complexes. The products do not necessarily have to be phosphine oxides and sulfides. Through choice of substrate and experimental conditions, OAT could be performed in the reverse way to make phosphines and sulfoxides from sulfides and phosphine oxides. In addition, sulfones could be used as the oxygen donor to selectively obtain sulfoxides.

OAT is not limited to phosphorus and sulfur as the donor and acceptor. OAT to olefins is well known, although often the metal is not directly involved and OAT takes places between substrates in the coordination sphere.[196]

Oxidation / reduction of carbon atoms is a large and important field, where any step in the chain C-H <-> alcohol <-> aldehyde / ketone <-> acid could potentially be achieved via OAT. The additionally required oxygen acceptor / donor would ideally be $O_2$ or water, as achieved by the molybdenum and tungsten enzymes, or any species that yields a useful or at least non-toxic by-product.

# Chapter 6 Experimental

## 6.1 General remarks and Instrumentation

Chemicals and solvents were obtained from commercial suppliers (Acros, Fluka, Sigma-Aldrich, Fluorochem, Alfa Aesar, Fischer Scientific, Tokyo Chemical Industry) and used without further purification unless stated otherwise.

$^{1}$H , $^{13}$C {$^{1}$H} decoupled and $^{31}$P {$^{1}$H} decoupled NMR spectra were recorded on a Jeol ECS400D 400 MHz spectrometer ($^{1}$H NMR 400 MHz, $^{13}$C NMR 100.6 MHz $^{31}$P NMR 161.9 MHz), a Bruker AV500b 500 MHz spectrometer ($^{1}$H NMR 500 MHz, $^{13}$C NMR 125.75, $^{31}$P NMR 202.4 MHz) and a Bruker AV600 600 MHz spectrometer ($^{1}$H NMR 600 MHz, $^{13}$C NMR 150.9 MHz, $^{31}$P NMR 242.9 MHz). The assignment of the spectra was aided by DEPT135, COSY, HMBC and HSQC experiments. MestReNova was used for processing and analysis of spectra. Chemical shifts are quoted as ppm referenced to residual solvent. Coupling constants are rounded to the nearest 0.5 Hz. Abbreviations for multiplicity are as follows: s for singlet, d for doublet, t for triplet, q for quartet, dd for doublet of doublet, td triplet of doublet, ddd for doublet of doublet of doublets, m for multiplet, br for broad.

ATR-FTIR spectra were recorded on a Perkin Elmer Spectrum Two in the region of 400-4000 cm$^{-1}$. Elemental analysis was carried out by Dr. G. McAllister on an Exeter Analytical Inc. CE-440 analyser. Calculated composition was empirically optimised by including residual water or methanol. Mass spectrometry was carried out by Mr. K. Heaton, Dr. R. Cercola and Mr. A. Lopez on Waters GCT Premier mass spectrometer (LIFDI) and Bruker compact® time of flight mass spectrometer (ESI). Masses for molybdenum and tungsten are calculated based on $^{98}$Mo and $^{184}$W, respectively. Melting points were recorded on a Stewart Scientific SMP3 melting point apparatus. Loss of MeOH in complexes was determined by colour change from yellow /orange to brown.

Electronic absorption spectra were recorded on a Shimadzu 1800 in the range of 330 to 700 nm (acetone) or 270 to 700 nm (DMSO), pathlength 1 cm.

Emission spectra were recorded on a Hitachi F-4500 spectrometer in acetone or DMSO and under nitrogen with the following parameters: Excitation at 410 nm, excitation slit width of 10 nm, emission slit width of 20 nm, 950 V photomultiplier tube (PMT) voltage, scan speed of 240 nm/min, pathlength 1 cm; spectra were corrected for instrument response. All measurements in a set of experiments were performed at an equal absorbance of 0.1 at 410 nm or at equal concentration. Details are provided in Table 6-1.

Excited state lifetimes were recorded on an Edinburgh Instruments FLS980 spectrometer in acetone or DMSO and under nitrogen with the following parameters: Excitation at 472.8 nm with a EPL-470 laser source and at 375.6 nm with a EPLED-380 LED source, excitation slit width 0.03 nm, emission slit width 10 nm, range 0 - 200 ns. All measurements in a set of experiments were performed at an equal absorbance of 0.1 at 473 nm or at equal concentration. Details are provided in Table 6-2. Data analysis and fitting were performed with the FLS980 software.

Single crystal X-ray crystallography was performed by Dr. A. Whitwood and T. Thanner. Data were collected at 110 K on an Oxford Diffraction SuperNova diffractometer with Cu-K radiation (λ = 1.54184 Å) using an EOS CCD camera.

*Table 6-1: Overview on experimental conditions for fluorescence spectroscopy.*

| Chapter | Compound | Concentration / mM | Additive | Concentration / mM | solvent |
|---|---|---|---|---|---|
| 4.3.1 | **L-1** | 0.45 | / | | acetone |
| | **L-2** | 0.07 | / | | acetone |
| | **L-4** | 0.01 | / | | acetone |
| | **Mo-1** | 0.02 | / | | acetone |
| | **Mo-2** | 0.019 | / | | acetone |
| | **Mo-4** | 0.009 | / | | acetone |
| 4.3.2 | **Mo-1, Mo-2, Mo-4, Mo-9, Mo-12, Mo-13, Mo-15, Mo-16** | 0.05 | | | acetone |
| 4.3.3 | **L-2** | 0.02 | / | | acetone |
| | **L-2** | 0.02 | $PPh_3$ | 6.5 | acetone |
| | **L-2** | 0.02 | $PPh_3$ and DMSO | 6.5 and 5000, respectively | acetone |
| | **Mo-2** | 0.02 | / | | acetone |
| | **Mo-2** | 0.02 | $PPh_3$ | 6.5 | acetone |
| | **Mo-2** | 0.02 | $PPh_3$ and DMSO | 6.5 and 5000, respectively | acetone |
| 4.3.4 | **Mo-1** | 0.022 | / | | DMSO |
| | **Mo-1** | 0.022 | $PPh_3$ | 6.6 | DMSO |
| | **Mo-1** | 0.022 | $OPPh_3$ | 6.6 | DMSO |
| | **Mo-2** | 0.015 | / | | DMSO |
| | **Mo-2** | 0.015 | $PPh_3$ | 4.5 | DMSO |
| | **Mo-2** | 0.015 | $OPPh_3$ | 4.5 | DMSO |
| | **W-1** | 0.18 | / | | DMSO |
| | **W-1** | 0.18 | $PPh_3$ | 54.0 | DMSO |
| | **W-1** | 0.18 | $OPPh_3$ | 54.0 | DMSO |
| | **W-2** | 0.15 | / | | DMSO |
| | **W-2** | 0.15 | $PPh_3$ | 45.0 | DMSO |
| | **W-2** | 0.15 | $OPPh_3$ | 45.0 | DMSO |

*Table 6-2: Overview on experimental conditions for excited state lifetime measurements.*

| Chapter | Compound | Concentration / mM | Additive | Concentration / mM | solvent |
|---|---|---|---|---|---|
| 4.4.1 | **Mo-1** | 0.056 | / | | DMSO |
| | **Mo-1** | 0.056 | $PPh_3$ | 16.8 | DMSO |
| | **Mo-1** | 0.056 | $OPPh_3$ | 16.8 | DMSO |
| 4.4.2 | **L-2** | 0.012 | / | | acetone |
| | **L-2** | 0.012 | $PPh_3$ | 0.12 | acetone |
| | **L-2** | 0.012 | DMSO | 500 | acetone |
| | **Mo-2** | 0.015 | / | | acetone |
| | **Mo-2** | 0.020 | $PPh_3$ | 0.20 | acetone |
| | **Mo-2** | 0.020 | DMSO | 500 | acetone |
| 4.4.3 | **Mo-2** | 0.013 | / | | DMSO |
| | **Mo-2** | 0.013 | $PPh_3$ | 3.9 | DMSO |
| | **Mo-2** | 0.013 | $OPPh_3$ | 3.9 | DMSO |
| 4.4.4 | **W-1** | 0.32 | / | | DMSO |
| | **W-1** | 0.32 | $PPh_3$ | 96 | DMSO |
| | **W-1** | 0.32 | $OPPh_3$ | 96 | DMSO |
| | **W-2** | 1.71 | / | | DMSO |
| | **W-2** | 1.71 | $PPh_3$ | 513 | DMSO |
| | **W-2** | 1.71 | $OPPh_3$ | 513 | DMSO |

## 6.2 Catalysis

**Set-up for irradiation:**

Samples prepared in (Young's) NMR tubes under nitrogen were irradiated by inserting them into a custom-made, 3-D printed chamber (shown in Figure 6-1 , schematics in Figure 6-2).

The tubes are inserted 8 cm deep, enough to ensure the part that contains the reaction mixture is fully inside. Up to three tubes can be inserted and positioned at an equal distance from the centrally placed LED. The inner walls of the chamber are covered with a reflective material to allow light to reach the tubes from all sides.

Three such chambers with different LEDs were made, allowing samples to be irradiated at 365, 410 or 460 nm.

The LEDs made by LED Engin, California, USA, were obtained from Mouser electronics, Buckinghamshire, UK. Powered by a constant current source (700 mA per LED) they produce a luminous flux of 1.2 W (365 nm), 1.05 W (410 nm) and 0.85 W (460 nm).

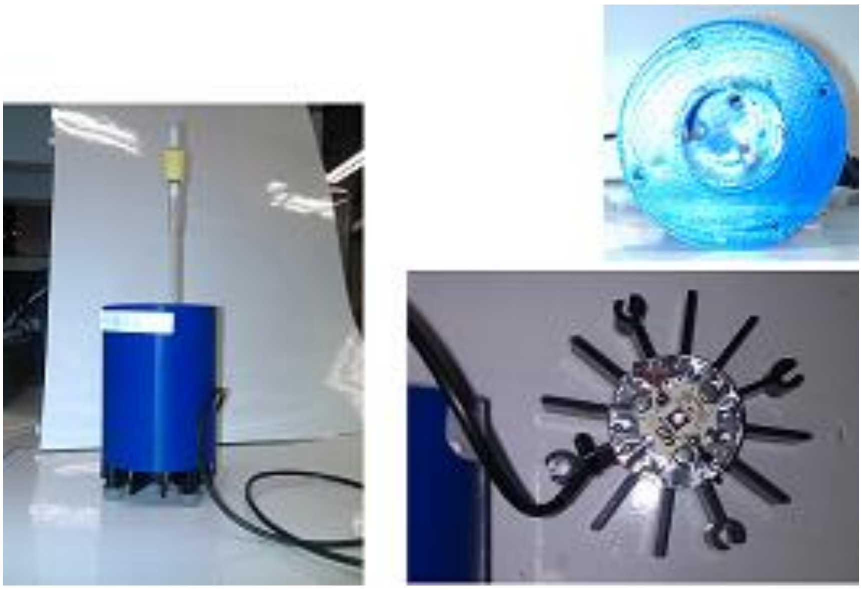

*Figure 6-1: Irradiation set-up. Fully assembled (left), plastic body (top right) and stand with electronics (bottom right)*

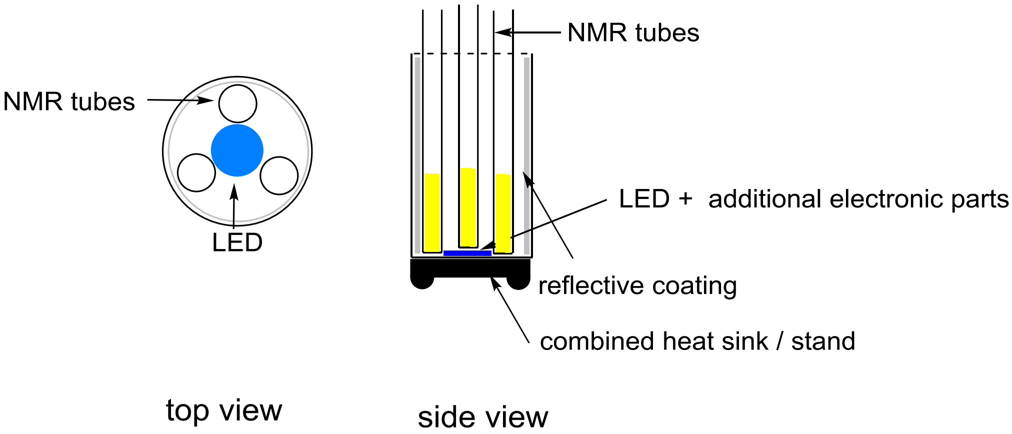

*Figure 6-2: Schematic top and side view of the irradiation set-up.*

**Sample preparation:**

Sample preparation was carried out in a glove box under nitrogen, solvents were dried over 3 Å molecular sieves and degassed via 3 freeze-pump-thaw cycles.

In a glove box under nitrogen atmosphere, appropriate amounts of phosphine, catalyst, sulfoxide and additional compounds as required were dissolved in the appropriate solvent (DMSO-$d_6$, acetone-$d_6$, DMF-$d_7$) to obtain the desired concentration. 700 µL of these solutions were then transferred into a Youngs NMR tube. Table 6-3 provides details on nature and concentrations of complexes, substrates and additives, solvents used and experimental condition. In a typical experiment **Mo-2** (0.34 mg, 0.7 µmol) and $PPh_3$ (55.08 mg, 0.21 mmol) were dissolved in DMSO-$d_6$ (700 µL).
Irradiation was conducted outside the glove box with the set-up described above.

Reactions were monitored by $^1$H NMR spectroscopy. Conversions were obtained through integrating and comparing characteristic resonances of phosphine and phosphine oxide, or sulfoxide and sulfide.
For the most used substrates, these resonances are: for $PPh_3$/$OPPh_3$ resonances around 7.2 to 7.3 ppm ($PPh_3$) and 7.5 to 7.59 ($OPPh_3$) , for **SO-2/S-2** resonances around 2.4 to 2.31 and 2.26 to 2.31 ppm.
The exact ranges that were integrated varied depending on the shape of the resonances and whether they overlapped with adjacent signals or not. Although overlap of signals from phosphine and sulfoxide occurred in some cases in the aromatic region, a pair of unambiguous signals of starting material and product could always be identified.
Conversion was calculated as follows:

$$\%\,Conversion = \frac{i(product)}{i(product) + i(starting\ material)} * 100$$

With i(x) the integrated value of the NMR signal, corrected for the number of protons represented.

*Table 6-3: Summary of concentrations of complex and substrates and solvents used for the indicated types of catalysis experiments.*

| Experiment | Chapter | c(complex) / mM | c(phosphine) / mM | c(sulfoxide) / mM | Additive / mM | Solvent | Irradiation / nm |
|---|---|---|---|---|---|---|---|
| complex screening | 3.2 and 3.3 | 1, (**Mo-1** to **Mo-16, W-1, W-2**) | 300, ($PPh_3$) | Excess | / | DMSO-$d_6$ | 410 |
| control | 3.2.3 | / | 300, ($PPh_3$) | Excess | / | DMSO-$d_6$ | 365, 410 and 460 |
| control | 3.2.3 | / | 300, ($PPh_3$) | 300, (**SO-2**) | / | acetone-$d_6$ | 410 |
| control | 3.2.4 | 1 **(Mo-2)** | 300, ($PPh_3$) | 300, (**SO-2**) | / | acetone-$d_6$ | 410 |
| control | 3.2.5 | / | 300, ($PPh_3$) | Excess | 1 (**L-1**, **L-2** or **L-3**) | acetone-$d_6$ | 365, 410, 460 |
| control [a] | 3.2.6 | 1 **(Mo-2)** | 300, ($PPh_3$) | Excess | / | DMSO-$d_6$ | none |
| control | 3.2.7 | 1 (**Mo-2)** | 300, ($PPh_3$) | 300, (**SO-2**) | water, 50 mM | acetone-$d_6$ | 410 |
| control [b] | 3.2.8 | 1 (**Mo-2)** | 300, ($PPh_3$) | 300, (**SO-2**) | / | acetone-$d_6$ | 410 |
| control [b] | 3.2.8 |  | 300, ($PPh_3$) | 300, (**SO-2**) | / | acetone-$d_6$ | 410 |
| control [b] | 3.2.8 | 1 (**Mo-2)** | 300, ($PPh_3$) | Excess | / | DMSO-$d_6$ | 410 |
| control [b] | 3.2.8 |  | 300, ($PPh_3$) | Excess | / | DMSO-$d_6$ | 410 |
| substrate scope | 3.4 | 1 (**Mo-2)** | 300, ($PPh_3$) | 300, (**SO-1** to **SO-10**) | / | acetone-$d_6$ | 410 |
| substrate scope | 3.4.1 | 1 (**Mo-2)** | 300, ($PPh_3$) | 300, (**SO-2**) | phenol , 100 mM | acetone-$d_6$ | 410 |
| substrate scope | 3.5 | 1 (**Mo-2)** | 300 (**P-1, P-2, P-3**) | 300, (**SO-1**) | / | acetone-$d_6$ | 410 |
| substrate scope | 3.5 | 1 (**Mo-2)** | 300 (**P-1, P-4, P-5, P-6, P-7**) | 300, (**SO-2**) | / | acetone-$d_6$ | 410 |
| kinetics | 3.6.1 | 1 (**Mo-2)** | varied, ($PPh_3$) | Excess | / | DMSO-$d_6$ | 410 |
| kinetics | 3.6.1 | 1 (**Mo-2)** | varied, ($PPh_3$) | 150, (**SO-2**) | / | acetone-$d_6$ | 410 |
| kinetics | 3.6.2 | 1 (**Mo-2)** | 300, ($PPh_3$) | Varied, (**SO-2**) | / | acetone-$d_6$ | 410 |
| kinetics | 3.6.2 | 1 (**Mo-2)** | 300, ($PPh_3$) | Varied, (**SO-2**) | / | acetone-$d_6$ | 410 |
| kinetics | 3.6.3 | Varied (**Mo-2**) | 300, ($PPh_3$) | Excess | / | DMSO-$d_6$ | 410 |
| kinetics | 3.6.3 | Varied (**Mo-2**) | 300, ($PPh_3$) | 300, (**SO-2**) | / | acetone-$d_6$ | 410 |
| stoichiometric reaction | 3.7 | 1 (**Mo-2**) | 1, ($PPh_3$) | / | / | acetone-$d_6$ | 410 |
| stoichiometric reaction | 3.7 | 1 (**W-2**) | 5, ($PPh_3$) | / | / | acetone-$d_6$ DMF-$d_7$ 1:1 | 410 |

[a] At 45 °C

[b] Samples prepared in air

## 6.3 Synthesis

### 6.3.1 3-Formyl-4-hydroxybenzoic acid, 1

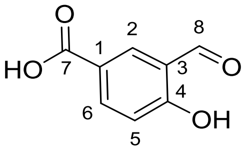

*$C_8H_6O_4$, 166.13 g/mol*

A literature preparation was used.[90]

HMTA (3.06 g, 21.7 mmol) was dissolved in trifluoroacetic acid (9 mL) under nitrogen and added dropwise to a suspension of para-hydroxybenzoic acid (3 g, 21.7 mmol) in trifluoracetic acid (8 mL) under nitrogen. The mixture was heated to 80 °C for 4 h whilst stirring. After cooling to RT, the then yellow mixture was poured into 4 M HCl (60 mL) and stirred for 3 h. The precipitate was isolated by filtration and washed with water (80 mL). The product was obtained as a pale-yellow solid. 1.206 g, 7.26 mmol, 40%
Characterisation data consistent with literature.[197]

**$^1$H NMR** (400 MHz, DMSO-$d_6$, 25 °C): δ = 12.82 (1H, COOH), 11.49 (1H, OH), 10.29 (1H, H-8), 8.23 (d, J = 2.5 Hz, 1H, H2) 8.04 (dd, J= 8.5 Hz, 2.5 Hz, 1H, H6), 7.08 (d, J = 8.5 Hz, 1H, H5) ppm.

**$^{13}$C NMR** (101 MHz, DMSO-$d_6$ , 25 °C): δ = 190.6, 166.5, 164.1, 136.9, 130.7, 122.1, 122.0, 117.6 ppm.

**ESI-MS**: negative ion, calculated for $(C_8H_5O_4)^-$: 165.0193, found 165.0189, error: 2.5 ppm.

**Mp.:** 230 °C

### 6.3.2 3-Formyl-4-hydroxybenzoic acid methyl ester, 2

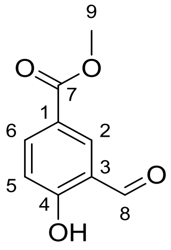

*$C_9H_8O_4$, 180.16 g/mol*

A literature preparation was used.[91]

**1** (1 g, 6 mmol) was suspended in MeOH (10 ml). Whilst stirring, sulfuric acid (0.66 mL, 10.9 mmol) was added and the mixture heated to reflux for 4.5 h. After letting the now pale pink solution cool to room temperature the solvent was removed under reduced pressure and the obtained solid dissolved in chloroform (30 ml). After washing with 10 % $NaHCO_3$ solution (20 ml) and drying over $MgSO_4$ the solvent was removed and the product dried *in vacuo*. 500 mg, 2.78 mmol, 46 %

Characterisation data consistent with literature.[197]

**$^1$H NMR** (600 MHz, $CDCl_3$, 25 °C): δ = 11.22 (br s,1H, OH), 9.87 (s, 1H, H8) 8.22 (d, *J* = 2.5 Hz, 1H, H2), 8.08 (dd, *J* = 8.5 Hz, 2.5 Hz, 1H,H6), 6.93 (d, *J* = 8.5 Hz, 1H, H5)., 3.85 (s, 3H, H9) ppm.

**$^{13}$C NMR** (151 MHz , $CDCl_3$, 25 °C): δ = 196.3, 165.4, 164.9, 137.7, 136.0, 122.2, 120.0, 117.8, 52.2 ppm.

**ESI-MS**: negative ion, calculated for $[C_9H_7O_4]^-$: 179.0350, found 179.0347, error: 1.4 ppm

**Mp.:** 76 °C

## 6.3.3 3-Amino-4-hydroxybenzoic acid methyl ester, 3

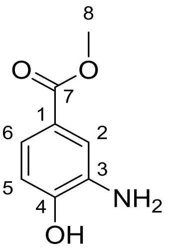

*$C_8H_9NO_3$, 167.16 g/mol*

A literature preparation was used.[92]
3-Amino-4-hydroxybenzoic acid (500 mg, 3.3 mmol) was dissolved in dry MeOH (20 ml) and sulfuric acid (0.4 mL, 6.61 mmol) added whilst stirring. The mixture was heated to reflux for 22 h. After cooling to room temperature, the solvent was removed under reduced pressure and the remaining oil was dissolved in ethyl acetate (20 mL) and saturated $NaHCO_3$ solution (20 mL). The phases were separated and the aqueous phase extracted with ethyl acetate two more times (10 mL each). The combined organic phases were washed with water (10 mL), dried over $MgSO_4$ and the solvent removed under reduced pressure. The product was obtained as a light brown solid. 425 mg, 2.54 mmol, 78 %.

**$^1$H NMR** (600 MHz, $CDCl_3$, 25 °C) δ = 7.46 (d, *J* = 1.5 Hz, 1H, H2), 7.42 (dd, *J* = 8.0 Hz, 1.5 Hz, 1H, H6), 6.75 (d, *J* = 8.0 Hz, 1H, H5), 3.86 (s, 3H, H8) ppm.

**$^{13}$C NMR** (151 MHz, $CDCl_3$, 25 °C) δ = 167.3, 148.5, 131.5, 123.4, 122.2, 118.4, 114.6, 52.1 ppm.

**ESI-MS**: positive ion, calculated for $[C_8H_{10}NO_3]^+$ : 168.0661, found 168.0655, error 0.3 ppm.

**Mp.:** 111-113 °C

### 6.3.4 4-Amino-3-hydroxybenzoic acid methyl ester, 4

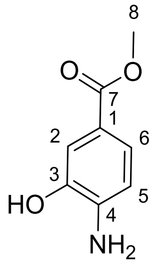

*$C_8H_9NO_3$, 167.16 g/mol*

The product was obtained from 4-amino-3-hydroxybenzoic acid (200 mg, 1.31 mmol) following the method from **3** as a brown solid. 111 mg, 0.66 mmol, 51%.

**$^1$H NMR** (600 MHz, $CDCl_3$, 25 °C) δ = 7.59 (d, *J* = 1.5 Hz, 1H, H2), 7.49 (dd, *J* = 8.0 Hz, 1.5 Hz, 1H, H6), 6.67 (d, *J* = 8.0 Hz, 1H, H5), 3.86 (s, 3H, H8) ppm.

**$^{13}$C NMR** (151 MHz, $CDCl_3$, 25 °C) δ = 167.9, 142.7, 140.5, 124.2, 119.6, 116.4, 114.4, 52.0 ppm.

**ESI-MS**: positive ion, calculated for $[C_8H_{10}NO_3]^+$ : 168.0661, found 168.0656, error 0.3 ppm.

**Mp.:** 118-119 °C

Characterisation data consistent with literature.[92]

### 6.3.5 [Bis(acetylacetonato)dioxomolybdenum(VI)], 5

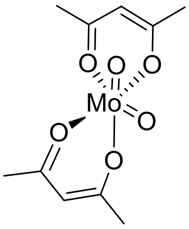

*$C_{10}H_{14}MoO_6$, 326.18 g/mol*

An adaptation of the method by H. Brunning was used.[97]
Sodium molybdate dihydrate (370 mg, 1.5 mmol) was dissolved in water (5.5 ml) and the solution acidified to pH 1 with 6M HCl. While stirring, acetylacetone (0.47 ml, 4.5 mmol) was added and the mixture kept in the dark. After 50 min the yellow solid that had formed was isolated by filtration and washed with ice cold water. The crude yellow product (680 mg) was dried *in vacuo*.
397 mg, 1.22 mmol, 81%
Analytical data consistent with literature.[198–200]

**IR** (ATR), $\nu$ (cm$^{-1}$): 2921 (m, $\nu_{C\text{-}H}$), 1582 (s, $\nu_{C=O}$), 932 (s, $\nu_{Mo=O/sym}$), 901 (s, $\nu_{Mo=O/asym}$).

**$^1$H NMR** (400 MHz, $CDCl_3$, 25°C) δ= 5.7 (1H, HC=C, enol form), 3.7 (2H, $CH_2$, keto form), 2.2 (6H, $CH_3$, keto form), 2.1(6H, $CH_3$, enol form) ppm.

**$^{13}$C NMR** (101 MHz, DMSO, 25°C) δ = 196.5, 184.2, 104.7, 27.6, 25.0 ppm.

**Mp.:** 179-181 °C

**General method for synthesis of L-1 to L-16, adapted from the literature.**[93]

In a typical reaction, around 150 mg of appropriate aldehyde and an equimolar amount of the appropriate amine were suspended in MeOH or EtOH (3 mL, dried over 3 Å molecular sieves) and heated to reflux whilst stirring for 5 h. After cooling to room temperature, the product was isolated by filtration, washed with MeOH and $Et_2O$ and dried *in vacuo.*

### 6.3.6 2-[(E)-(2-Hydroxybenzylidene)amino]phenol, L-1

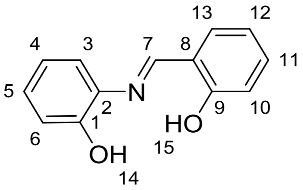

*$C_{13}H_{11}NO_2$, 213.24 g/mol.*

Using 2-amino phenol (270 mg, 2.45 mmol) and salicylic aldehyde (300 mg, 2.45 mmol) in ethanol (10 ml) the product was obtained as an orange-red crystalline solid. 399 mg, 1.87 mmol, 76 %

**$^1$H NMR** (600 MHz, DMSO-*d*$_6$, 25 °C) δ = 13.79 (s, 1H, H15), 9.74 (s, 1H, H14), 8.96 (s, 1H, H7), 7.61 (dd, *J* = 7.5 Hz, 1.0 Hz, 1H, H13), 7.38 (td, *J* = 8.0 Hz, 1.5 Hz, 1H, H11), 7.36 (dd, *J* = 8.0 Hz, 1.0 Hz, 1H, H3), 7.13 (td, *J* = 7.5 Hz, 1.0 Hz, 1H, H5), 6.97 (dd, *J* = 8.0 Hz, 1.0 Hz, 1H, H6), 6.94 (t, *J* = 8.0 Hz, 2H, H10/12), 6.88 (td, *J* = 7.5, 1.0 Hz, 1H, H4) ppm.

**$^{13}$C NMR** (151 MHz, DMSO-d$_6$, 25 °C) δ = 161.7 C7, 160.7 C9, 151.1 C1, 135.0 C2, 132.8 C11, 132.3 C13, 128.1 C5, 119.6 C3+4, 119.5 C8, 118.7 C10/12, 116.7 C10/12, 116.5 C6 ppm.

**IR** (ATR), $\nu$ (cm$^{-1}$): 2557-3048 (m, $\nu_{C\text{-}H}$), 1627 (s, $\nu_{C=N}$).

**ESI-MS**: positive ion, calculated for $[C_{13}H_{12}NO_2]^+$: 214.0863, measured: 214.0861, error 0.8 ppm.

**Mp.:** 185-187 °C

**Elemental analysis:** found: 73.13 % C, 4.77 % H, 5.60 % N, calculated for $C_{13}H_{10}NO_2$: 73.23 % C, 5.20 % H, 6.57 % N.

Analytical data consistent with literature.[95,96]

### 6.3.7 4-Hydroxy-3-[(E)-(4-methyl-oxycarbonyl-2-hydroxybenzylidene)amino]benzoic acid methyl ester, L-2

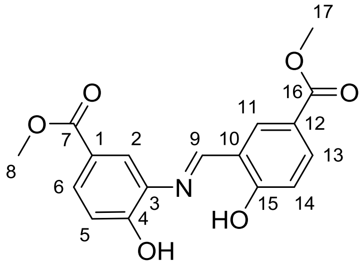

*$C_{17}H_{15}NO_6$, 329.09 g/mol*

Using **3** (139 mg, 0.83 mmol) and **2** (150 mg, 0.83 mmol) in MeOH (1 mL), the product was obtained as a yellow solid. 190 mg, 0.58 mmol, 70 %

**$^1$H NMR** (400 MHz, DMSO-d$_6$, 25 °C) δ = 14.53 (s, 1 H, OH), 10.90 (s, 1 H, OH), 9.23 (s, 1H, H9) 8.38 (d, *J* = 2.0 Hz, 1H, H11), 8.02 (d, *J* = 2.0 Hz, 1H, H2), 7.95 (dd, *J* = 8.5 Hz, 1.5 Hz, 1H, H13), 7.79 (dd, *J* = 8.5 Hz, 2.0 Hz, 1H, H6), 7.07 (d, *J* = 8.5 Hz, 1H, H5), 7.01 (d, *J* = 8.5 Hz, 1H, H14), 3.84 (s, 3H, H8/17), 3.83 (s, 3H, H8/17) ppm.

**$^{13}$C NMR (151 MHz, DMSO-d$_6$, 25 °C)** δ = 165.8 C7, 165.7 C15, 165.6 C16, 162.1 C9, 155.6 C4, 134.7 C11, 133.9 C10/13, 133.9 C10/13, 129.8 C6, 120.9 C1, 120.6 C2, 119.9 C12, 118.8 C10, 117.6 C14, 116.4 C5, 51.9 C8+C17 ppm.

**IR** (ATR), ν (cm$^{-1}$): 2789-3068 (m, $\nu_{C-H}$), 1716(s, $\nu_{C=O}$), 1677 (s, $\nu_{C=O}$), 1618 (s, $\nu_{C=N}$).

**ESI-MS**: positive ion, calculated for $[C_{17}H_{15}NO_6]^+$: 330.0972, found 330.0970, error 0.6 ppm.

**Mp.:** 201-204 °C

**Elemental analysis:** found: 61.23 % C, 4.53 % H, 4.32 % N, calculated for $C_{17}H_{15}NO_6$: 62.00 % C, 4.59 % H, 4.25 % N.

### 6.3.8 4-Hydroxy-3-[(E)-(5-carboxy-2-hydroxybenzylidene)amino]benzoic acid, L-3

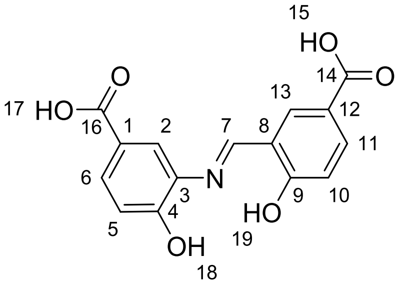

*$C_{15}H_{11}NO_6$, 301.25 g/mol*

Using **1** (1087 mg, 6.54 mmol) and 3-Amino-4-hydroxy benzoic acid (1 mg, 6.53 mmol) in ethanol (30 mL), the product was obtained as an orange solid. 1375 mg, 4.56 mmol, 70%

**$^1$H NMR** (400 MHz, DMSO, 25 °C): δ = 14.52 (br s, 1H, H19), 12.58 (br s, 2H, H15/17), 10.74 (br s, 1H, H18), 9.20 (s, 1H, H7), 8.34 (d, *J* = 2.0 Hz, 1H), 8.01 (d, *J* = 2.0 Hz, 1H), 7.94 (dd, *J* = 8.5 Hz, 2.0 Hz, 1H), 7.77 (dd, *J* = 8.5 Hz, 2.0 Hz, 1H), 7.05 (d, *J* = 8.5 Hz, 1H), 7.00 (d, *J* = 8.5 Hz, 1H) 8.35 (d, *J* = 2.0 Hz, 1H, H13), 8.02 (d, *J* = 2.0 Hz, 1H, H2), 7.94 (dd, *J* = 8.7 Hz, 2.1 Hz, 1H, H11), 7.77 (dd, *J* = 8.5 Hz, 2.0 Hz, 1H, H6), 7.05 (d, *J* = 8.5 Hz, 1H, H5), 7.00 (d, *J* = 8.7 Hz, 1H, H10) ppm.

**$^{13}$C NMR** (101 MHz, DMSO, 25 °C): δ = 167.0, 166.8, 165.5, 162.1, 155.4, 134.9, 134.2, 133.9, 130.0, 122.2, 121.1, 120.8, 118.9, 117.5, 116.3 ppm.

**IR** (ATR), $\nu$ (cm$^{-1}$):2789-3068 (m, $\nu_{C-H}$), 1725(s, $\nu_{C=O}$), 1657 (s, $\nu_{C=O}$), 1630 (s, $\nu_{C=N}$).

**ESI-MS:** negative ion, calculated for $(C_{15}H_{10}NO_6)^-$: 300.0514, found: 300.0512, error 0.5 ppm.

**Mp.:** decomposition > 300 °C

**Elemental analysis:** found: 53.33 % C, 4.20 % H, 4.01 % N, calculated for $C_{15}H_{11}NO_6$ *1.95 $H_2O$: 53.56 % C, 4.46 % H, 4.16 % N.

### 6.3.9 3-[(E)-[[4-(diethylamio)-2-hydroxyphenyl]methylidene]amino]-4-hdroxy benzoic acid methyl ester, L-4

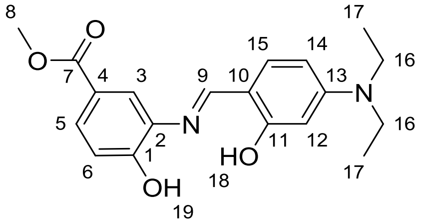

*$C_{19}H_{22}N_2O_4$, 342.40 g/mol*

Using **3** (100 mg, 0.6 mmol) and 4-formyl-3-hydroxyphenyl diethyl amine (116 mg, 0.6 mmol) in MeOH (2 mL), the product was obtained as an orange solid. 170 mg, 0.50 mmol, 83 %

**$^1$H NMR** (600 MHz, DMSO-*d*$_6$, 25 °C) δ = 13.92 (s br, 1H, H19), 10.56 (s br, 1H, H18), 8.72 (s, 1H, H9), 7.81 (d, *J* = 2.0 Hz, 1H, H3), 7.66 (dd, *J* = 8.5 Hz, 2.0 Hz, 1H, H5), 7.35 (d, *J* = 9.0 Hz, 1H, H14), 7.00 (d, *J* = 8.5 Hz, 1H, H6), 6.29 (dd, *J* = 9.0 Hz, 2.5 Hz, 1H, H15), 6.01 (d, *J* = 2.4 Hz, 1H, H12), 3.82 (s, 3H, H8), 3.39 (d, *J* = 7.0 Hz, 4H, H16), 1.12 (t, *J* = 7.0 Hz, 6H, H17) ppm.

**$^{13}$C NMR** (151 MHz, DMSO-*d*$_6$, 25 °C) δ = 166.0 C7, 164.7 C11, 160.3 C9, 155.0 C1, 151.7 C13, 135.4 C2, 134.2 C15, 127.8 C5, 120.8 C4, 119.7 C3, 116.0 C6, 109.0 C10, 103.8 C14, 97.0 C12, 51.8 C8, 43.9 C16, 12.6 C17 ppm.

**IR** (ATR), $\nu$ (cm$^{-1}$):2784-3023 (m, $\nu_{C-H}$), 1713(s, $\nu_{C=O}$), 1592 (s, $\nu_{C=N}$).

**ESI-MS**: positive ion, calculated for $[C_{19}H_{23}N_2O_4]^+$: 343.1652, found 343.1655, error 0.7 ppm.

**Mp.:** 221-223 °C

**Elemental analysis:** found: 65.61 % C, 6.16 % H, 7.62 % N, calculated for $C_{19}H_{22}N_2O_4$ : 66.65 % C, 6.48 % H, 8.18 % N.

## 6.3.10 4-Hydroxy-3-[(Z)-[2-hydroxy-5-(methoxycarbonyl)phenyl]imino]methyl]benzoic acid, L-5

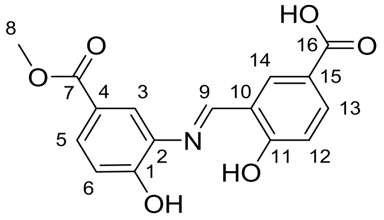

*$C_{16}H_{13}NO_6$, 315.28 g/mol*

Using **3** (106 mg, 0.63 mmol) and **1** (106 mg, 0.63 mmol) in MeOH (1 mL), the product was obtained as a yellow solid. 156 mg, 0.49 mmol, 79 %

**$^1$H NMR** (600 MHz, DMSO-*d*$_6$, 25 °C) δ = 14.42 (s, 1H), 12.61 (s br, 1H), 10.84 (s br, 1H), 9.20 (s, 1H, H9), 8.35 (s, 1H), 8.01 (s, 1H), 7.95 (d, *J* = 8.5 Hz, 1H), 7.78 (d, *J* = 8.5 Hz, 1H), 7.07 (d, *J* = 8.5 Hz, 1H), 7.00 (d, *J* = 8.5 Hz, 1H), 3.83 (s, 3H, H8) ppm.

**$^{13}$C NMR:** (151 MHz, DMSO-d$_6$, 25 °C) δ = 166.7, 165.8, 165.2, 162.3, 155.6, 134.7, 134.2, 134.2, 129.7, 121.2, 121.0, 120.7, 118.8, 117.3, 116.4, 51.9.

**IR** (ATR), ν (cm$^{-1}$):3228 (s, $\nu_{O-H}$), 2538-3076 (m, $\nu_{C-H}$), 1708(s, $\nu_{C=O}$), 1677(s, $\nu_{C=O}$), 1628 (s, $\nu_{C=N}$).

**ESI-MS**: positive ion, calculated for $[C_{16}H_{13}NO_6]^+$: 316.08016, found 316.0809, error 2.2 ppm.

**Mp.:** decomposition > 310 °C

**Elemental analysis:** found: 59.63 % C, 4.47 % H, 4.23 % N, calculated for $C_{19}H_{22}N_2O_4$ : 60.95 % C, 4.16 % H, 4.44 % N.

## 6.3.11 4-Hydroxy-3-[(E)-(4-methyl-oxycarbonyl-2-hydroxybenzylidene)amino]benzoic acid, L-6

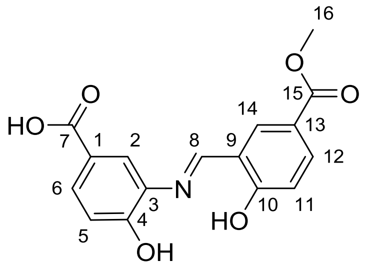

$C_{16}H_{13}NO_6$, *315.28 g/mol*

Using 3-amino-4-hydroxybenzoic acid (128 mg, 0.83 mmol) and **2** (150 mg, 0.83 mmol) in MeOH (2 mL), the product was obtained as a yellow solid. 260 mg, 0.76 mmol, 84 %

**$^1$H NMR** (600 MHz, DMSO-$d_6$, 25 °C) δ = 14.63 (s, 1H), 12.70 (s, 1H), 10.77 (s, 1H), 9.24 (s, 1H, H8), 8.38 (d, *J* = 2.5 Hz, 1H), 8.02 (d, *J* = 2.0 Hz, 1H), 7.95 (dd, *J* = 8.5 Hz, 2.5 Hz, 1H), 7.77 (dd, *J* = 8.5 Hz, 2.0 Hz, 1H), 7.05 (d, *J* = 8.5 Hz, 1H), 7.01 (d, *J* = 8.5 Hz, 1H), 3.84 (s, 3H) ppm.

**$^{13}$C NMR (**151 MHz, DMSO-d$_6$, 25 °C) δ = 166.9, 165.9, 165.6, 161.8, 155.2, 134.7, 133.9, 133.6, 123.0, 122.2, 120.7, 119.8, 118.8, 117.7, 116.2, 51.9 ppm.

**IR** (ATR), ν (cm$^{-1}$): 2538 - 3095 (m, $\nu_{C-H}$), 1723 (s, $\nu_{C=O}$), 1691 (s, $\nu C_{=O}$), 1615 (br, $\nu_{C=N}$).

**ESI-MS**: positive ion, calculated for $[C_{16}H_{13}NO_6]^+$: 316.0816, found 316.0816, error -0.1 ppm.

**Mp.:** 268-270 °C

**Elemental analysis:** found: 58.13 % C, 4.52 % H, 3.71 % N, calculated for $C_{16}H_{13}NO_6$: 60.95 % C, 4.16 % H, 4.44 % N.

### 6.3.12 4-Hydroxy-3-[(E)-(2-hydroxybenzylidene)amino]benzoic acid, L-7

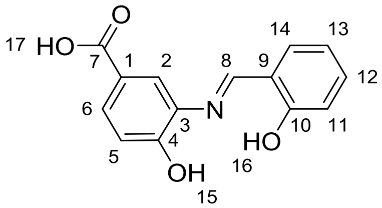

$C_{14}H_{11}NO_4$, *257.25 g/mol*

Using salicylic aldehyde (1.22 g, 10 mmol) and 3-amino-4-hydroxy benzoic acid (1.53 g, 10 mmol) in ethanol (30 ml), the product was obtained as an orange solid. 2.200 g, 8.55 mmol, 79 %

**$^1$H NMR** (400 MHz, DMSO, 25 °C) δ = 13.57 (s, 1H, H17), 12.64 (br s, 1H, H16), 10.65 (br s, 1H, H15), 9.05 (s, 1H, H8), 7.92 (d, *J* = 2.0 Hz, 1H, H7), 7.75 (dd, *J* = 8.5 Hz, 2.0 Hz, 1H, H3), 7.69 (dd, *J* = 8.0 Hz, 1.5 Hz, 1H, H14), 7.40 (td, J = 7.5 Hz, 1.5 Hz, 1H, H12), 7.04 (d, *J* = 8.5 Hz, 1H, H4), 6.99 – 6.92 (m, 2H, H11/13) ppm.

**$^{13}$C NMR** (101 MHz, DMSO, 25 °C): δ = 167.1 C1, 162.8 C8, 160.7 C10, 155.4 C5, 135.0 C6, 133.2 C12, 132.6 C14, 129.6 C3, 122.1 C2, 120.8 C7, 119.5 C9, 118.9 C11/13, 116.7 C11/13, 116.2 C4 ppm.

**IR** (ATR), ν (cm$^{-1}$): 2572 - 3075 (m, $\nu_{C-H}$),1608 (s, $\nu_{C=N}$), 1692 (s, $\nu_{C=O}$).

**ESI-MS**: positive ion, calculated for $C_{14}H_{12}NO_4$ [sap-acid +H]$^+$: 258.0761, measured: 258.0756, error 1.9 ppm.

**Mp.:** 272-277 °C

**Elemental analysis:** found: 65.15 % C, 4,47 % H, 5.32 % N, calculated for $C_{19}H_{22}N_2O_4$ : 65.37 % C, 4.31 % H, 5.45 % N.

## 6.3.13 4-Hydroxy-3-[(E)-[(2-hydroxyphenyl)imino]methyl]benzoic acid, L-8

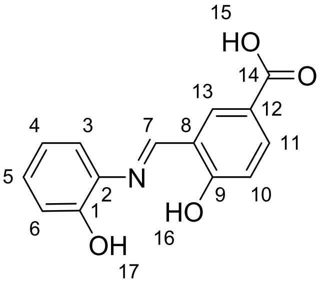

*$C_{14}H_{11}NO_4$, 257.25 g/mol*

Using 2-aminophenol (131 mg, 1.2 mmol) and **1** (200 mg, 1.2 mmol) in MeOH (3 mL), the product was obtained as a brown-yellow solid. 238 mg, 0.93 mmol, 77 %

**$^1$H NMR** (600 MHz, DMSO-$d_6$, 25 °C) δ = 14.86 (s, 1H), 12.16 (s br,1H, H15), 9.95 (s, 1H), 9.11 (s, 1H, H7), 8.26 (d, *J* = 2.0 Hz, 1H), 7.92 (dd, *J* = 8.5 Hz, 1.5 Hz, 1H), 7.45 (d, *J* = 8.0 Hz, 1H), 7.15 (t, *J* = 7.5 Hz, 1H), 6.98 (t, *J* = 9.0 Hz, 2H), 6.90 (t, *J* = 7.5 Hz, 1H) ppm.

**$^{13}$C NMR** (151 MHz, DMSO-d$_6$, 25 °C) δ = 166.7, 166.1, 160.8, 151.1, 134.7, 134.0, 133.4, 128.5, 120.7, 119.7, 119.3, 118.5, 117.7, 116.5.

**IR** (ATR), ν (cm$^{-1}$):2542-3057 (m, $\nu_{C-H}$), 1668 (s, $\nu_{C=O}$), 1612 (s, $\nu_{C=N}$).

**ESI-MS**: positive ion, calculated for $[C_{13}H_{12}NO_4]^+$: 258.0760 found 258.0761, error 0.3 ppm.

**Mp.:** 253-255 °C

**Elemental analysis:** found: 60.37 % C, 4.49 % H, 4.83 % N, calculated for $C_{14}H_{11}NO_4$ * 1.1 $H_2O$: 60.69 % C, 4.8 % H, 5.06 % N.

### 6.3.14 4-Hydroxy-3-[(E)-(2-hydroxybenzylidene)amino]benzoic acid methyl ester, L-9

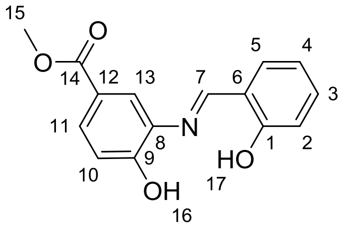

*$C_{15}H_{13}NO_4$, 271.27 g/mol*

Using 3-amino-4-hydroxybenzoic acid methyl ester (150 mg, 0.9 mmol) and salicylaldehyde (100 µL, 0.93 mmol) in MeOH (1 mL), the product was obtained as red crystallin solid. 181 mg, 0.67 mmol, 74 %

**$^1$H NMR** (400 MHz, DMSO-d$_6$, 25 °C) δ = 13.51 (0.75 H, Ar-OH), 10.77 (0.5 H, Ar-OH), 9.03 (1 H, H7), 7.76 (d, *J* = 8.3 Hz, 1H), 7.5 (d, *J* = 7.5 Hz, 1H), 7.5 (t, *J* = 7.5 Hz, 1H), 7.05 (d, *J* = 8.5 Hz, 1H), 6.96 (t, *J* = 8.5 Hz, 2H), 3.82 (3 H, H15) ppm.

**$^{13}$C NMR** (151 MHz, DMSO, 25 °C): δ = 165.8, 163.0, 160.5, 155.5, 135.3, 133.1, 132.5, 129.3, 120.9, 120.7, 119.4, 118.8, 116.6, 116.3, 51.7 ppm.

**IR** (ATR), $\nu$ (cm$^{-1}$): 2718 - 3095 (m, $\nu_{C-H}$), 1704 (s, $\nu_{C=O}$), 1618 (s, $\nu_{C=N}$).

**ESI-MS**: positive ion, calculated for $[C_{15}H_{13}NO_4]^+$: 279.0917 found 272.0919, error -0.5 ppm.

**Mp.:** 169-170 °C

**Elemental analysis:** found: 65.79 % C, 5.09 % H, 5.00 % N, calculated for $C_{15}H_{13}NO_4$: 66.41 % C, 4.83 % H, 5.16 % N.

### 6.3.15 4-Hydroxy-3-[(E)-[(2-hydroxyphenyl)imino]methyl]benzoic acid methyl ester, L-10

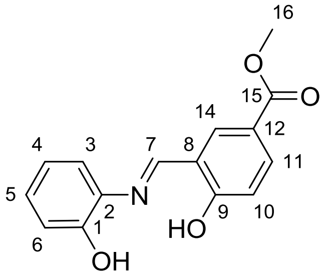

*$C_{15}H_{13}NO_4$, 271.27 g/mol*

Using 2-aminophenol (48 mg, 0.44 mmol) and **2** (79 mg, 0.44 mmol) in MeOH (1 mL), the product was obtained as a yellow solid. 105 mg, 0.39 mmol, 88%

**$^1$H NMR** (600 MHz, DMSO-d$_6$, 25 °C) δ = 15.00 (s, 1H), 9.95 (s, 1H), 9.15 (s, 1H, H7), 8.29 (d, *J* = 1.5 Hz, 1H), 7.93 (dd, *J* = 8.5 Hz, 2.0 Hz, 1H), 7.46 (d, *J* = 8.0 Hz, 1H), 7.16 (t, *J* = 7.5 Hz, 1H), 6.98 (d, *J* = 7.5 Hz, 1H), 6.98 (d, *J* = 9.0 Hz, 1H), 6.91 (t, *J* = 7.5 Hz, 1H), 3.84 (s, 3H).ppm.

**$^{13}$C NMR** (151 MHz, DMSO-d$_6$, 25 °C) δ = 166.8, 165.6, 160.5, 151.0, 134.6, 133.7, 133.0, 128.6, 119.7, 119.3, 119.2, 118.5, 118.1, 116.6, 51.8 ppm.

**IR** (ATR), ν (cm$^{-1}$): 2541-3060 (m, $\nu_{C-H}$), 1694 (s, $\nu_{C=O}$), 1613 (s, $\nu_{C=N}$).

**ESI-MS**: positive ion, calculated for $[C_{15}H_{13}NO_4]^+$: 272.0917 found 272.0909, error 2.9 ppm.

**Mp.:** 232-234 °C

**Elemental analysis:** found: 65.06 % C, 5.02% H, 5.12 % N, calculated for $C_{15}H_{13}NO_4$: 66.41 % C, 4.83 % H, 5.16 % N.

### 6.3.16 3-Hydroxy-4-[(E)-[2-hydroxyphenyl)methylidene]amino benzoic acid methyl ester, L-11

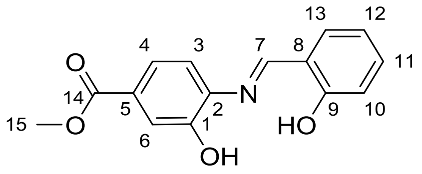

*$C_{15}H_{13}NO_4$, 271.272 g/mol*

Using salicylic aldehyde (59.07 mg, 0.59 mmol) and 4-amino-3-hydroxybenzoic acid (100 mg, 0.59 mmol) in MeOH (5 ml) the product was obtained as a red solid. 99 mg, 0.36 mmol, 68 %.

**$^1$H NMR** (600 MHz, DMSO-$d_6$, 25 °C) δ = 13.39 (s, 1H), 10.16 (s, 1H), 9.01 (s, 1H, H7), 7.65 (dd, *J* = 6.5 Hz, 1.0 Hz, 1H), 7.56 (d, *J* = 1.5 Hz, 1H), 7.49 (dd, *J* = 8.0 Hz, 1.5 Hz, 1H), 7.45-7.41 (m, 2H), 7.05 – 6.91 (m, 2H), 3.84 (s, 2H) ppm.

**$^{13}$C NMR** (151 MHz, DMSO-$d_6$ , 25 °C): δ = 165.8, 163.8, 160.7, 150.8, 139.6, 133.5, 132.6, 128.5, 120.8, 120.0, 119.4, 119.0, 116.9, 116.8, 52.1 ppm.

**IR** (ATR), ν (cm$^{-1}$): 2537 (s, $\nu_{O\text{-}H}$), 1717 (s, $\nu_{C=O}$), 1624 (s, $\nu_{C=N}$), 1218 (s, $\nu_{C\text{-}O}$ ester).

**ESI-MS**: positive ion, calculated for $[C_{15}H_{14}NO_4]^+$: 272.0917, found 272.0930, error -4.6 ppm.

**Mp.:** 168-171 °C

**Elemental analysis:** found: 62.77 % C, 4.54 % H, 4.86 % N, calculated for $C_{15}H_{13}NO_4$: 66.41 % C, 4.83 % H, 5.16 % N.

### 6.3.17 2-[(E)-[(2-hydroxyphenyl)methylidene]amino]-4-nitrophenol, L-12

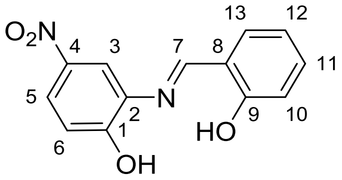

*$C_{13}H_{10}N_2O_4$, 258.23 g/mol*

Using 2-amino-4-nitrophenol (150 mg, 0.97 mmol) and 2-hydroxybenzaldehyde (118 mg, 0.97 mmol) in MeOH(5 ml) the product was obtained as a dark orange solid. 149 mg, 0.58 mmol, 60%

**$^1$H NMR** (400 MHz, DMSO-$d_6$, 25 °C): δ = 10.73 (br s, 1H), 9.10 (s, 1H, H7), 8.28 (d, 1H, *J* = 3.0 Hz), 8.08 (dd, 1H, *J* = 9.0 Hz, 3.0 Hz), 7.70 (dd, 1H, *J* = 8.0 Hz, 2.0 Hz), 7.45-7.14 (m, 1H), 7.13 (d, 1H, *J* = 9.0 Hz), 7.00-6.95 (m, 2H) ppm.

**$^{13}$C NMR** (101 MHz, DMSO-$d_6$ , 25 °C): δ = 164.5, 160.6, 157.8, 139.9, 135.7, 133.7, 132.8, 123.9, 119.4, 119.1, 116.8, 116.4, 115.4 ppm

**IR** (ATR), ν (cm$^{-1}$): 2362 (s, $\nu_{O-H}$), 1621 (s, $\nu_{C=N}$), 1525 ($\nu_{N-O}$).

**ESI-MS**: negative ion, calculated for $(C_{13}H_9N_2O_4)^-$: 257.0569 found: 257.0569, error -0.5 ppm.

**Mp.:** 238-239 °C

**Elemental analysis:** found: 59.06 % C, 4.27 % H, 10.37 % N, calculated for $C_{13}H_{10}N_2O_4$: 60.47 % C, 3.90 % H, 10.85 % N.

### 6.3.18 2-[(E)-[2-hydroxyphenyl)methylidene]amino-4-trifluoromethyl phenol, L-13

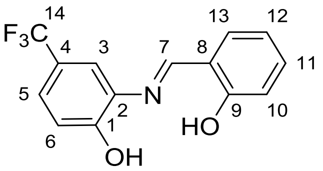

*$C_{14}H_{10}F_3NO_2$, 281.23 g/mol*

Using 2-amino-3-trifluoromethyl-phenol (150 mg, 0.85 mmol) and 2-hydroxybenzaldehyde (104 mg, 0.85 mmol) in MeOH (5 ml) the product was obtained as a bright orange solid. 122 mg, 0.43 mmol, 52 %

**$^1$H NMR** (400 MHz, DMSO-d$_6$, 25 °C): δ = 9.05 (s, 1H), 7.73 (d, *J* = 2.5 Hz, 1H), 7.66 (dd, *J* = 7.5 Hz, 1.5 Hz, 1H), 7.48 (dd, *J* = 8.5 Hz, 2.0 Hz, 1H), 7.41 (td, *J* = 7.5 Hz, 1.5 Hz, 1H), 7.12 (d, *J* = 8.0 Hz, 1H) ppm.

**$^{13}$C NMR** (101 MHz, DMSO-d$_6$ , 25 °C): δ = 163.8, 160.6, 154.4, 135.7, 133.4, 132.7, 124.82 (q, *J* = 4 Hz) C3/C5, 124.59 (q, *J* = 271 Hz) C14, 120.18 (q, *J* = 32.5 Hz) C4, 119.4, 119.0, 116.97 (q, *J* = 4 Hz) C3/C5, 116.78, 116.7 ppm. Note: due to low resolution all quartets appear as doublets.

**$^{19}$F NMR** (565 MHz, DMSO-*d*$_6$, 25 °C) δ = -59.5 (s, 3F) ppm.

**IR** (ATR), ν (cm$^{-1}$): 2494 (s, $\nu_{O-H}$), 1612 (s, $\nu_{C=N}$), 1106 (s, $\nu_{C-F}$).

**ESI-MS**: positive ion, calculated for $[C_{14}H_{11}F_3NO_2]^+$: 282.0736, found 282.0738, error -0.7 ppm.

**Mp.:** 186-188 °C

**Elemental analysis:** found: 59.43 % C, 3.5 % H, 4.51 % N, calculated for $C_{14}H_{10}F_3NO_2$: 59.79 % C, 3.58 % H, 4.98 % N.

## 6.3.19 Sulphonamide 4-hydroxy-3-[(E)-[(2-hydroxyphenyl)methylidene]amino]benzene-1-sulfonamide, L-14

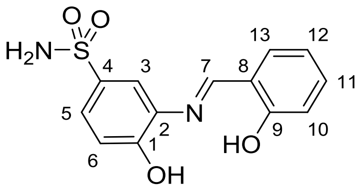

*$C_{13}H_{12}N_2O_4S$, 292.31 g/mol*

Using 3-amino-4-hydroxybenzenesulfonamide (150 mg, 0.8 mmol) and 2-hydroxybenzaldehyde (98 mg, 0.8 mmol) in MeOH (8.5ml) the product was obtained as an orange solid. 205 mg, 0.70 mmol, 88 %.

**$^1$H NMR** (400 MHz, DMSO-d$_6$, 25 °C): δ = 10.60 (br s, 1H), 9.01 (s, 1H), 7.77 (d, 1H, $J$ = 2.0 Hz), 7.71 (dd, 1H, $J$ = 8.0 Hz, 1.5 Hz), 7.60 (dd, 1H, $J$ = 8.0 Hz, 2.0 Hz), 7.44 (td, 1H, $J$ = 7.5 Hz, 1.5 Hz), 7.20 (s, 2H), 7.09 (d, 1H, $J$ = 8.5 Hz), 6.99 (t, 2H, $J$ = 8.5 Hz) ppm.

**$^{13}$C NMR** (101 MHz, DMSO-d$_6$ , 25 °C): δ = 163.0, 160.5, 154.1, 135.2, 135.1, 133.4, 132.5, 125.6, 119.5, 119.1, 117.7, 116.8, 116.3 ppm.

**IR** (ATR), $\nu$ (cm$^{-1}$): 3365 (s, $\nu_{N-H}$), 3265 (s, $\nu_{N-H}$),1615 (s, $\nu_{C=N}$).

**ESI-MS**: positive ion, calculated for $[C_{13}H_{13}N_2O_4S]^+$: 293.0591, found 293.0589, error 0.4 ppm.

**Mp.:** 268-274 °C

**Elemental analysis:** found: 53.01 % C, 3.56 % H, 9.38 % N, calculated for $C_{15}H_{13}NO_4$: 53.42 % C, 4.14 % H, 9.58 % N.

## 6.3.20 5-(Diethylamino)-2-[(E)-[2-hydroxyphenyl)imino]methyl]phenol, L-15

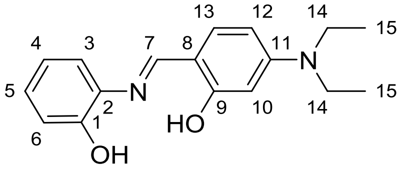

*$C_{17}H_{20}N_2O_2$, 284.36 g/mol*

Using 2-aminophenol (85 mg, 0.78 mmol) and 4-diethylamino salicylaldehyde (150 mg, 0.78 mmol) in MeOH (5 ml) the product was obtained as an orange solid. 112 mg, 0.39 mmol, 51 %

**$^1$H NMR** (400 MHz, DMSO-d$_6$, 25 °C): δ = 9.60 (s, 1H), 8.63 (s, 1H), 7.26 (dd, $J$ = 8.5 Hz, 7.0 Hz, 1H), 7.01 (td, $J$ = 7.5 Hz, 1.5 Hz, 1H), 6.90 (dd, $J$ = 8.0 Hz, 1.5 Hz, 1H), 6.83 (td, $J$ = 7.5 Hz, 1.5 Hz, 1H), 6.26 (dd, *J* = 9.0 Hz, 2.5 Hz, 1H), 5.97 (d, *J* = 2.5 Hz, 1H), 3.38 (p, *J* = 7.0 Hz, 2H), 1.11 (t, *J* = 7.0 Hz, 3H) ppm.

**$^{13}$C NMR** (101 MHz, DMSO-d$_6$ , 25 °C): δ = 165.8, 158.7, 151.6, 150.1, 134.6, 134.0, 126.2, 119.6, 118.5, 116.2, 109.0, 103.7, 97.2, 43.9 , 12.7 ppm.

**IR** (ATR), ν (cm$^{-1}$): 2974 (s, $\nu_{C-H}$), 1586 (s, $\nu_{C=N}$), 1366 (s, $\nu_{C-N}$).

**ESI-MS**: positive ion, calculated for $[C_{17}H_{20}N_2O_2]^+$: 258.1598, found 258.1598, error -0.3 ppm.

**Mp.:** 200-201 °C

**Elemental analysis:** found: 71.55 % C, 7.30 % H, 10.00 % N, calculated for $C_{17}H_{20}N_2O_2$: 71.81 % C, 7.09 % H, 9.85 % N.

## 6.3.21 3-[(E)-[(2-Hydroxyphenyl)methylidene]amino]naphthalen-2-ol, L-16

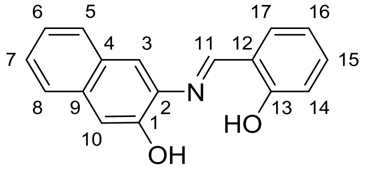

*$C_{17}H_{13}NO_2$, 263.30 g/mol*

Using 3-amino-2-naphtol (150 mg, 0.94 mol) and 2-hydroxybenzaldehyde (115 mg, 0.94 mmol) in MeOH (5 ml) the product was obtained as a red solid. 127 mg, 0.48 mmol, 51 %.

**$^1$H NMR** (400 MHz, DMSO-d$_6$, 25 °C): δ = 10.13 (br s, 1H), 9.08 (s, 1H), 7.82 (d, 2H, *J* = 8.0 Hz), 7.71 (t, 2H, *J* = 8.0 Hz), 7.45-7.36 (m, 2H), 7.31-7.28 (m, 2H), 7.00 (t, 2H, *J* = 8.0 Hz) ppm.

**$^{13}$C NMR** (101 MHz, DMSO-d$_6$ , 25 °C): δ = 163.3, 160.8, 150.1, 138.0, 133.3, 132.5, 128.0, 127.7, 126.0, 125.8, 123.4, 119.6, 119.0, 117.2, 116.8, 109.9 ppm.

**IR** (ATR), ν (cm$^{-1}$): 2511 (O-H), 1612 (C=N) cm$^{-1}$.

**ESI-MS**: positive ion, calculated for $[C_{17}H_{13}NO_2]^+$: 264.1019, found 264.1016, error 1.0 ppm.

**Mp.:** 253-256 °C

**Elemental analysis:** found: 76.95 % C, 4.61 % H, 5.11 % N, calculated for $C_{15}H_{13}NO_4$: 77.55 % C, 4.98 % H, 5.32 % N.

**General procedure for the synthesis of molybdenum dioxo complexes [MoO$_2$(L)(MeOH)] and [MoO$_2$(L)]**

In a typical reaction, 100 mg of the appropriate ligand and an equimolar amount of **5** were suspended in MeOH (2 mL, dried over 3 Å molecular sieves) and stirred for 4 h. The precipitate was isolated by filtration, washed with a small quantity MeOH and Et$_2$O (approximately 1 mL)and dried *in vacuo*.

## 6.3.22 MoO$_2$(2-[(E)-(2-Hydroxybenzylidene)amino]phenol)(MeOH), Mo-1

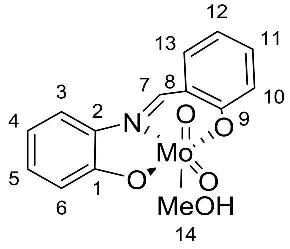

*C$_{14}$H$_{13}$MoNO$_5$, 371.22 g/mol*

Using **L-1** (69 mg, 0.32 mmol) and **5** (105 mg, 0.32 mmol) in methanol (8ml), the product was obtained as a yellow solid. 97 mg, 0.26 mmol, 81%

**$^1$H NMR** (400 MHz, ) δ = 9.28 (1H,H7), 7.82 (dd, *J* = 8.2 Hz, 1.0 Hz, 1H, H3), 7.77 (dd, *J* = 7.8 Hz, 1.5 Hz, 1H, H13), 7.54 (td, *J* = 7.5 Hz, 1.5 Hz, 1H, H11), 7.23 (td, *J* = 7.5 Hz, 1.0 Hz, 1H, H5), 7.06 (td, *J* = 7.5 Hz, 1.0 Hz, 1H, H12), 6.99 – 6.90 (m, 2H, H10+4), 6.85 (dd, *J* = 8.0 Hz, 1.0 Hz, 1H, H6), 4.12 (q, *J* = 5.5 Hz, 1H, MeO*H*), 3.17 (d, *J* = 5.5 Hz, 3H, H14).

**$^{13}$C NMR** (101 MHz, DMSO, 25 °C) δ = 161.2 C9, 160.1 C1, 156.7 C7, 135.6 C2+11, 135.2 C13, 130.1 C5, 122.0 C8, 120.9 C12, 120.4 C10, 118.9 C4/10, 117.4 C4/10, 116.5 C3, 48.7 C14 ppm.

**IR** (ATR), $\nu$ (cm$^{-1}$): 1611 (s, $\nu_{C=N}$), 908 (br, $\nu_{Mo=O/asym}$), 931 (s, $\nu_{Mo=O/sym}$).

**LIFDI-MS**: calculated for [C$_{13}$H$_9$MoNO$_4$]$^+$ : 340.9586, found: 340.9585, error: -0.3 ppm.

**UV-vis**, DMSO, λ / nm (ε / L * mol$^{-1}$ * cm$^{-1}$): 422 (4500), 352 (7800)

**Elemental analysis:** found: 45.05 % C, 3.34 % H, 3.63 % N, calculated: 45.30 % C, 3.53 % H, 3.77 % N.

**Mp.:** loss of MeOH > 120 °C, decomposition > 300 °C

### 6.3.23 [MoO$_2$(4-Hydroxy-3-[(E)-(4-methyl-oxycarbonyl-2-hydroxybenzylidene)amino]benzoic acid methyl ester)(MeOH)], Mo-2

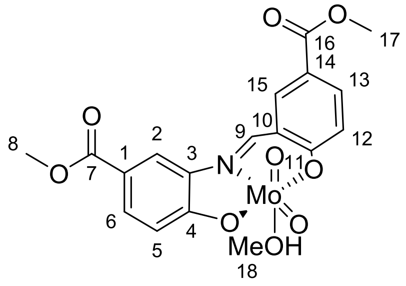

*$C_{18}H_{17}MoNO_9$, 487.29*

Using **L-2** (100 mg, 0.30 mmol) and **5** (100 mg, 0.30 mmol) in methanol (1.5 mL), the product was obtained as a yellow solid. 120 mg, 0.25 mmol, 82 %

**$^1$H NMR** (400 MHz, DMSO, 25 °C): δ = 9.66 (s, 1H, H9), 8.62 (s, 1H, H15), 8.51 (s, 1H, H2), 8.08 (dd, *J* = 9.0 Hz, 1.5 Hz, 1H, H13), 7.87 (d, *J* = 9.0 Hz, 1H, H6), 7.05 (d, *J* = 9.0 Hz, 1H, H12), 6.97 (d, *J* = 8.5 Hz, 1H, H5), 4.13 (q, *J* = 5.0 Hz, 1H, MeO*H*), 3.87 (s, 6H, H8+H17), 3.16 (d, *J* = 5.0 Hz, 3H, H18) ppm.

**$^{13}$C NMR** (101 MHz, DMSO, 25 °C) δ = 165.8 C7, 165.2 C16, 164.3 C11, 164.0 C4, 158.5 C9, 137.9 C15, 136.1 C13, 135.8 C3, 131.6 C6, 122.2 C10, 121.9 C1, 121.9 C14, 119.7 12, 118.5 C2, 117.6 C5, 52.3 C8/17, 52.2 C8/17, 48.7 C18 ppm.

**IR** (ATR), ν (cm$^{-1}$): 1689 (s br, $\nu_{C=O}$), 1608 (s, $\nu_{C=N}$), 936 (s, $\nu_{Mo=O/asym}$), 908 (s, $\nu_{Mo=O/sym}$).

**LIFDI-MS:** positive ion, calculated for $[C_{18}H_{17}MoNO_9]^+$: 456.96898, found: 456.97027, error: 2.84 ppm.

**UV-vis**, DMSO, λ / nm (ε / L * mol$^{-1}$ * cm$^{-1}$): 409 (4500), 347 (10000)

**Elemental analysis:** found: 43.50 % C, 3.19 % H, 2.52 % N, calculated for $C_{17}H_{15}MoNO_9$ *0.30 $H_2O$: 43.88 % C, 3.60 % H, 2.84 % N.

**Mp.:** loss of MeOH > 180 °C, decomposition > 300 °C

## 6.3.24 [MoO$_2$(4-Hydroxy-3-[(E)-(5-carboxy-2-hydroxybenzylidene)amino]benzoic acid)], Mo-3

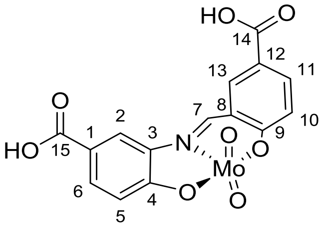

*$C_{15}H_9MoN_1O_8$, 427.20 g/mol*

Using **L-3** (196 mg, 0.65 mmol) and **5** (210 mg, 0.64 mmol) in methanol (6 mL), the product was obtained as a brown solid. 231 mg, 0.54 mmol, 78 %

**$^1$H NMR** (400 MHz, DMSO, 25 °C): δ = 13.00 (v br, 1.7H , COO*H*), 9.62 (1H, H7), 8.59 (d, *J* = 2.0 Hz, 1H, H13), 8.49 (d, *J* = 1.5 Hz, 1H, H2), 8.06 (dd, *J* = 8.5 Hz, 2.0 Hz, 1H, H11), 7.84 (dd, *J* = 8.5 Hz, 1.5 Hz, 1H, H6), 7.02 (d, *J* = 8.5 Hz, 1H, H10), 6.94 (d, *J* = 8.5 Hz, 1H, H5) ppm.

**$^{13}$C NMR** (101 MHz, DMSO, 25 °C) δ = 166.9 C15, 166.4 C14, 164.1 C9, 163.8 C4, 158.4 C7, 138.0 C13, 136.4 C11, 136.7 C3, 131.8 C6, 123.4 C12, 123.1 C1, 121.8 C8, 119.5 C10, 118.6 C2, 117.4 C5 ppm.

**IR** (ATR), ν (cm$^{-1}$): 1722 (s br, $\nu_{C=O}$), 1668 (s, $\nu_{C=O}$), 1607 (s, $\nu_{C=N}$), 946 (s, $\nu_{Mo=O}$), 808 (s, $\nu_{Mo\text{-}O\text{-}Mo}$).

**LIFDI-MS:** positive ion, calculated for [$C_{15}H_{19}MoNO_8$]$^+$: 428.9395, found: 428.9382, error: 3.0 ppm.

**UV-vis**, DMSO, λ / nm (ε / L * mol$^{-1}$ * cm$^{-1}$): 406 (4200), 3452 (2500)

**Elemental analysis:** found: 40.60 % C, 2.38 % H, 3.07 % N, calculated for $C_{30}H_{18}Mo_2N_2O_{16}$ *1.8 $H_2O$: 40.63 % C, 2.46 % H, 3.16 % N.

**Mp.:** decomposition > 300 °C

## 6.3.25 [MoO$_2$(3-[(E)-[[4-(diethylamio)-2-hydroxyphenyl]methylidene]amino]-4-hdroxy benzoic acid methyl ester)(MeOH)], Mo-4

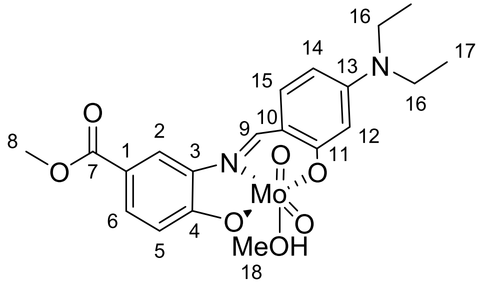

*$C_{20}H_{24}MoN_2O_7$, 500.38 g/mol*

Using **L-4** (100 mg, 0.29 mmol) and **5** (95 mg, 0.29 mmol) in MeOH (2.5 mL), the product was obtained as a dark red solid. 113 mg, 0.24 mmol, 82 %.

**$^1$H NMR** (400 MHz, DMSO, 25 °C): δ = 9.10 (s, 1H, H9), 8.22 (d, *J* = 2.0 Hz, 1H), 7.71 (dd, *J* = 8.5 Hz, 1.9 Hz, 1H), 7.61 (d, *J* = 9.1 Hz, 1H), 6.84 (d, *J* = 8.5 Hz, 1H), 6.47 (dd, *J* = 9.0 Hz, 2.5 Hz, 1H), 6.13 (d, *J* = 2.4 Hz, 1H), 4.12 (q, *J* = 5.2 Hz, 1H), 3.84 (s,3H, H8), 3.44 (q, *J* = 7.0 Hz, 4H, H16+18), 3.17 (d, *J* = 5.2 Hz, 3H,OH), 1.13 (t, *J* = 7.0 Hz, 6H, H17+19) ppm.

**$^{13}$C NMR** (101 MHz, DMSO, 25 °C) δ = 166.1 C7, 163.4 C4, 163.1 C11, 155.5 C9, 154.1 C13, 137.5 C3, 137.3 C15, 129.1 C6, 121.1 C1, 116.6 C5, 116.2 C2, 111.1 C10, 106.1 C14, 98.8 C12, 52.0 C18, 48.7 C16, 44.3 C8, 12.6 C17 ppm.

**IR** (ATR), $\nu$ (cm$^{-1}$): 1716 (s, $\nu_{C=O}$), 1613 (s, $\nu_{C=N}$), 929 (s, $\nu_{Mo=O/asym}$), 883(s, $\nu_{Mo=O/sym}$).

**LIFDI-MS:** positive ion, calculated for $[C_{19}H_{20}MoN_2O_6]^+$: 470.03700, found: 470.03744, error: 0.95 ppm.

**UV-vis**, DMSO, λ / nm (ε / L * mol$^{-1}$ * cm$^{-1}$): 466 (22000), 370 (19500)

**Elemental analysis:** found: 47.08 % C, 4.56 % H, 5.19 % N, calculated for $C_{20}H_{24}MoN_2O_9$ *0.35 $H_2O$: 47.41 % C, 4.91 % H, 5.53 % N.

**Mp.:** decomposition > 300 °C, solvent loss could not be determined

## 6.3.26 [$MoO_2$(4-Hydroxy-3-[(E)-[2-hydroxy-5-(methoxycarbonyl)phenyl]imino]methyl]benzoic acid)(MeOH)], Mo-5

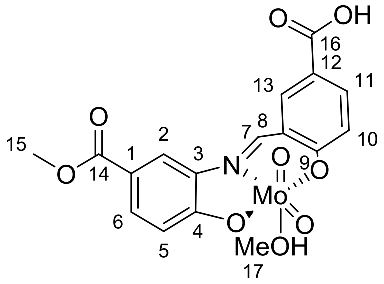

*$C_{17}H_{15}MoNO_9$, 473.27 g/mol*

Using **L-5** (100 mg, 0.32 mmol) and **5** (103.5 mg, 0.30 mmol) in methanol (1 mL), the product was obtained as a yellow-brown solid. 103 mg, 0.22 mmol, 68 %

**$^1$H NMR** (600 MHz, DMSO-*d*$_6$, 25 °C) δ = 12.87 (br s, 0.3H, COO*H*), 9.62 (s, 1H, H7), 8.59 (d, *J* = 2.0 Hz, 1H, H13), 8.50 (d, *J* = 2.0 Hz, 1H, H2), 8.06 (dd, *J* = 8.5 Hz, 2.0 Hz, 1H, H11), 7.86 (dd, *J* = 8.5 Hz, 2.0 Hz, 1H, H6), 7.02 (d, *J* = 8.5 Hz, 1H, H10), 6.96 (d, *J* = 8.5 Hz, 1H, H5), 3.87 (s, 3H, H15).

**$^{13}$C NMR** (101 MHz, DMSO, 25 °C) δ = 166.1 C16, 165.6 C14, 164.0 C9, 163.9 C4, 158.4 C7, 137.8 C13, 136.2 C11, 135.7 C3, 131.4 C6, 123.3 C8/12, 121.7 C1/8/12, 121.6 C1/8/12, 119.3 C10, 118.2 C2, 117.4 C5, 51.9 C15. ppm.

**IR** (ATR), $\nu$ (cm$^{-1}$): 1682 (s, $\nu_{C=O}$), 1618 (s, $\nu_{C=O}$), 1604 (s, $\nu_{C=N}$), 930 (s, $\nu_{Mo=O/asym}$), 909(s, $\nu_{Mo=O/sym}$).

**LIFDI-MS:** positive ion, calculated for [$C_{16}H_{11}MoNO_8$]$^+$: 442.95334, found: 442.95364, error: 0.70 ppm.

**UV-vis**, DMSO, λ / nm (ε / L * mol$^{-1}$ * cm$^{-1}$): 415 (3500), 348 (10300)

**Elemental analysis:** found: 42.16 % C, 2.96 % H, 2.61 % N, calculated for $C_{17}H_{15}MoNO_9$ *0.4 $H_2O$: 42.50 % C, 3.31. % H, 2.92 % N.

**Mp.:** loss of MeOH > 145 °C, decomposition > 300 °C

### 6.3.27 [MoO$_2$(4-Hydroxy-3-[(E)-(2-hydroxybenzylidene)amino]benzoic acid methyl ester)(MeOH)], Mo-6

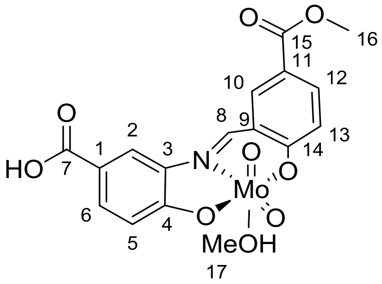

*$C_{17}H_{15}MoNO_9$, 473.27 g/mol*

Using **L-6** (100 mg, 0.37 mmol) and **5** (103.5 mg, 0.32 mmol) in methanol (1.5 mL), the product was obtained as a yellow solid. 102 mg, 0.22 mmol, 67%

**$^1$H NMR** (400 MHz, DMSO, 25 °C): δ = 9.65 (s, 1H, H8) , 8.62 (s, 1H, H10), 8.50 (s, 1H, H2), 8.07 (d, *J* = 5.5 Hz, 1H, H12), 7.84 (d, *J* = 6.5 Hz, 1H, H6), 7.04 (d, *J* = 7.5 Hz, 1H, H13), 6.95 (d, *J* = 6.9 Hz, 1H, H5), 4.13 (s 1H, MeO*H*), 3.87 (s, 3H, H16), 3.16 (s, 3H, H17) ppm.

**$^{13}$C NMR** (101 MHz, DMSO, 25 °C) δ = 166.9 C7, 165.2 C15, 164.4 C14, 163.8 C4, 158.4 C8, 137.8 C10, 136.1 C12, 135.7 C3, 131.8 C6, 123.1 C9, 122.2 C11, 121.9 C1, 119.8 C13, 118.6 C2, 117.4 C5, 52.3 C16, 48.7 C17 ppm.

**IR** (ATR), ν (cm$^{-1}$): 1721 (s, $\nu_{C=O}$), 1670 (s, $\nu_{C=O}$), 1608 (s, $\nu_{C=N}$), 931 (s, $\nu_{Mo=O/asym}$), 908(s, $\nu_{Mo=O/sym}$).

**LIFDI-MS:** positive ion, calculated for [$C_{16}H_{11}MoNO_8$]$^+$: 442.95333, found: 442.95364, error: 3.23 ppm.

**UV-vis**, DMSO, λ / nm (ε / L * mol$^{-1}$ * cm$^{-1}$): 412 (5100), 347 (11200)

**Elemental analysis:** found: 42.16 % C, 2.96 % H, 2.61 % N, calculated for $C_{17}H_{15}MoNO_9$ *0.40 $H_2O$: 42.50 % C, 3.33 % H, 2.92 % N.

**Mp.:** loss of MeOH > 155 °C, decomposition > 300 °C

### 6.3.28 [MoO2(4-Hydroxy-3-[(E)-(2-hydroxybenzylidene)amino]benzoic acid)(MeOH)], Mo-7

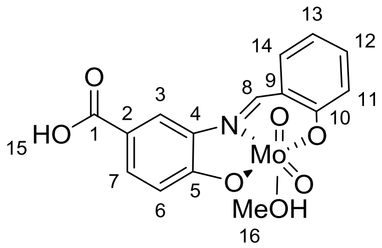

$C_{15}H_{13}MoNO_7$*, 415,23 g/mol.*

Using **L-7** (80 mg, 0.31 mmol) and **5** (100 mg, 0.31 mmol) in methanol (8 ml), the product was obtained as a yellow solid. 101 mg, 0.24 mmol, 79%

**$^1$H NMR** (400 MHz, DMSO-d6, 25°C) δ = 12.88 (br, 0.9H, H15), 9.47 (1H, H8), 8.43 (d, *J* = 2.0 Hz, 1H, H3), 7.90 (dd, *J* = 8.0 Hz, 1.5 Hz, 1H, H14), 7.83 (dd, *J* = 8.5 Hz, 2.0 Hz, 1H, H7), 7.57 (td, J= 7.5 Hz, 2 Hz, 1H, H12), 7.09 (td, J = 8.0 Hz, 1.0 Hz 1H, H13), 6.95 (d, *J* = 8.0 Hz, 1H, H11), 6.92 (d, *J* = 8.5 Hz, 1H, H6), 4.12(1H, $CH_3O$*H*), 3.16 (3H, H16) ppm.

**$^{13}$C NMR** (101 MHz, DMSO-d6, 25°C) δ = 166.9 C1, 163.8 C5, 161.1 C10, 158.2 C8, 136.0 C12, 135.7 C14+4, 131.5 C7, 122.6 C2, 122.0 C9, 121.2 C12, 118.8 C11, 118.1 C3, 117.3 C6, 48.7 C16 ppm.

**IR** (ATR), ν (cm$^{-1}$): 1666 (s, $\nu_{C=O}$), 1609 (s, $\nu_{C=N}$), 933 (s, $\nu_{Mo=O/sym}$), 911 (s, $\nu_{Mo=O/asym}$).

**LIFDI-MS**: calculated for $C_{14}H_9MoNO_6$ [$MoO_2$(sap-acid)]$^+$: 384.9485, found: 384.9484, error: 0.3 ppm.

**UV-vis**, DMSO, λ / nm (ε / L * mol$^{-1}$ * cm$^{-1}$): 414 (4700), 351 (10300)

**Elemental analysis:** found: 43.06 % C, 3.12 % H, 3.25 % N, calculated: 43.39 % C, 3.16 % H, 3.37 % N.

**Mp.:** loss of MeOH > 150 °C, decomposition > 300 °C

### 6.3.29 [$MoO_2$(4-Hydroxy-3-[(E)-[(2-hydroxyphenyl)imino]methyl]benzoic acid)(MeOH)], Mo-8

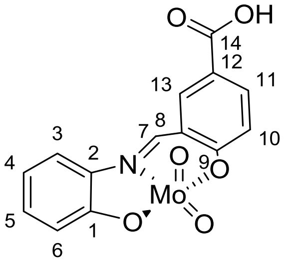

$C_{14}H_9MoNO_6$*, 383.19 g/mol*

Using **L-8** (100 mg, 0.39 mmol) and **5** (127 mg, 0.39 mmol) in methanol (1 mL), the product was obtained as a brown solid. 75 mg, 0.20 mmol, 50 %

**$^1$H NMR** (400 MHz, DMSO, 25 °C): δ = 12.95 (br s, 0.6 H, OH) 9.40 (s,1H, H7), 8.46 (d, *J* = 2.5 Hz, 1H, H13), 8.03 (dd, *J* = 8.5 Hz, 2.5 Hz, 1H, H11), 7.86 (d, *J* = 8.5 Hz, 1H, H3), 7.26 (t, *J* = 7.5 Hz, 1H, H5), 7.00 (d, *J* = 8.5 Hz, 1H, H10), 6.96 (d, *J* = 7.5 Hz, 1H, H4), 6.88 (d, *J* = 8.0 Hz, 1H, H6) ppm.

**$^{13}$C NMR** (101 MHz, DMSO, 25 °C) δ = 166.3 C14, 164.3 C9, 160.1 C1, 156.8 C7, 137.4 C13, 136.0 C11, 135.6 C2, 130.5 C5, 123.1 C8, 121.8 C12, 120.8 C4, 119.6 C10, 117.4 C6, 116.8 C3 ppm.

**IR** (ATR), $\nu$ (cm$^{-1}$): 1698 (s, $\nu_{C=O}$), 1610 (s, $\nu_{C=N}$), 924 (s, $\nu_{Mo=O}$), 802 (s, $\nu_{Mo\text{-}O\text{-}Mo}$).

**LIFDI-MS:** positive ion, calculated for $[C_{14}H_9MoNO_6]^+$: 384.94785, found: 384.94812, error: 0.72 ppm.

**UV-vis**, DMSO, λ / nm (ε / L * mol$^{-1}$ * cm$^{-1}$): 418 (4300), 352 (9000)

**Elemental analysis:** found: 42.84 % C, 2.06 % H, 3.21 % N, calculated for $C_{14}H_9MoNO_6$ *0.30 $H_2O$: 43.27 % C, 2.49 % H, 3.60 % N.

**Mp.:** decomposition > 300 °C

## 6.3.30 [MoO$_2$(4-Hydroxy-3-[(E)-(2-hydroxybenzylidene)amino]benzoic acid methyl ester)(MeOH)], Mo-9

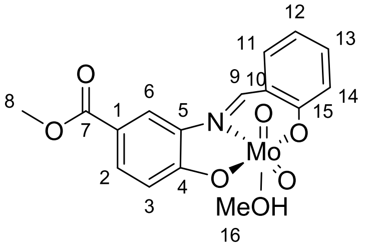

*$C_{16}H_{15}MoNO_7$, 429.26 g/mol*

Using **L-9** (90 mg, 0.33 mmol) and **5** (107 mg, 0.33 mmol) in methanol (1.5 mL), the product was obtained as a yellow solid. 120 mg, 0.28 mmol, 84 %

**$^1$H NMR** (400 MHz, DMSO, 25 °C): δ = 9.48 (s, 1H, H9), 8.44 (s,1H, H6), 7.90 (d, *J* = 7.5 Hz, 1H, H11), 7.85 (d, *J* = 8.5 Hz, 1H, H2), 7.58 (t, *J* = 7.6 Hz, 1H, H12), 7.10 (t, *J* = 7.4 Hz, 1H, H13), 6.97-6.94 (2* d, J= 8.5 Hz, 2H, H3/14) , 4.12 (br s, 0.2 H, OH), 3.86 (br s, 3H, H8), 3.17 (s, 2.6 H, H16) ppm.

**$^{13}$C NMR** (101 MHz, DMSO, 25 °C) δ = 165.9 C7, 164.1 C4, 161.1 C15, 158.5 C9, 136.1 C13, 135.9 C5, 135.8 C11, 131.4 C2, 122.0 C10, 121.5 C1, 121.3 C12, 118.8 C3/14, 118.0 C6, 117.6 C3/14, 52.1 C8, 48.7 C16 ppm.

**IR** (ATR), $\nu$ (cm$^{-1}$): 1713 (s, $\nu_{C=O}$), 1620 (s, $\nu_{C=N}$), 928 (s, $\nu_{Mo=O/sym}$), 891 (s, $\nu_{Mo=O/asym}$).

**LIFDI-MS:** positive ion, calculated for $[C_{15}H_{11}MoNO_6]^+$: 398.96327, found: 398.96350, error: -0.58 ppm.

**UV-vis**, DMSO, λ / nm (ε / L * mol$^{-1}$ * cm$^{-1}$): 415 (4700), 349 (10200)

**Elemental analysis:** found: 43.48 % C, 3.140 % H, 2.88 % N, calculated for $C_{16}H_{15}MoNO_7$ *0.45 $H_2O$: 43.94 % C, 3.66 % H, 3.20 % N.

**Mp.:** loss of MeOH > 130 °C, decomposition > 300 °C

### 6.3.31 [$MoO_2$(4-Hydroxy-3-[(E)-[(2-hydroxyphenyl)imino]methyl]benzoic acid methyl ester)(MeOH)], Mo-10

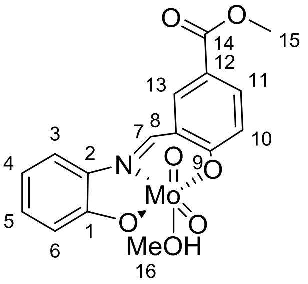

*$C_{16}H_{15}MoNO_7$, 429.26 g/mol*

Using **L-10** (80 mg, 0.29 mmol) and **5** (100 mg, 0.30 mmol) in methanol (1.5 mL), the product was obtained as an orange solid. 110 mg, 0.26 mmol, 88 %

**$^1$H NMR** (600 MHz, DMSO-*d*$_6$, 25 °C) δ = 9.43 (s, 1H, H8), 8.49 (s, 1H, H13), 8.05 (d, *J* = 8.5 Hz, 1H, H11), 7.86 (d, *J* = 8.0 Hz, 1H, J3), 7.26 (t, *J* = 7.5 Hz, 1H, H5), 7.02 (d, *J* = 8.5 Hz, 1H, H10), 6.98 (t, *J* = 7.5 Hz, 2H, H4), 6.88 (d, *J* = 8.1 Hz, 1H, H6), 4.09 (q, *J* = 5.5 Hz, 1H, MeO*H*), 3.87 (s, 3H, H15), 3.17 (d, *J* = 5 Hz, 3H, H16) ppm.

**$^{13}$C NMR** (151 MHz, DMSO-d$_6$, 25°C) δ = 165.2 C14, 164.5 C9, 160.1 C1, 156.7 C7, 137.2 C13, 135.6 C11, 135.5 C2, 130.4 C5, 121.8 C12/8, 121.8 C12/8, 120.8 C4, 119.7 C10, 117.3 C6, 116.7 C3, 52.1 C15, 48.6 C16 ppm.

**IR** (ATR), ν ($cm^{-1}$): 1688 (s, $\nu_{C=O}$), 1609 (s, $\nu_{C=N}$), 928 (s, $\nu_{Mo=O/sym}$), 904 (s, $\nu_{Mo=O/asym}$).

**LIFDI-MS:** positive ion, calculated for $[C_{15}H_{12}MoNO_6]^+$: 398.96350, found: 398.96436, error: 2.84 ppm.

**UV-vis**, DMSO, λ / nm (ε / L * $mol^{-1}$ * $cm^{-1}$): 421 (4400), 351 (9300)

**Elemental analysis:** found: 43.65 % C, 3.38 % H, 3.00 % N, calculated for $C_{16}H_{15}MoNO_7$ *0.45 $H_2O$: 43.94 % C, 3.66 % H, 3.20 % N.

**Mp.:** loss of MeOH > 170 °C, decomposition > 300 °C

### 6.3.32 [$MoO_2$(3-Hydroxy-4-[(E)-[2-hydroxyphenyl)methylidene]amino benzoic acid methyl ester)(MeOH)], Mo-11

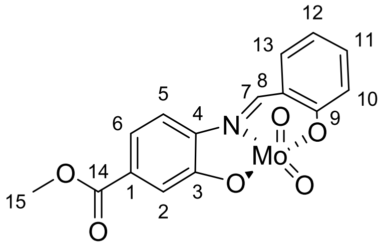

*$C_{15}H_{11}MoNO_6$, 397.21 g/mol*

Using **L-11** (41 mg, 0.15 mmol) and **5** (49 mg, 0.15 mmol) in MeOH (8 ml) the product was obtained as a brown solid. 91 mg, 0.23 mmol, 69 %.

**$^1$H NMR** (600 MHz, DMSO-$d_6$, 25 °C): δ = 9.40 (s, 1H, H7), 7.95 (d, *J* = 8.5 Hz, 1H, H6), 7.81 (dd, *J* = 8.0 Hz, 1.5 Hz, 1H, H13), 7.59 (td, *J* = 8.0 Hz, 1.5 Hz, 1H, H11), 7.54 (dd, *J* = 8.5 Hz, 1.5 Hz, 1H, H6), 7.35 (d, *J* = 1.5 Hz, 1H, H2), 7.09 (t, *J* = 7.0 Hz, 1H, H12), 6.96 (d, *J* = 8.5 Hz, 1H, H10), 3.85 (s, 3H, H15) ppm.

**$^{13}$C NMR** (151 MHz, DMSO-$d_6$, 25 °C): δ = 165.7 C14, 161.5 C9, 159.8 C3, 159.3 C7, 139.5 C4, 136.4 C11, 135.7 C13, 130.6 C1, 121.8 C8, 121.1 C6/11, 121.1 C6/11, 119.0 C10, 117.7 C2, 116.8 C5, 52.3 C15 ppm.

**IR** (ATR), $\nu$ (cm$^{-1}$): 1718 (s, $\nu_{C=O}$), 1616 (s, $\nu_{C=N}$), 918 (s, $\nu_{Mo=O}$), 813 (s br, $\nu_{Mo-O-Mo}$).

**MS-LIFDI**: positive ion, calculated for $[C_{15}H_{11}MoNO_6]^+$: 398.96350, found: 398.96232, error: -2.95 ppm.

**UV-vis**, DMSO, λ / nm (ε / L * mol$^{-1}$ * cm$^{-1}$): 431 (7300), 358 (10200)

**Elemental analysis:** found 44.38 % C, 2.35 % H, 2.90 % N, calculated for $C_{16}H_{15}MoNO_7$: 44.77 % C, 3.52 % H, 3.26 % N, rest 48.44 %.

**Mp.:** decomposition > 300 °C

### 6.3.33 [$MoO_2$(Nitro 2-[(E)-[(2-hydroxyphenyl)methylidene]amino]-4-nitrophenol)(MeOH)], Mo-12

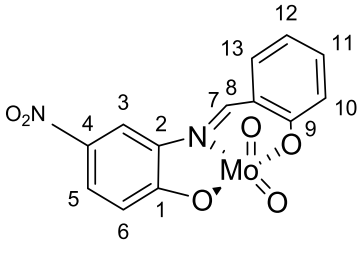

*$C_{13}H_8MoN_2O_6$, 384.18*

Using **L-12** (90.4 mg, 0.35 mmol) and **5** (114 mg, 0.35 mmol) in MeOH (8ml) the product was obtained as an orange solid. 36 mg, 0.09 mmol, 28 %.

**$^1$H NMR** (600 MHz, DMSO-$d_6$, 25 °C) δ = 9.58 (s, 1H, H7), 8.81 (d, *J* = 2.0 Hz, 1H, H3), 8.15 (dd, *J* = 9.0 Hz, 2.0 Hz, 1H, H5), 7.89 (d, *J* = 7.5 Hz, 1H, H13), 7.62 (t, *J* = 7.5 Hz, 1H, H11), 7.14 (t, *J* = 7.5 Hz, 1H, H10), 7.04 (d, *J* = 9.0 Hz, 1H, H6), 6.99 (d, *J* = 8.0 Hz, 1H, H10) ppm.

**$^{13}$C NMR** (151.5 MHz, DMSO-d$_6$, 25 °C) 165.7 C1, 161.1 C9, 160.1 C7, 140.3 C4, 136.5 C11, 135.9 C13, 135.9 C2, 125.7 C5, 121.8 C8, 121.5 C12, 118.8 C10, 117.6 C6, 113.2 C3 ppm.

**IR** (ATR), ν (cm$^{-1}$): 1610 (s, $\nu_{C=N}$), 1501 (s, $\nu_{N-O}$), 940 (s, $\nu_{Mo=O}$), 796 (s, $\nu_{Mo-O-Mo}$).

**MS-LIFDI:** positive ion, calculated for [$C_{13}H_8MoN_2O_6$]$^+$: 385.9431, found: 385.9416, error: -3.81 ppm.

**UV-vis**, DMSO, λ / nm (ε / L * mol$^{-1}$ * cm$^{-1}$): 430 - 450 very broad, no clear maximum, 365 (13100)

**Elemental analysis:** found 40.31 % C, 1.64 % H, 6.89 % N, calculated for $C_{13}H_8MoN_2O_6$: 40.64 % C, 2.10 % H, 7.29 % N.

**Mp.:** decomposition > 300 °C

## 6.3.34 [MoO$_2$(2-[(E)-[2-hydroxyphenyl)methylidene]amino]-4-trifluoromethyl phenol)], Mo-13

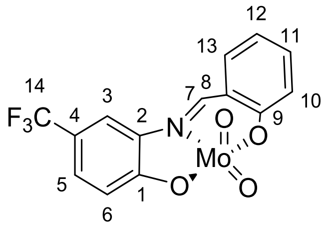

*$C_{14}H_8F_3MoNO_4$, 407.18 g/mol*

Using **L-13** (70 mg, 0.25 mmol) and **5** (81 mg, 0.25 mmol) in MeOH (8ml) the product was obtained as a red/brown solid. 90 mg, 0.22 mmol, 83 %.

**$^1$H NMR** (600 MHz, DMSO-$d_6$, 25 °C) δ = 9.48 (s, 1H, H7), 8.25 (s, 1H, H3), 7.82 (dd, *J* = 7.5 Hz, 1.5 Hz, 1H, H13), 7.59 (td, *J* = 8.0 Hz, 1.5 Hz, 1H, H11), 7.56 (dd, *J* = 8.5 Hz, 1.5 Hz, 1H, H5), 7.11 (td, *J* = 7.5 Hz, 1.0 Hz, 1H, H12), 7.02 (d, *J* = 8.5 Hz, 1H, H6), 6.97 (d, *J* = 8.5 Hz, 1H, H10) ppm.

**$^{13}$C NMR** (151 MHz, DMSO-d$_6$, 25 °C) δ = 162.8 C1, 161.0 C9, 159.0 C7, 136.2 C11, 135.9 C2, 135.6 C13, 126.7 (q, *J* = 3.0 Hz, C5), 124.5 (q, *J* = 271.5 Hz, C14), 121.8 C8, 121.3 C12, 120.5 (q, *J* = 32.0 Hz, C4), 118.9 C10, 118.0 C6, 114.4 (q, *J* = 4.0 Hz, C3) ppm. Note: due to low resolution all quartets appear as doublets.

**$^{19}$F NMR** (565 MHz, DMSO-$d_6$, 25 °C) δ = -59.4 (s, 3F) ppm.

**IR** (ATR), ν (cm$^{-1}$): 1601 (s, $\nu_{C=N}$), 1323 (s, $\nu_{C-F}$), 922 (s, $\nu_{Mo=O}$), 802 (s, $\nu_{Mo-O-Mo}$).

**MS-LIFDI:** positive ion, calculated for $[C_{14}H_8F_3MoNO_4]^+$: 408.94540, found: 408.94554, error: 0.34 ppm.

**UV-vis**, DMSO, λ / nm (ε / L * $mol^{-1}$ * $cm^{-1}$): 414 (4200), 348 (7900)

**Elemental analysis:** found 37.93 % C, 1.86 % H, 3.11 % N, calculated for $C_{14}H_8F_3MoNO_4$: 41.30 % C, 1.98 % H, 3.44 % N.

**Mp.:** decomposition > 300 °C

## 6.3.35 [$MoO_2$(4-hydroxy-3-[(E)-[(2-hydroxyphenyl)methylidene]amino]benzene-1-sulfonamide)(MeOH)], Mo-14

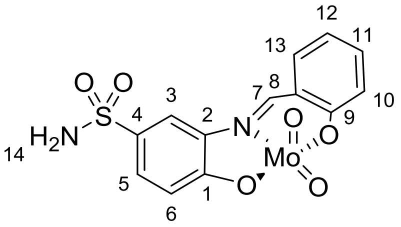

*$C_{14}H_{14}MoN_2O_7S$, 450.29 g/mol*

Using **L-14** (90 mg, 0.31 mmol) and **5** (100 mg, 0.31 mmol) in MeOH (8ml) the product was obtained a yellow solid. 62 mg, 0.14 mmol, 45 %.

**$^1$H NMR** (600 MHz, DMSO-*d*$_6$, 25 °C) δ = 9.41 (s, 1H, H7), 8.27 (d, *J* = 2.0 Hz, 1H, H3), 7.89 (dd, *J* = 8.0 Hz, 2.0 Hz, 1H, H13), 7.69 (dd, *J* = 8.5 Hz, 2.0 Hz, 1H, H5), 7.59 (td, *J* = 7.5 Hz, 1.5 Hz, 1H, H11), 7.26 (s, 2H, H14), 7.10 (t, *J* = 7.5 Hz, 1H, H12), 7.01 (d, *J* = 8.5 Hz, 1H, H6), 6.96 (d, *J* = 8.5 Hz, 1H, H10) ppm.

**$^{13}$C NMR** (151 MHz, DMSO-d$_6$, 25 °C) δ = 162.4 C1, 161.0 C9, 158.4 C7, 136.2 C11, 135.8 C2/4/8, 135.7 C13, 135.2 C2/4/8, 127.7 C5, 121.8 C2/4/8, 121.2 C12, 118.9 C10, 117.6 C6, 114.6 C3 ppm.

**IR** (ATR), ν ($cm^{-1}$): 3339 (s, $\nu_{O-H}$, MeOH), 3152 (s, $\nu_{N-H}$), 3057 (s, $\nu_{N-H}$), 1603 (s, $\nu_{C=N}$), 1386 (s, $\nu_{S=O}$),951 (s, $\nu_{Mo=O/sym}$), 910 (s, $\nu_{Mo=O/asym}$).

**MS-LIFDI**: positive ion, calculated for $[C_{14}H_{14}MoNO_7S]^+$: 419.93082, found: 419.93096, error: 0.35 ppm.

**UV-vis**, DMSO, λ / nm (ε / L * $mol^{-1}$ * $cm^{-1}$): 419 (4900), 351 (9700)

**Elemental analysis:** found 37.15 % C, 2.16 % H, 6.21 % N, calculated for $C_{14}H_{14}MoN_2O_7S$: 37.34 % C, 3.13 % H, 6.22 % N.

**Mp.:** decomposition > 300 °C

## 6.3.36 [MoO$_2$(5-(diethylamino)-2-[(E)-[2-hydroxyphenyl)imino]methyl]phenol)(MeOH)], Mo-15

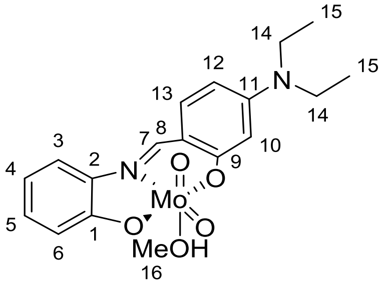

*$C_{18}H_{22}MoN_2O_5$, 442.34 g/mol*

Using **L-15** (72 mg, 0.25 mmol) and **5** (83 mg, 0.25 mmol) in MeOH (8ml) the product was obtained a red/brown solid. 40 mg, 0.09 mmol, 36 %.

**$^1$H NMR** (600 MHz, DMSO-*d*$_6$, 25 °C) δ = 8.91 (s, 1H, H7), 7.63 (d, *J* = 8.0 Hz, 1H), 7.47 (d, *J* = 9.0 Hz, 1H, H13), 7.07 (t, *J* = 7.5 Hz, 1H, H5 ), 6.86 (t, *J* = 7.5 Hz, 1H, H4), 6.75 (d, *J* = 8.0 Hz, 1H, H12), 6.44 (dd, *J* = 9.0 Hz, 2.5 Hz, 1H, H12), 6.10 (d, *J* = 2.5 Hz, 1H, H10), 4.10 (q, *J* = 5.5 Hz, 1H, O*H*), 3.43 (q, *J* = 7.0 Hz, 4H, H14), 3.17 (d, *J* = 5.5 Hz, 3H, H16), 1.13 (t, *J* = 7.0 Hz, 6H, H15) ppm.

**$^{13}$C NMR** (151 MHz, DMSO-d$_6$, 25 °C) δ = 163.0 C9, 159.2 C1, 154.3 C7, 153.7 C11, 137.1 C2, 136.6 C13, 127.5 C5, 119.9 C4, 116.5 C6, 115.0 C3, 111.1 C8, 105.9 C12, 99.0 C10, 48.6 C16, 44.2 C14, 12.6 C15 ppm.

**IR** (ATR), ν (cm$^{-1}$): 3395 (s, $\nu_{O\text{-}H}$, MeOH), 2973- 2872 (m, $\nu_{C\text{-}H}$), 1614 (s, $\nu_{C=N}$), 1248 (s, $\nu_{C\text{-}N}$), 933 (s, $\nu_{Mo=O/sym}$), 893 (s, $\nu_{Mo=O/asym}$).

**MS-LIFDI:** positive ion, calculated for $[C_{17}H_{18}MoN_2O_4]^+$: 412.0315, found: 412.0331, error: 3.83 ppm.

**UV-vis**, DMSO, λ / nm (ε / L * mol$^{-1}$ * cm$^{-1}$): 465 (18300), 366 (20200)

**Elemental analysis:** found 46.78 % C, 4.53 % H, 5.80 % N, calculated for $C_{18}H_{22}MoN_2O_5$: 48.88 % C, 5.01 % H, 6.33 % N.

**Mp.:** decomposition > 300 °C, solvent loss could not be determined

### 6.3.37 [MoO$_2$(3-[(E)-[(2-hydroxyphenyl)methylidene]amino]naphthalen-2-ol)(MeOH)], Mo-16

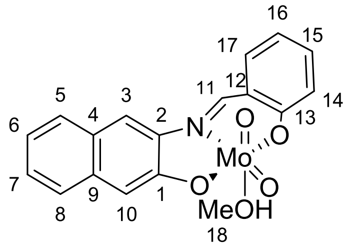

*$C_{18}H_{15}MoNO_5$, 421.28 g/mol*

Using **L-16** (81 mg, 0.3 mmol) and **5** (100 mg, 0.3 mmol) in MeOH (8ml) the product was obtained as an orange solid. 107 mg, 0.25 mmol, 85 %.

**$^1$H NMR** (600 MHz, DMSO-*d*$_6$, 25 °C ) δ = 9.54 (s, 1H, H11), 8.38 (s, 1H, H3), 7.85 (dd, *J* = 8.0 Hz, 1.5 Hz, 1H, H17), 7.83 (d, *J* = 8.5 Hz, 1H, H5), 7.73 (d, *J* = 8.0 Hz, 1H, H8), 7.60 (td, *J* = 7.5 Hz, 1.5 Hz, 1H, H15), 7.43 (td, *J* = 7.5 Hz, 1.0 Hz, 1H, H7), 7.34 (td, *J* = 7.5 Hz, 1.0 Hz, 1H, H6), 7.22 (s, 1H, H10), 7.11 (td, *J* = 7.5 Hz, 1.0 Hz, 1H, H16), 6.98 (d, *J* = 8.0 Hz, 1H, H14) ppm.

**$^{13}$C NMR** (151 MHz, DMSO-d$_6$, 25 °C) δ = 161.5 C13, 158.9 C11, 158.1 C1, 137.6 C2, 136.2 C15, 135.5 C17, 134.6 C9, 128.2 C5, 128.1 C4, 126.8 C7, 126.7 C8, 124.0 C6, 121.9 C12, 121.0 C16, 119.1 C14, 114.6 C3, 110.8 C10.

**IR** (ATR), ν (cm$^{-1}$): 1623 (s, $\nu_{C=N}$), 930 (s, $\nu_{Mo=O/sym}$), 888 (s br, $\nu_{Mo=O/asym}$).

**MS-LIFDI:** positive ion, calculated for $[C_{17}H_{11}MoNO_4]^+$: 390.97367, found: 390.97417, error: 1.27 ppm.

**UV-vis**, DMSO, λ / nm (ε / L * mol$^{-1}$ * cm$^{-1}$): 403 (11700), 339 (28800)

**Elemental analysis:** found 48.62 % C, 2.82 % H, 2.96 % N, calculated for $C_{18}H_{15}MoNO_5$: 51.32 % C, 3.59 % H, 3.32 % N.

**Mp.:** loss of MeOH > 130 °C, decomposition > 300 °C

## 6.3.38 [$WO_2$(2-[(E)-(2-Hydroxybenzylidene)amino]phenol)], W-1

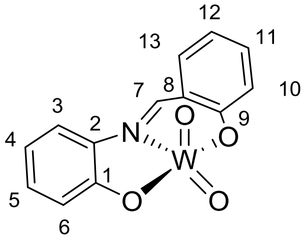

*$C_{13}H_9NO_4W$, 427.06 g/mol*

**L-1** (213.25 mg, 1 mmol) was dissolved in hot MeOH (20 ml) and $Na_2WO_4$ *2 $H_2O$ (329.85 mg, 1 mmol) was added to the orange solution. AcOH (0.1 ml, 1.75 mmol) was added resulting in a yellow solution and the mixture was heated to reflux for 22 h.
After cooling to room temperature, the formed precipitate was separated by filtration and dried *in vacuo*. The product was obtained as an orange solid. 303 mg, 0.71 mmol, 71 %

**$^1$H NMR** (400 MHz, DMSO, 25 °C): δ = 9.28 (s, 1H, H7), 7.86 (d, *J* = 8.0 Hz, 1H, H3), 7.79 (d, *J* = 7.5 Hz, 1H, H13), 7.61 (t, *J* = 8.0 Hz, 1H, H11), 7.29 (t, *J* = 7.5 Hz, 1H, H5), 7.10 (t, *J* = 7.5 Hz, 1H, H12), 7.01 (d, *J* = 8.0 Hz, 1H, H10), 6.97 (t, *J* = 8.0 Hz, 1H, H4), 6.90 (d, *J* = 8.0 Hz, 1H, H6) ppm.

**$^{13}$C NMR** (101 MHz, DMSO, 25 °C) δ = 159.7 C9, 158.9 C1, 157.5 C7, 136.1 C2+C11, 135.2 C13, 130.5 C5, 122.5 C8, 121.3 C11, 120.6 C4, 119.7 C10, 118.4 C6, 116.8 C3 ppm.

**IR** (ATR), ν ($cm^{-1}$): 1615 (s, $\nu_{C=N}$), 941 (s, $\nu_{W=O}$), 730 (s br, $\nu_{W-O-W}$).

**LIFDI-MS:** positive ion, calculated for $[C_{19}H_{20}MoN_2O_6]^+$: 427.00354, found: 427.00254, error: -2.35 ppm.

**UV-vis**, DMSO, λ / nm (ε / L * $mol^{-1}$ * $cm^{-1}$): 407 (7100), 362 (5600)

**Elemental analysis: f**ound 34.99 % C, 1.88 % H, 2.92 % N, calculated for $C_{13}H_9WNO_4$: 36.56 % C, 2.12 % H, 3.38 % N.

## 6.3.39 [$WO_2$ (4-Hydroxy-3-[(E)-(4-methyl-oxycarbonyl-2-hydroxybenzylidene)amino]benzoic acid methyl ester)], W-2

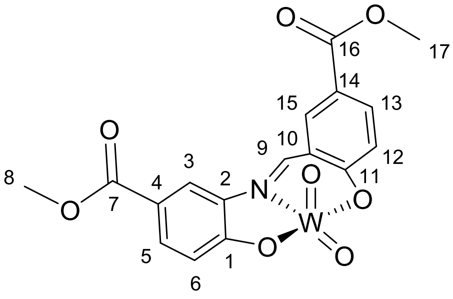

*$C_{17}H_{13}NO_8W$, 543.13 g/mol*

**L-2** (329.31 mg, 1 mmol) was dissolved in hot MeOH (25 ml) and $Na_2WO_4$ *2 $H_2O$ (329.85 mg, 1 mmol) was added to the orange solution. AcOH (0.1 ml, 1.75 mmol) was added, resulting in a yellow solution, and the reaction heated to reflux for 22 h.
After cooling to room temperature, the formed precipitate was separated by filtration and dried *in vacuo*. The product was obtained as an orange solid. 406 mg, 0.74 mmol, 75 %

**$^1$H NMR** (400 MHz, DMSO, 25 °C): δ = 9.67 (s, 1H, H9), 8.65 (s, 1H, H15), 8.55 (s, 1H, H3), 8.16 (d, *J* = 8.0 Hz, 1H, H13), 7.93 (d, *J* = 8.5 Hz, 1H, H5), 7.13 (d, *J* = 8.0 Hz, 1H, H12), 7.04 (d, *J* = 8.5 Hz, 1H, H6), 3.89 (s, 6H, H8+H17) ppm.

**$^{13}$C NMR** (101 MHz, DMSO, 25 °C) δ = 165.6 C7, 165.1 C14, 163.0 C1, 162.8 C11, 159.3 C9, 137.8 C15, 136.6 C13, 136.2 C2, 131.9 C5, 122.6 C10, 122.3 C14, 122.2 C4, 120.4 C12, 118.7 C3/6, 118.6 C3/6, 52.2 C8/17, 52.2 C8/17 ppm.

**IR** (ATR), $\nu$ (cm$^{-1}$): 1721 (s, $\nu_{C=O}$), 1610 (s, $\nu_{C=N}$), 964 (s, $\nu_{W=O}$), 736 (s br, $\nu_{W\text{-}O\text{-}W}$).

**LIFDI-MS:** positive ion, calculated for $[C_{17}H_{13}WNO_8]^+$: 543.01450, found: 543.01536, error: 1.59 ppm.

**UV-vis**, DMSO, λ / nm (ε / L * mol$^{-1}$ * cm$^{-1}$): 400 (7000), 359 (6300)

**Elemental analysis: f**ound 34.98 % C, 2.34 % H, 2.23 % N, calculated for $C_{17}H_{13}WNO_8$: 37.59 % C, 2.41 % H, 2.58 % N.

# Appendix

## A-1 Structures of complexes and substrates used in this work

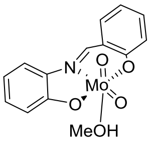

**Mo-1$^{H,H}$**

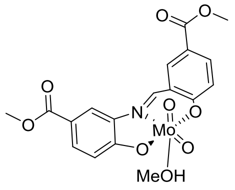

**Mo-2$^{COOMe,COOMe}$**

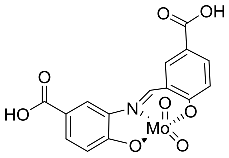

**Mo-3$^{COOH,COOH}$**

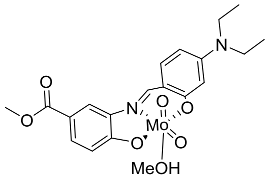

**Mo-4$^{COOMe,NEt2}$**

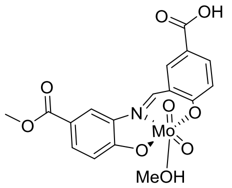

**Mo-5$^{COOMe,COOH}$**

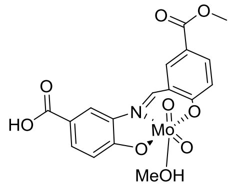

**Mo-6$^{COOH,COOMe}$**

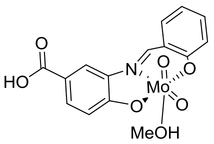

**Mo-7$^{COOH}$**

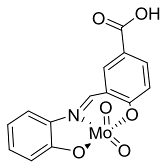

**Mo-8$^{H,COOH}$**

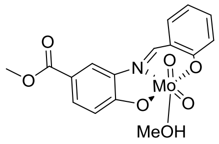

**Mo-9$^{COOMe}$**

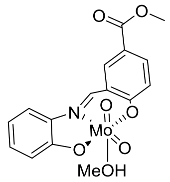

**Mo-10$^{H,COOMe}$**

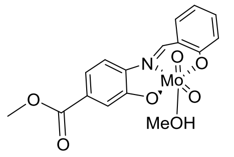

**Mo-11$^{COOMe}$**

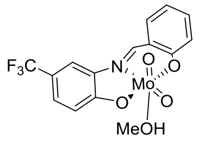

**Mo-12$^{CF3}$**

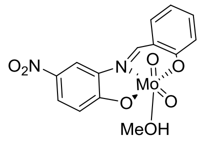

**Mo-13$^{NO2}$**

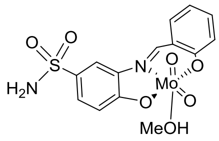

**Mo-14$^{SO2NH2}$**

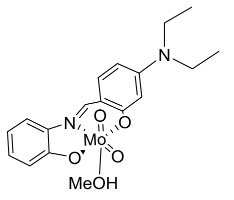

**Mo-15$^{H,NEt2}$**

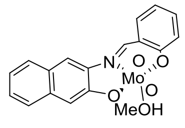

**Mo-16$^{Naph}$**

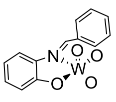

**W-1$^{H,H}$**

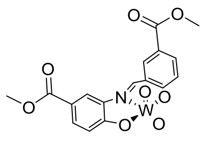

**W-2$^{COOMe,COOMe}$**

*Figure A-1-1: Structures of molybdenum and tungsten complexes synthesised in this work.*

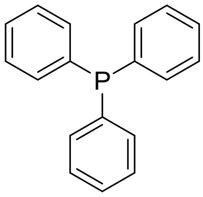

**P-1**

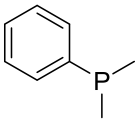

**P-2**

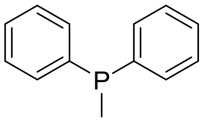

**P-3**

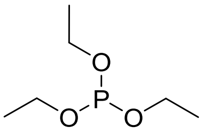

**P-4**

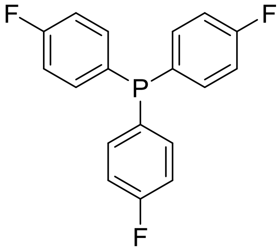

**P-5**

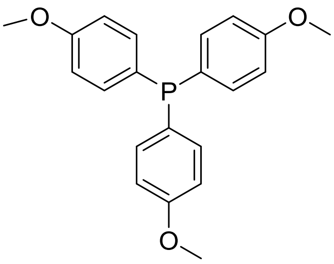

**P-6**

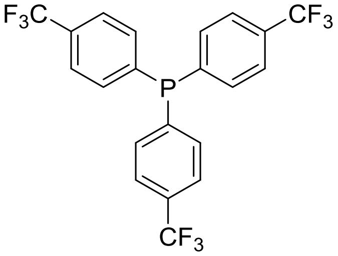

**P-7**

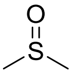

**SO-1**

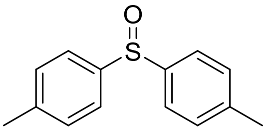

**SO-2**

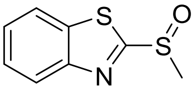

**SO-3**

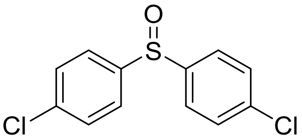

**SO-4**

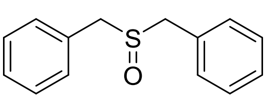

**SO-5**

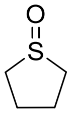

**SO-6**

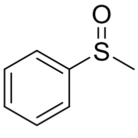

**SO-7**

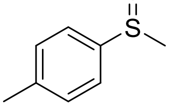

**SO-8**

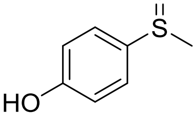

**SO-9**

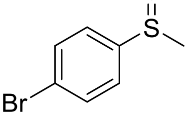

**SO-10**

*Figure A-1-2: Structures of phosphines and sulfoxides used in this work.*

## A-2 Screening of complexes: conversion after 3 h.

*Table A-2-1 Conversion of $PPh_3$ to $OPPh_3$ after 3h, catalysed by [Mo].*

| Complex | Conversion at a wavelength λ in % | | |
|---|---|---|---|
| | 365 nm | 410 nm | 460 nm |
| **Mo-1**$^{\mathrm{H,H}}$ | 0 | | |
| **Mo-2**$^{\mathrm{COOMe,COOMe}}$ | 69 | 78 | 77 |
| **Mo-3**$^{\mathrm{COOH,COOH}}$ | 32 | 35 | 32 |
| **Mo-4**$^{\mathrm{COOMe,NEt2}}$ | 0 | | |
| **Mo-5**$^{\mathrm{COOMe,COOH}}$ | 52 | 65 | 57 |
| **Mo-6**$^{\mathrm{COOH,COOMe}}$ | 32 | 39 | 31 |
| **Mo-7**$^{\mathrm{COOH}}$ | 7 | 12 | 12 |
| **Mo-8**$^{\mathrm{H,COOH}}$ | 4 | 2 | 2 |
| **Mo-9**$^{\mathrm{COOMe}}$ | 30 | 28 | 19 |
| **Mo-10**$^{\mathrm{H,COOMe}}$ | 5 | 2 | 2 |
| **Mo-11**$^{\mathrm{COOMe}}$ | | 23 | |
| **Mo-12**$^{\mathrm{NO2}}$ | | 32 | |
| **Mo-13**$^{\mathrm{CF3}}$ | | 25 | |
| **Mo-14**$^{\mathrm{SO2NH2}}$ | | 11 | |
| **Mo-15**$^{\mathrm{H,NEt2}}$ | 0 | | |
| **Mo-16**$^{\mathrm{Naph}}$ | 0 | | |
| **W-1**$^{\mathrm{H,H}}$ | 8 | 12 | 10 |
| **W-2**$^{\mathrm{COOMe,COOMe}}$ | 62 | 79 | 45 |

In DMSO-$d_6$, under $N_2$, c([Mo])= 1 mM, c($PPH_3$) = 300 mM, irradiation with a light source of the stated wavelength. [a] Catalyst deactivation observed, lower conversion obtained from a repeat of the experiment.

# A-3 Additional mass spectra for chapter 3.7.4

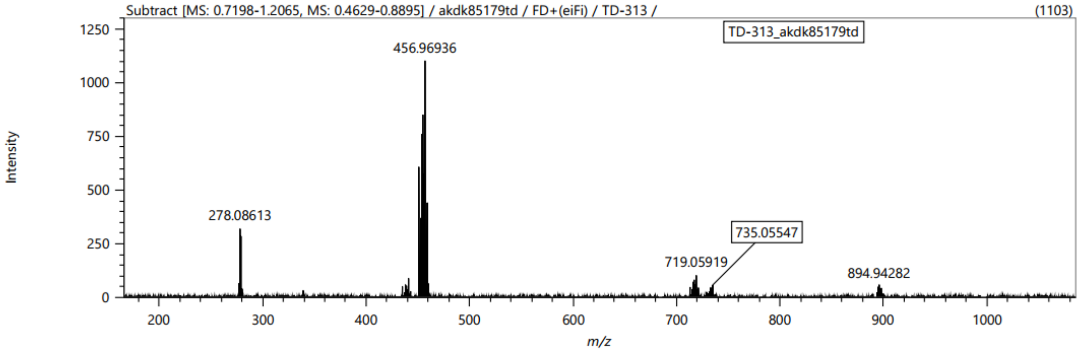

*Figure A-3-1: LIFDI-mass spectrum of a mixture of **Mo-2** and PPh$_3$ in acetone-d$_6$ after irradiation at 410 nm for16 h.*

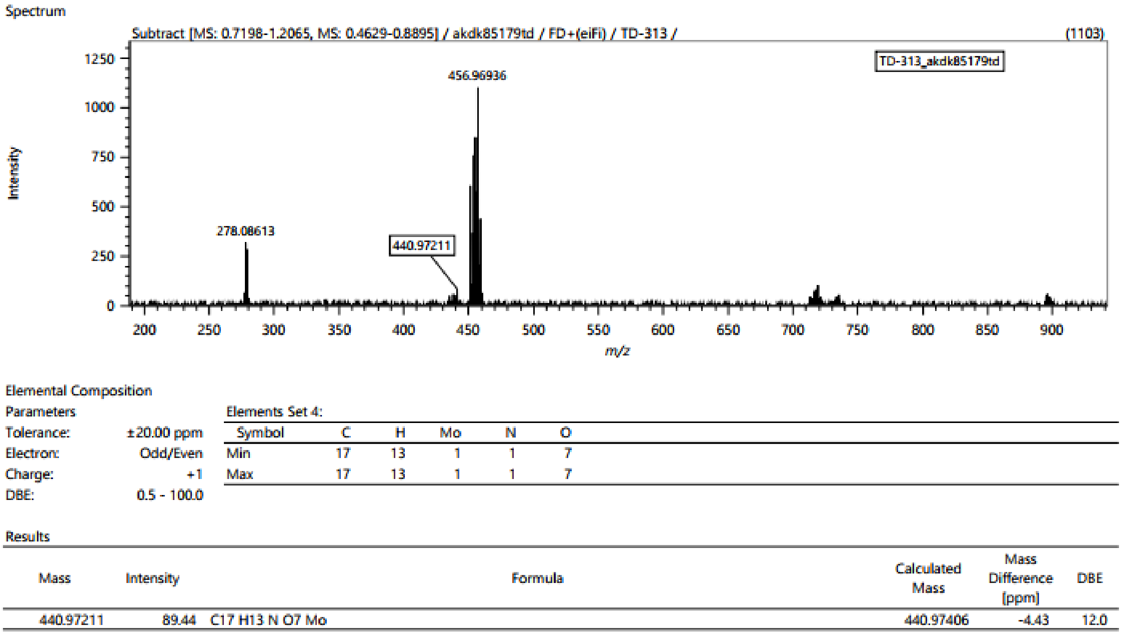

Elemental Composition

Parameters

Tolerance: ±20.00 ppm
Electron: Odd/Even
Charge: +1
DBE: 0.5 - 100.0

Elements Set 4:

| Symbol | C | H | Mo | N | O |
|---|---|---|---|---|---|
| Min | 17 | 13 | 1 | 1 | 7 |
| Max | 17 | 13 | 1 | 1 | 7 |

Results

| Mass | Intensity | Formula | Calculated Mass | Mass Difference [ppm] | DBE |
|---|---|---|---|---|---|
| 440.97211 | 89.44 | C17 H13 N O7 Mo | 440.97406 | -4.43 | 12.0 |

*Figure A-3-2: Mass accuracy calculation for m/z = 440.97211.*

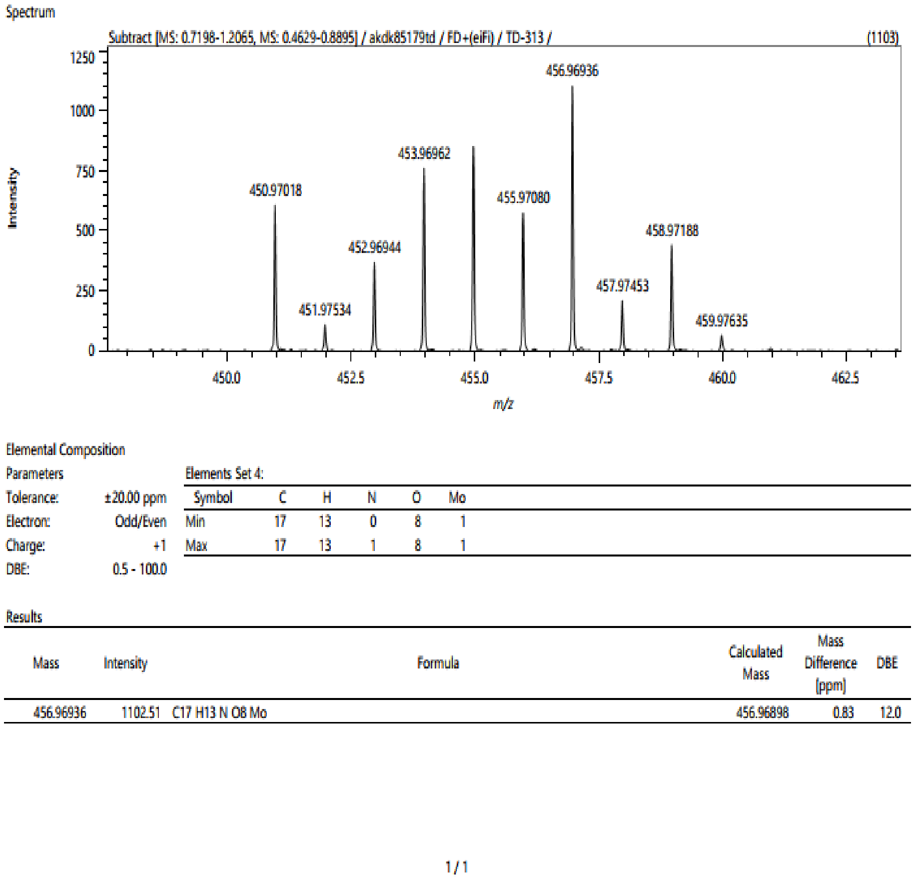

Spectrum

Subtract [MS: 0.7198-1.2065, MS: 0.4629-0.8895] / akdk85179td / FD+(eiFi) / TD-313 / (1103)

Elemental Composition

| Parameters | | Elements Set 4: | | | | | |
|---|---|---|---|---|---|---|---|
| Tolerance: | ±20.00 ppm | Symbol | C | H | N | O | Mo |
| Electron: | Odd/Even | Min | 17 | 13 | 0 | 8 | 1 |
| Charge: | +1 | Max | 17 | 13 | 1 | 8 | 1 |
| DBE: | 0.5 - 100.0 | | | | | | |

Results

| Mass | Intensity | Formula | Calculated Mass | Mass Difference (ppm) | DBE |
|---|---|---|---|---|---|
| 456.96936 | 1102.51 | C17 H13 N O8 Mo | 456.96898 | 0.83 | 12.0 |

1 / 1

*Figure A3-3: Mass accuracy calculation for m/z = 456.96936.*

Spectrum

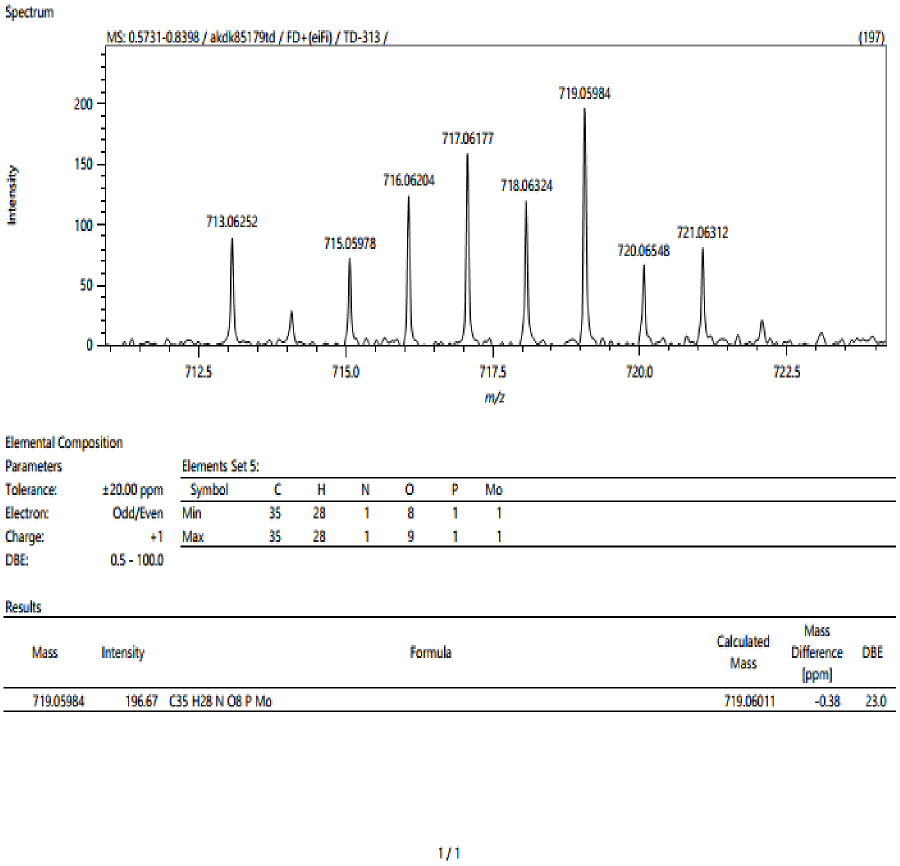

Elemental Composition

| Parameters | | Elements Set 5: | | | | | | |
|---|---|---|---|---|---|---|---|---|
| Tolerance: | ±20.00 ppm | Symbol | C | H | N | O | P | Mo |
| Electron: | Odd/Even | Min | 35 | 28 | 1 | 8 | 1 | 1 |
| Charge: | +1 | Max | 35 | 28 | 1 | 9 | 1 | 1 |
| DBE: | 0.5 - 100.0 | | | | | | | |

Results

| Mass | Intensity | Formula | Calculated Mass | Mass Difference [ppm] | DBE |
|---|---|---|---|---|---|
| 719.05984 | 196.67 | C35 H28 N O8 P Mo | 719.06011 | -0.38 | 23.0 |

1 / 1

*Figure A-3-4: Mass accuracy calculation for m/z = 719.05984.*

Spectrum

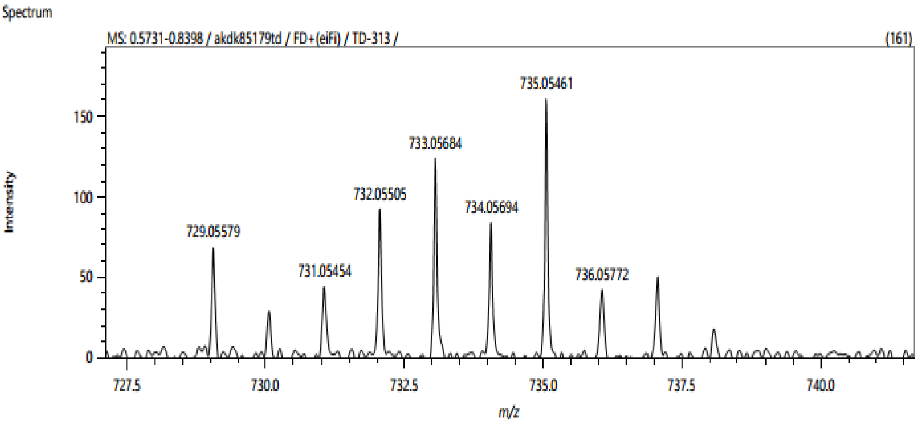

Elemental Composition

Parameters

Tolerance: ±20.00 ppm
Electron: Odd/Even
Charge: +1
DBE: 0.5 - 100.0

Elements Set 5:

| Symbol | C | H | N | O | P | Mo |
|---|---|---|---|---|---|---|
| Min | 35 | 28 | 1 | 9 | 1 | 1 |
| Max | 35 | 28 | 1 | 9 | 1 | 1 |

Results

| Mass | Intensity | Formula | Calculated Mass | Mass Difference [ppm] | DBE |
|---|---|---|---|---|---|
| 735.05461 | 160.72 | C35 H28 N O9 P Mo | 735.05503 | -0.57 | 23.0 |

1 / 1

*Figure A-3-5: Mass accuracy calculation for m/z = 735.05461.*

Spectrum

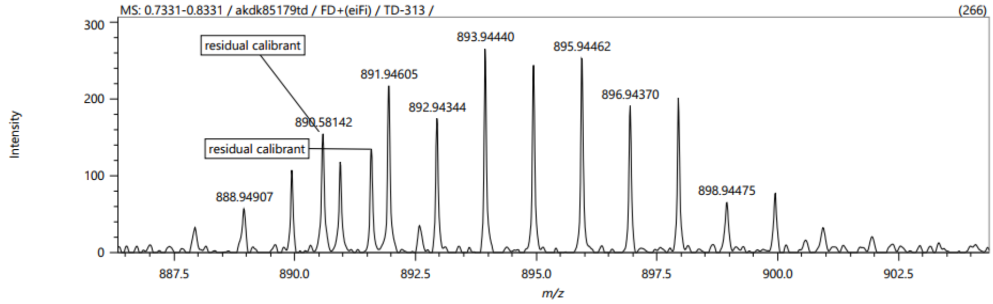

Elemental Composition

| Parameters | |
|---|---|
| Tolerance: | ±20.00 ppm |
| Electron: | Odd/Even |
| Charge: | +1 |
| DBE: | 0.5 - 100.0 |

Elements Set 4:

| Symbol | C | H | N | O | Mo |
|---|---|---|---|---|---|
| Min | 34 | 26 | 2 | 15 | 1 |
| Max | 34 | 26 | 2 | 15 | 2 |

Results

| Mass | Intensity | Formula | Calculated Mass | Mass Difference [ppm] | DBE |
|---|---|---|---|---|---|
| 897.94439 | 202.04 | C34 H26 N2 O15 Mo2 | 897.94359 | 0.90 | 23.0 |

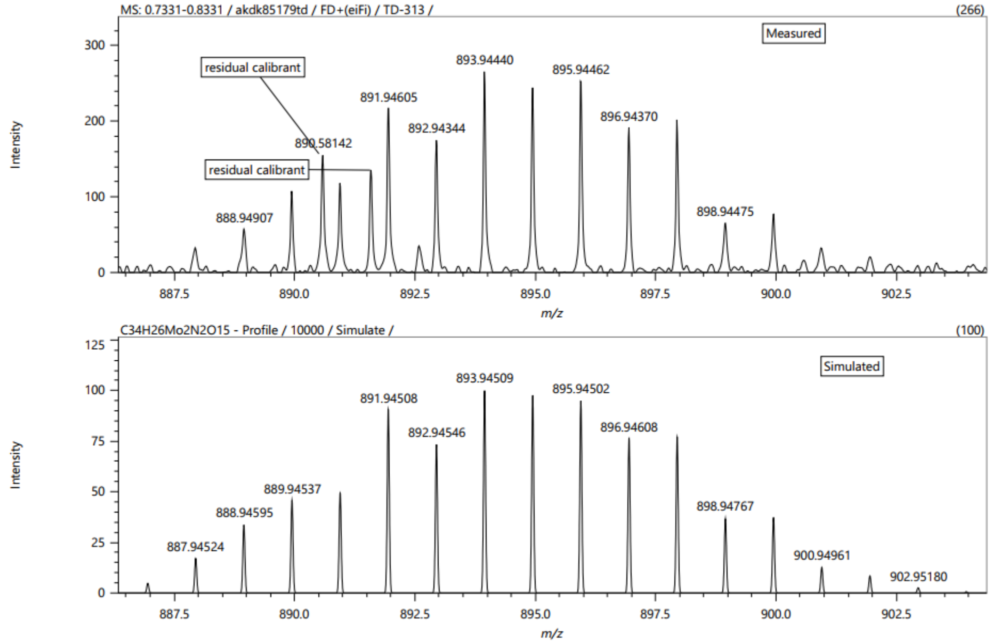

*Figure A-3-6: Mass accuracy calculation for m/z = 897.94439 (top) and comparison between measured and simulated isotope pattern (bottom).*

# A-4 Crystal structures of Mo-2, Mo-7 and W-1

## A-4.1 Crystal structure of Mo-2

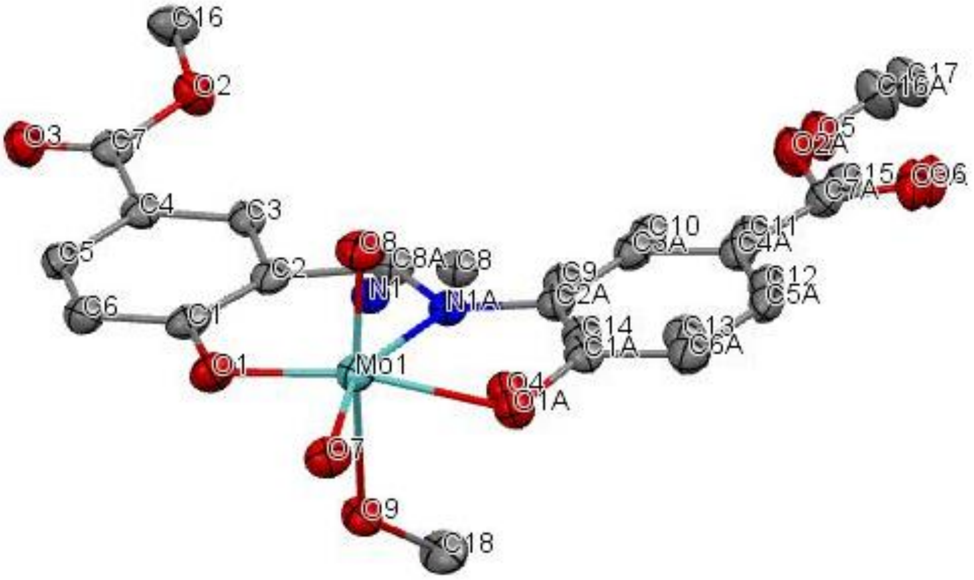

*Figure A-4.1-1: ORTEP plot (50 % probability) of the crystal structure of **Mo-2**. Hydrogen atoms omitted for clarity.*

Refinement Special Details

The ligand was disordered, and part was modelled in two positions with refined occupancies of 0.857:0.143(4). The ADP of adjacent or equivalent pairs of atoms in the disordered part were constrained to be equal as follows:
C8 & C8A, C9 & C2A, C10 & C3A, C11 & C4A, C12 & C5A, C13 & C6A, C14 & C1A, C15 & C7A, C17 & C16A, N1 & N1A, O4 & O1A, O5 & O2A, O6 & O3A.
Several pairs of bonds were restrained to be equal as follows:
N1-C8 & N1A-C8A, O5-C15 & O2A-C7A, C7A-C4A & C11-C15, O3A-C7A & O6-C15, O2A-C16A & O5-C17.

*Table A-4.1-1: Crystallographic data for* ***Mo-2.***

| | |
|---|---|
| Identification code | akdk2009 |
| Empirical formula | $C_{18}H_{17}MoNO_9$ |
| Formula weight | 487.27 |
| Temperature/K | 110.00(10) |
| Crystal system | monoclinic |
| Space group | $P2_1/c$ |
| a/Å | 6.8609(2) |
| b/Å | 31.9207(9) |
| c/Å | 8.6525(3) |
| α/° | 90 |
| β/° | 97.813(3) |
| γ/° | 90 |
| Volume/Å$^3$ | 1877.36(11) |
| Z | 4 |
| $\rho_{calc}$g/cm$^3$ | 1.724 |
| μ/mm$^{-1}$ | 6.208 |
| F(000) | 984.0 |
| Crystal size/mm$^3$ | 0.31 × 0.088 × 0.047 |
| Radiation | Cu Kα (λ = 1.54184) |
| 2Θ range for data collection/° | 10.686 to 134.16 |
| Index ranges | $-8 \le h \le 8, -34 \le k \le 38, -10 \le l \le 10$ |
| Reflections collected | 12024 |
| Independent reflections | 3349 [$R_{int}$ = 0.0489, $R_{sigma}$ = 0.0429] |
| Data/restraints/parameters | 3349/5/298 |
| Goodness-of-fit on F$^2$ | 1.092 |
| Final R indexes [I>=2σ (I)] | $R_1$ = 0.0339, w$R_2$ = 0.0850 |
| Final R indexes [all data] | $R_1$ = 0.0398, w$R_2$ = 0.0888 |
| Largest diff. peak/hole / e Å$^{-3}$ | 0.52/-0.82 |

**Table A-4.1-2 Fractional Atomic Coordinates (×10$^4$) and Equivalent Isotropic Displacement Parameters (Å$^2$×10$^3$) for Mo-2. $U_{eq}$ is defined as 1/3 of of the trace of the orthogonalised $U_{IJ}$ tensor.**

| **Atom** | ***x*** | ***y*** | ***z*** | **U(eq)** |
|---|---|---|---|---|
| $C_1$ | 2310(5) | 5501.0(10) | 4409(4) | 25.7(7) |
| $C_2$ | 3701(5) | 5818.9(10) | 4299(4) | 24.7(7) |
| $C_3$ | 5247(5) | 5753.3(9) | 3443(4) | 23.6(7) |
| $C_4$ | 5445(5) | 5361.3(9) | 2759(4) | 23.0(7) |
| $C_{4A}$ | 4230(40) | 7582(7) | 6550(30) | 27.1(9) |
| $C_{5A}$ | 2650(50) | 7674(6) | 7350(40) | 29.2(11) |
| $C_{6A}$ | 1300(40) | 7364(8) | 7570(30) | 29.4(10) |
| $C_{1A}$ | 1520(30) | 6962(6) | 7000(30) | 24.5(9) |
| $C_{2A}$ | 3100(30) | 6870(6) | 6210(20) | 23.0(9) |
| $C_{3A}$ | 4450(30) | 7180(8) | 5980(30) | 24.8(9) |
| $C_5$ | 4094(5) | 5039.8(9) | 2939(4) | 24.4(7) |
| $C_6$ | 2538(5) | 5108.8(10) | 3748(4) | 26.2(7) |

| | | | | |
|---|---|---|---|---|
| $C_{7}$ | 7039(5) | 5283.3(10) | 1808(4) | 25.6(7) |
| $C_{7A}$ | 5580(50) | 7929(9) | 6360(60) | 28.5(10) |
| $C_{8}$ | 4394(5) | 6500.6(12) | 5250(4) | 21.8(8) |
| $C_{8A}$ | 4080(40) | 6276(9) | 4860(30) | 21.8(8) |
| $C_{9}$ | 3956(7) | 6891.2(11) | 5984(5) | 23.0(9) |
| $C_{10}$ | 5214(6) | 7233.5(13) | 5852(5) | 24.8(9) |
| $C_{11}$ | 4788(7) | 7626.0(14) | 6417(6) | 27.1(9) |
| $C_{12}$ | 3093(8) | 7681.3(14) | 7119(6) | 29.2(11) |
| $C_{13}$ | 1877(7) | 7350.6(14) | 7315(6) | 29.4(10) |
| $C_{14}$ | 2316(7) | 6949.4(12) | 6763(5) | 24.5(9) |
| $C_{15}$ | 6025(8) | 8003.1(14) | 6256(8) | 28.5(10) |
| $C_{16}$ | 9546(6) | 5592.9(11) | 566(4) | 33.5(8) |
| $C_{16A}$ | 8370(60) | 8169(12) | 5340(50) | 39.5(12) |
| $C_{17}$ | 8838(9) | 8283.7(15) | 5354(7) | 39.5(12) |
| $C_{18}$ | 3867(6) | 6057.0(12) | 9008(4) | 38.1(9) |
| $Mo_{1}$ | 162.1(4) | 6134.9(2) | 5951.3(3) | 22.99(11) |
| $N_{1}$ | 3218(5) | 6183.2(9) | 5094(4) | 19.7(7) |
| $N_{1A}$ | 2940(30) | 6465(5) | 5680(20) | 19.7(7) |
| $O_{1}$ | 769(4) | 5577.7(7) | 5175(3) | 29.6(5) |
| $O_{1A}$ | 250(30) | 6671(6) | 7320(20) | 26.0(7) |
| $O_{2}$ | 8017(4) | 5631.3(7) | 1547(3) | 29.5(5) |
| $O_{2A}$ | 7090(40) | 7821(9) | 5610(40) | 35.4(9) |
| $O_{3}$ | 7421(4) | 4946.3(7) | 1275(3) | 32.1(6) |
| $O_{3A}$ | 5240(70) | 8290(10) | 6650(80) | 33.3(12) |
| $O_{4}$ | 1123(5) | 6635.7(8) | 7073(3) | 26.0(7) |
| $O_{5}$ | 7618(6) | 7921.6(10) | 5552(5) | 35.4(9) |
| $O_{6}$ | 5635(8) | 8346.7(14) | 6710(11) | 33.3(12) |
| $O_{7}$ | -1764(4) | 5983.3(7) | 6876(3) | 30.2(5) |
| $O_{8}$ | -857(4) | 6370.9(8) | 4281(3) | 31.9(5) |
| $O_{9}$ | 2279(4) | 5865.1(8) | 8015(3) | 28.2(5) |

**Table A-4.1-3 Anisotropic Displacement Parameters (Å$^2$×10$^3$) for Mo-2. The Anisotropic displacement factor exponent takes the form: $-2\pi^2[h^2a^{*2}U_{11}+2hka^*b^*U_{12}+…]$.**

| **Atom** | **$U_{11}$** | **$U_{22}$** | **$U_{33}$** | **$U_{23}$** | **$U_{13}$** | **$U_{12}$** |
|---|---|---|---|---|---|---|
| $C_{1}$ | 21.0(17) | 35.7(17) | 19.7(16) | 0.8(13) | 0.1(13) | 3.2(13) |
| $C_{2}$ | 27.5(18) | 24.8(15) | 19.7(16) | 0.4(12) | -4.2(13) | 7.1(13) |
| $C_{3}$ | 24.6(17) | 20.4(14) | 23.6(16) | 2.5(12) | -4.3(13) | -1.0(12) |
| $C_{4}$ | 20.6(17) | 24.6(15) | 22.4(16) | 2.9(12) | -2.6(13) | 1.7(12) |
| $C_{4A}$ | 29(3) | 23.7(19) | 26(2) | -0.2(15) | -4.7(19) | 0.5(18) |
| $C_{5A}$ | 37(3) | 23.2(16) | 24(2) | -4.2(14) | -5(2) | 0.8(16) |
| $C_{6A}$ | 30(3) | 29.1(18) | 28(2) | -0.8(16) | 0.9(19) | 2.8(19) |
| $C_{1A}$ | 21(2) | 24.1(17) | 26(2) | 2.4(15) | -4.4(19) | 0.6(17) |
| $C_{2A}$ | 23(2) | 23.5(18) | 21.6(19) | 0.3(14) | -1.2(17) | 0.7(18) |
| $C_{3A}$ | 23(2) | 27.9(19) | 22.6(18) | -1.1(14) | -0.9(18) | 0.4(18) |
| $C_{5}$ | 26.8(18) | 22.7(14) | 22.6(16) | -1.4(12) | -0.7(13) | 0.3(12) |
| $C_{6}$ | 24.6(18) | 27.6(16) | 25.4(17) | 1.7(13) | -0.6(14) | -3.9(13) |
| $C_{7}$ | 24.2(18) | 26.2(16) | 24.6(17) | 4.2(13) | -3.1(14) | 3.6(13) |
| $C_{7A}$ | 34(3) | 26(2) | 24(2) | -1(2) | -3(2) | -2.8(18) |
| $C_{8}$ | 15.5(18) | 27(2) | 23.1(19) | 2.7(16) | 1.8(15) | 0.6(15) |
| $C_{8A}$ | 15.5(18) | 27(2) | 23.1(19) | 2.7(16) | 1.8(15) | 0.6(15) |
| $C_{9}$ | 23(2) | 23.5(18) | 21.6(19) | 0.3(14) | -1.2(17) | 0.7(18) |
| $C_{10}$ | 23(2) | 27.9(19) | 22.6(18) | -1.1(14) | -0.9(18) | 0.4(18) |
| $C_{11}$ | 29(3) | 23.7(19) | 26(2) | -0.2(15) | -4.7(19) | 0.5(18) |
| $C_{12}$ | 37(3) | 23.2(16) | 24(2) | -4.2(14) | -5(2) | 0.8(16) |

| | | | | | | |
|---|---|---|---|---|---|---|
| $C_{13}$ | 30(3) | 29.1(18) | 28(2) | -0.8(16) | 0.9(19) | 2.8(19) |
| $C_{14}$ | 21(2) | 24.1(17) | 26(2) | 2.4(15) | -4.4(19) | 0.6(17) |
| $C_{15}$ | 34(3) | 26(2) | 24(2) | -1(2) | -3(2) | -2.8(18) |
| $C_{16}$ | 29.8(19) | 38.9(19) | 33.3(19) | 6.2(15) | 10.1(15) | 2.1(15) |
| $C_{16A}$ | 40(3) | 30(3) | 49(3) | 3(2) | 8(2) | -10(2) |
| $C_{17}$ | 40(3) | 30(3) | 49(3) | 3(2) | 8(2) | -10(2) |
| $C_{18}$ | 34(2) | 43(2) | 33(2) | 4.9(16) | -14.2(16) | -9.5(16) |
| $Mo_{1}$ | 18.49(16) | 26.01(16) | 23.43(16) | 1.29(10) | -0.85(10) | -2.01(10) |
| $N_{1}$ | 14.7(16) | 23.7(15) | 20.5(15) | 1.0(12) | 1.8(13) | 0.0(12) |
| $N_{1A}$ | 14.7(16) | 23.7(15) | 20.5(15) | 1.0(12) | 1.8(13) | 0.0(12) |
| $O_{1}$ | 26.6(13) | 36.2(12) | 26.8(12) | -1.5(10) | 6.8(10) | 1.3(10) |
| $O_{1A}$ | 24.1(19) | 26.2(13) | 28.0(15) | -0.1(11) | 4.9(13) | -0.2(13) |
| $O_{2}$ | 28.7(13) | 25.2(11) | 35.8(13) | 3.1(10) | 8.6(11) | 0.4(10) |
| $O_{2A}$ | 39(2) | 25(2) | 43.9(16) | -3.5(16) | 8.9(17) | -6.8(15) |
| $O_{3}$ | 37.4(15) | 22.9(11) | 37.4(14) | -1.1(10) | 9.6(11) | 3.8(10) |
| $O_{3A}$ | 35(3) | 21.6(19) | 40.6(17) | -8.8(18) | -6(3) | -0.7(16) |
| $O_{4}$ | 24.1(19) | 26.2(13) | 28.0(15) | -0.1(11) | 4.9(13) | -0.2(13) |
| $O_{5}$ | 39(2) | 25(2) | 43.9(16) | -3.5(16) | 8.9(17) | -6.8(15) |
| $O_{6}$ | 35(3) | 21.6(19) | 40.6(17) | -8.8(18) | -6(3) | -0.7(16) |
| $O_{7}$ | 24.9(13) | 35.9(12) | 29.3(13) | 1.3(10) | 1.9(10) | 2.3(10) |
| $O_{8}$ | 24.5(13) | 39.2(13) | 30.4(13) | 6.1(10) | -2.6(10) | -0.7(10) |
| $O_{9}$ | 24.9(13) | 26.9(12) | 30.3(13) | 5.1(10) | -5.1(10) | -4.3(10) |

**Table A-4.1-4 Bond Lengths for Mo-2.**

| Atom | Atom | Length/Å | | Atom | Atom | Length/Å |
|---|---|---|---|---|---|---|
| $C_{1}$ | $C_{2}$ | 1.405(5) | | $C_{8}$ | $N_{1}$ | 1.291(5) |
| $C_{1}$ | $C_{6}$ | 1.394(5) | | $C_{8A}$ | $N_{1A}$ | 1.276(17) |
| $C_{1}$ | $O_{1}$ | 1.345(4) | | $C_{9}$ | $C_{10}$ | 1.406(5) |
| $C_{2}$ | $C_{3}$ | 1.390(5) | | $C_{9}$ | $C_{14}$ | 1.401(6) |
| $C_{2}$ | $C_{8A}$ | 1.55(3) | | $C_{10}$ | $C_{11}$ | 1.390(5) |
| $C_{2}$ | $N_{1}$ | 1.413(4) | | $C_{11}$ | $C_{12}$ | 1.394(6) |
| $C_{3}$ | $C_{4}$ | 1.399(4) | | $C_{11}$ | $C_{15}$ | 1.490(5) |
| $C_{4}$ | $C_{5}$ | 1.406(4) | | $C_{12}$ | $C_{13}$ | 1.370(6) |
| $C_{4}$ | $C_{7}$ | 1.476(5) | | $C_{13}$ | $C_{14}$ | 1.414(6) |
| $C_{4A}$ | $C_{5A}$ | 1.3900 | | $C_{14}$ | $O_{4}$ | 1.343(5) |
| $C_{4A}$ | $C_{3A}$ | 1.3900 | | $C_{15}$ | $O_{5}$ | 1.347(5) |
| $C_{4A}$ | $C_{7A}$ | 1.466(19) | | $C_{15}$ | $O_{6}$ | 1.207(5) |
| $C_{5A}$ | $C_{6A}$ | 1.3900 | | $C_{16}$ | $O_{2}$ | 1.442(4) |
| $C_{6A}$ | $C_{1A}$ | 1.3900 | | $C_{16A}$ | $O_{2A}$ | 1.450(19) |
| $C_{1A}$ | $C_{2A}$ | 1.3900 | | $C_{17}$ | $O_{5}$ | 1.451(5) |
| $C_{1A}$ | $O_{1A}$ | 1.33(2) | | $C_{18}$ | $O_{9}$ | 1.431(4) |
| $C_{2A}$ | $C_{3A}$ | 1.3900 | | $Mo_{1}$ | $N_{1}$ | 2.322(4) |
| $C_{2A}$ | $N_{1A}$ | 1.37(2) | | $Mo_{1}$ | $N_{1A}$ | 2.216(18) |
| $C_{5}$ | $C_{6}$ | 1.372(5) | | $Mo_{1}$ | $O_{1}$ | 1.966(2) |
| $C_{7}$ | $O_{2}$ | 1.333(4) | | $Mo_{1}$ | $O_{1A}$ | 2.077(19) |
| $C_{7}$ | $O_{3}$ | 1.213(4) | | $Mo_{1}$ | $O_{4}$ | 1.938(3) |
| $C_{7A}$ | $O_{2A}$ | 1.345(19) | | $Mo_{1}$ | $O_{7}$ | 1.705(2) |
| $C_{7A}$ | $O_{3A}$ | 1.209(18) | | $Mo_{1}$ | $O_{8}$ | 1.695(2) |
| $C_{8}$ | $C_{9}$ | 1.449(5) | | $Mo_{1}$ | $O_{9}$ | 2.309(2) |

**Table A-4.1-5 Bond Angles for Mo-2.**

| Atom | Atom | Atom | Angle/˚ | | Atom | Atom | Atom | Angle/˚ |
|---|---|---|---|---|---|---|---|---|
| $C_{6}$ | $C_{1}$ | $C_{2}$ | 120.4(3) | | $C_{9}$ | $C_{14}$ | $C_{13}$ | 120.3(4) |
| $O_{1}$ | $C_{1}$ | $C_{2}$ | 119.2(3) | | $O_{4}$ | $C_{14}$ | $C_{9}$ | 123.3(4) |

|  |  |  |  |  |  |  |  |  |
|---|---|---|---|---|---|---|---|---|
| $O_1$ | $C_1$ | $C_6$ | 120.4(3) |  | $O_4$ | $C_{14}$ | $C_{13}$ | 116.4(4) |
| $C_1$ | $C_2$ | $C_{8A}$ | 138.1(9) |  | $O_5$ | $C_{15}$ | $C_{11}$ | 113.2(4) |
| $C_1$ | $C_2$ | $N_1$ | 110.8(3) |  | $O_6$ | $C_{15}$ | $C_{11}$ | 123.3(5) |
| $C_3$ | $C_2$ | $C_1$ | 120.1(3) |  | $O_6$ | $C_{15}$ | $O_5$ | 123.5(5) |
| $C_3$ | $C_2$ | $C_{8A}$ | 101.7(9) |  | $N_{1A}$ | $Mo_1$ | $O_9$ | 78.4(5) |
| $C_3$ | $C_2$ | $N_1$ | 129.0(3) |  | $O_1$ | $Mo_1$ | $N_1$ | 73.07(10) |
| $C_2$ | $C_3$ | $C_4$ | 119.1(3) |  | $O_1$ | $Mo_1$ | $N_{1A}$ | 99.7(4) |
| $C_3$ | $C_4$ | $C_5$ | 120.2(3) |  | $O_1$ | $Mo_1$ | $O_{1A}$ | 161.6(6) |
| $C_3$ | $C_4$ | $C_7$ | 120.6(3) |  | $O_1$ | $Mo_1$ | $O_9$ | 77.68(10) |
| $C_5$ | $C_4$ | $C_7$ | 119.2(3) |  | $O_{1A}$ | $Mo_1$ | $N_{1A}$ | 73.1(7) |
| $C_{5A}$ | $C_{4A}$ | $C_{3A}$ | 120.0 |  | $O_{1A}$ | $Mo_1$ | $O_9$ | 84.2(5) |
| $C_{5A}$ | $C_{4A}$ | $C_{7A}$ | 116(2) |  | $O_4$ | $Mo_1$ | $N_1$ | 81.06(12) |
| $C_{3A}$ | $C_{4A}$ | $C_{7A}$ | 124(2) |  | $O_4$ | $Mo_1$ | $O_1$ | 147.54(12) |
| $C_{6A}$ | $C_{5A}$ | $C_{4A}$ | 120.0 |  | $O_4$ | $Mo_1$ | $O_9$ | 77.60(10) |
| $C_{5A}$ | $C_{6A}$ | $C_{1A}$ | 120.0 |  | $O_7$ | $Mo_1$ | $N_1$ | 163.66(11) |
| $C_{2A}$ | $C_{1A}$ | $C_{6A}$ | 120.0 |  | $O_7$ | $Mo_1$ | $N_{1A}$ | 156.3(4) |
| $O_{1A}$ | $C_{1A}$ | $C_{6A}$ | 117.9(19) |  | $O_7$ | $Mo_1$ | $O_1$ | 96.72(11) |
| $O_{1A}$ | $C_{1A}$ | $C_{2A}$ | 122.0(19) |  | $O_7$ | $Mo_1$ | $O_{1A}$ | 86.0(6) |
| $C_{3A}$ | $C_{2A}$ | $C_{1A}$ | 120.0 |  | $O_7$ | $Mo_1$ | $O_4$ | 103.40(13) |
| $N_{1A}$ | $C_{2A}$ | $C_{1A}$ | 109.4(19) |  | $O_7$ | $Mo_1$ | $O_9$ | 88.70(10) |
| $N_{1A}$ | $C_{2A}$ | $C_{3A}$ | 130.5(18) |  | $O_8$ | $Mo_1$ | $N_1$ | 89.07(12) |
| $C_{2A}$ | $C_{3A}$ | $C_{4A}$ | 120.0 |  | $O_8$ | $Mo_1$ | $N_{1A}$ | 87.7(5) |
| $C_6$ | $C_5$ | $C_4$ | 120.7(3) |  | $O_8$ | $Mo_1$ | $O_1$ | 101.11(11) |
| $C_5$ | $C_6$ | $C_1$ | 119.5(3) |  | $O_8$ | $Mo_1$ | $O_{1A}$ | 95.6(5) |
| $O_2$ | $C_7$ | $C_4$ | 112.5(3) |  | $O_8$ | $Mo_1$ | $O_4$ | 97.66(12) |
| $O_3$ | $C_7$ | $C_4$ | 125.1(3) |  | $O_8$ | $Mo_1$ | $O_7$ | 105.67(12) |
| $O_3$ | $C_7$ | $O_2$ | 122.4(3) |  | $O_8$ | $Mo_1$ | $O_9$ | 165.59(11) |
| $O_{2A}$ | $C_{7A}$ | $C_{4A}$ | 114(2) |  | $O_9$ | $Mo_1$ | $N_1$ | 76.80(10) |
| $O_{3A}$ | $C_{7A}$ | $C_{4A}$ | 124(3) |  | $C_2$ | $N_1$ | $Mo_1$ | 112.5(2) |
| $O_{3A}$ | $C_{7A}$ | $O_{2A}$ | 122(4) |  | $C_8$ | $N_1$ | $C_2$ | 120.8(4) |
| $N_1$ | $C_8$ | $C_9$ | 123.9(4) |  | $C_8$ | $N_1$ | $Mo_1$ | 126.7(3) |
| $N_{1A}$ | $C_{8A}$ | $C_2$ | 122(2) |  | $C_{2A}$ | $N_{1A}$ | $Mo_1$ | 116.4(14) |
| $C_{10}$ | $C_9$ | $C_8$ | 117.9(4) |  | $C_{8A}$ | $N_{1A}$ | $C_{2A}$ | 127(2) |
| $C_{14}$ | $C_9$ | $C_8$ | 123.6(4) |  | $C_{8A}$ | $N_{1A}$ | $Mo_1$ | 115.7(19) |
| $C_{14}$ | $C_9$ | $C_{10}$ | 118.5(3) |  | $C_1$ | $O_1$ | $Mo_1$ | 123.4(2) |
| $C_{11}$ | $C_{10}$ | $C_9$ | 120.8(4) |  | $C_{1A}$ | $O_{1A}$ | $Mo_1$ | 115.4(16) |
| $C_{10}$ | $C_{11}$ | $C_{12}$ | 119.6(4) |  | $C_7$ | $O_2$ | $C_{16}$ | 116.9(3) |
| $C_{10}$ | $C_{11}$ | $C_{15}$ | 123.1(4) |  | $C_{7A}$ | $O_{2A}$ | $C_{16A}$ | 114(3) |
| $C_{12}$ | $C_{11}$ | $C_{15}$ | 117.2(4) |  | $C_{14}$ | $O_4$ | $Mo_1$ | 133.6(3) |
| $C_{13}$ | $C_{12}$ | $C_{11}$ | 121.0(4) |  | $C_{15}$ | $O_5$ | $C_{17}$ | 114.6(4) |
| $C_{12}$ | $C_{13}$ | $C_{14}$ | 119.7(4) |  | $C_{18}$ | $O_9$ | $Mo_1$ | 130.7(2) |

**Table A-4.1-6 Torsion Angles for Mo-2.**

| **A** | **B** | **C** | **D** | **Angle/˚** |  | **A** | **B** | **C** | **D** | **Angle/˚** |
|---|---|---|---|---|---|---|---|---|---|---|
| $C_1$ | $C_2$ | $C_3$ | $C_4$ | -2.9(5) |  | $C_6$ | $C_1$ | $C_2$ | $N_1$ | -177.9(3) |
| $C_1$ | $C_2$ | $C_{8A}$ | $N_{1A}$ | 0(3) |  | $C_6$ | $C_1$ | $O_1$ | $Mo_1$ | -173.2(2) |
| $C_1$ | $C_2$ | $N_1$ | $C_8$ | 174.1(3) |  | $C_7$ | $C_4$ | $C_5$ | $C_6$ | -176.6(3) |
| $C_1$ | $C_2$ | $N_1$ | $Mo_1$ | -7.5(3) |  | $C_{7A}$ | $C_{4A}$ | $C_{5A}$ | $C_{6A}$ | 179(3) |
| $C_2$ | $C_1$ | $C_6$ | $C_5$ | -2.4(5) |  | $C_{7A}$ | $C_{4A}$ | $C_{3A}$ | $C_{2A}$ | -179(4) |
| $C_2$ | $C_1$ | $O_1$ | $Mo_1$ | 7.6(4) |  | $C_8$ | $C_9$ | $C_{10}$ | $C_{11}$ | 174.7(4) |
| $C_2$ | $C_3$ | $C_4$ | $C_5$ | 0.0(5) |  | $C_8$ | $C_9$ | $C_{14}$ | $C_{13}$ | -173.7(4) |
| $C_2$ | $C_3$ | $C_4$ | $C_7$ | 178.4(3) |  | $C_8$ | $C_9$ | $C_{14}$ | $O_4$ | 8.5(6) |
| $C_2$ | $C_{8A}$ | $N_{1A}$ | $C_{2A}$ | -178.2(18) |  | $C_{8A}$ | $C_2$ | $C_3$ | $C_4$ | 178.4(10) |
| $C_2$ | $C_{8A}$ | $N_{1A}$ | $Mo_1$ | -9(3) |  | $C_9$ | $C_8$ | $N_1$ | $C_2$ | 177.0(3) |
| $C_3$ | $C_2$ | $C_{8A}$ | $N_{1A}$ | 178.7(19) |  | $C_9$ | $C_8$ | $N_1$ | $Mo_1$ | -1.2(5) |

| | | | | | | | | | |
|---|---|---|---|---|---|---|---|---|---|
| $C_3$ | $C_2$ | $N_1$ | $C_8$ | -8.2(5) | $C_9$ | $C_{10}$ | $C_{11}$ | $C_{12}$ | -0.1(6) |
| $C_3$ | $C_2$ | $N_1$ | $Mo_1$ | 170.2(3) | $C_9$ | $C_{10}$ | $C_{11}$ | $C_{15}$ | -177.6(5) |
| $C_3$ | $C_4$ | $C_5$ | $C_6$ | 1.8(5) | $C_9$ | $C_{14}$ | $O_4$ | $Mo_1$ | -36.3(6) |
| $C_3$ | $C_4$ | $C_7$ | $O_2$ | -7.9(4) | $C_{10}$ | $C_9$ | $C_{14}$ | $C_{13}$ | 3.9(6) |
| $C_3$ | $C_4$ | $C_7$ | $O_3$ | 173.8(3) | $C_{10}$ | $C_9$ | $C_{14}$ | $O_4$ | -174.0(4) |
| $C_4$ | $C_5$ | $C_6$ | $C_1$ | -0.6(5) | $C_{10}$ | $C_{11}$ | $C_{12}$ | $C_{13}$ | 2.5(6) |
| $C_4$ | $C_7$ | $O_2$ | $C_{16}$ | -177.1(3) | $C_{10}$ | $C_{11}$ | $C_{15}$ | $O_5$ | -1.8(8) |
| $C_{4A}$ | $C_{5A}$ | $C_{6A}$ | $C_{1A}$ | 0.0 | $C_{10}$ | $C_{11}$ | $C_{15}$ | $O_6$ | 178.1(7) |
| $C_{4A}$ | $C_{7A}$ | $O_{2A}$ | $C_{16A}$ | 177(4) | $C_{11}$ | $C_{12}$ | $C_{13}$ | $C_{14}$ | -1.7(6) |
| $C_{5A}$ | $C_{4A}$ | $C_{3A}$ | $C_{2A}$ | 0.0 | $C_{11}$ | $C_{15}$ | $O_5$ | $C_{17}$ | 179.0(5) |
| $C_{5A}$ | $C_{4A}$ | $C_{7A}$ | $O_{2A}$ | 179(3) | $C_{12}$ | $C_{11}$ | $C_{15}$ | $O_5$ | -179.4(5) |
| $C_{5A}$ | $C_{4A}$ | $C_{7A}$ | $O_{3A}$ | -10(7) | $C_{12}$ | $C_{11}$ | $C_{15}$ | $O_6$ | 0.6(10) |
| $C_{5A}$ | $C_{6A}$ | $C_{1A}$ | $C_{2A}$ | 0.0 | $C_{12}$ | $C_{13}$ | $C_{14}$ | $C_9$ | -1.6(6) |
| $C_{5A}$ | $C_{6A}$ | $C_{1A}$ | $O_{1A}$ | 176(2) | $C_{12}$ | $C_{13}$ | $C_{14}$ | $O_4$ | 176.4(4) |
| $C_{6A}$ | $C_{1A}$ | $C_{2A}$ | $C_{3A}$ | 0.0 | $C_{13}$ | $C_{14}$ | $O_4$ | $Mo_1$ | 145.8(3) |
| $C_{6A}$ | $C_{1A}$ | $C_{2A}$ | $N_{1A}$ | -176(2) | $C_{14}$ | $C_9$ | $C_{10}$ | $C_{11}$ | -3.0(6) |
| $C_{6A}$ | $C_{1A}$ | $O_{1A}$ | $Mo_1$ | 163.4(13) | $C_{15}$ | $C_{11}$ | $C_{12}$ | $C_{13}$ | -179.8(5) |
| $C_{1A}$ | $C_{2A}$ | $C_{3A}$ | $C_{4A}$ | 0.0 | $N_1$ | $C_2$ | $C_3$ | $C_4$ | 179.6(3) |
| $C_{1A}$ | $C_{2A}$ | $N_{1A}$ | $C_{8A}$ | 177(2) | $N_1$ | $C_8$ | $C_9$ | $C_{10}$ | -169.9(3) |
| $C_{1A}$ | $C_{2A}$ | $N_{1A}$ | $Mo_1$ | 8.1(18) | $N_1$ | $C_8$ | $C_9$ | $C_{14}$ | 7.7(6) |
| $C_{2A}$ | $C_{1A}$ | $O_{1A}$ | $Mo_1$ | -20(2) | $N_{1A}$ | $C_{2A}$ | $C_{3A}$ | $C_{4A}$ | 175(2) |
| $C_{3A}$ | $C_{4A}$ | $C_{5A}$ | $C_{6A}$ | 0.0 | $O_1$ | $C_1$ | $C_2$ | $C_3$ | -176.6(3) |
| $C_{3A}$ | $C_{4A}$ | $C_{7A}$ | $O_{2A}$ | -2(6) | $O_1$ | $C_1$ | $C_2$ | $C_{8A}$ | 1.3(15) |
| $C_{3A}$ | $C_{4A}$ | $C_{7A}$ | $O_{3A}$ | 169(5) | $O_1$ | $C_1$ | $C_2$ | $N_1$ | 1.3(4) |
| $C_{3A}$ | $C_{2A}$ | $N_{1A}$ | $C_{8A}$ | 2(3) | $O_1$ | $C_1$ | $C_6$ | $C_5$ | 178.5(3) |
| $C_{3A}$ | $C_{2A}$ | $N_{1A}$ | $Mo_1$ | -167.7(13) | $O_{1A}$ | $C_{1A}$ | $C_{2A}$ | $C_{3A}$ | -176(2) |
| $C_5$ | $C_4$ | $C_7$ | $O_2$ | 170.5(3) | $O_{1A}$ | $C_{1A}$ | $C_{2A}$ | $N_{1A}$ | 7(2) |
| $C_5$ | $C_4$ | $C_7$ | $O_3$ | -7.8(5) | $O_3$ | $C_7$ | $O_2$ | $C_{16}$ | 1.2(5) |
| $C_6$ | $C_1$ | $C_2$ | $C_3$ | 4.2(5) | $O_{3A}$ | $C_{7A}$ | $O_{2A}$ | $C_{16A}$ | 6(7) |
| $C_6$ | $C_1$ | $C_2$ | $C_{8A}$ | -177.9(14) | $O_6$ | $C_{15}$ | $O_5$ | $C_{17}$ | -0.9(10) |

**Table A-4.1-7 Hydrogen Atom Coordinates (Å×$10^4$) and Isotropic Displacement Parameters (Å$^2$×$10^3$) for Mo-2.**

| **Atom** | ***x*** | ***y*** | ***z*** | **U(eq)** |
|---|---|---|---|---|
| $H_3$ | 6156.23 | 5971.48 | 3324.7 | 28 |
| $H_{5A}$ | 2500.83 | 7948.91 | 7734.94 | 35 |
| $H_{6A}$ | 218.5 | 7426.92 | 8114.11 | 35 |
| $H_{3A}$ | 5531.71 | 7117.44 | 5441.8 | 30 |
| $H_5$ | 4260.32 | 4772.06 | 2495.66 | 29 |
| $H_6$ | 1622.76 | 4890.99 | 3857.03 | 31 |
| $H_8$ | 5618.5 | 6476.67 | 4859.74 | 26 |
| $H_{8A}$ | 5191.22 | 6420.2 | 4587.98 | 26 |
| $H_{10}$ | 6367.02 | 7196.12 | 5372.08 | 30 |
| $H_{12}$ | 2776.69 | 7952.19 | 7465.74 | 35 |
| $H_{13}$ | 745.32 | 7390.77 | 7820.18 | 35 |
| $H_{16A}$ | 10361.74 | 5347.78 | 887.93 | 50 |
| $H_{16B}$ | 10366.1 | 5845.46 | 665.14 | 50 |
| $H_{16C}$ | 8951.12 | 5559.38 | -522.47 | 50 |
| $H_{16D}$ | 9634.71 | 8060.97 | 5112.46 | 59 |
| $H_{16E}$ | 8580.94 | 8344.27 | 6280.75 | 59 |
| $H_{16F}$ | 7751.77 | 8336.24 | 4460.57 | 59 |
| $H_{17A}$ | 10058.62 | 8192.29 | 4986.35 | 59 |
| $H_{17B}$ | 9150.53 | 8429.11 | 6354.3 | 59 |

| | | | | |
|---|---|---|---|---|
| $H_{17C}$ | 8127.55 | 8474.35 | 4586.57 | 59 |
| $H_{18A}$ | 5008.31 | 6083.46 | 8445.73 | 57 |
| $H_{18B}$ | 4218.04 | 5883.33 | 9938.63 | 57 |
| $H_{18C}$ | 3464.02 | 6335.46 | 9320.84 | 57 |
| $H_9$ | 2330(70) | 5636(14) | 8020(60) | 51(15) |

**Table A-4.1-8 Atomic Occupancy for Mo-2.**

| **Atom** | ***Occupancy*** | | **Atom** | ***Occupancy*** | | **Atom** | ***Occupancy*** |
|---|---|---|---|---|---|---|---|
| $C_{4A}$ | 0.143(4) | | $C_{5A}$ | 0.143(4) | | $H_{5A}$ | 0.143(4) |
| $C_{6A}$ | 0.143(4) | | $H_{6A}$ | 0.143(4) | | $C_{1A}$ | 0.143(4) |
| $C_{2A}$ | 0.143(4) | | $C_{3A}$ | 0.143(4) | | $H_{3A}$ | 0.143(4) |
| $C_{7A}$ | 0.143(4) | | $C_8$ | 0.857(4) | | $H_8$ | 0.857(4) |
| $C_{8A}$ | 0.143(4) | | $H_{8A}$ | 0.143(4) | | $C_9$ | 0.857(4) |
| $C_{10}$ | 0.857(4) | | $H_{10}$ | 0.857(4) | | $C_{11}$ | 0.857(4) |
| $C_{12}$ | 0.857(4) | | $H_{12}$ | 0.857(4) | | $C_{13}$ | 0.857(4) |
| $H_{13}$ | 0.857(4) | | $C_{14}$ | 0.857(4) | | $C_{15}$ | 0.857(4) |
| $C_{16A}$ | 0.143(4) | | $H_{16D}$ | 0.143(4) | | $H_{16E}$ | 0.143(4) |
| $H_{16F}$ | 0.143(4) | | $C_{17}$ | 0.857(4) | | $H_{17A}$ | 0.857(4) |
| $H_{17B}$ | 0.857(4) | | $H_{17C}$ | 0.857(4) | | $N_1$ | 0.857(4) |
| $N_{1A}$ | 0.143(4) | | $O_{1A}$ | 0.143(4) | | $O_{2A}$ | 0.143(4) |
| $O_{3A}$ | 0.143(4) | | $O_4$ | 0.857(4) | | $O_5$ | 0.857(4) |
| $O_6$ | 0.857(4) | | | | | | |

## A-4.2 Crystal structure of Mo-7

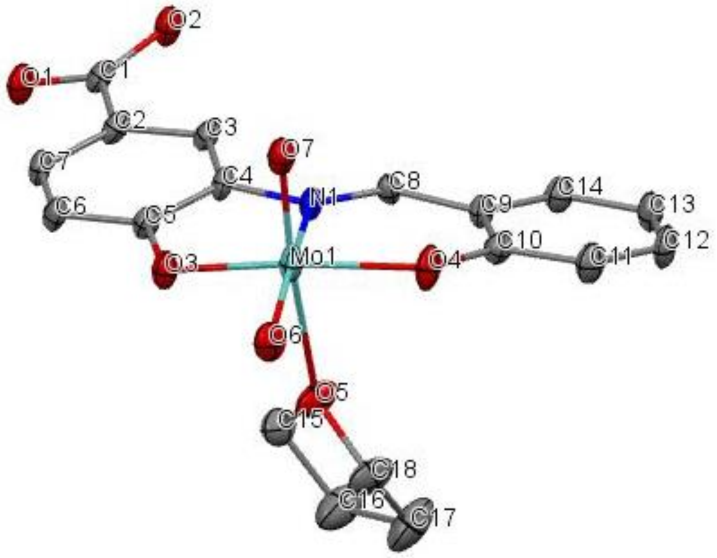

*Figure A-4.2-1: ORTEP plot (50 % probability) of the crystal structure of* ***Mo-7****. Hydrogen atoms omitted for clarity.*

Refinement special detail

The carboxylic acid proton was located by difference map, forced to ride on the oxygen and then the bond length reduced to 0.983 angstroms in the direction of the O-H bond.

The unit cell contained a highly disordered tetrahydrofuran which was modelled using a solvent mask. The volume masked was 195.6 cubic angstroms containing an estimated 42.7 electrons - consistent with the presence of a single THF.

*Table A-4.2-1: Crystallographic data for **Mo-7.***

| | |
|---|---|
| Identification code | akdk1803 |
| Empirical formula | $C_{20}H_{21}MoNO_{7.5}$ |
| Formula weight | 491.32 |
| Temperature/K | 110.00(14) |
| Crystal system | triclinic |
| Space group | P-1 |
| a/Å | 6.7460(4) |
| b/Å | 12.9235(11) |
| c/Å | 13.1613(11) |
| α/° | 61.601(9) |
| β/° | 87.263(6) |
| γ/° | 80.349(6) |
| Volume/Å$^3$ | 994.39(15) |
| Z | 2 |
| $\rho_{calc}$g/cm$^3$ | 1.641 |
| μ/mm$^{-1}$ | 5.806 |
| F(000) | 500.0 |
| Crystal size/mm$^3$ | 0.173 × 0.03 × 0.01 |
| Radiation | CuKα (λ = 1.54184) |
| 2Θ range for data collection/° | 7.642 to 134.156 |
| Index ranges | $-8 \leq h \leq 7$, $-15 \leq k \leq 14$, $-14 \leq l \leq 15$ |
| Reflections collected | 6214 |
| Independent reflections | 3537 [$R_{int}$ = 0.0423, $R_{sigma}$ = 0.0597] |
| Data/restraints/parameters | 3537/40/290 |
| Goodness-of-fit on F$^2$ | 1.052 |
| Final R indexes [I>=2σ (I)] | $R_1$ = 0.0376, $wR_2$ = 0.0931 |
| Final R indexes [all data] | $R_1$ = 0.0433, $wR_2$ = 0.0982 |
| Largest diff. peak/hole / e Å$^{-3}$ | 0.67/-0.83 |

**Table A-4.2-2 Fractional Atomic Coordinates (×10$^4$) and Equivalent Isotropic Displacement Parameters (Å$^2$×10$^3$) for Mo-7. $U_{eq}$ is defined as 1/3 of of the trace of the orthogonalised $U_{IJ}$ tensor.**

| Atom | *x* | *y* | *z* | U(eq) |
|---|---|---|---|---|
| C1 | 2409(5) | 164(3) | 9132(3) | 19.1(7) |
| C2 | 4271(5) | 328(3) | 8471(3) | 18.5(7) |
| C3 | 4336(5) | 1405(3) | 7478(3) | 17.6(7) |
| C4 | 6049(5) | 1565(3) | 6844(3) | 17.3(7) |
| C5 | 7756(5) | 660(3) | 7220(3) | 18.4(7) |
| C6 | 7688(5) | -409(3) | 8224(3) | 20.0(7) |
| C7 | 5944(5) | -580(3) | 8835(3) | 19.6(7) |
| C8 | 4839(5) | 3382(3) | 5191(3) | 17.2(7) |
| C9 | 4969(5) | 4391(3) | 4081(3) | 18.1(7) |
| C10 | 6795(5) | 4654(3) | 3511(3) | 20.0(7) |
| C11 | 6771(6) | 5686(3) | 2461(3) | 25.5(8) |
| C12 | 4967(6) | 6420(3) | 1951(3) | 28.3(9) |
| C13 | 3153(6) | 6178(3) | 2487(3) | 26.7(8) |
| C14 | 3170(5) | 5167(3) | 3541(3) | 21.7(7) |
| C15 | 6814(6) | 922(3) | 4506(3) | 28.1(8) |
| C16 | 6064(8) | 1083(4) | 3375(3) | 44.1(12) |
| C17 | 7119(7) | 2004(5) | 2442(4) | 47.5(12) |
| C18 | 8870(6) | 2067(4) | 3054(3) | 34.7(10) |
| Mo1 | 9613.6(4) | 2467.2(2) | 5302.7(2) | 18.68(10) |
| N1 | 6338(4) | 2569(2) | 5774(2) | 17.7(6) |
| O1 | 2211(4) | -878(2) | 9908(2) | 24.9(6) |
| O2 | 1069(4) | 1084(2) | 8892(2) | 25.1(6) |
| O3 | 9385(3) | 855(2) | 6572.1(19) | 21.0(5) |
| O4 | 8556(4) | 3953(2) | 3952(2) | 25.2(6) |
| O5 | 8202(4) | 1764(2) | 4204(2) | 29.9(6) |
| O6 | 11832(4) | 2079(2) | 4801(2) | 24.5(5) |
| O7 | 10247(4) | 3075(2) | 6105(2) | 22.8(5) |

**Table A-4.2-3 Anisotropic Displacement Parameters (Å$^2$×10$^3$) for Mo-7. The Anisotropic displacement factor exponent takes the form: $-2\pi^2[h^2a^{*2}U_{11}+2hka^*b^*U_{12}+\ldots]$.**

| Atom | $U_{11}$ | $U_{22}$ | $U_{33}$ | $U_{23}$ | $U_{13}$ | $U_{12}$ |
|---|---|---|---|---|---|---|
| C1 | 19.4(18) | 23.0(18) | 11.1(15) | -4.7(14) | -1.8(13) | -3.6(14) |
| C2 | 14.7(17) | 24.1(18) | 12.7(15) | -5.1(14) | -1.2(13) | -3.8(14) |
| C3 | 15.4(17) | 21.0(17) | 11.9(16) | -4.6(14) | -2.2(13) | -0.5(13) |
| C4 | 18.2(18) | 15.9(16) | 10.9(15) | -1.0(13) | -3.2(13) | -1.3(13) |
| C5 | 16.4(18) | 20.5(17) | 14.0(16) | -5.2(14) | 0.8(13) | -1.8(13) |
| C6 | 17.2(18) | 19.5(17) | 13.9(16) | -2.1(14) | -2.3(13) | 3.3(13) |
| C7 | 20.6(19) | 16.7(16) | 11.9(16) | 0.7(13) | -1.8(13) | -1.3(13) |
| C8 | 16.3(17) | 13.7(16) | 16.2(16) | -3.9(14) | 2.0(13) | 0.5(13) |
| C9 | 19.2(18) | 15.3(16) | 14.2(16) | -2.6(14) | 0.1(13) | -2.4(13) |
| C10 | 18.2(18) | 20.7(17) | 17.1(17) | -6.3(14) | -0.5(14) | -0.9(14) |
| C11 | 24(2) | 23.7(19) | 19.5(18) | -2.6(15) | 4.5(15) | -5.3(15) |
| C12 | 33(2) | 21.1(18) | 14.9(17) | 4.1(15) | 1.5(15) | -3.9(16) |
| C13 | 27(2) | 20.1(18) | 19.6(18) | -0.3(15) | -1.7(15) | 2.2(15) |
| C14 | 20.0(19) | 21.5(18) | 18.5(17) | -5.5(15) | 1.6(14) | -3.8(14) |
| C15 | 34(2) | 23.8(19) | 25(2) | -9.0(16) | 5.3(17) | -10.6(16) |
| C16 | 52(3) | 55(3) | 27(2) | -16(2) | 4(2) | -26(2) |
| C17 | 41(3) | 70(3) | 21(2) | -11(2) | 0.0(19) | -17(2) |
| C18 | 36(2) | 48(3) | 22(2) | -16.3(19) | 14.1(17) | -18(2) |
| Mo1 | 14.22(16) | 17.88(16) | 14.67(15) | -0.66(11) | 1.30(10) | -1.70(10) |

| | | | | | | |
|---|---|---|---|---|---|---|
| N1 | 16.6(15) | 15.6(14) | 13.0(13) | -0.9(11) | -0.8(11) | -0.3(11) |
| O1 | 25.0(14) | 21.3(13) | 17.5(12) | -0.2(10) | 4.9(10) | -6.0(10) |
| O2 | 20.7(14) | 25.0(13) | 16.5(12) | -0.8(10) | 0.5(10) | 0.7(11) |
| O3 | 14.5(12) | 20.8(12) | 17.9(12) | -2.4(10) | 1.7(9) | -0.1(9) |
| O4 | 16.7(13) | 24.3(13) | 18.8(12) | 2.6(10) | 2.5(10) | -4.5(10) |
| O5 | 30.4(15) | 42.3(16) | 19.7(13) | -14.0(12) | 9.0(11) | -17.1(13) |
| O6 | 19.7(13) | 24.0(13) | 23.1(13) | -5.6(11) | 6.8(10) | -5.9(10) |
| O7 | 18.8(13) | 20.5(12) | 19.8(12) | -3.5(10) | 1.1(10) | 1.1(10) |

**Table A-4.2-4 Bond Lengths for Mo-7.**

| **Atom** | **Atom** | **Length/Å** | | **Atom** | **Atom** | **Length/Å** |
|---|---|---|---|---|---|---|
| C1 | C2 | 1.479(5) | | C10 | O4 | 1.332(4) |
| C1 | O1 | 1.271(4) | | C11 | C12 | 1.385(5) |
| C1 | O2 | 1.281(4) | | C12 | C13 | 1.389(5) |
| C2 | C3 | 1.390(4) | | C13 | C14 | 1.380(4) |
| C2 | C7 | 1.397(5) | | C15 | C16 | 1.503(5) |
| C3 | C4 | 1.378(5) | | C15 | O5 | 1.453(4) |
| C4 | C5 | 1.411(5) | | C16 | C17 | 1.498(5) |
| C4 | N1 | 1.423(4) | | C17 | C18 | 1.496(6) |
| C5 | C6 | 1.391(4) | | C18 | O5 | 1.442(4) |
| C5 | O3 | 1.341(4) | | Mo1 | N1 | 2.266(3) |
| C6 | C7 | 1.382(5) | | Mo1 | O3 | 1.982(2) |
| C8 | C9 | 1.433(4) | | Mo1 | O4 | 1.942(2) |
| C8 | N1 | 1.291(4) | | Mo1 | O5 | 2.344(3) |
| C9 | C10 | 1.416(5) | | Mo1 | O6 | 1.702(2) |
| C9 | C14 | 1.407(5) | | Mo1 | O7 | 1.691(2) |
| C10 | C11 | 1.390(5) | | | | |

**Table A-4.2-5 Bond Angles for Mo-7.**

| **Atom** | **Atom** | **Atom** | **Angle/˚** | | **Atom** | **Atom** | **Atom** | **Angle/˚** |
|---|---|---|---|---|---|---|---|---|
| O1 | C1 | C2 | 118.7(3) | | C17 | C16 | C15 | 106.9(3) |
| O1 | C1 | O2 | 123.0(3) | | C18 | C17 | C16 | 104.5(3) |
| O2 | C1 | C2 | 118.2(3) | | O5 | C18 | C17 | 104.8(3) |
| C3 | C2 | C1 | 118.9(3) | | N1 | Mo1 | O5 | 77.30(10) |
| C3 | C2 | C7 | 120.2(3) | | O3 | Mo1 | N1 | 74.77(9) |
| C7 | C2 | C1 | 120.9(3) | | O3 | Mo1 | O5 | 82.24(9) |
| C4 | C3 | C2 | 119.5(3) | | O4 | Mo1 | N1 | 81.88(10) |
| C3 | C4 | C5 | 120.4(3) | | O4 | Mo1 | O3 | 152.61(10) |
| C3 | C4 | N1 | 127.2(3) | | O4 | Mo1 | O5 | 78.78(10) |
| C5 | C4 | N1 | 112.3(3) | | O6 | Mo1 | N1 | 160.67(11) |
| C6 | C5 | C4 | 119.7(3) | | O6 | Mo1 | O3 | 97.11(10) |
| O3 | C5 | C4 | 118.2(3) | | O6 | Mo1 | O4 | 100.45(11) |
| O3 | C5 | C6 | 122.1(3) | | O6 | Mo1 | O5 | 84.31(11) |
| C7 | C6 | C5 | 119.7(3) | | O7 | Mo1 | N1 | 94.01(11) |
| C6 | C7 | C2 | 120.4(3) | | O7 | Mo1 | O3 | 98.67(10) |
| N1 | C8 | C9 | 124.9(3) | | O7 | Mo1 | O4 | 97.03(11) |
| C10 | C9 | C8 | 123.9(3) | | O7 | Mo1 | O5 | 170.75(10) |
| C14 | C9 | C8 | 117.6(3) | | O7 | Mo1 | O6 | 104.65(12) |
| C14 | C9 | C10 | 118.6(3) | | C4 | N1 | Mo1 | 111.1(2) |
| C11 | C10 | C9 | 119.4(3) | | C8 | N1 | C4 | 121.0(3) |
| O4 | C10 | C9 | 122.3(3) | | C8 | N1 | Mo1 | 127.9(2) |

| | | | | | | | | |
|---|---|---|---|---|---|---|---|---|
| O4 | C10 | C11 | 118.2(3) | | C5 | O3 | Mo1 | 121.0(2) |
| C12 | C11 | C10 | 120.2(3) | | C10 | O4 | Mo1 | 139.0(2) |
| C11 | C12 | C13 | 121.5(3) | | C15 | O5 | Mo1 | 131.2(2) |
| C14 | C13 | C12 | 118.5(3) | | C18 | O5 | C15 | 108.4(3) |
| C13 | C14 | C9 | 121.7(3) | | C18 | O5 | Mo1 | 120.1(2) |
| O5 | C15 | C16 | 105.5(3) | | | | | |

**Table A-4.2-6 Hydrogen Atom Coordinates (Å×10$^{4}$) and Isotropic Displacement Parameters (Å$^{2}$×10$^{3}$) for Mo-7.**

| **Atom** | ***x*** | ***y*** | ***z*** | **U(eq)** |
|---|---|---|---|---|
| H3 | 3206.05 | 2027.3 | 7237.32 | 21 |
| H6 | 8836.08 | -1019.69 | 8487.21 | 24 |
| H7 | 5880.76 | -1318.85 | 9506.89 | 24 |
| H8 | 3553.77 | 3305.6 | 5520.79 | 21 |
| H11 | 7997.68 | 5887.49 | 2090.68 | 31 |
| H12 | 4969.74 | 7105.61 | 1218.27 | 34 |
| H13 | 1927.39 | 6697.62 | 2136.03 | 32 |
| H14 | 1935.78 | 4989.44 | 3911.32 | 26 |
| H15A | 5684.08 | 1096.39 | 4939.66 | 34 |
| H15B | 7510.42 | 95.46 | 4987.44 | 34 |
| H16A | 6369.67 | 320.72 | 3347.05 | 53 |
| H16B | 4589.79 | 1351.98 | 3277.81 | 53 |
| H17A | 7580.4 | 1761.11 | 1849.2 | 57 |
| H17B | 6220.04 | 2784.98 | 2063.29 | 57 |
| H18A | 10062.47 | 1493.5 | 3075.82 | 42 |
| H18B | 9218.31 | 2880.09 | 2665.8 | 42 |
| H2 | -100.86 | 883.63 | 9381.85 | 160(30) |

**Table A-4.2-7 Solvent masks information for Mo-7.**

| **Number** | **X** | **Y** | **Z** | **Volume** | **Electron count** | **Content** |
|---|---|---|---|---|---|---|
| 1 | -0.406 | 0.500 | 0.000 | 195.6 | 42.7 | ? |

## A-4.3 Crystal structure of W-1

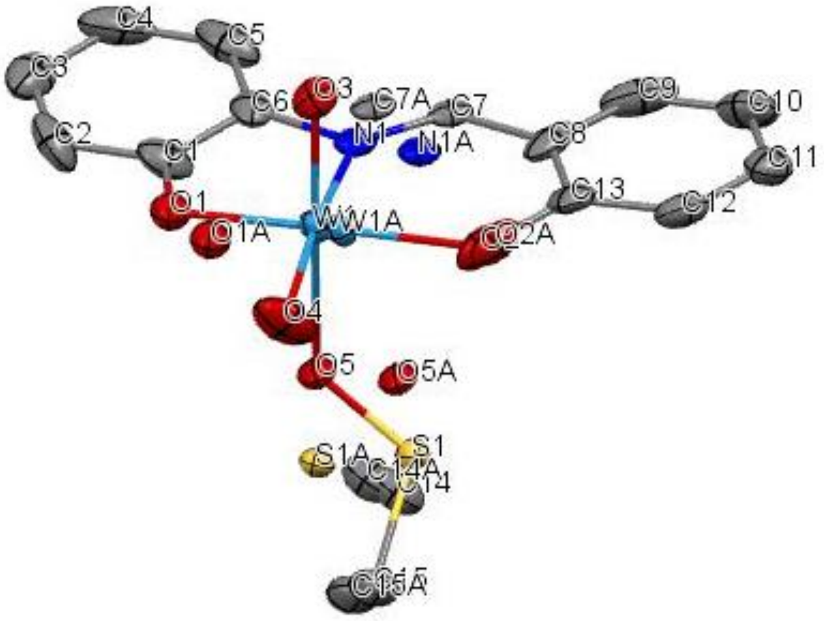

*Figure A-4.3-1: ORTEP plot (50 % probability) of the crystal structure of **W-1**. Hydrogen atoms omitted for clarity.*

### Refinement special detail

The structure was disordered by reflection in a plane defined by O3, O4 and the midpoint point between the two tungsten positions. The tungsten, imine bridge, phenoxy oxygens and the coordinated DMSO were modelled in two positions in a refined ratio of 0.541:0.459(2). Attempts to model the aromatic rings led to poor ADP due to close proximity of the two positions for each carbon. The ADP of pairs of disordered atoms were constrained to be equal (W1 & W1A, N1 & N1A, C7 & C7A, O1 & O1A, O2 & O2A, O5 & O5A, C14 & C14a, C15 & C15A). The ADP of C14, C14a, C15 & C15A were restrained to be approximately isotropic.

*Table A-4.3-1: Crystallographic data for **W-1.***

| | |
|---|---|
| Empirical formula | $C_{17}H_{21}NO_6S_2W$ |
| Formula weight | 583.32 |
| Temperature / K | 109.9 (4) |
| Crystal system | Monoclinic |
| Space group | $P2_1/c$ |
| a/Å | 12.48131 (15) |
| b/Å | 6.72402 (8) |
| c/Å | 23.5573(3) |
| α/° | 90 |
| β/° | 94.1359(11) |
| γ/° | 90 |
| Volume/Å$^3$ | 1971.89 (4) |
| Z | 4 |
| $\rho_{calc}$ / g/cm$^3$ | 1.965 |
| μ/mm$^{-1}$ | 13.141 |
| F(000) | 1136.0 |
| Crystal size/mm$^3$ | 0.24 x 0.16 x 0.13 |
| Radiation | CuKα (λ = 1.54184) |
| 2Θ range for data collection/° | 7.1 to 134.156 |
| Index ranges | $-14 \le h \le 14$, $-8 \le k \le 7$, $-28 \le l \le 20$ |
| Reflections collected | 12136 |
| Independent reflections | 3503 [$R_{int}$ = 0.0233, $R_{sigma}$ = 0.0219] |
| Data/restraints/parameters | 2502/24/285 |
| Goodness-of-fit on F$^2$ | 1.105 |
| Final R indexes [I>=2σ (I)] | $R_1$ = 0.0246, w$R_2$ = 0.0529 |
| Final R indexes [all data] | $R_1$ = 0.0265, w$R_2$ = 0.0538 |
| Largest diff. peak/hole / e Å$^{-3}$ | 0.89/-0.87 |

**Table A-4.3-2 Fractional Atomic Coordinates (×10$^4$) and Equivalent Isotropic Displacement Parameters (Å$^2$×10$^3$) for W-1. $U_{eq}$ is defined as 1/3 of the trace of the orthogonalised $U_{IJ}$ tensor.**

| **Atom** | ***x*** | ***y*** | ***z*** | **U(eq)** |
|---|---|---|---|---|
| C1 | 1354(3) | 3812(7) | 3787.6(18) | 33.2(10) |
| C2 | 1033(4) | 3878(7) | 4336.6(18) | 39.4(12) |
| C3 | 407(4) | 2391(8) | 4523.2(19) | 42.9(13) |
| C4 | 97(4) | 820(8) | 4171(2) | 50.1(15) |
| C5 | 428(4) | 742(7) | 3624(2) | 42.9(12) |
| C6 | 1047(3) | 2235(7) | 3432.8(17) | 30.1(10) |
| C7 | 1395(5) | 1553(11) | 2472(3) | 17.6(11) |
| C7A | 1221(6) | 1616(14) | 2860(4) | 17.6(11) |
| C8 | 1795(3) | 2115(8) | 1934.4(18) | 35.9(11) |
| C9 | 1543(4) | 528(8) | 1573(3) | 47.5(14) |
| C10 | 1823(4) | 551(8) | 1019(2) | 45.9(13) |
| C11 | 2349(3) | 2181(8) | 821.9(18) | 37.3(11) |
| C12 | 2602(3) | 3781(7) | 1168.1(18) | 30.6(10) |
| C13 | 2330(3) | 3749(7) | 1730.9(18) | 30.6(10) |

| | | | | |
|---|---|---|---|---|
| C14 | 4893(18) | 1120(40) | 3263(7) | 36(3) |
| C14A | 4730(20) | 1180(50) | 3396(9) | 36(3) |
| C15 | 5680(20) | 4790(30) | 3144(7) | 36(3) |
| C15A | 5720(20) | 4520(40) | 3291(8) | 36(3) |
| N1 | 1498(5) | 2827(10) | 2876(3) | 17.4(10) |
| N1A | 1680(6) | 2856(12) | 2550(3) | 17.4(10) |
| O1 | 1818(5) | 5538(11) | 3653(3) | 26.0(12) |
| O1A | 2155(7) | 4994(14) | 3536(4) | 26.0(12) |
| O2 | 2622(11) | 5035(16) | 2133(5) | 29.2(17) |
| O2A | 2587(14) | 5610(20) | 1996(7) | 29.2(17) |
| O3 | 933(2) | 6826(4) | 2629.3(11) | 23.7(6) |
| O4 | 2959(3) | 8067(5) | 2943.6(14) | 42.6(8) |
| O5 | 3585(4) | 4279(8) | 3221(2) | 26.6(9) |
| O5A | 3766(5) | 4009(10) | 2834(2) | 26.6(9) |
| S1 | 4512.0(13) | 3405(3) | 2911.1(7) | 21.2(4) |
| S1A | 4445.2(16) | 3664(4) | 3393.7(8) | 27.7(6) |
| W1 | 2160(2) | 6001(5) | 2874.2(8) | 14.8(3) |
| W1A | 2237(3) | 5910(5) | 2754.4(10) | 14.8(3) |
| C16 | 7094(5) | 673(11) | 5456(3) | 81(2) |
| C17 | 5393(5) | 2815(12) | 5603(2) | 80(2) |
| O6 | 5972(3) | 2232(6) | 4585.8(13) | 50.4(9) |
| S2 | 6444.8(12) | 2794(3) | 5154.1(6) | 56.4(4) |

**Table A-4.3-3 Anisotropic Displacement Parameters (Å$^2$×10$^3$) for W-1. The Anisotropic displacement factor exponent takes the form: $-2\pi^2[h^2a^{*2}U_{11}+2hka^*b^*U_{12}+\ldots]$.**

| Atom | $U_{11}$ | $U_{22}$ | $U_{33}$ | $U_{23}$ | $U_{13}$ | $U_{12}$ |
|---|---|---|---|---|---|---|
| C1 | 31(2) | 35(3) | 31(2) | 12.8(19) | -12.8(18) | -4(2) |
| C2 | 57(3) | 35(3) | 23(2) | -2.4(19) | -17(2) | 6(2) |
| C3 | 32(2) | 69(4) | 28(2) | 15(2) | 0.2(19) | 17(3) |
| C4 | 27(2) | 55(3) | 65(4) | 29(3) | -16(2) | -11(2) |
| C5 | 40(3) | 28(3) | 57(3) | -4(2) | -25(2) | 5(2) |
| C6 | 20(2) | 45(3) | 24(2) | -1.3(19) | -7.2(16) | 14.3(19) |
| C7 | 11(2) | 14(3) | 27(3) | 7(3) | -1(2) | 4(2) |
| C7A | 11(2) | 14(3) | 27(3) | 7(3) | -1(2) | 4(2) |
| C8 | 17(2) | 59(3) | 33(2) | 20(2) | 8.4(17) | 18(2) |
| C9 | 20(2) | 42(3) | 81(4) | 29(3) | 6(2) | 0(2) |
| C10 | 25(2) | 49(3) | 62(3) | -5(3) | -4(2) | -10(2) |
| C11 | 22(2) | 62(3) | 27(2) | 7(2) | -2.3(17) | 1(2) |
| C12 | 15.6(19) | 37(3) | 40(2) | 12(2) | 4.9(17) | 0.6(18) |
| C13 | 10.8(18) | 44(3) | 37(2) | 2(2) | 2.1(16) | 6.8(18) |
| C14 | 35(5) | 40(3) | 33(7) | -1(5) | -10(5) | -2(4) |
| C14A | 35(5) | 40(3) | 33(7) | -1(5) | -10(5) | -2(4) |
| C15 | 23(3) | 42(5) | 43(7) | -8(5) | 0(5) | -9(3) |
| C15A | 23(3) | 42(5) | 43(7) | -8(5) | 0(5) | -9(3) |
| N1 | 13(2) | 14(2) | 25(3) | 4(3) | -2(3) | 3(2) |
| N1A | 13(2) | 14(2) | 25(3) | 4(3) | -2(3) | 3(2) |
| O1 | 22(4) | 33(4) | 23(3) | -1(2) | 0(2) | 4(2) |
| O1A | 22(4) | 33(4) | 23(3) | -1(2) | 0(2) | 4(2) |
| O2 | 28.2(19) | 22(6) | 39(6) | 10(3) | 17(4) | 2(4) |
| O2A | 28.2(19) | 22(6) | 39(6) | 10(3) | 17(4) | 2(4) |
| O3 | 24.7(14) | 13.0(13) | 33.8(15) | 1.4(11) | 5.6(11) | 2.4(11) |
| O4 | 43.0(19) | 33.7(18) | 49.2(19) | 5.1(15) | -9.4(15) | -22.0(16) |
| O5 | 14.7(19) | 41(2) | 23.7(19) | -5(2) | 0.2(18) | 8.7(18) |
| O5A | 14.7(19) | 41(2) | 23.7(19) | -5(2) | 0.2(18) | 8.7(18) |
| S1 | 14.0(9) | 26.8(10) | 22.7(10) | -7.4(7) | 0.1(6) | 1.0(7) |

| | | | | | | |
|---|---|---|---|---|---|---|
| S1A | 12.1(10) | 53.3(15) | 17.3(11) | -6.5(9) | -1.5(7) | -0.8(9) |
| W1 | 16.2(4) | 13.5(3) | 14.4(7) | -1.7(5) | -0.6(5) | -3.6(2) |
| W1A | 16.2(4) | 13.5(3) | 14.4(7) | -1.7(5) | -0.6(5) | -3.6(2) |
| C16 | 77(4) | 101(6) | 60(4) | -27(4) | -35(3) | 61(4) |
| C17 | 92(5) | 115(6) | 35(3) | 9(3) | 13(3) | 65(5) |
| O6 | 55(2) | 70(3) | 25.9(16) | -11.1(17) | -0.5(15) | 14(2) |
| S2 | 54.1(8) | 73.7(10) | 39.5(7) | -16.3(7) | -10.3(6) | 9.0(7) |

**Table A-4.3-4 Bond Lengths for W-1.**

| Atom | Atom | Length/Å | | Atom | Atom | Length/Å |
|---|---|---|---|---|---|---|
| C1 | C2 | 1.382(6) | | C14 | S1 | 1.79(3) |
| C1 | C6 | 1.387(6) | | C14A | S1A | 1.71(3) |
| C1 | O1 | 1.345(9) | | C15 | S1 | 1.78(2) |
| C1 | O1A | 1.438(11) | | C15A | S1A | 1.72(3) |
| C2 | C3 | 1.362(7) | | N1 | W1 | 2.288(7) |
| C3 | C4 | 1.382(8) | | N1A | W1A | 2.210(9) |
| C4 | C5 | 1.381(7) | | O1 | W1 | 1.938(8) |
| C5 | C6 | 1.363(7) | | O1A | W1A | 1.952(10) |
| C6 | C7A | 1.444(10) | | O2 | W1 | 1.987(14) |
| C6 | N1 | 1.518(8) | | O2A | W1A | 1.882(16) |
| C7 | C8 | 1.445(8) | | O3 | W1 | 1.690(4) |
| C7 | N1 | 1.279(11) | | O3 | W1A | 1.744(4) |
| C7A | N1A | 1.272(13) | | O4 | W1 | 1.711(4) |
| C8 | C9 | 1.387(7) | | O4 | W1A | 1.748(5) |
| C8 | C13 | 1.389(6) | | O5 | S1 | 1.529(5) |
| C8 | N1A | 1.549(8) | | O5 | W1 | 2.228(6) |
| C9 | C10 | 1.374(7) | | O5A | S1A | 1.532(6) |
| C10 | C11 | 1.376(7) | | O5A | W1A | 2.294(7) |
| C11 | C12 | 1.373(7) | | C16 | S2 | 1.765(6) |
| C12 | C13 | 1.392(6) | | C17 | S2 | 1.745(6) |
| C13 | O2 | 1.315(16) | | O6 | S2 | 1.473(3) |
| C13 | O2A | 1.425(18) | | | | |

**Table A-4.3-5 Bond Angles for W-1.**

| Atom | Atom | Atom | Angle/˚ | | Atom | Atom | Atom | Angle/˚ |
|---|---|---|---|---|---|---|---|---|
| C2 | C1 | C6 | 120.2(4) | | S1A | O5A | W1A | 124.1(3) |
| C2 | C1 | O1A | 128.6(5) | | C15 | S1 | C14 | 97.0(10) |
| C6 | C1 | O1A | 110.2(5) | | O5 | S1 | C14 | 107.0(6) |
| O1 | C1 | C2 | 110.6(5) | | O5 | S1 | C15 | 106.5(8) |
| O1 | C1 | C6 | 128.5(5) | | C14A | S1A | C15A | 97.6(13) |
| C3 | C2 | C1 | 119.4(4) | | O5A | S1A | C14A | 104.8(8) |
| C2 | C3 | C4 | 120.7(4) | | O5A | S1A | C15A | 106.6(7) |
| C5 | C4 | C3 | 120.0(5) | | O1 | W1 | N1 | 75.2(3) |
| C6 | C5 | C4 | 119.7(4) | | O1 | W1 | O2 | 151.2(4) |
| C1 | C6 | C7A | 136.9(6) | | O1 | W1 | O5 | 78.1(2) |
| C1 | C6 | N1 | 102.5(4) | | O2 | W1 | N1 | 79.9(4) |
| C5 | C6 | C1 | 120.2(4) | | O2 | W1 | O5 | 82.9(4) |
| C5 | C6 | C7A | 102.9(5) | | O3 | W1 | N1 | 89.3(2) |
| C5 | C6 | N1 | 137.2(5) | | O3 | W1 | O1 | 96.9(2) |
| N1 | C7 | C8 | 117.0(6) | | O3 | W1 | O2 | 96.9(4) |
| N1A | C7A | C6 | 116.9(8) | | O3 | W1 | O4 | 105.9(2) |
| C9 | C8 | C7 | 105.1(5) | | O3 | W1 | O5 | 167.3(2) |
| C9 | C8 | C13 | 119.3(4) | | O4 | W1 | N1 | 164.8(2) |
| C9 | C8 | N1A | 142.2(5) | | O4 | W1 | O1 | 101.9(3) |

| | | | | | | | | |
|---|---|---|---|---|---|---|---|---|
| C13 | C8 | C7 | 135.6(5) | | O4 | W1 | O2 | 98.3(4) |
| C13 | C8 | N1A | 98.5(5) | | O4 | W1 | O5 | 86.7(2) |
| C10 | C9 | C8 | 120.8(4) | | O5 | W1 | N1 | 78.1(2) |
| C9 | C10 | C11 | 119.4(5) | | N1A | W1A | O5A | 75.3(3) |
| C12 | C11 | C10 | 121.2(4) | | O1A | W1A | N1A | 82.9(4) |
| C11 | C12 | C13 | 119.5(4) | | O1A | W1A | O5A | 81.2(3) |
| C8 | C13 | C12 | 119.8(4) | | O2A | W1A | N1A | 77.5(5) |
| C8 | C13 | O2A | 130.0(7) | | O2A | W1A | O1A | 153.4(5) |
| C12 | C13 | O2A | 109.9(6) | | O2A | W1A | O5A | 76.6(5) |
| O2 | C13 | C8 | 112.8(5) | | O3 | W1A | N1A | 91.0(2) |
| O2 | C13 | C12 | 127.0(6) | | O3 | W1A | O1A | 99.2(3) |
| C6 | N1 | W1 | 113.7(4) | | O3 | W1A | O2A | 98.9(5) |
| C7 | N1 | C6 | 116.3(6) | | O3 | W1A | O4 | 102.0(2) |
| C7 | N1 | W1 | 129.8(5) | | O3 | W1A | O5A | 166.2(3) |
| C7A | N1A | C8 | 113.7(7) | | O4 | W1A | N1A | 167.1(3) |
| C7A | N1A | W1A | 129.2(7) | | O4 | W1A | O1A | 94.7(3) |
| C8 | N1A | W1A | 117.0(5) | | O4 | W1A | O2A | 100.4(5) |
| C1 | O1 | W1 | 119.3(5) | | O4 | W1A | O5A | 91.7(2) |
| C1 | O1A | W1A | 130.4(6) | | C17 | S2 | C16 | 96.1(3) |
| C13 | O2 | W1 | 139.9(9) | | O6 | S2 | C16 | 107.5(3) |
| C13 | O2A | W1A | 116.7(7) | | O6 | S2 | C17 | 106.5(3) |
| S1 | O5 | W1 | 129.5(3) | | | | | |

**Table A-4.3-6 Torsion Angles for W-1.**

| A | B | C | D | Angle/˚ | | A | B | C | D | Angle/˚ |
|---|---|---|---|---|---|---|---|---|---|---|
| C1 | C2 | C3 | C4 | 0.3(7) | | C9 | C8 | N1A | C7A | 2.4(10) |
| C1 | C6 | C7A | N1A | -9.1(10) | | C9 | C8 | N1A | W1A | -174.3(5) |
| C1 | C6 | N1 | C7 | 175.4(5) | | C9 | C10 | C11 | C12 | 0.2(7) |
| C1 | C6 | N1 | W1 | -8.8(4) | | C10 | C11 | C12 | C13 | 0.6(6) |
| C2 | C1 | C6 | C5 | -0.1(6) | | C11 | C12 | C13 | C8 | -0.8(6) |
| C2 | C1 | C6 | C7A | -178.7(6) | | C11 | C12 | C13 | O2 | 171.3(8) |
| C2 | C1 | C6 | N1 | 176.3(4) | | C11 | C12 | C13 | O2A | -175.3(8) |
| C2 | C1 | O1 | W1 | -171.3(4) | | C12 | C13 | O2 | W1 | 158.1(6) |
| C2 | C1 | O1A | W1A | -148.4(5) | | C12 | C13 | O2A | W1A | 177.9(7) |
| C2 | C3 | C4 | C5 | 0.4(7) | | C13 | C8 | C9 | C10 | 0.4(6) |
| C3 | C4 | C5 | C6 | -1.0(7) | | C13 | C8 | N1A | C7A | -178.7(6) |
| C4 | C5 | C6 | C1 | 0.9(6) | | C13 | C8 | N1A | W1A | 4.6(5) |
| C4 | C5 | C6 | C7A | 179.8(5) | | C13 | O2A | W1A | N1A | -0.2(9) |
| C4 | C5 | C6 | N1 | -174.0(5) | | C13 | O2A | W1A | O1A | 43(2) |
| C5 | C6 | C7A | N1A | 172.2(6) | | C13 | O2A | W1A | O3 | -89.2(10) |
| C5 | C6 | N1 | C7 | -9.2(9) | | C13 | O2A | W1A | O4 | 166.7(9) |
| C5 | C6 | N1 | W1 | 166.6(4) | | C13 | O2A | W1A | O5A | 77.4(10) |
| C6 | C1 | C2 | C3 | -0.5(6) | | N1 | C7 | C8 | C9 | -177.5(5) |
| C6 | C1 | O1 | W1 | -1.4(8) | | N1 | C7 | C8 | C13 | 2.9(9) |
| C6 | C1 | O1A | W1A | 43.3(8) | | N1A | C8 | C9 | C10 | 179.3(6) |
| C6 | C7A | N1A | C8 | -177.6(5) | | N1A | C8 | C13 | C12 | -178.9(4) |
| C6 | C7A | N1A | W1A | -1.5(10) | | N1A | C8 | C13 | O2A | -5.7(10) |
| C7 | C8 | C9 | C10 | -179.2(4) | | O1 | C1 | C2 | C3 | 170.3(5) |
| C7 | C8 | C13 | C12 | 179.8(5) | | O1 | C1 | C6 | C5 | -169.1(5) |
| C7 | C8 | C13 | O2 | 6.6(9) | | O1 | C1 | C6 | N1 | 7.3(7) |
| C8 | C7 | N1 | C6 | 178.4(4) | | O1A | C1 | C2 | C3 | -167.8(6) |
| C8 | C7 | N1 | W1 | 3.4(8) | | O1A | C1 | C6 | C5 | 169.3(5) |
| C8 | C9 | C10 | C11 | -0.7(7) | | O1A | C1 | C6 | C7A | -9.2(8) |
| C8 | C13 | O2 | W1 | -29.3(12) | | W1 | O5 | S1 | C14 | -145.3(8) |
| C8 | C13 | O2A | W1A | 4.2(15) | | W1 | O5 | S1 | C15 | 111.8(7) |

| | | | | | | | | | | |
|---|---|---|---|---|---|---|---|---|---|---|
| C9 | C8 | C13 | C12 | 0.3(6) | | W1A | O5A | S1A | C14A | 136.0(10) |
| C9 | C8 | C13 | O2 | -172.9(7) | | W1A | O5A | S1A | C15A | -121.2(10) |
| C9 | C8 | C13 | O2A | 173.5(9) | | | | | | |

**Table A-4.3-7 Hydrogen Atom Coordinates (Å×$10^4$) and Isotropic Displacement Parameters (Å$^2$×$10^3$) for W-1.**

| **Atom** | ***x*** | ***y*** | ***z*** | **U(eq)** |
|---|---|---|---|---|
| H2 | 1247.33 | 4951.59 | 4581.38 | 47 |
| H3 | 180.62 | 2433.72 | 4899.59 | 52 |
| H4 | -344.26 | -206.18 | 4304.09 | 60 |
| H5 | 225.6 | -346.85 | 3382.96 | 51 |
| H7 | 1070.13 | 294.56 | 2523.57 | 21 |
| H7A | 1001.62 | 342.41 | 2720.75 | 21 |
| H9 | 1172.4 | -588.75 | 1709.51 | 57 |
| H10 | 1654.53 | -547.31 | 775.42 | 55 |
| H11 | 2541.06 | 2199.67 | 438.96 | 45 |
| H12 | 2959.75 | 4901.68 | 1024.71 | 37 |
| H14A | 4944.24 | 1326.51 | 3675.63 | 55 |
| H14B | 5590.53 | 685.11 | 3142.35 | 55 |
| H14C | 4351.05 | 99.71 | 3162.44 | 55 |
| H14D | 4066.02 | 410.84 | 3391.87 | 55 |
| H14E | 5190.54 | 846.78 | 3739.61 | 55 |
| H14F | 5114.08 | 844.99 | 3058.56 | 55 |
| H15A | 5629.58 | 6132.01 | 2982.6 | 54 |
| H15B | 6319.18 | 4123.57 | 3016.13 | 54 |
| H15C | 5734.91 | 4870.95 | 3560.07 | 54 |
| H15D | 5950.28 | 3993.62 | 2932.08 | 54 |
| H15E | 6215.71 | 4086.32 | 3606.4 | 54 |
| H15F | 5708.81 | 5979.99 | 3274.64 | 54 |
| H16A | 6592.96 | -451.59 | 5438.19 | 122 |
| H16B | 7332.46 | 944.59 | 5853.7 | 122 |
| H16C | 7717.21 | 346.34 | 5243.11 | 122 |
| H17A | 5686.66 | 2809.99 | 6000.67 | 121 |
| H17B | 4944.24 | 1633.17 | 5531 | 121 |
| H17C | 4957.39 | 4013.07 | 5531.15 | 121 |

**Table A-4.3-8 Atomic Occupancy for W-1.**

| **Atom** | ***Occupancy*** | | **Atom** | ***Occupancy*** | | **Atom** | ***Occupancy*** |
|---|---|---|---|---|---|---|---|
| C7 | 0.541(2) | | H7 | 0.541(2) | | C7A | 0.459(2) |
| H7A | 0.459(2) | | C14 | 0.541(2) | | H14A | 0.541(2) |
| H14B | 0.541(2) | | H14C | 0.541(2) | | C14A | 0.459(2) |
| H14D | 0.459(2) | | H14E | 0.459(2) | | H14F | 0.459(2) |
| C15 | 0.541(2) | | H15A | 0.541(2) | | H15B | 0.541(2) |
| H15C | 0.541(2) | | C15A | 0.459(2) | | H15D | 0.459(2) |
| H15E | 0.459(2) | | H15F | 0.459(2) | | N1 | 0.541(2) |
| N1A | 0.459(2) | | O1 | 0.541(2) | | O1A | 0.459(2) |
| O2 | 0.541(2) | | O2A | 0.459(2) | | O5 | 0.541(2) |
| O5A | 0.459(2) | | S1 | 0.541(2) | | S1A | 0.459(2) |
| W1 | 0.541(2) | | W1A | 0.459(2) | | | |

# Abbreviations

| | |
|---|---|
| acac | acetylacetonate |
| AcOH | acetic acid |
| Asp | asparagine |
| asym | asymmetric |
| ATR | attenuated total reflection |
| br | broad |
| Cys | cysteine |
| c | concentration |
| d | doublet |
| Da | Dalton |
| DCM | dichloromethane |
| dd | doublet of doublets |
| DMF | dimethyl formamide |
| DMSO | dimethyl sulfoxide |
| DMSOR | DMSO reductase |
| ESI | electron spray ionisation |
| EPR | electron paramagnetic resonance |
| eq | equatorial |
| EXFAS | Extended X-ray absorption fine structure |
| FAD | flavin adenine dinucleotide |
| FT | Fourier transformed |
| gc | gas chromatography |
| HMPA | hexamethylphosphoramide |
| IR | infrared |
| LIFDI | liquid introduction field desorption ionisation |
| m | multiplet |
| mnt | maleonitriledithiolate |
| mp | melting point |
| MS | mass spectrometry |

| | |
|---|---|
| NAD | nicotinamide adenosine dinucleotide |
| OAT | oxygen atom transfer |
| Phen | phenanthroline |
| s | singlet |
| salan | N,N′ -bis(2-hydroxy-5-chloromethylbenzyl)-1,2-diaminocyclohexane |
| sap | salicylidene amino phenol |
| sae | salicylidene amino ethanol |
| sse | thio salicylidene amino ethanol |
| ssp | thio salicylidene amino phenol |
| Ser | serine |
| SO | sulfite oxidase |
| st | strong |
| sym | symmetric |
| t | triplet |
| TBHP | *tert*-butyl hydroperoxide |
| THF | tetrahydrofuran |
| TOF | turn-over frequency |
| V | very |
| w | weak |
| XO | xanthine oxidase |

# References

1 D. Friedmann, A. Hakki, H. Kim, W. Choi and D. Bahnemann, Heterogeneous photocatalytic organic synthesis: state-of-the-art and future perspectives, *Green Chem.*, 2016, **18**, 5391–5411.

2 S. Muthusamy, N. Kumarswamyreddy, V. Kesavan and S. Chandrasekaran, Recent advances in aerobic oxidation with ruthenium catalysts, *Tetrahedron Lett.*, 2016, **57**, 5551–5559.

3 F. E. Kühn, S. A. Hauser and M. Cokoja, Epoxidation of olefins with homogeneous catalysts – quo vadis?, *Catal Sci Technol*, 2013, **3**, 552–561.

4 D. G. Nocera, T. R. Cook, D. K. Dogutan, S. Y. Reece, Y. Surendranath and T. S. Teets, Solar Energy Supply and Storage for the Legacy and Nonlegacy Worlds, *Chem. Rev.*, 2010, **110**, 6474–6502.

5 G. Strukul and A. Scarso, in *Liquid Phase Oxidation via Heterogeneous Catalysis: Organic Synthesis and Industrial Applications*, eds. M. G. Clerici and O. A. Kholdeeva, John Wiley & Sons, Inc., Hoboken, New Jersey, 2013, pp. 1–20.

6 V. R. Landaeta and R. E. Rodríguez-Lugo, Catalytic oxygenation of organic substrates: Toward greener ways for incorporating oxygen, *Inorganica Chim. Acta*, 2015, **431**, 21–47.

7 P. Tang, Q. Zhu, Z. Wu and D. Ma, Methane activation: the past and future, *Energy Env. Sci*, 2014, **7**, 2580–2591.

8 R. H. Holm and J. P. Donahue, A thermodynamic scale for oxygen atom transfer reactions, *Polyhedron*, 1993, **12**, 571–589.

9 S. A. Buckler, Autoxidation of Trialkylphosphines, *J. Am. Chem. Soc.*, 1962, **84**, 3093–3097.

10 K. A. Hofmann, Sauerstoff-übertragung durch Osmiumtetroxyd und Aktivierung von Chlorat-Lösungen, *Berichte Dtsch. Chem. Ges.*, 1912, **45**, 3329–3336.

11 J. Halperin and H. Taube, Oxygen atom transfer in the reaction of chlorate with sulfite in aqueous solution, *J. Am. Chem. Soc.*, 1950, **72**, 3319–3320.

12 R. H. Holm, Metal-centered oxygen atom transfer reactions, *Chem. Rev.*, 1987, **87**, 1401–1449.

13 A. L. Balch, Y. W. Chan, R. J. Cheng, G. N. La Mar, L. Latos-Grazynski and M. W. Renner, Oxygenation patterns for iron(II) porphyrins. Peroxo and ferryl ($Fe^{IV}O$) intermediates detected by proton nuclear magnetic resonance spectroscopy during the oxygenation of (tetramesitylporphyrin)iron(II), *J. Am. Chem. Soc.*, 1984, **106**, 7779–7785.

14 L. Keith. Woo, Intermetal oxygen, sulfur, selenium, and nitrogen atom transfer reactions, *Chem. Rev.*, 1993, **93**, 1125–1136.

15 Tungsten - Element information, properties and uses | Periodic Table, https://www.rsc.org/periodic-table/element/74/Tungsten, (accessed 18 April 2022).

16 Molybdenum - Element information, properties and uses | Periodic Table, https://www.rsc.org/periodic-table/element/42/molybdenum, (accessed 18 April 2022).

17 A. Lennartson, Made by molybdenum, *Nat. Chem.*, 2014, **6**, 746–746.

18 L. E. Bevers, P.-L. Hagedoorn and W. R. Hagen, The bioinorganic chemistry of tungsten, *Coord. Chem. Rev.*, 2009, **253**, 269–290.

19 webelements, www.webelements.com, (accessed 3 April 2022).

20 L. B. Maia, I. Moura and J. J. G. Moura, in *Metallobiology*, eds. R. Hille, C. Schulzke and M. L. Kirk, Royal Society of Chemistry, Cambridge, 2016, pp. 1–80.

21 M. Dixon and S. Thurlow, CXXXI. Studies on xanthine oxidase, *Biochem. J.*, **18**, 976–988.

22 M. J. Romão, M. Archer, I. Moura, J. J. G. Moura, J. LeGall, R. Engh, M. Schneider, P. Hof and R. Huber, Crystal Structure of the Xanthine Oxidase-Related Aldehyde Oxido-Reductase from *D. gigas*, *Science*, 1995, **270**, 1170–1176.

23 I. Yamamoto, T. Saiki, S. M. Liu and L. G. Ljungdahl, Purification and properties of NADP-dependent formate dehydrogenase from *Clostridium thermoaceticum* , a tungsten-selenium-iron protein, *J. Biol. Chem.*, 1983, **258**, 1826–1832.

24 M. K. Chan, S. Mukund, A. Kletzin, M. W. W. Adams and D. C. Rees, Structure of a Hyperthermophilic Tungstopterin Enzyme, Aldehyde Ferredoxin Oxidoreductase, *Science*, 1995, **267**, 1463–1469.

25 H. Schindelin, C. Kisker, J. Hilton, K. V. Rajagopalan and D. C. Rees, Crystal Structure of DMSO Reductase: Redox-Linked Changes in Molybdopterin Coordination, *Science*, 1996, **272**, 1615–1621.

26 C. Kisker, H. Schindelin, A. Pacheco, W. A. Wehbi, R. M. Garrett, K. V. Rajagopalan, J. H. Enemark and D. C. Rees, Molecular Basis of Sulfite Oxidase Deficiency from the Structure of Sulfite Oxidase, *Cell*, 1997, **91**, 973–983.

27 P. Basu and S. J. N. Burgmayer, Pterin chemistry and its relationship to the molybdenum cofactor, *Coord. Chem. Rev.*, 2011, **255**, 1016–1038.

28 J. H. Enemark and C. D. Garner, The coordination chemistry and function of the molybdenum centres of the oxomolybdoenzymes, *JBIC*, 1997, **2**, 817–822.

29 V. N. Gladyshev and Y. Zhang, in *Molybdenum and Tungsten Enzymes: Biochemistry*, eds. R. Hille, C. Schulzke and M. L. Kirk, The Royal Society of Chemistry, 2017, pp. 81–99.

30 H. Dobbek, Structural aspects of mononuclear Mo/W-enzymes, *Coord. Chem. Rev.*, 2011, **255**, 1104–1116.

31 T. Nishino, K. Okamoto and S. Leimkühler, in *Molybdenum and Tungsten Enzymes: Biochemistry*, eds. R. Hille, C. Schulzke and M. L. Kirk, The Royal Society of Chemistry, 2017, pp. 192–239.

32 R. Hille and T. Nishino, Xanthine oxidase and xanthine dehydrogenase, *FASEB J.*, 1995, **9**, 995–1003.

33 K. Heinze, Bioinspired functional analogs of the active site of molybdenum enzymes: Intermediates and mechanisms, *Coord. Chem. Rev.*, 2015, **300**, 121–141.

34 F. Schardinger, Ueber das Verhalten der Kuhmilch gegen Methylenblau und seine Verwendung zur Unterscheidung von ungekochter und gekochter Milch, *Z. Für Unters. Nahr.-Genussm.*, 1902, **5**, 1113–1121.

35 R. O. Day, G. G. Graham, M. Hicks, A. J. McLachlan, S. L. Stocker and K. M. Williams, Clinical Pharmacokinetics and Pharmacodynamics of Allopurinol and Oxypurinol:, *Clin. Pharmacokinet.*, 2007, **46**, 623–644.

36 U. Kappler and G. Schwarz, in *Molybdenum and Tungsten Enzymes: Biochemistry*, eds. R. Hille, C. Schulzke and M. L. Kirk, The Royal Society of Chemistry, 2017, pp. 240–273.

37 F. Schneider, J. Löwe, R. Huber, H. Schindelin, C. Kisker and J. Knäblein, Crystal Structure of Dimethyl Sulfoxide Reductase from Rhodobacter capsulatus at 1.88 Å Resolution, *J. Mol. Biol.*, 1996, **263**, 53–69.

38 J. H. Enemark, J. J. A. Cooney, J.-J. Wang and R. H. Holm, Synthetic Analogues and Reaction Systems Relevant to the Molybdenum and Tungsten Oxotransferases, *Chem. Rev.*, 2004, **104**, 1175–1200.

39 E. I. Stiefel, D. Coucouvanis and W. E. Newton, Eds., *Molybdenum Enzymes, Cofactors, and Model Systems*, American Chemical Society, Washington, DC, 1993, vol. 535.

40 B. Bradshaw, A. Dinsmore, W. Ajana, D. Collison, C. D. Garner and J. A. Joule, Synthesis of the organic ligand of the molybdenum cofactor, in protected form, *J. Chem. Soc. Perkin Trans.*, 2001, **1**, 3239–3244.

41 A. Thapper, J. P. Donahue, K. B. Musgrave, M. W. Willer, E. Nordlander, B. Hedman, K. O. Hodgson and R. H. Holm, The Unperturbed Oxo-Sulfido Functional Group cis-$Mo^{VI}$ OS Related to That in the Xanthine Oxidase Family of Molybdoenzymes: Synthesis, Structural Characterization, and Reactivity Aspects, *Inorg. Chem.*, 1999, **38**, 4104–4114.

42 M. A. Ehweiner, F. Belaj, K. Kirchner and N. C. Mösch-Zanetti, Synthesis and Reactivity of a Bioinspired Molybdenum(IV) Acetylene Complex, *Organometallics*, 2021, **40**, 2576–2583.

43 C. Vidovič, F. Belaj and N. C. Mösch-Zanetti, Soft Scorpionate Hydridotris(2-mercapto-1-methylimidazolyl) borate) Tungsten-Oxido and -Sulfido Complexes as Acetylene Hydratase Models, *Chem. – Eur. J.*, 2020, **26**, 12431–12444.

44 R. D. Chakravarthy and D. K. Chand, Synthesis, structure and applications of [*cis*-dioxomolybdenum(VI)-(ONO)] type complexes, *J. Chem. Sci.*, 2011, **123**, 187–199.

45 A. Majumdar, Structural and functional models in molybdenum and tungsten bioinorganic chemistry: description of selected model complexes, present scenario and possible future scopes, *Dalton Trans.*, 2014, **43**, 8990.

46 C.-X. Zhang, D.-W. Fang, J.-L. Wang, A.-Q. Jia and Q.-F. Zhang, Syntheses, characterizations, and reactivities of new 1,4,7-trimethyl-l,4,7-triazacyclononane ($Me_3$tacn) molybdenum and tungsten complexes, *Inorganica Chim. Acta*, 2020, **507**, 119599.

47 A. Hochheimer, R. Hedderich and R. K. Thauer, The formylmethanofuran dehydrogenase isoenzymes in Methanobacterium wolfei and Methanobacterium thermoautotrophicum : induction of the molybdenum isoenzyme by molybdate and constitutive synthesis of the tungsten isoenzyme, *Arch. Microbiol.*, 1998, **170**, 389–393.

48 R. A. Schmitz, S. P. J. Albracht and R. K. Thauer, A molybdenum and a tungsten isoenzyme of formylmethanofuran dehydrogenase in the thermophilic archaeon *Methanobacterium wolfei*, *Eur. J. Biochem.*, 1992, **209**, 1013–1018.

49 S. Groysman and R. H. Holm, Synthesis and Structures of Bis(dithiolene)tungsten(IV,VI) Thiolate and Selenolate Complexes: Approaches to the Active Sites of Molybdenum and Tungsten Formate Dehydrogenases, *Inorg. Chem.*, 2007, **46**, 4090–4102.

50 J. Jiang and R. H. Holm, An Expanded Set of Functional Groups in Bis(dithiolene)tungsten(IV,VI) Complexes Related to the Active Sites of Tungstoenzymes, Including $W^{IV}$ –SR and $W^{VI}$ –O(SR), *Inorg. Chem.*, 2004, **43**, 1302–1310.

51 S. K. Das, D. Biswas, R. Maiti and S. Sarkar, Modeling the Tungsten Sites of Inactive and Active Forms of Hyperthermophilic *Pyrococcus furiosus* Aldehyde Ferredoxin Oxidoreductase, *J. Am. Chem. Soc.*, 1996, **118**, 1387–1397.

52 S. K. Das, P. K. Chaudhury, D. Biswas and S. Sarkar, Modeling for the Active Site of Sulfite Oxidase: Synthesis, Characterization, and Reactivity of $[Mo^{VI}O_2(mnt)_2]^{2-}$ ($mnt^{2-}$ = 1,2-Dicyanoethylenedithiolate), *J. Am. Chem. Soc.*, 1994, **116**, 9061–9070.

53 D. Eierhoff, W. C. Tung, A. Hammerschmidt and B. Krebs, Molybdenum complexes with O,N,S donor ligands as models for active sites in oxotransferases and hydroxylases, *Inorganica Chim. Acta*, 2009, **362**, 915–928.

54 M. R. Maurya, B. Uprety and F. Avecilla, Dioxidomolybdenum(VI) Complexes of Tripodal Tetradentate Ligands for Catalytic Oxygen Atom Transfer between Benzoin and Dimethyl Sulfoxide and for Oxidation of Pyrogallol, *Eur. J. Inorg. Chem.*, 2016, **2016**, 4802–4813.

55 Md. K. Hossain, J. A. Schachner, M. Haukka, A. Lehtonen, N. C. Mösch-Zanetti and E. Nordlander, Dioxidomolybdenum(VI) and -tungsten(VI) complexes with tripodal amino bisphenolate ligands as epoxidation and oxo-transfer catalysts, *Polyhedron*, 2017, **134**, 275–281.

56 Y.-L. Wong, J.-F. Ma, W.-F. Law, Y. Yan, W.-T. Wong, Z.-Y. Zhang, T. C. W. Mak and D. K. P. Ng, Synthesis, Electrochemistry, and Oxygen-Atom Transfer Reactions of Dioxotungsten(VI) and -molybdenum(VI) Complexes with $N_2O_2$ and $N_2S_2$ Tetradentate Ligands, *Eur. J. Inorg. Chem.*, 1999, **1999**, 313–321.

57 A. Thapper, A. Behrens, J. Fryxelius, M. H. Johansson, F. Prestopino, M. Czaun, D. Rehder and E. Nordlander, Synthesis and characterization of molybdenum oxo complexes of two tripodal ligands: reactivity studies of a functional model for molybdenum oxotransferases, *Dalton Trans.*, 2005, 3566.

58 F. J. Arnáiz, R. Aguado, M. R. Pedrosa, A. De Cian and J. Fischer, Synthesis, characterization and catalytic activity of addition compounds of dioxomolybdenum(VI) pyridine-2,6-dicarboxylate. Crystal structure of $MoO_2$(dipic)(L) (L=DMF, DMSO, $OPPh_3$), *Polyhedron*, 2000, **19**, 2141–2147.

59 A. Syamal and M. R. Maurya, Dioxotungsten VI complexes of ONO donor tridentated dibasic schiff bases derived from aminophenol & salicylaldehydes, *Indian J. Chem.*, 1986, **25A**, 934–938.

60 P. Basu, A. M. Raitsimring, M. J. LaBarre, I. K. Dhawan, J. L. Weibrecht and J. H. Enemark, Covalently linked oxomolybdenum(V) and iron(III) porphyrin centers: Synthetic models for the molybdenum-iron interaction in sulfite oxidase, *J. Am. Chem. Soc.*, 1994, **116**, 7166–7176.

61 K. Hanauer, C. Förster and K. Heinze, Redox-Controlled Stabilization of an Open-Shell Intermediate in a Bioinspired Enzyme Model, *Eur. J. Inorg. Chem.*, 2018, **2018**, 3537–3547.

62 N. Chrysochos, M. Ahmadi, S. Wahlefeld, Y. Rippers, I. Zebger, M. A. Mroginski and C. Schulzke, Comparison of molybdenum and rhenium oxo bis-pyrazine-dithiolene complexes – in search of an alternative metal centre for molybdenum cofactor models, *Dalton Trans.*, 2019, **48**, 2701–2714.

63 H. Arzoumanian, G. Agrifoglio and L. Maurino, Thiocyanatodioxomolybdenum (VI) complexes as efficient oxidizing agents, *J. Mol. Catal. Chem.*, 1997, **117**, 471–478.

64 H. Martinez Q, Á. A. Amaya, E. A. Paez-Mozo, F. Martinez O and S. Valange, Photo-assisted O-atom transfer to monoterpenes with molecular oxygen and a dioxo Mo(VI) complex immobilized on $TiO_2$ nanotubes, *Catal. Today*, 2021, **375**, 441–457.

65 N. J. Castellanos, H. Martínez Q, F. Martínez O, K. Leus and P. V. D. Voort, Photo-epoxidation of (α, β)-pinene with molecular $O_2$ catalyzed by a dioxo-molybdenum (VI)-based Metal–Organic Framework, *Res. Chem. Intermed.*, 2021, **47**, 4227–4244.

66 A. B. Ducrot, B. A. Coulson, R. N. Perutz and A.-K. Duhme-Klair, Light-Induced Activation of a Molybdenum Oxotransferase Model within a Ru(II)–Mo(VI) Dyad, *Inorg. Chem.*, 2016, **55**, 12583–12594.

67 D. Yu, W.-P. To, G. S. M. Tong, L.-L. Wu, K.-T. Chan, L. Du, D. L. Phillips, Y. Liu and C.-M. Che, Luminescent tungsten(VI) complexes as photocatalysts for light-driven C–C and C–B bond formation reactions, *Chem. Sci.*, 2020, **11**, 6370–6382.

68 H. Schiff, Mittheilungen aus dem Universitätslaboratorium in Pisa: Eine neue Reihe organischer Basen, *Ann. Chem. Pharm.*, 1864, **131**, 118–119.

69 X. Liu and J.-R. Hamon, Recent developments in penta-, hexa- and heptadentate Schiff base ligands and their metal complexes, *Coord. Chem. Rev.*, 2019, **389**, 94–118.

70 A. Dupé, M. E. Judmaier, F. Belaj, K. Zangger and N. C. Mösch-Zanetti, Activation of molecular oxygen by a molybdenum complex for catalytic oxidation, *Dalton Trans.*, 2015, **44**, 20514–20522.

71 P. E. Aranha, M. P. dos Santos, S. Romera and E. R. Dockal, Synthesis, characterization, and spectroscopic studies of tetradentate Schiff base chromium(III) complexes, *Polyhedron*, 2007, **26**, 1373–1382.

72 A. A. El-Sherif and M. S. Aljahdali, Review: protonation, complex-formation equilibria, and metal–ligand interaction of salicylaldehyde Schiff bases, *J. Coord. Chem.*, 2013, **66**, 3423–3468.

73 W. Qin, S. Long, M. Panunzio and S. Biondi, Schiff Bases: A Short Survey on an Evergreen Chemistry Tool, *Molecules*, 2013, **18**, 12264–12289.

74 Y. Shichida and T. Matsuyama, Evolution of opsins and phototransduction, *Philos. Trans. R. Soc. B Biol. Sci.*, 2009, **364**, 2881–2895.

75 D. Dutta, N. K. Bhattacharyya and J. Biswas, A review on synthesis and biological activity of Schiff Bases, *Indian J Chem*, 2021, 12.

76 H. M. Junaid, M. Batool, F. W. Harun, M. S. Akhter and N. Shabbir, Naked Eye Chemosensing of Anions by Schiff Bases, *Crit. Rev. Anal. Chem.*, 2020, **52**, 463–480.

77 A. L. Berhanu, Gaurav, I. Mohiuddin, A. K. Malik, J. S. Aulakh, V. Kumar and K.-H. Kim, A review of the applications of Schiff bases as optical chemical sensors, *Trends Anal. Chem.*, 2019, **116**, 74–91.

78 S. Khan, X. Chen, A. Almahri, E. S. Allehyani, F. A. Alhumaydhi, M. M. Ibrahim and S. Ali, Recent developments in fluorescent and colorimetric chemosensors based on schiff bases for metallic cations detection: A review, *J. Environ. Chem. Eng.*, 2021, **9**, 106381.

79 K. C. Gupta and A. K. Sutar, Catalytic activities of Schiff base transition metal complexes, *Coord. Chem. Rev.*, 2008, **252**, 1420–1450.

80 M. N. Uddin, S. S. Ahmed and S. M. R. Alam, REVIEW: Biomedical applications of Schiff base metal complexes, *J. Coord. Chem.*, 2020, **73**, 3109–3149.

81 P. Ghanghas, A. Choudhary, D. Kumar and K. Poonia, Coordination metal complexes with Schiff bases: Useful pharmacophores with comprehensive biological applications, *Inorg. Chem. Commun.*, 2021, **130**, 108710.

82 S. Shekhar, A. M. Khan, S. Sharma, B. Sharma and A. Sarkar, Schiff base metallodrugs in antimicrobial and anticancer chemotherapy applications: a comprehensive review, *Emergent Mater.*, 2021, **5**, 279–293.

83 S. Kagatikar and D. Sunil, Schiff Bases and Their Complexes in Organic Light Emitting Diode Application, *J. Electron. Mater.*, 2021, **50**, 6708–6723.

84 A. Wesley Jeevadason, K. Kalidasa Murugavel and M. A. Neelakantan, Review on Schiff bases and their metal complexes as organic photovoltaic materials, *Renew. Sustain. Energy Rev.*, 2014, **36**, 220–227.

85 C. G. Young, Scorpionate Complexes as Models for Molybdenum Enzymes, *Eur. J. Inorg. Chem.*, 2016, **2016**, 2357–2376.

86 R. H. Holm, The biologically relevant oxygen atom transfer chemistry of molybdenum: from synthetic analogue systems to enzymes, *Coord. Chem. Rev.*, 1990, **100**, 183–221.

87 R. Hille, The Mononuclear Molybdenum Enzymes, *Chem Rev*, 1996, **96**, 2757–2816.

88 A. E. Martell, R. D. Hancock and R. J. Motekaitis, Factors affecting stabilities of chelate, macrocyclic and macrobicyclic complexes in solution, *Coord. Chem. Rev.*, 1994, **133**, 39–65.

89 J. Topich and J. O. Bachert, Solution IR spectroscopic studies of cis-dioxomolybdenum(VI) complexes, *Inorg. Chem.*, 1992, **31**, 511–515.

90 V. Béreau, V. Jubéra, P. Arnaud, A. Kaiba, P. Guionneau and J.-P. Sutter, Modulation of the luminescence quantum efficiency for blue luminophor {Al(salophen)}$^+$ by ester-substituents, *Dalton Trans.*, 2010, **39**, 2070.

91 Akanksha and D. Maiti, Microwave-assisted palladium mediated decarbonylation reaction: synthesis of eulatachromene, *Green Chem.*, 2012, **14**, 2314.

92 P. Jaikhan, B. Buranrat, Y. Itoh, J. Chotitumnavee, T. Kurohara and T. Suzuki, Identification of ortho-hydroxy anilide as a novel scaffold for lysine demethylase 5 inhibitors, *Bioorg. Med. Chem. Lett.*, 2019, **29**, 1173–1176.

93 A. Guha, R. Sanyal, T. Chattopadhyay, Y. Han, T. K. Mondal and D. Das, Self-assembled nanostructures of specially designed Schiff-bases and their zinc complexes: Preparation, characterization and photoluminescence property, *J. Mol. Struct.*, 2013, **1042**, 104–111.

94 A. Makal, W. Schilf, B. Kamieński, A. Szady-Chelmieniecka, E. Grech and K. Woźniak, Hydrogen bonding in Schiff bases – NMR, structural and experimental charge density studies, *Dalton Trans.*, 2011, **40**, 421–430.

95 B. Das, A. Chakraborty and S. Chakraborty, Experimental and theoretical investigation of ground state intramolecular proton transfer (GSIPT) in salicylideneaniline Schiff base derivatives in polar protic medium, *Spectrochim. Acta. A. Mol. Biomol. Spectrosc.*, 2020, **225**, 117443.

96 S. Kim, J. Y. Noh, K. Y. Kim, J. H. Kim, H. K. Kang, S.-W. Nam, S. H. Kim, S. Park, C. Kim and J. Kim, Salicylimine-Based Fluorescent Chemosensor for Aluminum Ions and Application to Bioimaging, *Inorg. Chem.*, 2012, **51**, 3597–3602.

97 H. Brunning, *Year 3 Miniproject*, University of York, York, 2018.

98 J. Morlot, N. Uyttebroeck, D. Agustin and R. Poli, Solvent-Free Epoxidation of Olefins Catalyzed by “[$MoO_2$(SAP)]”: A New Mode of *tert*-Butylhydroperoxide Activation, *ChemCatChem*, 2013, **5**, 601–611.

99 M. Minelli, F. Namuswe, D. Jeffrey, A. L. Morrow, I. A. Guzei, D. Swenson, E. Bothe and T. Weyhermüller, Synthesis, Structure, and Characterization of Molybdenum(VI) Imido Complexes with N-Salicylidene-2-aminophenol, *Inorg. Chem.*, 2006, **45**, 5455–5464.

100 W. Wang, T. Guerrero, S. R. Merecias, H. García-Ortega, R. Santillan, J.-C. Daran, N. Farfán, D. Agustin and R. Poli, Substituent effects on solvent-free epoxidation catalyzed by

dioxomolybdenum(VI) complexes supported by ONO Schiff base ligands, *Inorganica Chim. Acta*, 2015, **431**, 176–183.

101 M. Cindrić, N. Strukan, V. Vrdoljak and B. Kamenar, Synthesis, Characterization, and Crystal Structure of Mononuclear and Dinuclear Dioxomolybdenum(VI) Complexes with Tridentate Schiff-base Ligands. Part 2, *Z. Für Anorg. Allg. Chem.*, 2004, **630**, 585–590.

102 L. B. Jerzykiewicz, J. M. Sobczak and J. J. Ziółkowski, Synthesis, X-ray structure and spectroscopic studies of $MoO_2$(3,5-di-tert-Busap)(EtOH), *J. Chem. Res.*, 2000, **2000**, 423–425.

103 R. Takjoo, A. Akbari, S. Y. Ebrahimipour, H. Amiri Rrudbari and G. Brunò, Synthesis, characterization, X-ray structure and DFT calculation of two Mo(VI) and Ni(II) Schiff-base complexes, *Comptes Rendus Chim.*, 2014, **17**, 1144–1153.

104 J. A. Craig, E. W. Harlan, B. S. Snyder, M. A. Whitener and R. H. Holm, Oxomolybdenum(IV,V,VI) complexes: structures, reactivities, and criteria of detection of binuclear (μ-oxo) molybdenum(V) products in oxygen atom transfer systems, *Inorg. Chem.*, 1989, **28**, 2082–2091.

105 M. Cindrić, D. Agustin, G. Pavlovic and R. Katava, Towards a global greener process: from solvent-less synthesis of molybdenum(VI) ONO Schiff base complexes to catalyzed olefin epoxidation under organic-solvent-free conditions, *New J. Chem.*, , DOI:10.1039/c6nj03174a.

106 T. Tunç, M. Sarı, M. Sadıkoğlu and O. Büyükgüngör, Synthesis, Crystal Structure and Spectroscopic Studies of 2-{(E)-[2-Hydroxyphenyl)imino]methyl} Phenol Schiff Base Molecule, *J. Chem. Crystallogr.*, 2009, **39**, 672–676.

107 Cambridge Crystallographic Data Centre, https://www.ccdc.cam.ac.uk/structures/, (accessed 1 February 2022).

108 A. L. Spek, J. Terheijden, J. G. Kraaykamp and K. Timmer, Structure of Dioxo[2-(salicylidenamino)phenolato(2-)-O,N,O']-[tris(dimethylamino)phosphine oxide]tungsten(VI), *Acta Crystallogr. C*, 1990, **46**, 693–695.

109 A. L. Spek and H. A. Meinema, CCDC 228317 Experimental Crystal Structure Determination, *CCDC*, , DOI:10.5517/cc7nl2j.

110 S. B. Yu and R. H. Holm, Aspects of the oxygen atom transfer chemistry of tungsten, *Inorg. Chem.*, 1989, **28**, 4385–4391.

111 P. K. Nath and K. C. Dash, cis-Dioxo(N-salicylidene-2-aminophenolato)(imidazole)-molybdenum(VI) complexes, *Transit. Met. Chem.*, 1985, **10**, 262–264.

112 A. Ducrot, B. Scattergood, B. Coulson, R. N. Perutz and A.-K. Duhme-Klair, Electronic Fine-Tuning of Oxygen Atom Transfer Reactivity of cis -Dioxomolybdenum(VI) Complexes with Thiosemicarbazone Ligands, *Eur. J. Inorg. Chem.*, 2015, **2015**, 3562–3571.

113 C. Hansch, A. Leo and R. W. Taft, A survey of Hammett substituent constants and resonance and field parameters, *Chem. Rev.*, 1991, **91**, 165–195.

114 O. A. Rajan and A. Chakravorty, Molybdenum complexes. 1. Acceptor behavior and related properties of $Mo^{(VI)}O_2$(tridentate) systems, *Inorg. Chem.*, 1981, **20**, 660–664.

115 J. M. Sobczak, T. Glowiak and J. J. Ziólkowski, The structure of binuclear molybdenum(VI) oxocomplexes with dianionic tridentate Schiff bases, *Transit. Met. Chem.*, 1990, **15**, 208–211.

116 J. Coates, in *Encyclopedia of Analytical Chemistry*, ed. R. A. Meyers, John Wiley & Sons, Ltd, Chichester, UK, 2006, p. a5606.

117 E. I. Stiefel, in *Progress in Inorganic Chemistry*, ed. S. J. Lippard, John Wiley & Sons, Inc., Hoboken, NJ, USA, 1977, pp. 1–223.

118 J. M. Hawkins, J. C. Dewan and K. B. Sharpless, Dioxomolybdenum(VI)-substituted 2,6-pyridinedimethanol complexes: new five-coordinate species, *Inorg. Chem.*, 1986, **25**, 1501–1503.

119 T. Guerrero, P. G. Lacroix, H. García-Ortega, O. G. Morales-Saavedra, D. Agustin and N. Farfán, Enhanced NLO properties of molybdenum push–pull coordination compounds with tridentate ONO organic ligands, *Inorganica Chim. Acta*, 2016, **442**, 10–15.

120 J. U. Mondal, F. A. Schultz, T. D. Brennan and W. R. Scheidt, Synthesis, electrochemistry, and spectroscopic properties of six-coordinate monooxomolybdenum(VI) complexes containing

tridentate Schiff base and bidentate catecholate ligands. Crystal and molecular structure of (N-salicylidene-2-aminophenolato)(naphthalene-2,3-diolato)oxomolybdenum(VI), *Inorg. Chem.*, 1988, **27**, 3950–3956.
121 B. W. Kail, L. M. Pérez, S. D. Zarić, A. J. Millar, C. G. Young, M. B. Hall and P. Basu, Mechanistic Investigation of the Oxygen-Atom-Transfer Reactivity of Dioxo-molybdenum(VI) Complexes, *Chem. - Eur. J.*, 2006, **12**, 7501–7509.
122 M. A. Pietsch and M. B. Hall, Theoretical Studies on Models for the Oxo-Transfer Reaction of Dioxomolybdenum Enzymes, *Inorg. Chem.*, 1996, **35**, 1273–1278.
123 J. Topich and J. T. Lyon III, Kinetic study on the reaction of cis-dioxo-(N-(5-X-salicylidene)-2-aminobenzene thiolato) molybdenum(VI) with ethyldiphenylphosphine, *Polyhedron*, 1984, **3**, 61–65.
124 J. Topich, Ligand control of the redox properties of dioxomolybdenum(VI) coordination complexes, *Inorg. Chem.*, 1981, **20**, 3704–3707.
125 J. Topich and J. T. Lyon III, Kinetic study of the oxidation of ethyldiphenylphosphine by cis-dioxo-[N-(5-X-salicylidene)-2-aminoethanethiolato] molybdenum(VI), *Inorganica Chim. Acta*, 1983, **80**, L41–L43.
126 J. Topich and J. T. Lyon III, Ligand control of cis-dioxomolybdenum(VI) redox chemistry: kinetic and activation parameter data for oxygen atom transfer, *Inorg. Chem.*, 1984, **23**, 3202–3206.
127 C. J. Whiteoak, G. J. P. Britovsek, V. C. Gibson and A. J. P. White, Electronic effects in oxo transfer reactions catalysed by salan molybdenum(VI) cis-dioxo complexes, *Dalton Trans.*, 2009, 2337.
128 P. Basu, V. N. Nemykin and R. S. Sengar, Substituent Effect on Oxygen Atom Transfer Reactivity from Oxomolybdenum Centers: Synthesis, Structure, Electrochemistry, and Mechanism, *Inorg. Chem.*, 2009, **48**, 6303–6313.
129 O. A. Rajan and A. Chakravorty, New molybdenum systems: Trends in cyclic voltammetric reduction potentials, *Inorganica Chim. Acta*, 1979, **37**, L503–L504.
130 C. Lorber, M. R. Plutino, L. I. Elding and E. Nordlander, Kinetics of oxygen-atom transfer reactions involving molybdenum dithiolene complexes, *J. Chem. Soc. Dalton Trans.*, 1997, 3997–4004.
131 R. Barral and C. Bocard, Activation de l’oxygène moléculaire en phase liquide homogène par des complexes oxo du molybdène - oxydation catlytique des phosphines tertiaires, *Tetrahedron Lett.*, 1972, 4.
132 Z. Xiao, C. G. Young, J. H. Enemark and A. G. Wedd, A single model displaying all the important centers and processes involved in catalysis by molybdoenzymes containing $[Mo^{VI}O_2]^{2+}$ active sites, *J. Am. Chem. Soc.*, 1992, **114**, 9194–9195.
133 J. Leppin, C. Förster and K. Heinze, Molybdenum Complex with Bulky Chelates as a Functional Model for Molybdenum Oxidases, *Inorg. Chem.*, 2014, **53**, 12416–12427.
134 P. Arroyo, S. Gil, A. Muñoz, P. Palanca, J. Sanchis and V. Sanz, Polymer-supported molybdenyl thioglycolate as oxygen atom transfer reagent, *J. Mol. Catal. Chem.*, 2000, **160**, 403–408.
135 M. Masteri-Farahani and M. Modarres, Superiority of Activated Carbon versus MCM-41 for the Immobilization of Molybdenum Dithiocarbamate Complex as Heterogeneous Epoxidation Catalyst, *ChemistrySelect*, 2017, **2**, 1163–1169.
136 J. M. Berg and R. H. Holm, Synthetic approach to the mononuclear active sites of molybdoenzymes: catalytic oxygen atom transfer reactions by oxomolybdenum(IV,VI) complexes with saturation kinetics and without molybdenum(V) dimer formation, *J. Am. Chem. Soc.*, 1984, **106**, 3035–3036.
137 J. M. Berg and R. H. Holm, Model for the active site of oxo-transfer molybdoenzymes: synthesis, structure, and properties, *J. Am. Chem. Soc.*, 1985, **107**, 917–925.
138 J. M. Berg and R. H. Holm, Model for the active sites of oxo-transfer molybdoenzymes: reactivity, kinetics, and catalysis, *J. Am. Chem. Soc.*, 1985, **107**, 925–932.
139 C. J. Doonan, D. A. Slizys and C. G. Young, New Insights into the Berg–Holm Oxomolybdoenzyme Model, *J. Am. Chem. Soc.*, 1999, **121**, 6430–6436.

140 M. Castiñeira Reis, M. Marín-Luna, C. Silva López and O. N. Faza, $[MoO_2]^{2+}$ -Mediated Oxygen Atom Transfer via an Unusual Lewis Acid Mechanism, *Inorg. Chem.*, 2017, **56**, 10570–10575.

141 R. Sanz, J. Escribano, R. Aguado, M. R. Pedrosa and F. J. Arnáiz, Selective Deoxygenation of Sulfoxides to Sulfides with Phosphites Catalyzed by Dichlorodioxomolybdenum(VI), *Synthesis*, 2004, **2004**, 1629–1632.

142 I. W. Boyd and J. T. Spence, Molybdenum(IV)-oxo complexes with oxygen, nitrogen and sulfur ligands. Syntheses and electrochemical studies, *Inorg. Chem.*, 1982, **21**, 1602–1606.

143 C. Franco and J. Olmsted III, Photochemical determination of the solubility of oxygen in various media, *Talanta*, 1990, **37**, 905–909.

144 S. T. Heller and T. P. Silverstein, pKa values in the undergraduate curriculum: introducing pKa values measured in DMSO to illustrate solvent effects, *ChemTexts*, 2020, **6**, 15.

145 N. Neeraj, A. Kumar, V. Kumar, R. Prajapati, S. K. Asthana, K. K. Upadhyay and J. Zhao, A remarkable effect of N,N-diethylamino functionality on the optoelectronic properties of a salicylimine-based probe for $Al^{3+}$, *Dalton Trans.*, 2014, **43**, 5831–5839.

146 J. Cheng, K. Wei, X. Ma, X. Zhou and H. Xiang, Synthesis and Photophysical Properties of Colorful Salen-Type Schiff Bases, *J. Phys. Chem. C*, 2013, **117**, 16552–16563.

147 L. J. Stewart, S. Bailey, D. Collison, G. A. Morris, I. Preece and C. D. Garner, In Vivo Oxo Transfer: Reactions of Native and W-Substituted Dimethyl Sulfoxide Reductase Monitored by $^1$H NMR Spectroscopy, *ChemBioChem*, 2001, **2**, 703–706.

148 J. Buc, C.-L. Santini, R. Giordani, M. Czjzek, L.-F. Wu and G. Giordano, Enzymatic and physiological properties of the tungsten-substituted molybdenum TMAO reductase from *Escherichia coli*, *Mol. Microbiol.*, 1999, **32**, 159–168.

149 L. J. Stewart, S. Bailey, B. Bennett, J. M. Charnock, C. D. Garner and A. S. McAlpine, Dimethylsulfoxide reductase: an enzyme capable of catalysis with either molybdenum or tungsten at the active site, *J. Mol. Biol.*, 2000, **299**, 593–600.

150 T. Arumuganathan, R. Mayilmurugan, M. Volpe and N. C. Mösch-Zanetti, Faster oxygen atom transfer catalysis with a tungsten dioxo complex than with its molybdenum analog, *Dalton Trans.*, 2011, **40**, 7850–7857.

151 M. Kaupp, Trigonal Prismatic or not Trigonal Prismatic? On the Mechanisms of Oxygen-Atom Transfer in Molybdopterin-Based Enzymes, *Angew. Chem. Int. Ed.*, 2004, **43**, 546–549.

152 M. Feng, B. Tang, S. H. Liang and X. Jiang, Sulfur Containing Scaffolds in Drugs: Synthesis and Application in Medicinal Chemistry, *Curr. Top. Med. Chem.*, 2016, **16**, 1200–1216.

153 Anna and G. Wypych, in *Databook of Solvents*, Elsevier, 2014, pp. 715–732.

154 V. Ji Ram, R. Pratap, A. Sethi and M. Nath, *The Chemistry of Heterocycles*, Elsevier, 2017.

155 C. A. Tolman, Steric effects of phosphorus ligands in organometallic chemistry and homogeneous catalysis, *Chem. Rev.*, 1977, **77**, 313–348.

156 D. G. Blackmond, Reaction Progress Kinetic Analysis: A Powerful Methodology for Mechanistic Studies of Complex Catalytic Reactions, *Angew. Chem. Int. Ed.*, 2005, **44**, 4302–4320.

157 J. Burés, A Simple Graphical Method to Determine the Order in Catalyst, *Angew. Chem. Int. Ed.*, 2016, **55**, 2028–2031.

158 J. Burés, Variable Time Normalization Analysis: General Graphical Elucidation of Reaction Orders from Concentration Profiles, *Angew. Chem. Int. Ed.*, 2016, **55**, 16084–16087.

159 A. Martínez-Carrión, M. G. Howlett, C. Alamillo-Ferrer, A. D. Clayton, R. A. Bourne, A. Codina, A. Vidal-Ferran, R. W. Adams and J. Burés, Kinetic Treatments for Catalyst Activation and Deactivation Processes based on Variable Time Normalization Analysis, *Angew. Chem. Int. Ed.*, 2019, **58**, 10189–10193.

160 C. D.-T. Nielsen and J. Burés, Visual kinetic analysis, *Chem. Sci.*, 2019, **10**, 348–353.

161 R. H. Holm, G. C. Tucci and J. P. Donahue, Comparative Kinetics of Oxo Transfer to Substrate Mediated by Bis(dithiolene)dioxomolybdenum and -tungsten Complexes, *Inorg. Chem.*, 1998, **37**, 1602–1608.

162 J. P. Caradonna, E. W. Harlan and R. H. Holm, Thiol as an electron donor in molybdenum oxo-transferase analog reaction systems: observations by fluorine-$^{19}$ NMR spectroscopy and biological implications, *J. Am. Chem. Soc.*, 1986, **108**, 7856–7858.
163 S. R. Logan, Does a Photochemical Reaction Have a Reaction Order?, *J. Chem. Educ.*, 1997, **74**, 1303.
164 M. Hippler, Photochemical Kinetics: Reaction Orders and Analogies with Molecular Beam Scattering and Cavity Ring-Down Experiments, *J. Chem. Educ.*, 2003, **80**, 1074.
165 S. Toby, Does a Photochemical Reaction Have a Kinetic Order?, *J. Chem. Educ.*, 2005, **82**, 37.
166 D. M. Kaphan, K. R. Brereton, R. C. Klet, R. J. Witzke, A. J. M. Miller, K. L. Mulfort, M. Delferro and D. M. Tiede, Photocatalytic Transfer Hydrogenation in Water: Insight into Mechanism and Catalyst Speciation, *Organometallics*, 2021, **40**, 1482–1491.
167 C. E. Housecroft and A. G. Sharpe, *Inorganic chemistry*, Pearson Education Ltd, Essex, United Kingdom, 4th edn., 2012.
168 A. J. Pell, G. Pintacuda and C. P. Grey, Paramagnetic NMR in solution and the solid state, *Prog. Nucl. Magn. Reson. Spectrosc.*, 2019, **111**, 1–271.
169 M. T. Pope, in *Progress in Inorganic Chemistry*, ed. S. J. Lippard, John Wiley & Sons, Inc., Hoboken, NJ, USA, 1991, pp. 181–257.
170 E. I. Stiefel, in *Kirk-Othmer Encyclopedia of Chemical Technology*, 5th edn., vol. 17, pp. 19–43.
171 H. B. Linden, Liquid Injection Field Desorption Ionization: A New Tool for Soft Ionization of Samples Including Air-Sensitive Catalysts and Non-Polar Hydrocarbons, *Eur. J. Mass Spectrom.*, 2004, **10**, 459–468.
172 M. H. Dickman and M. T. Pope, Peroxo and Superoxo Complexes of Chromium, Molybdenum, and Tungsten, *Chem. Rev.*, 1994, **94**, 569–584.
173 N. J. Castellanos, F. Martínez, E. A. Páez-Mozo, F. Ziarelli and H. Arzoumanian, Bis(3,5-dimethylpyrazol-1-yl)acetate bound to titania and complexed to molybdenum dioxido as a bidentate N,N′-ligand. Direct comparison with a bipyridyl analog in a photocatalytic arylalkane oxidation by $O_2$, *Transit. Met. Chem.*, 2012, **37**, 629–637.
174 H. Martínez and S. Valange, Photo-epoxidation of cyclohexene, cyclooctene and 1-octene with molecular oxygen catalyzed by dichloro dioxo-(4,4′-dicarboxylato-2,2′-bipyridine) molybdenum (VI) grafted on mesoporous TiO 2, *J. Mol. Catal. Chem.*, 2016, **423**, 248–255.
175 D. J. Abrams, J. G. West and E. J. Sorensen, Toward a mild dehydroformylation using base-metal catalysis, *Chem. Sci.*, 2017, **8**, 1954–1959.
176 A. Maldotti, A. Molinari and F. Bigi, Selective photooxidation of diols with silica bound $W_{10}O_{32}^{4-}$, *J. Catal.*, 2008, **253**, 312–317.
177 N. Petkov, A. Ivanova, A. A. Trifonov, I. C. Buchvarov and S. S. Stanimirov, Transient absorption, femtosecond dynamics, vibrational coherence and molecular modelling of the photoisomerization of N-salicylidene- o -aminophenol in solution, *Phys. Chem. Chem. Phys.*, 2021, **23**, 20989–21000.
178 A. A. Abdel Aziz, A. N. M. Salem, M. A. Sayed and M. M. Aboaly, Synthesis, structural characterization, thermal studies, catalytic efficiency and antimicrobial activity of some M(II) complexes with ONO tridentate Schiff base N-salicylidene-o-aminophenol (saph$H_2$), *J. Mol. Struct.*, 2012, **1010**, 130–138.
179 Q. Song, W. Ma, M. Jia, D. Johnson and Y. Huang, Degradation of organic pollutants in waters by a water-insoluble iron(III) Schiff base complex, *Appl. Catal. Gen.*, 2015, **505**, 70–76.
180 T. I. Robertson and P. N. Nelson, A DFT and experimental study of the spectroscopic and hydrolytic degradation behaviour of some benzylideneanilines, *J. Mol. Struct.*, 2022, **1249**, 131625.
181 S. Y. Ebrahimipour, M. Khosravan, J. White and S. Fekri, Preparation, crystal structure, spectroscopic studies, DFT calculations, antibacterial activities and molecular docking of a tridentate Schiff base ligand and its cis -MoO2 complex: biological activity of a cis MoO2 complex, *Appl. Organomet. Chem.*, 2018, **32**, e4233.

182 B. Agrahari, S. Layek, R. Ganguly, N. Dege and D. D. Pathak, Synthesis, characterization and single crystal X-ray studies of pincer type Ni(II)-Schiff base complexes: Application in synthesis of 2-substituted benzimidazoles, *J. Organomet. Chem.*, 2019, **890**, 13–20.

183 C. Reichardt and T. Welton, in *Solvents and Solvent Effects in Organic Chemistry*, Wiley-VCH Verlag GmbH & Co. KGaA, Weinheim, Germany, 3rd edn., 2010, pp. 549–586.

184 V. Balzani, P. Ceroni and A. Juris, *Photochemistry and Photophysics : Concepts, Research, Applications*, Wiley-VCH Verlag GmbH & Co. KGaA, Weinheim, Germany, first., 2014.

185 J.-S. Wu, W.-M. Liu, X.-Q. Zhuang, F. Wang, P.-F. Wang, S.-L. Tao, X.-H. Zhang, S.-K. Wu and S.-T. Lee, Fluorescence Turn On of Coumarin Derivatives by Metal Cations: A New Signaling Mechanism Based on C=N Isomerization, *Org. Lett.*, 2007, **9**, 33–36.

186 N. Klinhom, N. Saengsuwan, S. Sriyab, P. Prompinit, S. Hannongbua and S. Suramitr, Photophysical properties for excited-state intramolecular proton transfer (ESIPT) reaction of N-salicylidene-o-aminophenol: Experimental and DFT based approaches, *Spectrochim. Acta. A. Mol. Biomol. Spectrosc.*, 2019, **206**, 359–366.

187 S. K. Kurapati, U. Ugandhar, S. Maloth and S. Pal, Dioxomolybdenum(VI) complexes with 2-((2-(pyridin-2-yl)hydrazono)methyl)phenol and its derivatives, *Polyhedron*, 2012, **42**, 161–167.

188 Y. Wang, Y. Guo, Y. Liang, Y. Pan, Y. Shi, Y. Wang, S. Zhang, B. Jin and G. Zhao, Coordination-promoted photoluminescence induced by configuration twisting regulation, *J. Lumin.*, 2021, **231**, 117783.

189 M. L. Ramos, L. L. G. Justino, P. E. Abreu, S. M. Fonseca and H. D. Burrows, Oxocomplexes of Mo(VI) and W(VI) with 8-hydroxyquinoline-5-sulfonate in solution: structural studies and the effect of the metal ion on the photophysical behaviour, *Dalton Trans.*, 2015, **44**, 19076–19089.

190 Edinburgh Instruments Ltd, 2013.

191 N. R. Pramanik, J. Ray, T. K. Raychaudhuri, S. Ghosh and S. S. Mandai, The absorption and emission characteristics of some dithiocarbazate ligands and their Mo(VI) complexes, *J. Indian Chem. Soc.*, 2011, **88**, 531–535.

192 D. M. Arias-Rotondo and J. K. McCusker, The photophysics of photoredox catalysis: a roadmap for catalyst design, *Chem. Soc. Rev.*, 2016, **45**, 5803–5820.

193 J. R. Ochola and M. O. Wolf, The effect of photocatalyst excited state lifetime on the rate of photoredox catalysis, *Org. Biomol. Chem.*, 2016, **14**, 9088–9092.

194 A. K. Clarke, A. Parkin, R. J. K. Taylor, W. P. Unsworth and J. A. Rossi-Ashton, Photocatalytic Deoxygenation of Sulfoxides Using Visible Light: Mechanistic Investigations and Synthetic Applications, *ACS Catal.*, 2020, 5814–5820.

195 P. Subramaniam, S. Anbarasan, S. Sugirtha Devi and A. Ramdass, Modulation of catalytic activity by ligand oxides in the sulfoxidation of phenylmercaptoacetic acids by oxo(salen)chromium(V) complexes, *Polyhedron*, 2016, **119**, 14–22.

196 Y. Shen, P. Jiang, P. T. Wai, Q. Gu and W. Zhang, Recent Progress in Application of Molybdenum-Based Catalysts for Epoxidation of Alkenes, *Catalysts*, 2019, **9**, 31.

197 M. Livendahl, J. Jamroskovic, M. Hedenström, T. Görlich, N. Sabouri and E. Chorell, Synthesis of phenanthridine spiropyrans and studies of their effects on G-quadruplex DNA, *Org. Biomol. Chem.*, 2017, **15**, 3265–3275.

198 M. M. Folkendt, B. E. Weiss-Lopez, J. P. Chauvel and N. S. True, Gas-phase proton NMR studies of keto-enol tautomerism of acetylacetone, methyl acetoacetate, and ethyl acetoacetate, *J. Phys. Chem.*, 1985, **89**, 3347–3352.

199 H. Mahmoudi, M. Bagherzadeh, S. Ataie, R. Kia, S. Heydar Moravej, M. Zare, P. R. Raithby, F. Ferlin and L. Vaccaro, Synthesis and X-ray crystal structure of a Molybdenum(VI) Schiff base complex: Design of a new catalytic system for sustainable olefin epoxidation, *Inorganica Chim. Acta*, 2020, **511**, 119775.

200 B. Soptrajanov, A. Nikolovski and I. Petrov, Infra-red spectra of dioxobis(acetylacetonato) tungsten (VI) and dioxobis (acetylacetonato) molybdenum (VI), *Spectrochim. Acta*, 1968, **24A**, 1617–1621.